m 56

Rudolf Haussmann

Self-consistent Quantum-Field Theory and Bosonization for Strongly Correlated Electron Systems

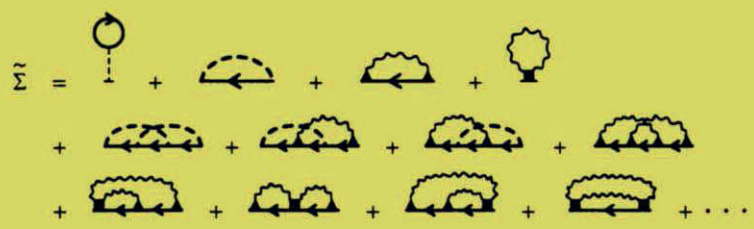

Springer

Lecture Notes in Physics

Monographs

Editorial Board

R. Beig, Vienna, Austria
J. Ehlers, Potsdam, Germany
U. Frisch, Nice, France
K. Hepp, Zürich, Switzerland
R. L. Jaffe, Cambridge, MA, USA
R. Kippenhahn, Göttingen, Germany
I. Ojima, Kyoto, Japan
H. A. Weidenmüller, Heidelberg, Germany
J. Wess, München, Germany
J. Zittartz, Köln, Germany

Managing Editor

W. Beiglböck
Assisted by Ms. Monika Eisenächer
c/o Springer-Verlag, Physics Editorial Department II
Tiergartenstrasse 17, D-69121 Heidelberg, Germany

Springer
Berlin
Heidelberg
New York
Barcelona
Hong Kong
London
Milan
Paris
Singapore
Tokyo

The Editorial Policy for Monographs

The series Lecture Notes in Physics reports new developments in physical research and teaching - quickly, informally, and at a high level. The type of material considered for publication in the monograph Series includes monographs presenting original research or new angles in a classical field. The timeliness of a manuscript is more important than its form, which may be preliminary or tentative. Manuscripts should be reasonably self-contained. They will often present not only results of the author(s) but also related work by other people and will provide sufficient motivation, examples, and applications.
The manuscripts or a detailed description thereof should be submitted either to one of the series editors or to the managing editor. The proposal is then carefully refereed. A final decision concerning publication can often only be made on the basis of the complete manuscript, but otherwise the editors will try to make a preliminary decision as definite as they can on the basis of the available information.
Manuscripts should be no less than 100 and preferably no more than 400 pages in length. Final manuscripts should be in English. They should include a table of contents and an informative introduction accessible also to readers not particularly familiar with the topic treated. Authors are free to use the material in other publications. However, if extensive use is made elsewhere, the publisher should be informed. Authors receive jointly 30 complimentary copies of their book. They are entitled to purchase further copies of their book at a reduced rate. No reprints of individual contributions can be supplied. No royalty is paid on Lecture Notes in Physics volumes. Commitment to publish is made by letter of interest rather than by signing a formal contract. Springer-Verlag secures the copyright for each volume.

The Production Process

The books are hardbound, and quality paper appropriate to the needs of the author(s) is used. Publication time is about ten weeks. More than twenty years of experience guarantee authors the best possible service. To reach the goal of rapid publication at a low price the technique of photographic reproduction from a camera-ready manuscript was chosen. This process shifts the main responsibility for the technical quality considerably from the publisher to the author. We therefore urge all authors to observe very carefully our guidelines for the preparation of camera-ready manuscripts, which we will supply on request. This applies especially to the quality of figures and halftones submitted for publication. Figures should be submitted as originals or glossy prints, as very often Xerox copies are not suitable for reproduction. For the same reason, any writing within figures should not be smaller than 2.5 mm. It might be useful to look at some of the volumes already published or, especially if some atypical text is planned, to write to the Physics Editorial Department of Springer-Verlag direct. This avoids mistakes and time-consuming correspondence during the production period.
As a special service, we offer free of charge LaTeX and TeX macro packages to format the text according to Springer-Verlag's quality requirements. We strongly recommend authors to make use of this offer, as the result will be a book of considerably improved technical quality.
Manuscripts not meeting the technical standard of the series will have to be returned for improvement.
For further information please contact Springer-Verlag, Physics Editorial Department II, Tiergartenstrasse 17, D-69121 Heidelberg, Germany.

Rudolf Haussmann

Self-consistent Quantum Field Theory and Bosonization for Strongly Correlated Electron Systems

Springer

Author

Rudolf Haussmann
Sektion Physik
Universität München
Theresienstrasse 37
D-80333 München, Germany

Library of Congress Cataloging-in-Publication Data applied for.

Die Deutsche Bibliothek - CIP-Einheitsaufnahme

Haussmann, Rudolf:
Self-consistent quantum field theory and bosonization for strongly correlated electron systems / Rudolf Haussmann. - Berlin ; Heidelberg ; New York ; Barcelona ; Hong Kong ; London ; Milan ; Paris ; Singapore ; Tokyo : Springer, 1999
(Lecture notes in physics : N.s. M, Monographs ; 56)
ISBN 3-540-65812-2

ISSN 0940-7677 (Lecture Notes in Physics. Monographs)
ISBN 3-540-65812-2 Springer-Verlag Berlin Heidelberg New York

This work is subject to copyright. All rights are reserved, whether the whole or part of the material is concerned, specifically the rights of translation, reprinting, reuse of illustrations, recitation, broadcasting, reproduction on microfilm or in any other way, and storage in data banks. Duplication of this publication or parts thereof is permitted only under the provisions of the German Copyright Law of September 9, 1965, in its current version, and permission for use must always be obtained from Springer-Verlag. Violations are liable for prosecution under the German Copyright Law.

© Springer-Verlag Berlin Heidelberg 1999
Printed in Germany

The use of general descriptive names, registered names, trademarks, etc. in this publication does not imply, even in the absence of a specific statement, that such names are exempt from the relevant protective laws and regulations and therefore free for general use.

Typesetting: Camera-ready by the author
Cover design: *design & production*, Heidelberg

SPIN: 10552635 55/3144 - 5 4 3 2 1 0 – Printed on acid-free paper

Preface

In quantum liquids the interaction between the particles leads to a variety of interesting and unusual states of condensed-matter systems, e.g. superconductivity and the fractional quantum Hall effect (FQHE) in electron systems. In this book we investigate quantum-field-theoretical approaches for interacting fermion systems. Originally, the quantum-field theory is designed as a perturbation theory to describe weakly interacting many-particle systems. For a proper treatment of interaction and correlation effects beyond the perturbation theory, the series of Feynman diagrams must be resummed partially. We present several resummation schemes which depend on the particular physical effect considered. We start with a compact description of the self-consistent quantum-field theory and the conserving approximations.

Superconductivity in fermion systems is caused by the interplay of two phenomena: formation of bound pairs by attractive interaction between the fermions and condensation of the pairs at low temperatures leading to long-range order and superfluidity. We consider a three-dimensional system of fermions with short-range attractive interaction which shows a crossover from BCS superconductivity to Bose–Einstein condensation of bound pairs if the interaction strength is tuned from weak to strong coupling. While the self-consistent version of the quantum-field theory is well suited to describe condensation of pairs and superfluidity, a second resummation leading to the Bethe–Salpeter equation describes the formation of bound pairs.

The local particle-number conservation is related to a fundamental symmetry: invariance with respect to local gauge transformations. The self-consistent quantum-field theory is gauge invariant only if all Feynman diagrams are resummed, but not if the perturbation series is truncated at finite order. Thus, by a local gauge transformation the self-consistent quantum-field theory can be modified to incorporate nonperturbative effects. We develop an approach which may be viewed as a generalized bosonization and which can be used as a perturbation theory for systems with degenerate levels.

The approach is applied to the two-dimensional electron system in a strong perpendicular magnetic field. Degeneracies are implied by the Landau-level quantization for noninteger filling factors ν so that the Coulomb interaction leads to strong correlations of the electrons at low temperatures. We calculate the spectral function $A(\epsilon)$ of the lowest Landau level and the mag-

netization $M(T)$ for systems in the FQHE regime. We find good agreement of our theoretical results with recent experiments. Finally, we discuss some further applications of the modified self-consistent quantum-field theory to Coulomb plasmas and to interacting boson systems.

I would like to thank Prof. Dr. W. Zwerger for many discussions from which I have learned a great deal about many-particle physics, superconductivity, bosonization, and the quantum Hall effect. I am especially grateful to Prof. Dr. A. H. MacDonald for an enjoyable collaboration at the Indiana University in Bloomington, which gave me a deep insight into the quantum Hall effect and into the American way of research. Finally, I thank Dr. M. Kasner for discussions about magnetic properties in FQHE systems.

München, February 1999 *Rudolf Haussmann*

Contents

1. **Introduction** 1

2. **Self-consistent quantum-field theory** 7
   - 2.1 Legendre transformation 9
   - 2.2 Perturbation series expansion 12
   - 2.3 Conserving approximations 17
   - 2.4 Two-particle functions and Ward identities 20

3. **Superconductivity and pairing of electrons in three dimensions** 27
   - 3.1 Derivation of the self-consistent equations for a superfluid Fermi system with s-wave pairing 31
   - 3.2 Discussion of the self-consistent equations, weak- and strong-coupling limit 46
   - 3.3 Numerical results for $T = T_c$ and discussion 61

4. **Gauge transformation and bosonization** 73
   - 4.1 Conventional bosonization for one- and higher-dimensional fermion systems 76
   - 4.2 Modification of the self-consistent quantum-field theory by gauge transformation 81
   - 4.3 Application to the Luttinger model 101
   - 4.4 Application to the independent-boson model 111

5. **Two-dimensional electron systems in the FQHE regime** 117
   - 5.1 Theory of the FQHE 118
   - 5.2 General properties of the spectral functions for FQHE systems 128
   - 5.3 Modified SC-RPA theory for the two-dimensional electron system in a homogeneous magnetic field 133
   - 5.4 Electronic excitation spectrum of the partially filled lowest Landau level 143
   - 5.5 Magnetization of FQHE electron systems 153

6. Further applications 161
6.1 Coulomb plasma 161
6.2 Interacting boson systems 164

References 169

Index 173

1. Introduction

The quantum-field theory is a powerful approach for interacting many-particle systems as e.g. electrons in condensed-matter systems at low temperatures where quantum effects are observed. This approach is originally designed as a perturbation theory with respect to the interaction of the particles, which is well organized in a very elegant and efficient way by the use of Feynman diagrams. Thus, the quantum-field theory is suited for the description of weakly interacting Fermi and Bose systems where the interaction effects are calculated order by order in perturbation theory. However, in condensed-matter systems many phenomena have been observed, which are not accessible by perturbation theory, as e.g. phase transitions and strong correlation effects. For a description of these systems nonperturbative methods are needed which must be incorporated into the quantum-field theory.

In this work we investigate quantum-field-theoretical approaches for interacting fermion systems beyond the conventional perturbation theory. We consider several partial resummations of the Feynman diagrams to improve the perturbation series and to include nonperturbative effects. Each resummation scheme will be related to and suited for a particular nonperturbative physical effect. We use the quantum-field theory in the self-consistent version where in the Feynman diagrams the propagator lines are identified by the dressed Green's function. This theory anticipates the resummation of all self-energy subdiagrams and is suited to describe nontrivial spectra of the elementary excitations, because via the dressed Green's function these spectra are incorporated into each term of the perturbation series. The self-consistent quantum-field theory is a standard approach for interacting many-particle systems which we will use throughout this work as the basic approach. For this reason, in Chap. 2 we describe the self-consistent quantum-field theory, the related resummation, and the conserving approximations on a general level. Formulas derived there will be used in later chapters.

Interacting electron systems may be viewed as model systems for the delocalized valence electrons in condensed-matter systems as e.g. metals and doped semiconductors. The electrons are moving in the potential of the ions and atoms which form the positively charged neutralizing background. The electrons interact with each other by the repulsive Coulomb forces and also indirectly via collective excitations of the ionic and atomic background as e.g.

phonons. Furthermore, there may be external electric and magnetic fields. The physical effects observed in these electron systems can be divided into two classes: single-particle effects and interaction effects. Single-particle effects are caused by the motion of the individual electrons in the background potential and in the electric and magnetic fields. In crystals the background potential is periodic in space which leads to a band structure for the energies of the electrons. Impurity atoms cause irregularities in the background potential which imply disorder effects as e.g. a metal-insulator transition. Special structures of the background potential can restrict the effective motion of the electrons into two, one, and zero dimensions. Electron systems of these kinds are realized in semiconductor devices as quantum wells, quantum wires, and quantum dots, respectively. A homogeneous external magnetic field implies the quantization of the electron motion into Landau levels. On the other hand interaction effects cause correlations between the electrons and elementary excitations with finite lifetimes and nontrivial spectra. Furthermore, interaction effects lead to unusual states and properties of condensed-matter systems as e.g. superconductivity, pair formation, ferromagnetism, antiferromagnetism, and the fractional quantum Hall effect.

In this work we focus on interaction and correlation effects. For this reason we simplify the single-particle properties implied by the background potential as much as possible. We omit all nontrivial bandstructure effects. To do this we approximate the valence band by a quadratic and isotropic dispersion relation $\varepsilon_{\mathbb{k}} = \hbar^2 \mathbb{k}^2 / 2m^*$ so that the electrons move like free particles of effective mass m^* in a homogeneous positively charged neutralizing background. This approximation is valid for metal like systems where in the valence band only the states with small wave vectors $\mathbb{k}$ are occupied. Furthermore, we consider only very clean systems so that disorder by impurities is neglected. There may be an external potential which restricts the effective motion of the electrons to lower dimensions. Furthermore, there may be or may be not a homogeneous magnetic field. Thus, in this work we consider interacting electron systems in $d = 1$, 2, and 3 dimensions which in second-quantization representation are described by the Hamiltonian

$$H = \int d^d r \sum_\sigma \Big\{ \frac{1}{2m^*} \Big| \big(\mathbb{p} + \frac{e}{c}\mathbb{A}\big) \Psi_\sigma(\mathbb{r}) \Big|^2 + g\mu_{\mathrm{B}} \mathbb{B} \cdot \mathbb{s}/\hbar \Big\} + \frac{1}{2} \int d^d r \int d^d r' : [\varrho(\mathbb{r}) - \varrho_{\mathrm{b}}]\, V(\mathbb{r} - \mathbb{r}')\, [\varrho(\mathbb{r}') - \varrho_{\mathrm{b}}] : \qquad (1.1)$$

where $\Psi_\sigma(\mathbb{r})$ and $\Psi_\sigma^+(\mathbb{r})$ are the fermion field operators of the electrons. The electron-density operator is defined by $\varrho(\mathbb{r}) = \sum_\sigma \Psi_\sigma^+(\mathbb{r}) \Psi_\sigma(\mathbb{r})$, and the spin-density operator is defined by $\mathbb{s}(\mathbb{r}) = (\hbar/2) \sum_{\sigma\sigma'} \Psi_\sigma^+(\mathbb{r}) \boldsymbol{\sigma}_{\sigma\sigma'} \Psi_{\sigma'}(\mathbb{r})$. The first term represents the quadratic dispersion relation of the kinetic energy where m^* is the effective electron mass. The magnetic field $\mathbb{B}$ couples to the electrons via the vector potential $\mathbb{A}$ in the kinetic energy and via the Zeeman coupling term. The last term describes the interaction between the electrons

by the two-particle potential $V(\boldsymbol{r})$, where ϱ_{b} is the homogeneous density of the positively charged neutralizing background.

In Chap. 3 we consider the tree-dimensional fermion system with an attractive short-range interaction. We tune the strength of the interaction in the whole range between weak coupling and strong coupling. While for weak coupling the system is a weakly interacting Fermi gas, for strong coupling the fermions are bound into pairs which form a weakly interacting Bose gas. In the intermediate region the system is a mixture of single fermions and bound pairs which interact strongly with each other. For low temperatures a superfluid transition is found which is related to superconductivity in condensed-matter systems. Depending on the strength of the interaction we find a crossover between BCS superconductivity and Bose–Einstein condensation of bound pairs. In interacting fermion systems superfluidity is related to two phenomena: formation of bound pairs and condensation of fermion pairs leading to a long-range order. For this reason we need two partial resummations of the Feynman diagrams. First of all, the self-consistent quantum-field theory, which anticipates the resummation of all self-energy subdiagrams, is well suited to describe the condensation of pairs and superfluidity, because the order parameter is included in the fermion Green's function (as the anomalous Green's functions), which is treated self-consistently here. Secondly, the formation of bound pairs is described be a resummation of subdiagrams which leads to the Bethe–Salpeter equation for the vertex function. In a self-consistent ladder approximation we derive four self-consistent equations for the fermion Green's function and for the vertex function. A considerable simplification is achieved by the short range of the interaction, so that the interaction strength can be described by the s-wave scattering length. The four self-consistent equations represent a simple model for the crossover from BCS superconductivity to Bose–Einstein condensation, which can be solved numerically by iteration and Fourier transformation and which describes the essential physical properties of the crossover. We calculate the superfluid transition temperature T_{c} as a function of the coupling strength. Furthermore, we calculate the fermion distribution function $n(\boldsymbol{k})$, the electronic spectral function $A(\boldsymbol{k}, \varepsilon)$, and the effective mass of the bound pairs at $T = T_{\mathrm{c}}$ for various coupling strengths.

In many-particle systems the local conservation of the particle number is related to a fundamental symmetry: invariance with respect to local gauge transformations. However, since a single Feynman diagram is not gauge invariant, at least certain classes of diagrams must be resummed to achieve gauge invariance. It turns out that the self-consistent quantum-field theory is not gauge invariant order by order in perturbation theory. By exploiting this observation in Chap. 4 we modify the self-consistent quantum-field theory by a local gauge transformation to incorporate nonperturbative effects. We choose the local phase of the gauge transformation as a real boson field operator, which eventually is identified by the collective excitations. In this

way we obtain a nonperturbative method which in the literature is known as *bosonization*. It turns out that by this method the Luttinger model for the one-dimensional interacting fermion system can be solved exactly in an easy and elegant way. Furthermore, the independent-boson model can be solved exactly. By applying our theory to more general and more realistic fermion systems we may combine nonperturbative properties of the exactly solvable models with the perturbation theory. The modified self-consistent quantum-field theory can be used as a perturbation theory for systems with degenerate levels, where the degenerate degrees of freedom are treated by bosonization while the remaining degrees of freedom are treated perturbatively.

In Chap. 5 we consider the two-dimensional electron system in a strong perpendicular magnetic field. Degeneracies are implied by the Landau-level quantization if the filling factor ν is noninteger so that the Coulomb interaction leads to strong correlations of the electron system at low temperatures. The modified self-consistent quantum-field theory turns out to be the appropriate approach here. Including self-consistent Feynman diagrams up to first order we find that the degenerate degrees of freedom in the partially filled level are treated by an independent-boson model while the other nearly empty or nearly filled levels are treated perturbatively. We calculate the spectral functions $A_{n\sigma}(\varepsilon)$ for the Landau levels n with spin polarization σ. To compare with experiments we focus on electron systems in the regime of the fractional quantum Hall effect (FQHE), where only the lowest Landau level is filled partially while all the higher Landau levels are nearly empty. In this case it turns out that the higher Landau levels imply only small perturbations so that in leading approximation the motion of the electrons can be restricted to the lowest Landau level. For filling factors ν in the interval $0 < \nu < 1$ where the system is assumed to be spin polarized, we calculate the electronic spectral function $A(\varepsilon)$ of the lowest spin-polarized Landau level. At low temperatures we obtain a double-peak structure for $A(\varepsilon)$, a hole peak for $\varepsilon < \mu$ and an electron peak for $\varepsilon > \mu$ which are separated by a pseudogap around the Fermi energy $\varepsilon = \mu$. The spectral function $A(\varepsilon)$ may be interpreted as a generalized density of states for interacting electron systems so that it can be related to the current-voltage characteristic $I(V)$ of a tunneling experiment. Our theoretical results for $A(\varepsilon)$ and $I(V)$ agree with the observations of a tunneling experiment with two FQHE layers (Eisenstein et al. 1992 and 1994, Brown et al. 1994). Furthermore, we consider the magnetic properties of the electron system for filling factors ν in the interval $0 < \nu < 2$. In this case the electrons occupy the lowest Landau levels with both spin directions. Since the Zeeman energy is small compared to the characteristic interaction energy, the magnetic properties are influenced by strong correlations. For $\nu = 1$ we calculate the magnetic polarization $M(T)$ as a function of temperature and find a surprisingly good agreement with the experiment of Barrett et al. (1995). Nevertheless, the FQHE is not explained by our theory, because the

FQHE would appear in $A(\varepsilon)$ only as a small detail close to the Fermi energy $\varepsilon = \mu$ which is not resolved by our approximations.

Finally, in Chap. 6 we discuss some further applications of the modified self-consistent quantum-field theory. First of all, we note that our method can be used as a bosonization technique for interacting fermion systems in $d = 1$ and $d > 1$ dimensions alternatively to existing approaches. Secondly, we apply our method to the three-dimensional Coulomb plasma with the intention to calculate the electronic spectral function $A(\boldsymbol{k}, \varepsilon)$ at large r_s. It turns out that our theory works at high temperatures, where the Coulomb plasma is a classical liquid, but fails for low temperatures, where quantum effects like the Fermi surface appear. Furthermore, we discuss the possible application of our method to interacting boson systems with the intention to describe superfluid systems where the order parameter is averaged to zero by strong phase fluctuations. For this purpose we consider a simple interacting boson system with one bosonic degree of freedom, which can be solved exactly. We demonstrate that our theory works very well for this model and conclude that it is suited to describe also more realistic interacting boson systems at low temperatures.

2. Self-consistent quantum-field theory

In this work we use the quantum-field theory as the basic approach to study strongly correlated many-particle systems in the quantum regime. The quantum-field theory is a perturbation-series expansion which is well organized by the use of the Feynman diagrams. However, from the beginning it is designed for weakly interacting quantum many-particle systems because the interaction between the particles is treated perturbatively. Thus, to consider strongly-correlated quantum liquids it is necessary to go beyond perturbation theory. To do this one usually tries to find one or more partial resummations of the series of Feynman diagrams which cover the essential part of the physical effect. In this chapter we describe a standard resummation procedure, the so called *self-consistent quantum-field theory*, in which the terms depend on the exact or dressed Green's function. This resummation has been invented first by Luttinger and Ward (1960) and can be found in standard text books as e.g. Abrikosov, Gorkov, and Dzyaloshinskii (1963). Later it has been extended and formulated in terms of Legendre transformations by De Dominicis and Martin (1964). The self-consistent quantum-field theory implies approximations in a natural way which satisfy conservation laws for particle number, momentum, and energy (Baym and Kadanoff 1961, Baym 1962) and the Luttinger theorem (Luttinger 1960). Since we will use this approach as a starting point for applications and further developments beyond perturbation theory, we will give a brief account in the following to exhibit the general structure of the self-consistent quantum-field theory.

The quantum-field theory exists in three different versions for nonrelativistic many-particle systems: the ground-state theory at zero temperature, the Matsubara formalism for systems in thermal equilibrium at finite temperatures (Matsubara 1955), and the Keldysh formalism for nonequilibrium systems (Keldysh 1965). While the ground-state theory and the Matsubara formalism are described in standard text books (Abrikosov, Gorkov, and Dzyaloshinskii 1963, Fetter and Walecka 1971, Mahan 1990, Negele and Orland 1988), there exist only a few good review articles for the Keldysh formalism as e.g. Rammer and Smith (1986) and Serene and Rainer (1983). We are studying quantum many-particle systems at finite temperatures T so that we are using only the Matsubara formalism with temperature dependent Green's functions in the following. All formulas and theories that we

will derive in this work can be translated also into the other two versions of the quantum-field theory.

Properties of many-particle systems are described by averages of physical quantities and correlation functions which are defined by thermal averages of a product of some quantum operators. Since the particle number is a conserved quantity, the thermal averages are defined with the grand-canonical ensemble,

$$\langle \cdots \rangle = Z^{-1} \mathrm{Tr}\{\cdots \mathrm{e}^{-\beta K}\} \tag{2.1}$$

where $\beta = 1/k_{\mathrm{B}}T$ and $K = H - \mu N$. The grand-canonical partition function

$$Z = \mathrm{Tr}\{\mathrm{e}^{-\beta K}\} \tag{2.2}$$

is the normalization factor. In quantum-field theory the most important correlation function is the one-particle Green's function

$$G_{XX'} = \langle T[\Psi_X \Psi_{X'}^{+}] \rangle \tag{2.3}$$

where Ψ_X and Ψ_X^{+} are the field operators of the particles. While in our work we consider only fermion systems, in this chapter we want to describe the general formalism briefly and hence allow for generality the particles to be either bosons or fermions. For brevity we use a short-hand notation for the arguments of the fields: the index X comprises the space-time coordinates and the spin index σ. In the Matsubara formalism it is

$$X = (\boldsymbol{r}, \tau, \sigma) \tag{2.4}$$

where τ is the imaginary time which varies in the interval $0 \leq \tau \leq \hbar\beta = \hbar/k_{\mathrm{B}}T$. Furthermore we assume the sum convention which means that whenever an index X appears twice, the "sum" over X is taken, defined by

$$\sum_X = \hbar^{-1} \int_0^{\hbar\beta} \mathrm{d}\tau \int \mathrm{d}^d r \sum_\sigma \,. \tag{2.5}$$

In (2.3) by $T[\cdots]$ we understand the usual time ordered product of the field operators with respect to τ. The one-particle Green's function (2.3) describes the properties of the one-particle excitations: it yields the distribution function $n(\boldsymbol{k})$ of bosons or fermions and the spectrum $A(\boldsymbol{k}, \varepsilon)$ of the one-particle excitations with wave vector $\boldsymbol{k}$ and energy ε.

The averages or traces in (2.1)-(2.3) are evaluated perturbatively. The Hamiltonian $H = H_0 + V$ is decomposed into a free Hamiltonian H_0 which describes the noninteracting system and an interaction part V which usually is a two-particle interaction with a potential. Analogously we decompose $K = K_0 + V$. Defining the S matrix

$$S = T \exp\Big\{-\hbar^{-1} \int_0^{\hbar\beta} \mathrm{d}\tau \, V(\tau)\Big\} \tag{2.6}$$

where $V(\tau) = \mathrm{e}^{K_0\tau/\hbar} V \mathrm{e}^{-K_0\tau/\hbar}$ the exponential factor in (2.1) and (2.2) can be rewritten as $\mathrm{e}^{-\beta K} = \mathrm{e}^{-\beta K_0} S$ (Abrikosov, Gorkov, and Dzyaloshinskii 1963, Fetter and Walecka 1971). Thus, we can rewrite the partition function as

$$Z = Z_0 \langle T \exp\Big\{-\hbar^{-1} \int_0^{\hbar\beta} \mathrm{d}\tau\, V(\tau)\Big\}\rangle_0 \tag{2.7}$$

where $\langle \cdots \rangle_0 = Z_0^{-1} \mathrm{Tr}\{\cdots \mathrm{e}^{-\beta K_0}\}$ is the average and $Z_0 = \mathrm{Tr}\{\mathrm{e}^{-\beta K_0}\}$ the partition function of the noninteracting system. The perturbation series expansion is generated by expanding the S matrix in powers of the interaction $V(\tau)$ and evaluating the averages $\langle \cdots \rangle_0$ by the Wick theorem, which implies a very economical identification of the terms of the perturbation series in terms of Feynman diagrams (Abrikosov, Gorkov, and Dzyaloshinskii 1963, Fetter and Walecka 1971). The perturbation series of the one-particle Green's function (2.3) is generated in an analogous manner.

2.1 Legendre transformation

By the way described above we obtain the bare perturbation series. This means that in the Feynman diagrams the propagator lines are identified by the free Green's function $G_{0,XX'}$ (of the noninteracting system). To obtain the self-consistent quantum-field theory we will perform several partial resummations of the Feynman diagrams so that we obtain a perturbation series in terms of a smaller number of *irreducible* or *skeleton* diagrams for which the propagator lines are identified by the exact or dressed Green's function $G_{XX'}$ defined by (2.3).

Following De Dominicis and Martin (1964) the resummation can be performed by Legendre transformations. To do this we introduce an external field $A_{XX'}$ so that the generalized partition function $Z[A]$ generates the Green's function $G_{XX'}$ by a functional derivative. Later the Legendre transformation from $A_{XX'}$ to $G_{XX'}$ as the explicit variable will be performed. The appropriate partition function is defined by

$$Z[A] = Z \langle T \exp\{\Psi_X^+ A_{XX'} \Psi_{X'}\}\rangle \tag{2.8}$$

so that

$$\frac{\delta Z[A]}{\delta A_{XX'}}\Big|_{A=0} = Z\langle T[\Psi_X^+ \Psi_{X'}]\rangle = \pm Z\langle T[\Psi_{X'} \Psi_X^+]\rangle = \pm Z G_{X'X} \tag{2.9}$$

Since in this chapter we consider bosons and fermions, the upper sign (+) is related to the bosonic case and the lower sign (−) to the fermionic case. We use this convention throughout this chapter. The structure of the partition function (2.8) is quite similar to that of (2.7). The external field $A_{XX'}$ is treated as perturbation while the average $\langle \cdots \rangle$ and Z are evaluated with the

statistical operator $\mathrm{e}^{-\beta K}$. By applying the coherent state representation of the boson or fermion fields, it is possible to cast (2.7) and (2.8) into nice functional integrals which generate the perturbation series in an alternative and very lucid way compared to the operator formalism (Negele and Orland 1988).

It is not necessary to set $A_{XX'} = 0$ in (2.9) so that we may define a generalized Green's function $G_{XX'}$ which depends on $A_{XX'}$. To abolish the normalization factor on the right-hand side of (2.9) it is useful to define the "free energy"

$$F[A] = -\ln Z[A] \tag{2.10}$$

so that the A dependent Green's function G is obtained from the first variation

$$\delta F[A] = \mp G_{X'X} \delta A_{XX'} \ . \tag{2.11}$$

Now, we perform the Legendre transformation from $A_{XX'}$ to $G_{XX'}$ as explicit variable by defining the "enthalpy"

$$H[G] = F[A] \pm G_{X'X} A_{XX'} \ , \tag{2.12}$$

so that $A_{XX'}$ is obtained by the functional derivative of $H[G]$ or

$$\delta H[G] = \pm A_{X'X} \delta G_{XX'} \ . \tag{2.13}$$

First we consider the noninteracting system. In this case the partition function $Z_0[A]$ can be evaluated easily. To do this we represent $Z_0[A]$ in terms of a functional integral. Since in (2.8) the external field $A_{XX'}$ couples quadratically to the boson or fermion field operators the functional integral is Gaussian and can be evaluated exactly. As a result we obtain the determinant

$$Z_0[A] = [\det(G_0^{-1} - A)]^{\mp 1} = \exp\{\mp \mathrm{Tr} \ln(G_0^{-1} - A)\} \tag{2.14}$$

where $G_{0,XX'}$ is the free Green's function. Here we have applied a further shorthand notation by considering G_0^{-1} and A as matrices and omitting the indices X and X'. The determinant and the trace are defined appropriately. For $A = 0$ we obtain

$$\begin{aligned} Z_0 &= \exp\{\mp \mathrm{Tr} \ln G_0^{-1}\} = \exp\{\mp \lim_{\tau \to -0} \sum_{\boldsymbol{k}} \sum_{\omega_n} \mathrm{e}^{-\mathrm{i}\omega_n \tau} \ln G_0^{-1}(\boldsymbol{k}, \omega_n)\} \\ &= \exp\{\mp \sum_{\boldsymbol{k}} \ln(1 \mp \mathrm{e}^{-\beta(\varepsilon_{\boldsymbol{k}} - \mu)})\} = \prod_{\boldsymbol{k}} (1 \mp \mathrm{e}^{-\beta(\varepsilon_{\boldsymbol{k}} - \mu)})^{\mp 1} \end{aligned} \tag{2.15}$$

which is indeed the partition function of a free boson or fermion gas. Here we have inserted the inverse free Green's function $G_0^{-1}(\boldsymbol{k}, \omega_n) = -\mathrm{i}\hbar\omega_n + \varepsilon_{\boldsymbol{k}} - \mu$ depending on the wave vector $\boldsymbol{k}$ and the Matsubara frequency ω_n. Now, taking the logarithm of (2.14) we obtain the "free energy"

$$F_0[A] = \pm \mathrm{Tr} \ln(G_0^{-1} - A) \ . \tag{2.16}$$

Performing a functional derivative according to (2.11) we obtain the dressed Green's function $G^{-1} = G_0^{-1} - A$. Then, inserting (2.16) into (2.12) and replacing $A = G_0^{-1} - G^{-1}$ we obtain the "enthalpy" of the noninteracting system

$$H_0[G] = \pm \mathrm{Tr}\{-\ln G + [G_0^{-1}G - 1]\} \tag{2.17}$$

and its first variation

$$\delta H_0[G] = \mp \mathrm{Tr}\{(G^{-1} - G_0^{-1})\delta G\} \; . \tag{2.18}$$

For the interacting many-particle system we write the "enthalpy" in the form

$$H[G] = H_0[G] - \Phi[G] \tag{2.19}$$

where $H_0[G]$ is given by (2.17) and $\Phi[G]$ contains all terms due to the interaction. In the next section we determine $\Phi[G]$ as a perturbation series of irreducible skeleton diagrams. We define the self energy $\Sigma_{XX'}$ by the functional derivative

$$\Sigma_{X'X} = \pm \delta\Phi[G]/\delta G_{XX'} \tag{2.20}$$

so that $\delta\Phi[G] = \pm \mathrm{Tr}\{\Sigma\delta G\} = \pm\Sigma_{X'X}\delta G_{XX'}$. Then we obtain the first variation of the "enthalpy"

$$\delta H[G] = \mp \mathrm{Tr}\{(G^{-1} - G_0^{-1} + \Sigma)\delta G\} = \pm \mathrm{Tr}\{A\delta G\} \; . \tag{2.21}$$

The external field $A_{XX'}$ is an auxiliary quantity to perform the Legendre transformation. In a real physical system it is $A_{XX'} = 0$, so that the physical Green's function $G_{XX'}$ is determined by the condition

$$\frac{\delta H[G]}{\delta G_{X'X}} = \mp(G^{-1}_{XX'} - G^{-1}_{0,XX'} + \Sigma_{XX'}) = 0 \; . \tag{2.22}$$

Actually, Eq. (2.22) is the necessary condition for an extremum of the "enthalpy" $H[G]$. In standard thermodynamics this extremum is usually a minimum. However, in the present case the "enthalpy" $H[G]$ is determined by the Matsubara theory which includes the imaginary time τ and thus contains dynamical terms. Thus, the extremization condition must be weakened, the extremum of $H[G]$ is only a saddle point so that only the necessary condition (2.22) holds true (De Dominicis and Martin 1964).

In quantum-field theory (2.22) is well known as the Dyson equation which usually is written as

$$G^{-1}_{XX'} = G^{-1}_{0,XX'} - \Sigma_{XX'} \; . \tag{2.23}$$

The Dyson equation (2.23) together with the self energy (2.20) forms a set of *self-consistent* equations to determine the Green's function $G_{XX'}$, because the self energy is a functional of the exact Green's function $G_{XX'}$. To summarize, the self-consistent quantum-field theory works as follows: one writes down a thermodynamic potential $H[G]$ given by (2.19) and (2.17) which is

a functional of the exact $G_{XX'}$. The Green's function $G_{XX'}$ is determined by the necessary condition (2.22) which is equivalent to the Dyson equation and which is a self-consistent equation. Finally, the grand-canonical thermodynamic potential $\Omega(T,\mu)$ is obtained by

$$\Omega(T,\mu) = -k_B T \ln Z = k_B T F[0] = k_B T \,\mathrm{extr}\{H[G]\} \tag{2.24}$$

where "extr" means extremum (in the sense of a saddle point) with respect to G.

2.2 Perturbation series expansion

For explicit calculations and practical applications of the self-consistent quantum-field theory we need to know the explicit form of the "enthalpy" functional $H[G]$. While in (2.19) the first contribution is given by the free functional (2.17), the remaining terms in $\Phi[G]$ are given by a perturbation series which we will determine below. The functional $H[G]$ and the perturbation series of $\Phi[G]$ have been first proposed by Luttinger and Ward (1960).

We start with the partition function $Z[A]$ and perform the resummation of the perturbation series in three steps. The perturbation series of $Z[A]$ is generated by expanding the S matrix in powers of the interaction and evaluating the averages by the Wick theorem. We find as usual

$$Z[A] = Z_0[A]\,\{1 + \text{sum of all vacuum diagrams}\}\ . \tag{2.25}$$

The diagrams may consist of several parts that are disconnected from each other. In a first step we take the logarithm $F[A] = -\ln Z[A]$. As a consequence of the so called *linked cluster theorem* the perturbation series is reduced to the subclass of connected diagrams. For the "free-energy" functional we obtain

$$F[A] = F_0[A] - \{\text{sum of all connected vacuum diagrams}\}\ . \tag{2.26}$$

Since the number of diagrams has reduced, a first resummation of the perturbation series has been achieved. More details of this resummation and the linked cluster theorem are found in chapter 5 of Amit (1978).

The explicit form of the Feynman diagrams depends on the physical system that is considered. For boson or fermion systems with a two-particle interaction the diagrams consist of elements that are shown in Fig. 2.1. The propagator line (Fig. 2.1a) is identified by the free Green's function $G_0^A = (G_0^{-1} - A)^{-1}$. Since in (2.8) the external field A couples quadratically to the field operator, A must be incorporated into the free Green's function G_0^A. The dashed interaction line (Fig. 2.1b) is identified by minus the two-particle interaction potential $-V_{XX'}$. The dashed lines are attached to the propagator lines by three vertices as shown in Fig. 2.1c. Finally, for each three

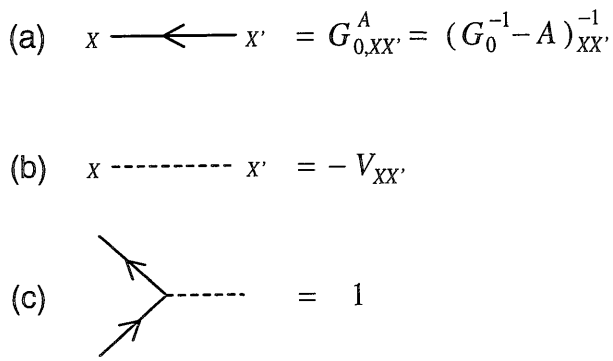

Fig. 2.1. The elements of the Feynman diagrams for interacting bosons or fermions: (a) propagator line, (b) dashed interaction line (interaction via two-particle potential $V_{XX'}$), and (c) three vertex.

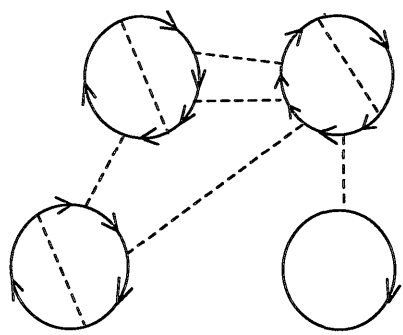

Fig. 2.2. A typical diagram of the free energy (2.26). It consists of a certain number of propagator loops that are connected with each other by dashed interaction lines. All parts of the diagram must be connected with each other.

vertex we must perform a summation over X as defined in (2.5). The diagrams of the perturbation series are constructed from the elements of Fig. 2.1 in all possible ways where some topological restrictions as e.g. "connected" must be satisfied. We assume that the averages of the field operators are zero, $\langle \Psi_X \rangle = 0$ and $\langle \Psi_X^+ \rangle = 0$. This requirement is satisfied for all Fermi systems and for normal fluid Bose liquids. Then the vacuum diagrams consist of a certain number of closed propagator loops (loops of full lines) which are connected with each other by dashed interaction lines in any possible way. A typical diagram of the "free energy" (2.26) is shown in Fig. 2.2. The dashed lines may be attached with their two ends to two different loops or to the same loop.

The one-particle Green's function $G_{XX'}$ is obtained by the functional derivative $\delta F[A]/\delta A_{X'X} = \mp G_{XX'}$. This means that in the diagrams of $F[A]$ one of the propagator loops is opened by cutting a full line. Thus, a typical

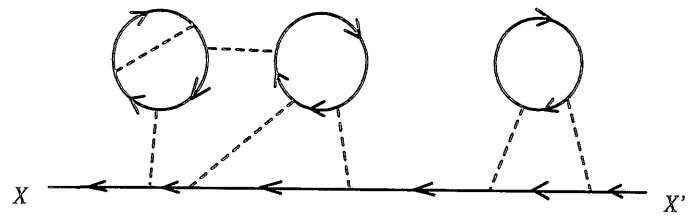

Fig. 2.3. A typical diagram of the one-particle Green's function $G_{XX'}$. It consists of an open propagator line from X' to X and a certain number of propagator loops that are connected with each other by dashed interaction lines. All parts of the diagram must be connected with each other.

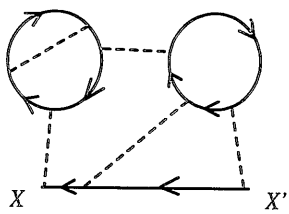

Fig. 2.4. A typical diagram of the self energy $\Sigma_{XX'}$. It consists of an open propagator line from X' to X and a certain number of propagator loops that are connected with each other by dashed interaction lines. The diagram is connected and one-particle irreducible. The external lines are amputated.

diagram of the Green's function looks like as shown in Fig. 2.3. It consists of one open propagator line that connects the points X and X' and of a certain number of propagator loops. The loops and the open propagator line are connected with each other by dashed lines in any possible way. The diagrams are "connected" so that there may not be disconnected parts.

In a second step a resummation is performed that reduces the perturbation series to the so called *one-particle irreducible diagrams*. Diagrams, that fall into two disconnected pieces if a propagator line is cut, are called one-particle reducible. Otherwise the diagrams are one-particle irreducible. A closed propagator loop never falls into pieces if it is cut. For this reason the diagrams of $F[A]$ for Fermi liquids and normal fluid Bose liquids as this one in Fig. 2.2 are already one-particle irreducible. On the other hand the diagrams of the one-particle Green's function need not be one-particle irreducible as it is clearly seen in Fig. 2.3: this diagram falls into two pieces if the open propagator line is cut at a certain position. However, the diagrams can be classified and regrouped so that the Green's function can be written as the series

$$G = G_0^A + G_0^A \Sigma G_0^A + G_0^A \Sigma G_0^A \Sigma G_0^A + \cdots \tag{2.27}$$

where Σ is the self energy which consists of one-particle irreducible diagrams with amputated external lines. The series (2.27) can be resummed as a geometrical series and thus yields the Dyson equation

$$G^{-1} = (G_0^A)^{-1} - \Sigma = G^{-1} - \Sigma - A \,. \tag{2.28}$$

A typical one-particle irreducible self-energy diagram is shown in Fig. 2.4.

In the third step we perform a resummation over self-energy subdiagrams, which formally is done by the Legendre transformation described above. To demonstrate how this resummation works we consider the diagrams of the self energy $\Sigma_{XX'}$ up to second order which are shown in Fig. 2.5a. The first two diagrams are first-order diagrams. In the next four second-order diagrams one clearly sees that the first two diagrams appear as subdiagrams. The last two diagrams do not contain self-energy subdiagrams. Thus, there are four second-order diagrams that contain self-energy subdiagrams. Now, we take only the *skeleton diagrams*, i.e. these diagrams which do not contain self-energy subdiagrams, and draw the propagator lines thick. In Fig. 2.5b the skeleton diagrams of the self energy are shown up to second order. The thick propagator lines are identified by the exact Green's function $G_{XX'}$ as shown in Fig. 2.5c. Inserting the series (2.27) for $G_{XX'}$ one can show order by order in perturbation theory that this procedure corresponds to the resummation of all self-energy subdiagrams. Thus, the first diagram in Fig. 2.5b corresponds

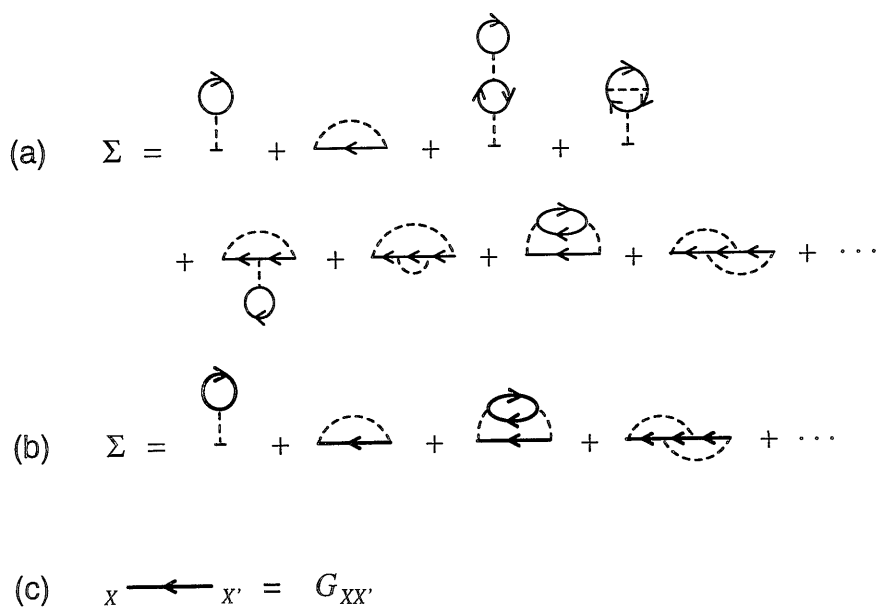

Fig. 2.5. The self energy (a) in terms of bare Feynman diagrams up to second order and (b) in terms of skeleton diagrams with thick propagator lines. (c) Thick propagator lines are identified by the exact Green's function $G_{XX'}$.

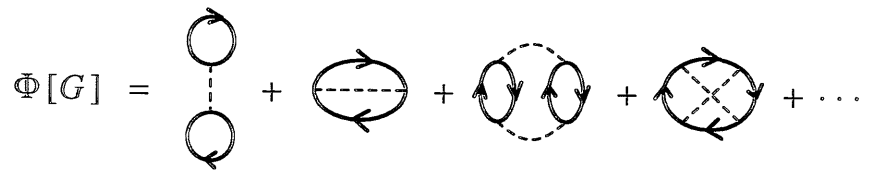

Fig. 2.6. The vacuum skeleton diagrams with thick propagator lines of $\Phi[G]$ up to second order.

up to second order to the sum of the first, third, and fourth diagram in Fig. 2.5a. The second diagram in Fig. 2.5b corresponds to the sum of the second, fifth, and sixth diagram in Fig. 2.5a. The last two diagrams in Fig. 2.5b correspond to the last two diagrams in Fig. 2.5a.

Thus, by the resummation of the self-energy subdiagrams we obtain the self energy Σ as a functional of the exact Green's function G where the perturbation series of Σ is given by the sum of all skeleton diagrams with thick propagator lines. The skeleton diagrams are irreducible in the sense that they do not contain self-energy subdiagrams. This irreducibility may be formulated more precisely by the topological requirement that the diagrams may not fall into pieces if the propagator lines are cut twice at any two points. (By this formulation it is clear that skeleton diagrams are automatically also one-particle irreducible.) On the other hand in the previous section we have formally shown by the Legendre transformation that the self energy $\Sigma_{XX'}$ is the functional derivative (2.20) of a functional $\Phi[G]$. We find the perturbation series of $\Phi[G]$ by comparing (2.20) diagram by diagram with the perturbation series of skeleton diagrams of the self energy Σ. Up to second order the functional $\Phi[G]$ is given by the vacuum skeleton diagrams shown in Fig. 2.6 which correspond to the self energy skeleton diagrams in Fig. 2.5b. The full perturbation series of $\Phi[G]$ is given by (Luttinger and Ward 1960, De Dominicis and Martin 1964)

$$\Phi[G] = \left\{ \begin{array}{c} \text{sum of all vacuum skeleton diagrams} \\ \text{with thick propagator lines identified by } G \end{array} \right\} \tag{2.29}$$

where the vacuum skeleton diagrams are irreducible vacuum diagrams that do not fall into pieces if the propagator lines are cut twice at any two points. Thus, by (2.19), (2.17), and (2.29) we now have the perturbation series of the "enthalpy functional" $H[G]$ in terms of vacuum skeleton diagrams, which may be taken as the starting point of the self-consistent quantum-field theory to derive approximations and to perform explicit calculations.

The resummation procedure can be generalized and performed also for superfluid Bose systems. Following De Dominicis and Martin (1964) one introduces additionally the external field h_X which couples linearly to Ψ_X. Then the "free energy" $F[h, A]$ is a functional of h_X and $A_{XX'}$. The resummation leading to one-particle irreducible diagrams is performed by the Legendre

transformation from h_X to $\langle\Psi_X\rangle$. The resulting functional $\Gamma[\langle\Psi\rangle, A]$ is the so called *generating functional of the vertex functions* (see chapter 5 in Amit 1978). Later, the functional $H[\langle\Psi\rangle, G]$ is obtained by the Legendre transformation from $A_{XX'}$ to $G_{XX'}$. It is possible to achieve further resummations by introducing external fields that couple to higher order products of the operators Ψ_X and Ψ_X^+ and performing the respective Legendre transformations. In this way one obtains functionals which depend additionally on higher-order Green's functions as e.g. the two-particle Green's function (De Dominicis and Martin 1964).

2.3 Conserving approximations

Since the functional $\Phi[G]$ is given by an infinite perturbation series (2.29), for practical calculations of the Green's function $G_{XX'}$ it is necessary to make approximations which can be handled. The most natural approximations of the self-consistent quantum-field theory are obtained by truncating the perturbation series of $\Phi[G]$ so that either a finite number of diagrams is taken or an infinite subclass of diagrams is resummed exactly. Approximations of this kind are the so called *conserving approximations* which have been first considered by Baym and Kadanoff (1961) and Baym (1962). Because, whenever the self energy $\Sigma_{XX'}$ can be written as the functional derivative (2.20) of a functional $\Phi[G]$, the approximation satisfies certain conservation laws if $\Phi[G]$ possesses the respective symmetries. Thus, if $\Phi[G] = \Phi[\tilde{G}]$ is invariant under the local gauge transformation $\tilde{G}_{XX'} = \mathrm{e}^{\mathrm{i}\Lambda_X} G_{XX'} \mathrm{e}^{-\mathrm{i}\Lambda_{X'}}$, then the particle number is conserved locally, i.e. the continuity equation for the average particle density $\langle\varrho\rangle$ and the average current $\langle\boldsymbol{j}\rangle$ is valid,

$$\partial_t\langle\varrho\rangle + \boldsymbol{\nabla}\langle\boldsymbol{j}\rangle = 0\,. \tag{2.30}$$

Furthermore, if the functional $\Phi[G]$ is invariant under spatial and time translations, the total momentum and total energy are conserved, respectively (Baym and Kadanoff 1961, Baym 1962).

On the other hand for Fermi systems the conserving approximations satisfy the Luttinger theorem which states (Luttinger 1960) that the volume enclosed by the Fermi surface in $\boldsymbol{k}$ space is not affected by the interaction but only depends on the particle density. The proof of the Luttinger theorem is based on the representation of the self energy $\Sigma_{XX'}$ in terms of the functional derivative (2.20) and on certain analyticity properties of the spectral function of the self energy close to the Fermi energy, where for a truncated perturbation series the analyticity properties are always guaranteed (Luttinger 1961).

We briefly describe the three most popular examples of conserving approximations which have been considered by Baym and Kadanoff (1961) and which we will use in the following chapters. As the simplest example, the

quantum-field theoretic version of the Hartree–Fock approximation is obtained by taking only the first two diagrams of $\Phi[G]$ in Fig. 2.6 or the self energy Σ in Fig. 2.5b, respectively. The first diagram is called the *Hartree diagram*, and the second diagram is called the *Fock diagram.* For electrons with Coulomb interaction the contribution of $H[G]$ due to the Hartree diagram is the electrostatic energy implied by the average charge density $-e\langle\varrho\rangle$ of the negatively charged electrons. The positively charged background of the ions which neutralizes the system implies that the contribution of the Hartree diagram is canceled at least partially. In the case of a homogeneous positively charged background as for the *jellium model* the cancellation is complete so that the Hartree diagram may be omitted.

An approximation which incorporates the screening of the long-range Coulomb interaction is given by the sum of the ring diagrams shown in Fig. 2.7a. The Hartree diagram is omitted for the above reason. The self energy Σ is represented by a Fock diagram shown in Fig. 2.7b where the thick dashed line is identified by minus the effective screened interaction $U_{\text{eff},XX'}$. The analytical expression of the self energy is

$$\Sigma_{XX'} = -U_{\text{eff},XX'} G_{XX'} \tag{2.31}$$

(where here it is not summed over X or X', i.e. no sum convention). The effective screened interaction U_{eff} is given by the series of bubble diagrams shown in Fig. 2.7c. This series can be resummed as a geometric series so that

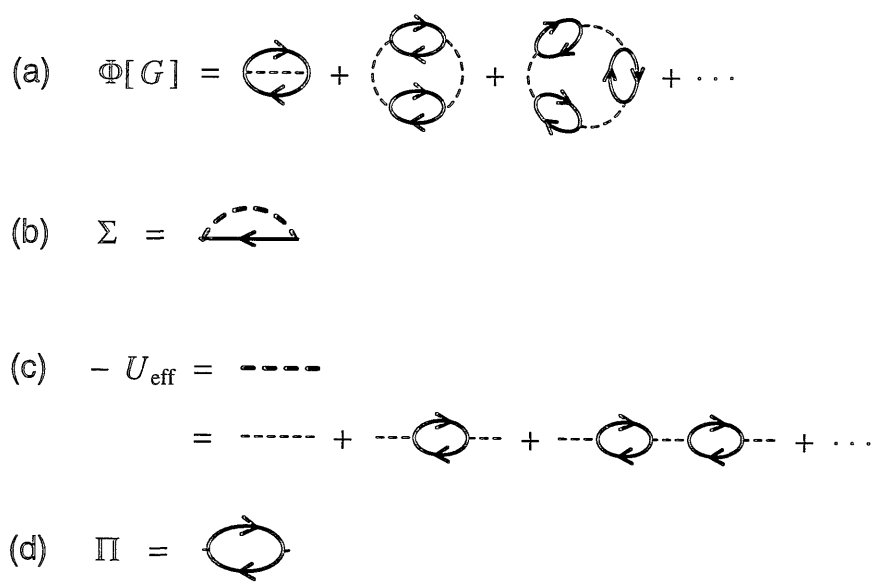

Fig. 2.7. The diagrams of the self-consistent RPA for (a) the functional $\Phi[G]$, (b) the self energy Σ, (c) the effective screened interaction U_{eff}, and (d) the polarization function Π.

$$U^{-1}_{\mathrm{eff},XX'} = V^{-1}_{XX'} + \Pi_{XX'} \,, \tag{2.32}$$

where $\Pi_{XX'}$ is the polarization function given by the bubble diagram shown in Fig. 2.7d or explicitly by

$$\Pi_{XX'} = \pm G_{XX'} G_{X'X} \tag{2.33}$$

(where again it is not summed over X or X', no sum convention). The Dyson equation (2.23) together with (2.31)-(2.33) form a set of self-consistent equations which can be solved iteratively to determine the Green's function $G_{XX'}$. For homogeneous systems this can be done numerically involving Fourier transformations with not too great effort. The approximation based on these four equations and the diagrams of Fig. 2.7 is a self-consistent version of the so called random-phase approximation or RPA (see e.g. Fetter and Walecka 1971). We will call it the self-consistent RPA or shortly SC-RPA.

For dilute systems of bosons or fermions with a short-range interaction we may use an approximation based on ladder diagrams shown in Fig. 2.8. The two classes of diagrams involved in the infinite series reflect the sym-

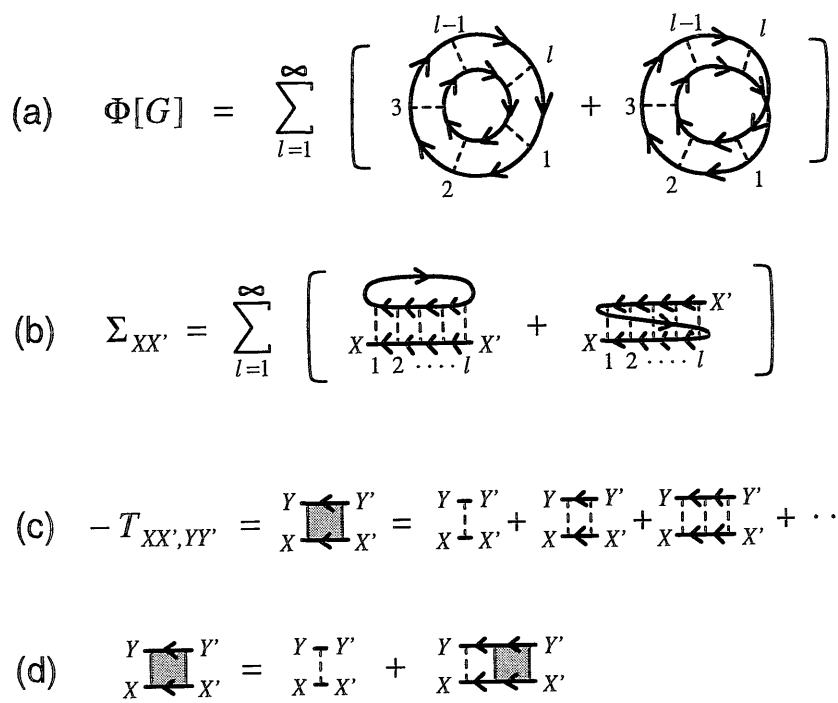

Fig. 2.8. The diagrams of the self-consistent ladder approximation for (a) the functional $\Phi[G]$ and (b) the self energy Σ. The infinite series of ladder diagrams (c) is identified by minus the scattering matrix T. The Bethe–Salpeter equation (d) is obtained by resumming the series.

metrization or antisymmetrization for bosons or fermions. This approximation treats two-particle collisions correctly. The series of ladder diagrams shown in Fig. 2.8c may be interpreted as the effective scattering matrix T of two particles scattering each other in a medium of particles with a finite density $\langle\varrho\rangle$. The series of ladder diagrams can be resummed so that an integral equation for T is obtained which is shown in Fig. 2.8d in terms of Feynman diagrams. This integral equation is the Bethe–Salpeter equation in self-consistent ladder approximation. From the Dyson equation Kadanoff and Baym (1962) have derived quantum kinetic equations to describe nonequilibrium phenomena in quantum systems. In the dilute limit $\langle\varrho\rangle \to 0$ it is possible do derive the Boltzmann equation for the dilute quantum gas, where the collision integral arises from the ladder diagrams of Fig. 2.8a and includes the two-particle collisions correctly with the exact scattering cross section. For a dilute classical gas where $n(\boldsymbol{k}) \ll 1$ it can be shown that for $\Phi[G]$ up to second order in $\langle\varrho\rangle$ the diagrams shown in Fig. 2.8a are all that must be included. The Bethe–Salpeter equation is known to describe the formation of bound pairs in quantum-field theory if the interaction V is attractive (see e.g. Itzykson and Zuber 1980). The T matrix obtained as a solution of the Bethe–Salpeter equation has poles at the energies of the bound-pair states. Thus, the self-consistent ladder approximation defined by the diagrams in Fig. 2.8 is well suited to describe quantum liquids with attractive interaction between the particles which may cause the formation of bound pairs. In Chap. 3 we will generalize this approximation for superfluid Fermi systems to describe the crossover from BCS superconductivity to Bose–Einstein condensation of strongly bound pairs.

For nonequilibrium processes described by quantum kinetic equations the conservation laws are essential. Especially the number of particles should not change with time. However, the conservation laws are also essential for systems in thermal equilibrium. Because, the equilibrium state of an interacting system may emerge from the equilibrium state of the noninteracting system by adiabatic switching on of the interaction. It would be fatal for an approximation, if the particle number would change during this process. Thus, the conserving approximations are well behaving with respect to this aspect.

2.4 Two-particle functions and Ward identities

The two-particle Green's function

$$G^{(2)}_{XX',YY'} = \langle T[\Psi_X \Psi_Y \Psi^+_{Y'} \Psi^+_{X'}] \rangle \tag{2.34}$$

is generated by the second functional derivative of the partition function $Z[A]$ which is

$$\frac{\delta^2 Z[A]}{\delta A_{XX'} \delta A_{YY'}} = Z[A]\, G^{(2)}_{X'X,Y'Y} \ . \tag{2.35}$$

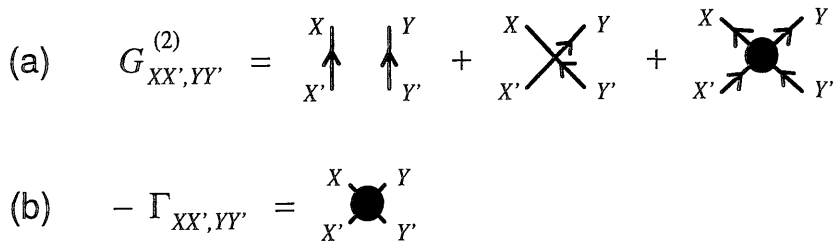

Fig. 2.9. (a) the two-particle Green's function $G^{(2)}$ expressed in terms of the vertex function Γ, (b) diagrammatical identification of the vertex function.

By inserting (2.25) the perturbation series of $G^{(2)}_{XX',YY'}$ in terms of Feynman diagrams is obtained. The possibility to separate the factor $Z[A]$ on the right-hand side of (2.35) is due to the so called cancellation of vacuum diagrams (see e.g. Amit 1978). The diagrams of the two-particle Green's function $G^{(2)}_{XX',YY'}$ can be divided into classes so that subdiagrams can be resummed partially. Thus, by

$$G^{(2)}_{XX',YY'} = G_{XX'}G_{YY'} \pm G_{XY'}G_{YX'} - G_{XU}G_{U'X'}\Gamma_{UU',WW'}G_{YW}G_{W'Y'} \tag{2.36}$$

we can express the two-particle Green's function in terms of the vertex function $\Gamma_{XX',YY'}$ which is given by a series of one-particle irreducible diagrams with four amputated external lines. In Fig. 2.9a the equation (2.36) is shown diagrammatically where the thick propagator lines represent the exact one-particle Green's function G and the black filled circle represents minus the vertex function Γ as shown in Fig. 2.9b. Equation (2.36) can be derived by the Legendre transformation from h_X to $\langle\Psi_X\rangle$ which leads to the generating functional of the vertex functions $\Gamma[\langle\Psi\rangle, A]$ given by the series of one-particle irreducible diagrams (see chapter 5 in Amit 1978). For convenience of the notation we introduce the pair propagator

$$\chi_{XX',YY'} = \pm G_{XY'}G_{YX'} \tag{2.37}$$

so that Eq. (2.36) can be written in the form

$$G^{(2)}_{XX',Y'Y} = G_{XX'}G_{Y'Y} + \chi_{XX',Y'Y} - \chi_{XX',U'U}\Gamma_{UU',W'W}\chi_{WW',Y'Y} \,. \tag{2.38}$$

The vertex function $\Gamma_{XX',YY'}$ may be expanded in terms of an irreducible vertex function $\Gamma_{1,XX',YY'}$ as shown diagrammatically in Fig. 2.10a (see e.g. Abrikosov, Gorkov, and Dzyaloshinskii 1963). Here, the irreducible vertex function $\Gamma_{1,XX',YY'}$ is represented by a grey filled circle as shown in Fig. 2.10b and is given by the series of a subset of vertex diagrams which are irreducible in the sense that they do not fall into pieces with X and X' disconnected from Y and Y' if any two propagator lines are cut. Thus, the vertex function can be written as the series

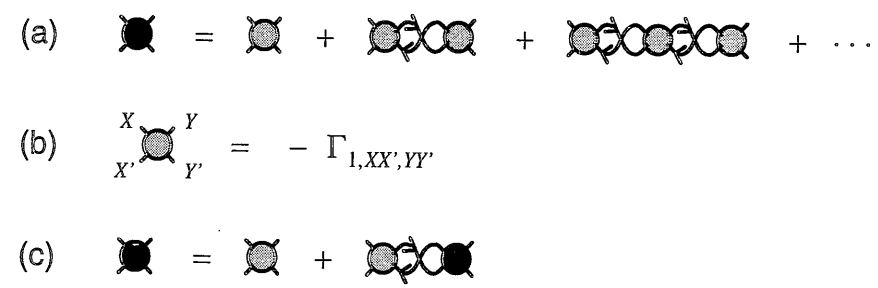

Fig. 2.10. (a) expansion of the vertex function Γ in terms of the irreducible vertex function Γ_1, (b) diagrammatical identification of the irreducible vertex function, and (c) diagrammatical representation of the integral equation (2.40).

$$\Gamma_{XX',Y'Y} = \Gamma_{1,XX',Y'Y} - \Gamma_{1,XX',U'U}\chi_{UU',W'W}\Gamma_{1,WW',Y'Y} + \Gamma_{1,XX',U'U}\chi_{UU',V'V}\Gamma_{1,VV',W'W}\chi_{WW',Z'Z}\Gamma_{1,ZZ',Y'Y} - \cdots . \quad (2.39)$$

This series can be resummed so that we obtain the integral equation

$$\Gamma_{XX',Y'Y} = \Gamma_{1,XX',Y'Y} - \Gamma_{1,XX',U'U}\chi_{UU',W'W}\Gamma_{WW',Y'Y} \quad (2.40)$$

which is shown diagrammatically in Fig. 2.10c. One clearly sees that in a short-hand notation these two equations can be written as

$$\Gamma = \Gamma_1 - \Gamma_1\chi\Gamma_1 + \Gamma_1\chi\Gamma_1\chi\Gamma_1 - \cdots = \Gamma_1 - \Gamma_1\chi\Gamma . \quad (2.41)$$

Furthermore, after some manipulations we can write (2.40) in the equivalent forms

$$\Gamma^{-1} = \Gamma_1^{-1} + \chi , \quad (2.42)$$

$$\chi^{-1}\Gamma^{-1}\Gamma_1 = \chi^{-1} + \Gamma_1 , \quad (2.43)$$

$$\chi - \chi\Gamma\chi = [\chi^{-1} + \Gamma_1]^{-1} \quad (2.44)$$

where $\chi^{-1}_{XX',YY'} = \pm G^{-1}_{XY'}G^{-1}_{YX'}$.

The Jacobi matrix of the Legendre transformation from $A_{XX'}$ to $G_{XX'}$ is given by the functional derivative

$$\frac{\delta G_{XX'}}{\delta A_{YY'}} = \mp\frac{\delta^2 F[A]}{\delta A_{X'X}\delta A_{YY'}} \quad (2.45)$$

which is related to the second functional derivative of the "free energy" $F[A]$. Thus, the Jacobi matrix can be expressed in terms of the two-particle Green's function $G^{(2)}$ or in terms of the vertex function Γ as

$$\frac{\delta G_{XX'}}{\delta A_{YY'}} = \pm[G^{(2)}_{XX',Y'Y} - G_{XX'}G_{Y'Y}] = \pm[\chi_{XX',Y'Y} - \chi_{XX',U'U}\Gamma_{UU',W'W}\chi_{WW',Y'Y}] . \quad (2.46)$$

For the Legendre transformation to be well defined it is important that the Jacobi matrix is non singular so that it can be inverted. The inverse Jacobi matrix is given by the functional derivative

$$\frac{\delta A_{XX'}}{\delta G_{YY'}} = \pm \frac{\delta^2 H[G]}{\delta G_{X'X} \delta G_{YY'}} \tag{2.47}$$

which is related to the second functional derivative of the "enthalpy" $H[G]$. Since we identify the right-hand side of (2.46) by (2.44) we obtain the inverse Jacobi matrix

$$\frac{\delta A_{XX'}}{\delta G_{YY'}} = \pm [\chi^{-1}_{XX',Y'Y} + \Gamma_{1,XX',Y'Y}] \,. \tag{2.48}$$

From (2.20) we obtain the functional derivative of the self energy

$$\frac{\delta \Sigma_{XX'}}{\delta G_{YY'}} = \pm \frac{\delta^2 \Phi[G]}{\delta G_{X'X} \delta G_{YY'}} = \mp \Gamma_{1,XX',Y'Y} \,. \tag{2.49}$$

For the last equality sign we have inserted $\Phi[G] = H_0[G] - H[G]$. Thus, the variation of the self energy $\delta\Sigma$ is related to the variation of the Green's function δG by

$$\delta \Sigma_{XX'} = \mp \Gamma_{1,XX',Y'Y} \delta G_{YY'} \,. \tag{2.50}$$

While Γ_1 is usually finite, the vertex function Γ may have poles which are related to physical phenomena as sound, pair formation, superconductivity, or a Goldstone mode of a second-order phase transition. Singularities of the Jacobi matrix due to poles of the vertex function Γ are not problematic for the Legendre transformation because they exist only on a subset of measure zero of the index set.

Symmetries of the system and conservation laws imply relations between Green's functions and vertex functions which are called Ward identities (see e.g. Itzykson and Zuber 1980). These relations are derived exactly and hold true for all orders in perturbation theory. Thus, Ward identities are suitable to obtain results beyond perturbation theory. Let us consider a transformation which depends continuously on a parameter λ. We assume that the variation of the Green's function $\delta_\lambda G_{XX'}$ and the respective variation of the external field $\delta_\lambda A_{XX'}$ implied by the transformation can be determined explicitly. Then from (2.46) we obtain the relation

$$\delta_\lambda G_{XX'} = \pm [\chi_{XX',Y'Y} - \chi_{XX',U'U} \Gamma_{UU',W'W} \chi_{WW',Y'Y}] \, \delta_\lambda A_{YY'} \tag{2.51}$$

which can be transformed into

$$\delta_\lambda G^{-1}_{XX'} = -\delta_\lambda A_{XX'} + \Gamma_{XX',W'W} \chi_{WW',Y'Y} \, \delta_\lambda A_{YY'} \,. \tag{2.52}$$

By considering gauge transformations and Galilei transformations it is possible to derive four Ward identities from (2.51) or (2.52) which are useful to derive the basic relations of the Fermi liquid theory (Abrikosov, Gorkov,

and Dzyaloshinskii 1963, Landau and Lifshitz vol. 9). Furthermore, Ward identities have turned out to be useful tools for Luttinger liquids, i.e. one-dimensional Fermi systems (Sólyom 1979, Metzner and Di Castro 1993). The exact solution of the Luttinger model can be obtained by the use of Ward identities.

Ward identities can also be derived for systems with a spontaneously broken continuous symmetry related to a second-order phase transition to show the existence of massless Goldstone modes (see e.g. Amit 1978). The inverse relation

$$\delta_\lambda A^{-1}_{XX'} = \pm[\chi^{-1}_{XX',Y'Y} + \Gamma_{1,XX',Y'Y}]\,\delta_\lambda G_{YY'} \tag{2.53}$$

obtained from (2.48) can be used for this purpose. Inserting (2.43) for the square bracket and multiplying from the left by χ we cast (2.53) into

$$\pm\Gamma^{-1}_{XX',Y'Y}\Gamma_{1,YY',W'W}\,\delta_\lambda G_{WW'} = \chi_{XX',Y'Y}\,\delta_\lambda A_{YY'}\ . \tag{2.54}$$

Then, because of (2.50) we obtain a Ward identity for the variation of the self energy $\delta_\lambda \Sigma_{XX'}$ which reads

$$\Gamma^{-1}_{XX',Y'Y}\,\delta_\lambda \Sigma_{YY'} = -\chi_{XX',Y'Y}\,\delta_\lambda A_{YY'}\ . \tag{2.55}$$

Let us assume that the continuous transformation is a rotation in the order-parameter space so that $\delta_\lambda \Sigma_{XX'}$ is related directly to the order parameter. Supposed the system is invariant under this transformation so that $\delta_\lambda H[G] = 0$ for all G, then we obtain

$$\delta_\lambda A_{XX'} = \pm\frac{\delta}{\delta G_{X'X}}\big[\delta_\lambda H[G]\big] = 0\ . \tag{2.56}$$

Thus, we obtain the Ward identity

$$\Gamma^{-1}_{XX',Y'Y}\,\delta_\lambda \Sigma_{YY'} = 0\ . \tag{2.57}$$

Above the critical temperature T_c in the disordered phase the order parameter is zero and hence $\delta_\lambda \Sigma_{XX'} = 0$ so that (2.57) is satisfied trivially. Below T_c in the ordered phase $\delta_\lambda \Sigma_{XX'}$ is nonzero so that the inverse vertex function $\Gamma^{-1}_{XX',Y'Y}$ must possess a zero eigenvalue which implies the existence of massless Goldstone modes and which corresponds to a pole in the vertex function $\Gamma_{XX',Y'Y}$.

The Ward identity (2.57) has a direct application for superfluid Fermi systems as we will see in the next chapter. The global gauge transformation $\Psi_X \to \mathrm{e}^{\mathrm{i}\lambda}\Psi_X$ and $\Psi^+_X \to \mathrm{e}^{-\mathrm{i}\lambda}\Psi^+_X$ implies that $\delta_\lambda \Sigma_{XX'}$ is the natural choice for the order parameter. The consequence of the Ward identity (2.57) that the vertex function $\Gamma_{XX',YY'}$ has a pole below T_c is known as the Thouless criterion for superconductivity (Thouless 1960).

While the Ward identities are derived for the exact theory and hold true up to all orders in perturbation theory, they can be used also for approximations supposed the Green's functions and vertex functions are defined appropriately and in a consistent way. For the conserving approximations the Ward identity (2.57) can be derived from the functional $H[G] = H_0[G] - \Phi[G]$ where $\Phi[G]$ may be given by a truncated perturbation series. While the self energy $\Sigma_{XX'}$ and the irreducible vertex function are defined by the first and the second functional derivative of $\Phi[G]$, for the validity of the Ward identity (2.57) and the Thouless criterion it is very important to define the vertex function $\Gamma_{XX',YY'}$ by the integral equation (2.40) or equivalently by (2.42). Furthermore, for the conserving approximations it can be shown that density and current correlation functions, which are defined from the two-particle Green's function using this vertex function in (2.36), satisfy the continuity equation (Baym and Kadanoff 1961, Baym 1962).

3. Superconductivity and pairing of electrons in three dimensions

At low temperatures quantum liquids can become superfluid for both bosons and also for fermions where however the mechanisms are quite different. A Bose liquid as e.g. ^{4}He becomes superfluid due to Bose–Einstein condensation. This means that a macroscopic number of the bosons condenses into the zero momentum state. The average of the boson field operator $\langle \Psi(\boldsymbol{r}, t) \rangle$ becomes nonzero which reflects a macroscopic quantum coherence of the bosons in the condensate and which may be viewed as the order parameter of the superfluid transition. On the other hand Fermi systems become superfluid (as e.g. ^{3}He) or superconducting (electrons in a metal) if the interaction between the fermions is attractive. In this case the mechanism may be understood roughly as follows. Due to the attractive interaction the fermions form bound pairs which are bosons. These pairs condense into the zero momentum state and develop a macroscopic quantum coherence. Since the bosons consist of two fermions, the order parameter is the average of two fermion operators, i.e. $\langle \Psi_{\sigma_1}(\boldsymbol{r}_1, t_1) \Psi_{\sigma_2}(\boldsymbol{r}_2, t_2) \rangle$, which becomes nonzero below T_c.

However, usually the fermion pairs are not well defined particles because the interaction need not be very strong. The pairs may be large and penetrate each other. Cooper has shown (Cooper 1956) that in a weakly interacting Fermi gas already an infinitesimal small attractive interaction is sufficient for the formation of a bound pair. Based on this observation the Bardeen–Cooper–Schrieffer theory (BCS theory) of superconductivity has been developed (Bardeen, Cooper, and Schrieffer 1957, see also Schrieffer 1964). Already for an infinitesimal small attractive interaction a Fermi liquid becomes superfluid and bound pairs, the Cooper pairs, are formed, supposed the temperature is sufficiently small. On the other hand for a very strong attractive interaction the fermions are tightly bound into pairs, which are well defined bosons. These pairs may be small so that they form a dilute weakly interacting Bose gas which at low temperatures becomes superfluid via the Bose–Einstein condensation.

The BCS theory and the Bose–Einstein condensation of tightly bound fermion pairs may be viewed as the two limiting mechanisms of superfluidity in Fermi systems for weak and strong attractive interaction, respectively. The strength of the interaction can be characterized by the dimensionless quantity $k_F \xi$, where ξ is the diameter of the pairs and k_F^{-1} is the Fermi wave length

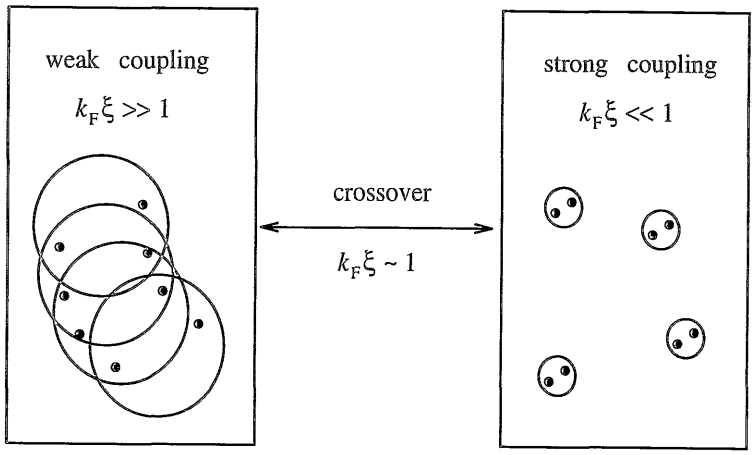

Fig. 3.1. The pairs for weak and strong coupling. ξ is the size of a pair and k_F^{-1} is the average distance between the fermions. For weak coupling, according to the BCS theory the Cooper pairs are very large and penetrate each other. For strong coupling the pairs are well defined bosons which are far away from each other.

which ist the average distance between the fermions. Hence $k_F\xi$ is the ratio of the pair size and the average fermion distance. For weak coupling in the regime where the BCS theory is valid it is $k_F\xi \gg 1$. The diameter of the Cooper pairs is much larger than the average distance between the fermions. Hence, the Cooper pairs are overlapping each other as it is shown in Fig. 3.1 on the left-hand side. On the other hand for strong coupling it is $k_F\xi \ll 1$. In this case the pairs are small, well defined bosons, and far away from each other, as it is shown in Fig. 3.1 on the right-hand side. In the intermediate regime where $k_F\xi \sim 1$ the crossover from BCS superconductivity to Bose–Einstein condensation of bound pairs happens.

The BCS theory has been remarkably successful for the conventional superconductors, i.e. metals and alloys, because the electron density is very high and the interaction is very weak. For these systems it is $k_F\xi \sim 10^4 - 10^5$. On the other hand for the high T_c superconductors as the copper oxides and more recently the n doped fullerites $k_F\xi \sim 10 - 20$ is comparatively small, which is due to the small electron density $n_F = k_F^3/3\pi^2$ of the doped systems and the small coherence length. Thus, the understanding of superconductivity for stronger couplings beyond the BCS theory and the crossover to Bose–Einstein condensation is of particular interest. In Fig. 3.2 the phase diagram of a three dimensional fermion system with attractive interaction between the particles from weak to strong coupling is shown. For weak coupling the system is a Fermi liquid with single fermions as the particles, while for strong coupling it is a Bose liquid of bound fermion pairs. These two regimes are separated by a region of *dissociation* shown as the shaded area in Fig. 3.2, where single fermions and bound pairs coexist. By thermody-

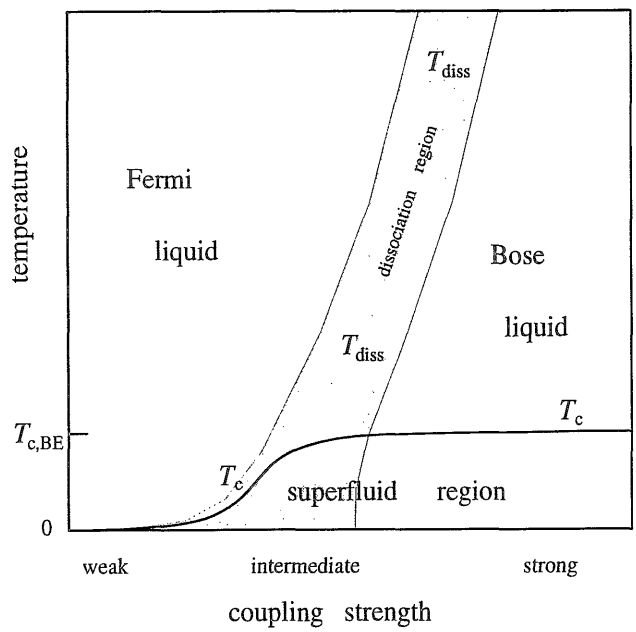

Fig. 3.2. Phase diagram of a Fermi system with attractive interaction: temperature versus coupling strength. While for weak coupling the system is a Fermi liquid, for strong coupling it is a Bose liquid of bound pairs, separated by the dissipation region (shaded area) where single fermions and bound pairs coexist. For low temperatures the system becomes superfluid. The critical temperature T_c is indicated by the full line.

namic arguments the temperature of dissociation T_{diss} can be estimated as $k_B T_{diss} = c \cdot \varepsilon_b$ where ε_b is the binding energy of the pairs and c is a factor of order unity. (For higher temperatures c is reduced logarithmically by entropic corrections.) Since the dissociation of pairs into single fermions happens on atomic scale, the transition is continuous so that T_{diss} is not sharply defined. Below a certain critical temperature T_c which is shown as full line in Fig. 3.2 the system becomes superfluid. Since in the strong-coupling limit the system is a weakly interacting Bose gas, in this limit the critical temperature is approximately the Bose–Einstein condensation temperature $T_{c,BE}$, which only depends on the density of bosons $n_B = n_F/2$ but not on the interaction between the fermions or bosons. For this reason, T_c is nearly constant for strong couplings as seen in Fig. 3.2, supposed the particle density is kept constant. On the other hand, the binding energy ε_b and hence the dissociation temperature T_{diss} strongly depend on the interaction strength. For strong couplings T_{diss} is much larger than T_c, i.e. $T_{diss} \gg T_c$. Now, if the coupling strength is reduced, T_{diss} decreases considerably while T_c remains nearly constant. In the crossover region T_{diss} will reach the same order of magnitude as T_c. If the coupling strength is reduced furthermore, the weak coupling regime is

reached where the BCS theory is valid and the superconducting transition is linked to the formation of Cooper pairs. The BCS theory predicts a critical temperature T_c which becomes exponentially small with decreasing coupling strength. In the crossover regime the full line shown in Fig. 3.2 is an interpolation of the critical temperature T_c as a function of the coupling strength between the exponentially small $T_{c,BCS}$ and the constant $T_{c,BE}$, which will be the subject of the investigations in this chapter.

The crossover problem has been first investigated by Leggett (1980) at zero temperature. Via a variational ansatz with a BCS trial wave function he derived two equations to determine the energy gap Δ and the chemical potential μ as functions of the coupling strength at $T = 0$ and for constant fermion density n_F. This variational ansatz has also been applied to the two-dimensional fermion system by Randeria et al. (1989 and 1990). Nozières and Schmitt-Rink (1985) have extended the theory to finite temperatures by using the many-particle quantum-field theory with temperature dependent Green's functions and the ladder approximation, but *without* self consistency. While this theory was designed for $T \geq T_c$, they determined the critical temperature T_c in the whole crossover region from weak to strong coupling by the Thouless criterion (Thouless 1960). A third approach is due to Drechsler and Zwerger (1992). Starting from a functional integral representation of the interacting fermion system Drechsler and Zwerger introduced the order parameter $\Delta(\mathbf{r}, \tau)$ via a Hubbard Stratonovich transformation. Integrating out the fermion degrees of freedom and expanding in powers of $\Delta(\mathbf{r}, \tau)$ they obtained a Ginzburg–Landau theory. Though this theory was originally designed for a two-dimensional system (Drechsler and Zwerger 1992), it has been extended also to three dimensions (Drechsler 1991, Stintzing 1996). Sá de Melo et al. (1993) have proposed a time-dependent Ginzburg–Landau theory, and in close analogy to Nozières and Schmitt-Rink (1985) they determined the superfluid transition temperature T_c as a function of the coupling strength.

All the above mentioned theories are based on an approximation scheme which is equivalent to a mean-field approximation and which uses free fermion Green's functions to take the fermionic degrees of freedom into account, while the bosonic properties lead to the superfluid transition. In the two limiting cases of weak and strong coupling this approximation is exact: while for weak coupling the BCS theory is recovered, for strong coupling an ideal Bose gas is found in $d = 3$ dimensions. The critical temperature T_c versus the coupling strength obtained by these theories looks qualitatively like the full line in Fig. 3.2. However, this T_c is not a monotonic increasing function in the coupling strength but rather has a small maximum in the crossover region. This maximum is an artifact of the approximation as we will show below. In the crossover region the approximation using free fermion Green's functions is invalid because the fermionic quasiparticles are rather short living and far from being free particles. For this reason the self-consistent quantum-field theory has turned out to be the proper approach (Haussmann 1993 and

1994a) because it is a perturbation theory in terms of the exact or dressed fermion Green's function so that the nontrivial spectrum of the short-living fermionic quasiparticles is taken into account in a natural way. Furthermore, the approximation of the above theories does not include the repulsive interaction between the noncondensed bosons. This repulsive interaction actually implies that T_c is a monotonic increasing function in the coupling strength for $d = 3$ as shown in Fig. 3.2 so that there is no maximum present in the crossover region (Haussmann 1994a). For a two-dimensional system Tokumitu, Miyake, and Yamada (1991) extended the Nozières-Schmitt-Rink theory including the repulsive interactions between the composite bosons due to the Pauli exclusion principle. This was done by a quantum mechanical mode-coupling scheme known from the spin-fluctuation theory of itinerant magnetism (Moriya 1985). Furthermore, the Ginzburg–Landau theory can be extended to include also the interaction between the noncondensed bosons if one considers the functional integral for the order parameter $\Delta(\boldsymbol{r}, \tau)$ beyond the mean-field approximation (Stintzing 1996).

In this chapter we always consider a continuous system of fermions which means that the kinetic energy of the fermions is just $\frac{1}{2}m\boldsymbol{v}^2$ and the dispersion relation $\varepsilon_{\boldsymbol{k}} = \hbar^2\boldsymbol{k}^2/2m$ is quadratic. However, the crossover from weak to strong coupling superconductivity has been investigated also for fermion systems on a two- or three-dimensional lattice within the negative-U Hubbard model (Nozières and Schmitt-Rink 1985, Scalettar et al. 1989, Denteneer et al. 1991, Sofo et al. 1992, Frésard et al. 1992). For the high-T_c superconductors (the copper oxides) a model with fermions on a lattice may be more realistic. The much more complicated pairing phenomena in fluid hydrogen under high pressure have been considered recently by Moulopoulos and Ashcroft (1991) within a functional integral approach similar to that of Drechsler and Zwerger (1992).

3.1 Derivation of the self-consistent equations for a superfluid Fermi system with s-wave pairing

In this and the following sections we apply the self-consistent quantum-field theory, which we have described in Chap. 2, to the crossover problem. The following presentation will mainly be a review of previous publications (Haussmann 1993, 1994a, and 1994b) but with some modifications and improvements. While the electrostatic interaction between the electrons is repulsive, for superconductivity a second kind of interaction by phonons or spin-wave fluctuations (for the copper oxides) is necessary which leads to an *attractive* effective interaction between the electrons. Since we want to investigate the interplay between pairing and superconductivity for various coupling strengths on a basic level, we do not care about the origin of the interaction. For this reason we assume that the fermions interact via a spin-independent two-particle potential $U(\boldsymbol{r} - \boldsymbol{r}')$ which is attractive. Thus, in

second-quantization representation the system is described by the Hamiltonian

$$H = \int \mathrm{d}^d r \sum_\sigma \frac{\hbar^2}{2m} [\nabla \Psi_\sigma^+(r)][\nabla \Psi_\sigma(r)] + \frac{1}{2} \int \mathrm{d}^d r \int \mathrm{d}^d r' \sum_{\sigma\sigma'} \Psi_\sigma^+(r) \Psi_{\sigma'}^+(r') U(r - r') \Psi_{\sigma'}(r') \Psi_\sigma(r) \,. \quad (3.1)$$

Furthermore, we assume that the fermion system is dilute and the range of the interaction is short, i.e. the average particle distance is much larger than the range of the interaction. More precisely we assume the interaction potential to be a delta function

$$U(r - r') = V \, \delta(r - r') \,, \quad (3.2)$$

where V may be considered as the parameter of the coupling strength. For attractive interaction it is $V < 0$. While eventually we investigate superconductivity and pairing for $d = 3$ dimensions, in this section we let the dimension d be arbitrary and continuous for generality. The singularity of the delta potential (3.2) implies ultraviolet divergences in the Feynman diagrams for $d \geq 2$. Thus, a renormalization of the coupling strength V will be necessary. For this reason we restrict the dimension to the interval $2 < d < 4$.

In quantum-field theory with temperature dependent Green's functions (Matsubara formalism) the fermionic degrees of freedom of a superfluid Fermi liquid are described by the normal Green's function

$$\langle \mathrm{T}[\Psi_{\sigma_1}(r_1, \tau_1) \Psi_{\sigma_2}^+(r_2, \tau_2)] \rangle = \delta_{\sigma_1 \sigma_2} \cdot G(r_1 - r_2, \tau_1 - \tau_2) \quad (3.3)$$

and the anomalous Green's function

$$\langle \mathrm{T}[\Psi_{\sigma_1}(r_1, \tau_1) \Psi_{\sigma_2}(r_2, \tau_2)] \rangle = \varepsilon_{\sigma_1 \sigma_2} \cdot F(r_1 - r_2, \tau_1 - \tau_2) \quad (3.4)$$

Since the interaction between the fermions $U(r - r')$ is assumed to be spin independent, the normal Green's function (3.3) is diagonal in the spin indices and proportional to the Kronecker symbol $\delta_{\sigma_1 \sigma_2}$. Because of its zero range the delta potential (3.2) favors s-wave pairing. Thus, we assume that the pairs which may form have zero spin. This fact is represented by the Levi-Civita tensor $\varepsilon_{\sigma_1 \sigma_2}$ on the right-hand side of (3.4), which is the spin function of a spin zero singlet state. For a more compact notation it is useful to combine the two Green's functions (3.3) and (3.4) into a matrix Green's function. Following Nambu (1960) we introduce the vectorial field operators

$$(\Phi_\sigma^\alpha) = \begin{pmatrix} \Psi_\sigma \\ \Psi_\sigma^+ \end{pmatrix} \,, \qquad (\bar{\Phi}_\sigma^\alpha) = (\Psi_\sigma^+, \Psi_\sigma) \,. \quad (3.5)$$

The index $\alpha = 1, 2$ distinguishes between Ψ_σ and Ψ_σ^+ while σ is the spin index. We define the matrix Green's function by

$$G^{\alpha_1\alpha_2}_{\sigma_1\sigma_2}(r_1 - r_2, \tau_1 - \tau_2) = \langle \mathrm{T}[\Phi^{\alpha_1}_{\sigma_1}(r_1, \tau_1)\bar{\Phi}^{\alpha_2}_{\sigma_2}(r_2, \tau_2)]\rangle \tag{3.6}$$

and we find

$$\left(G^{\alpha_1\alpha_2}_{\sigma_1\sigma_2}(r, \tau)\right) = \begin{pmatrix} \delta_{\sigma_1\sigma_2}G(r, \tau) & \varepsilon_{\sigma_1\sigma_2}F(r, \tau) \\ -\varepsilon_{\sigma_1\sigma_2}F^*(-r, \tau) & -\delta_{\sigma_1\sigma_2}G(-r, -\tau) \end{pmatrix} . \tag{3.7}$$

The Hamiltonian (3.1) and the action functional of the functional integral for the grand-canonical partition function can also be written in terms of the Nambu fields (3.5). Then, for the construction of the diagrams the Feynman rules are obtained which are shown in Fig. 3.3. While for a normal fluid system the propagator line is directed as shown in Fig. 2.1a, here for the superfluid Fermi system the propagator line of Fig. 3.3a is *undirected.* The Nambu representation includes both directions in the matrix Green's function (3.7). This can be seen clearly e.g. in the diagonal elements which contain $G(r, \tau)$ and $G(-r, -\tau)$. (Actually, in the Nambu representation the Green's function (3.7) is not perfectly symmetric but rather a Hermitian matrix with respect to the arguments with index 1 and index 2, because the Nambu fields Φ^α_σ and $\bar{\Phi}^\alpha_\sigma$ of (3.5) are complex field operators which are Hermitian

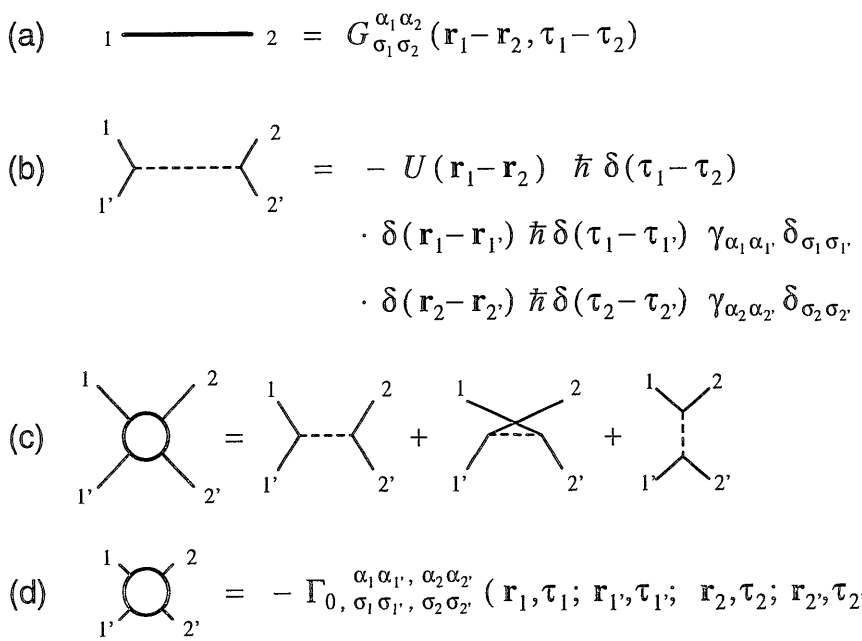

Fig. 3.3. Feynman rules for a superfluid Fermi system: (a) the dressed Green's function (3.6) identified by an undirected thick propagator line, (b) the elementary interaction vertex with amputated external lines where $\gamma_{\alpha\alpha'}$ is defined in (3.8), (c) the bare interaction vertex as a symmetric combination of elementary interaction vertices, and (d) the bare interaction vertex with amputated external lines identified by minus the bare vertex function Γ_0.

conjugated with respect to each other. A perfectly symmetric representation with a perfectly undirected matrix Green's function will be obtained by using a representation with real fields (Hermitian field operators) φ_σ^α which are defined by $\Psi_\sigma = \varphi_\sigma^1 + \mathrm{i}\,\varphi_\sigma^2$ and $\Psi_\sigma^+ = \varphi_\sigma^1 - \mathrm{i}\,\varphi_\sigma^2$.) The two-particle interaction between the fermions implies an elementary interaction vertex which is shown in Fig. 3.3b. In the analytic expression of this vertex the fact that two fermion field operators anticommute is represented by the diagonal matrix

$$(\gamma_{\alpha_1\alpha_2}) = \begin{pmatrix} 1 & 0 \\ 0 & -1 \end{pmatrix} . \tag{3.8}$$

The Nambu representation allows the introduction of a symmetric bare interaction vertex which is defined by the sum of three elementary interaction vertices as shown in Fig. 3.3c. This symmetric vertex is invariant under permutations of the four external lines and identified by the bare vertex function Γ_0 according to Fig. 3.3d.

The matrix Green's function (3.7) is composed of blocks of 2×2 spin matrices. Hence it is a 4×4 matrix. Since the interaction potential $U(\boldsymbol{r} - \boldsymbol{r}')$ in (3.1) is spin independent, in the field theoretic considerations the spin indices need not be treated explicitly. Due to the special structure of the elementary vertex in Fig. 3.3b with respect to the indices α and σ, in the Feynman diagrams of the perturbation series only summations and matrix multiplications of matrices with the structure (3.7) occur. One can convince oneself easily that the matrix structure of (3.7) with respect to the spin indices will be retained under summations and matrix multiplications. Hence we may omit the spin indices and reduce all considerations to the 2×2 matrix Green's function

$$\big(G_{\alpha_1\alpha_2}(\boldsymbol{r},\tau)\big) = \begin{pmatrix} G(\boldsymbol{r},\tau) & F(\boldsymbol{r},\tau) \\ F^*(-\boldsymbol{r},\tau) & -G(-\boldsymbol{r},-\tau) \end{pmatrix} . \tag{3.9}$$

In order to account for the spin degrees of freedom it is sufficient to multiply by a factor 2 for each closed fermion loop in a Feynman diagram. The Feynman rules of Fig. 3.3 are modified appropriately by omitting the spin indices σ and replacing $\delta_{\sigma\sigma'}$ by unity.

In the notation of Chap. 2 we identify $X = (\boldsymbol{r}, \tau, \alpha)$ where the spin index σ is omitted. The matrix Green's function $G_{X_1X_2} = G_{\alpha_1\alpha_2}(\boldsymbol{r}_1 - \boldsymbol{r}_2, \tau_1 - \tau_2)$ can be expressed via the Dyson equation (2.23) in terms of the matrix self energy $\Sigma_{X_1X_2} = \Sigma_{\alpha_1\alpha_2}(\boldsymbol{r}_1 - \boldsymbol{r}_2, \tau_1 - \tau_2)$. For a homogeneous system the matrix Green's function and also the matrix self energy can be diagonalized partially by the Fourier transformation

$$G_{\alpha_1\alpha_2}(\boldsymbol{r},\tau) = \int \frac{\mathrm{d}^d k}{(2\pi)^d} \frac{1}{\beta} \sum_{\omega_n} \exp[\mathrm{i}(\boldsymbol{k}\boldsymbol{r} - \omega_n\tau)]\, G_{\alpha_1\alpha_2}(\boldsymbol{k},\omega_n) \tag{3.10}$$

where $\boldsymbol{k}$ is the wave vector corresponding to the momentum of the fermions and $\omega_n = \pi(2n+1)/\hbar\beta$ are the fermionic Matsubara frequencies. Thus, the Dyson equation (2.23) can be written in the form

$$G^{-1}_{\alpha_1\alpha_2}(\boldsymbol{k},\omega_n) = -\mathrm{i}\hbar\omega_n\delta_{\alpha_1\alpha_2} + (\varepsilon_{\boldsymbol{k}} - \mu)\gamma_{\alpha_1\alpha_2} - \Sigma_{\alpha_1\alpha_2}(\boldsymbol{k},\omega_n) \ , \qquad (3.11)$$

where the several terms are 2×2 matrices which depend on $\boldsymbol{k}$ and ω_n. The first two terms on the right-hand side represent the inverse free matrix Green's function which is obtained by inserting the free fermion Green's function $G_0(\boldsymbol{k},\omega_n) = 1/[-\mathrm{i}\hbar\omega_n + \varepsilon_{\boldsymbol{k}} - \mu]$ and $F_0(\boldsymbol{k},\omega_n) = 0$ into (3.9). Since we consider a continuous system of fermions the kinetic energy is $\varepsilon_{\boldsymbol{k}} = \hbar^2\boldsymbol{k}^2/2m$. According to (2.20) the self energy $\Sigma_{\alpha_1\alpha_2}(\boldsymbol{k},\omega_n)$ can be written as the functional derivative of a functional $\Phi[G]$ which in the present notation reads

$$\Sigma_{\alpha_1\alpha_2}(\boldsymbol{k},\omega_n) = -\frac{1}{2}\,\frac{1}{\beta L^d}\,\frac{\delta\Phi[G]}{\delta\, G_{\alpha_2\alpha_1}(\boldsymbol{k},\omega_n)} \ . \qquad (3.12)$$

The factor $\frac{1}{2}$ occurs because we have omitted the spin index: since $\Phi[G]$ has a closed fermion loop more than $\Sigma_{\alpha_1\alpha_2}(\boldsymbol{k},\omega_n)$, there will be a factor 2 more for $\Phi[G]$ which must be canceled. The factor $1/\beta L^d$ is needed for the correct normalization because here the functional derivative is defined in Fourier space. (L^d is the volume of the system.) The functional $\Phi[G]$ is given by the sum of all vacuum skeleton diagrams (2.29), i.e. all diagrams which can be constructed from the elements shown in Fig. 3.3a (thick propagator line) and Fig. 3.3d (bare interaction vertex) and which do not fall into disconnected pieces if any two propagator lines are cut.

The self energy $\Sigma_{\alpha_1\alpha_2}(\boldsymbol{k},\omega_n)$ can be expressed exactly in terms of the two diagrams shown in Fig. 3.4a which involve the exact matrix Green's function (thick propagator line) and the exact vertex function which is represented by the black filled circle. This equation together with the Dyson equation (3.11) is obtained from the equation of motion for the fermion Green's function: because of the interaction term in (3.1) the equation of motion for G involves the two-particle Green's function $G^{(2)}$ which can be expressed in terms of the exact vertex function Γ by (2.36), so that an integral equation involving G

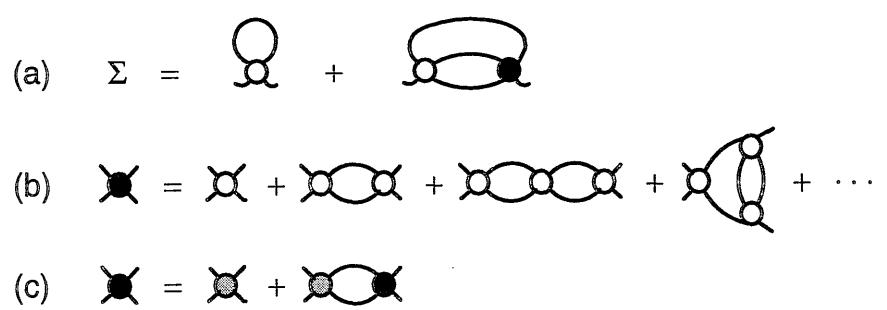

Fig. 3.4. (a) Self energy Σ in terms of the exact Green's function (thick propagator lines) and the exact vertex function (black filled circle), which represents together with the Dyson equation the equation of motion of the fermion Green's function, (b) self-consistent perturbation series for the exact vertex function, and (c) the Bethe–Salpeter equation for the exact vertex function.

and Γ is obtained which is equivalent to (3.11) and Fig. 3.4a. On the other hand the exact vertex function Γ can be expanded in terms of a self-consistent perturbation series as shown in Fig. 3.4b. Since the propagator lines are thick, the diagrams in Fig. 3.4b must be skeleton diagrams which means that no self-energy subdiagrams are present. In Fig. 3.4a one clearly sees that the introduction of the exact vertex function Γ implies a further resummation of the self-consistent perturbation series of the self energy (3.12) which will turn out to be useful for the description of pair formation in the Fermi system, because the vertex function Γ is a two-particle function.

A resummation of the perturbation series of the vertex function in Fig. 3.4b can be achieved by the Bethe–Salpeter equation which is shown in Fig. 3.4c, where the grey circle is identified by the irreducible vertex function Γ_1. For normal fluid systems this resummation has been considered in Sect. 2.4 and in Fig. 2.10. In short-hand notation the Bethe–Salpeter equation reads

$$\Gamma = \Gamma_1 - \Gamma_1 \chi \Gamma \tag{3.13}$$

or

$$\Gamma^{-1} = \Gamma_1^{-1} + \chi \tag{3.14}$$

where χ is the pair propagator which represents the two thick propagator lines in Fig. 3.4c which connect the grey and the black circle. The explicit form of the Bethe–Salpeter equation as an integral equation depends on the details of the matrix multiplications and matrix inversions in (3.13) and (3.14). The Bethe–Salpeter equation is known to be well suited to describe the formation of bound pairs (see e.g. Itzykson and Zuber 1980).

Now, all possible resummations for the calculation of the matrix Green's function (3.9) have been performed. The resummation is represented by three integral equations, the Dyson equation (3.11), the equation for the self energy Σ in Fig. 3.4a, and the Bethe–Salpeter equation (3.13) shown in Fig. 3.4c to determine the vertex function Γ. Eventually, the irreducible vertex function Γ_1 must be determined by the perturbation series, because Γ_1 is needed as input for the Bethe–Salpeter equation. While the perturbation series of Γ_1 is still infinite, the number of diagrams is reduced considerably because the diagrams of Γ_1 are irreducible with respect to several criteria. Since Γ_1 is a functional of the exact Green's function G, the three integral equations are self-consistent and can be solved iteratively. For an explicit calculation an approximation must be introduced by truncating the perturbation series of Γ_1 so that the three integral equations can be solved explicitly. As shown in Fig. 3.5a the lowest order diagram of the irreducible vertex function (the grey circle) is the bare interaction vertex, i.e. the open circle. Thus, in a lowest order approximation we replace Γ_1 by Γ_0. Then, in the Bethe–Salpeter equation the grey circles are replaced approximately by open circles as shown in Fig. 3.5b. Now, in Fig. 3.4a one clearly sees that in this approximation the two diagrams of the self energy can be summed by the Bethe–Salpeter equation, so that a single diagram remains which is shown in Fig. 3.5c. The

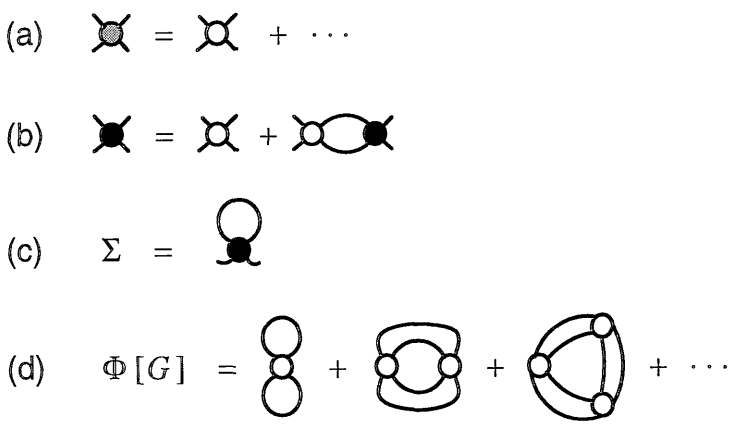

Fig. 3.5. (a) In lowest-order approximation the irreducible vertex function (grey circle) can be replaced by the bare vertex function (open circle). (b) The Bethe–Salpeter equation, (c) the self energy, and (d) the functional $\Phi[G]$ in this approximation.

approximation is conserving. It is possible to find a functional $\Phi[G]$ so that the self energy is the functional derivative (3.12). The functional $\Phi[G]$ is given by the series of Feynman diagrams shown in Fig. 3.5d. Thus, after replacing Γ_1 by Γ_0, the three integral equations simplify into (3.11), Fig. 3.5c, and Fig. 3.5b.

For explicit calculations we need the analytical form of the latter two equations. A considerable simplification of these integral equations occurs because of the local interaction: the delta interaction potential (3.2) implies that the elementary interaction vertex of Fig. 3.3b and hence the bare interaction vertex Γ_0 of Fig. 3.3d is local in space and imaginary time. Since superfluidity in Fermi systems is related to the formation of pairs which is described by two-particle functions, we combine the four external lines of a vertex function into pairs: according to Fig. 3.3d the external lines 1, 1′ and 2, 2′ are pairs, respectively. Since the vertex function Γ may be interpreted as an effective scattering matrix, in the language of scattering theory 2, 2′ are the incoming particles which collide and scatter, and 1, 1′ are the outgoing particles. For the simplification of the Bethe–Salpeter equation it is useful to express the two-particle functions in terms of center of mass and relative coordinates and imaginary times with respect to the pairs. The locality of the interaction implies that in Γ_0 the dependence on the relative coordinates and imaginary times factorizes in terms of delta functions. Hence the bare interaction vertex can be written as

$$\begin{aligned}
&\Gamma_{0,\alpha_1\alpha_{1'},\alpha_2\alpha_{2'}}(\boldsymbol{r}_1,\tau_1;\boldsymbol{r}_{1'},\tau_{1'};\boldsymbol{r}_2,\tau_2;\boldsymbol{r}_{2'},\tau_{2'}) \\
&\quad = \delta(\boldsymbol{r}_1-\boldsymbol{r}_{1'})\,\hbar\delta(\tau_1-\tau_{1'}) \\
&\qquad \cdot \Gamma_{0,\alpha_1\alpha_{1'},\alpha_2\alpha_{2'}}\left(\frac{\boldsymbol{r}_1+\boldsymbol{r}_{1'}}{2}-\frac{\boldsymbol{r}_2+\boldsymbol{r}_{2'}}{2},\frac{\tau_1+\tau_{1'}}{2}-\frac{\tau_2+\tau_{2'}}{2}\right)
\end{aligned}$$

$$\cdot\delta(\boldsymbol{r}_2-\boldsymbol{r}_{2'})\;\hbar\delta(\tau_2-\tau_{2'})\;. \tag{3.15}$$

Because of translational invariance in space and imaginary time, the bare vertex function $\Gamma_{0,\alpha_1\alpha_{1'},\alpha_2\alpha_{2'}}(\boldsymbol{R}_1-\boldsymbol{R}_2,T_1-T_2)$ depends on the difference of the center of mass coordinates $\boldsymbol{R}_1=\frac{1}{2}(\boldsymbol{r}_1+\boldsymbol{r}_{1'})$, $\boldsymbol{R}_2=\frac{1}{2}(\boldsymbol{r}_2+\boldsymbol{r}_{2'})$ and center of mass imaginary times $T_1=\frac{1}{2}(\tau_1+\tau_{1'})$, $T_2=\frac{1}{2}(\tau_2+\tau_{2'})$. Furthermore, the locality of the interaction implies

$$\Gamma_{0,\alpha_1\alpha_{1'},\alpha_2\alpha_{2'}}(\boldsymbol{R}_1-\boldsymbol{R}_2,T_1-T_2)\;\sim\;\delta(\boldsymbol{R}_1-\boldsymbol{R}_2)\;\hbar\delta(T_1-T_2)\;. \tag{3.16}$$

Now, inserting Γ_0 into the approximate Bethe–Salpeter equation of Fig. 3.5b we find that the vertex function Γ has the same structure as (3.15), thus

$$\begin{aligned}
&\Gamma_{\alpha_1\alpha_{1'},\alpha_2\alpha_{2'}}(\boldsymbol{r}_1,\tau_1;\boldsymbol{r}_{1'},\tau_{1'};\boldsymbol{r}_2,\tau_2;\boldsymbol{r}_{2'},\tau_{2'})\\
&\quad=\delta(\boldsymbol{r}_1-\boldsymbol{r}_{1'})\;\hbar\delta(\tau_1-\tau_{1'})\\
&\qquad\cdot\Gamma_{\alpha_1\alpha_{1'},\alpha_2\alpha_{2'}}\Big(\frac{\boldsymbol{r}_1+\boldsymbol{r}_{1'}}{2}-\frac{\boldsymbol{r}_2+\boldsymbol{r}_{2'}}{2},\frac{\tau_1+\tau_{1'}}{2}-\frac{\tau_2+\tau_{2'}}{2}\Big)\\
&\qquad\cdot\delta(\boldsymbol{r}_2-\boldsymbol{r}_{2'})\;\hbar\delta(\tau_2-\tau_{2'})
\end{aligned} \tag{3.17}$$

where now $\Gamma_{\alpha_1\alpha_{1'},\alpha_2\alpha_{2'}}(\boldsymbol{R}_1-\boldsymbol{R}_2,T_1-T_2)$ is a nontrivial function of $\boldsymbol{R}_1-\boldsymbol{R}_2$ and T_1-T_2. By (3.15) and (3.17) we find that the Bethe–Salpeter equation $\Gamma=\Gamma_0-\Gamma_0\chi\Gamma$ can be written as the integral equation

$$\begin{aligned}
\Gamma_{\alpha_1\alpha_{1'},\alpha_4\alpha_4}(\boldsymbol{r}_1-\boldsymbol{r}_4,\tau_1-\tau_4)&=\Gamma_{0,\alpha_1\alpha_{1'},\alpha_4\alpha_4}(\boldsymbol{r}_1-\boldsymbol{r}_4,\tau_1-\tau_4)\\
&-\int\mathrm{d}^dr_2\frac{1}{\hbar}\int_0^{\hbar\beta}\mathrm{d}\tau_2\sum_{\alpha_2\alpha_{2'}}\int\mathrm{d}^dr_3\frac{1}{\hbar}\int_0^{\hbar\beta}\mathrm{d}\tau_3\sum_{\alpha_3\alpha_{3'}}\\
&\qquad\Gamma_{0,\alpha_1\alpha_{1'},\alpha_{2'}\alpha_2}(\boldsymbol{r}_1-\boldsymbol{r}_2,\tau_1-\tau_2)\\
&\qquad\cdot\chi_{\alpha_2\alpha_{2'},\alpha_{3'}\alpha_3}(\boldsymbol{r}_2-\boldsymbol{r}_3,\tau_2-\tau_3)\\
&\qquad\cdot\Gamma_{\alpha_3\alpha_{3'},\alpha_{4'}\alpha_4}(\boldsymbol{r}_3-\boldsymbol{r}_4,\tau_3-\tau_4)
\end{aligned} \tag{3.18}$$

where

$$\begin{aligned}
&\chi_{\alpha_1\alpha_{1'},\alpha_2\alpha_{2'}}(\boldsymbol{r}_1-\boldsymbol{r}_2,\tau_1-\tau_2)\\
&\quad=-G_{\alpha_1\alpha_{2'}}(\boldsymbol{r}_1-\boldsymbol{r}_2,\tau_1-\tau_2)G_{\alpha_2\alpha_{1'}}(\boldsymbol{r}_2-\boldsymbol{r}_1,\tau_2-\tau_1)
\end{aligned} \tag{3.19}$$

is the pair propagator. (The structure of the indices is the same as in (2.37).) Because of the translational invariance, the vertex functions Γ, Γ_0, and the pair propagator χ can be diagonalized partially by the Fourier transformation

$$\Gamma_{\alpha_1\alpha_{1'},\alpha_2\alpha_{2'}}(\boldsymbol{r},\tau)=\int\frac{\mathrm{d}^dk}{(2\pi)^d}\,\frac{1}{\beta}\sum_{\Omega_n}\exp[\mathrm{i}(\mathbb{K}\boldsymbol{r}-\Omega_n\tau)]\,\Gamma_{\alpha_1\alpha_{1'},\alpha_2\alpha_{2'}}(\mathbb{K},\Omega_n) \tag{3.20}$$

where $\mathbb{K}$ is the wave vector corresponding to the total momentum and $\Omega_n=2\pi n/\hbar\beta$ are the bosonic Matsubara frequencies corresponding to the total

energy of the incoming or outgoing fermion pairs. Eq. (3.16) implies that the bare vertex function

$$\Gamma_{0,\alpha_1\alpha_{1'},\alpha_2\alpha_{2'}}(\boldsymbol{K},\Omega_n) = \Gamma_{0,\alpha_1\alpha_{1'},\alpha_2\alpha_{2'}} \tag{3.21}$$

does not depend on $\boldsymbol{K}$ and Ω_n. Thus, by the Fourier transformation the integral equation (3.18) becomes a simple matrix equation which reads

$$\begin{aligned}\Gamma_{\alpha_1\alpha_{1'},\alpha_{4'}\alpha_4}(\boldsymbol{K},\Omega_n) &= \Gamma_{0,\alpha_1\alpha_{1'},\alpha_{4'}\alpha_4} \\ &- \sum_{\alpha_2\alpha_{2'}}\sum_{\alpha_3\alpha_{3'}} \Gamma_{0,\alpha_1\alpha_{1'},\alpha_{2'}\alpha_2}\,\chi_{\alpha_2\alpha_{2'},\alpha_{3'}\alpha_3}(\boldsymbol{K},\Omega_n)\,\Gamma_{\alpha_3\alpha_{3'},\alpha_{4'}\alpha_4}(\boldsymbol{K},\Omega_n)\end{aligned} \tag{3.22}$$

Since (3.22) has the structure of (2.41) with the appropriate matrix multiplications, the Bethe–Salpeter equation can be transformed into the equivalent form (2.42) which reads

$$\Gamma^{-1}_{\alpha_1\alpha_{1'},\alpha_{2'}\alpha_2}(\boldsymbol{K},\Omega_n) = \Gamma^{-1}_{0,\alpha_1\alpha_{1'},\alpha_{2'}\alpha_2} + \chi_{\alpha_1\alpha_{1'},\alpha_{2'}\alpha_2}(\boldsymbol{K},\Omega_n) \tag{3.23}$$

where the inverse matrices Γ^{-1} and Γ_0^{-1} are defined appropriately. On the other hand the pair propagator is a simple product in real space and imaginary time representation,

$$\chi_{\alpha_1\alpha_{1'},\alpha_{2'}\alpha_2}(\boldsymbol{r},\tau) = -G_{\alpha_1\alpha_2}(\boldsymbol{r},\tau)G_{\alpha_{2'}\alpha_{1'}}(-\boldsymbol{r},-\tau)\ . \tag{3.24}$$

From the diagram in Fig. 3.5c we obtain the self energy. Inserting (3.17) for the vertex function we obtain

$$\begin{aligned}&\Sigma_{\alpha_1\alpha_2}(\boldsymbol{r}_1-\boldsymbol{r}_2,\tau_1-\tau_2) \\ &\quad= -\sum_{\alpha_{1'}\alpha_{2'}} G_{\alpha_{1'}\alpha_{2'}}(\boldsymbol{r}_1-\boldsymbol{r}_2,\tau_1-\tau_2)\Gamma_{\alpha_1\alpha_{1'},\alpha_{2'}\alpha_2}(\boldsymbol{r}_1-\boldsymbol{r}_2,\tau_1-\tau_2)\end{aligned} \tag{3.25}$$

which simply is a sum of products in real space,

$$\Sigma_{\alpha_1\alpha_2}(\boldsymbol{r},\tau) = -\sum_{\alpha_{1'}\alpha_{2'}} G_{\alpha_{1'}\alpha_{2'}}(\boldsymbol{r},\tau)\Gamma_{\alpha_1\alpha_{1'},\alpha_{2'}\alpha_2}(\boldsymbol{r},\tau)\ . \tag{3.26}$$

Now, by (3.11), (3.26), (3.23), and (3.24) we have four equations which form a set of self-consistent equations for the matrix Green's function $G_{\alpha_1\alpha_2}(\boldsymbol{k},\omega_n)$ and the vertex function $\Gamma_{\alpha_1\alpha_{1'},\alpha_2\alpha_{2'}}(\boldsymbol{K},\Omega_n)$. The structure of the equations has simplified considerably with respect to the space and imaginary-time coordinates, which is a result of the local interaction. There are no integral equations any more. To solve the equations iteratively to determine G and Γ, only matrix multiplications, matrix inversions, and Fourier transformations as (3.10) and (3.20) are needed.

A further simplification of the self-consistent equations with respect to the indices α is possible for dimensions $d \geq 2$: the local interaction with the

delta potential (3.2) implies an ultraviolet divergence in the pair propagator χ which requires a renormalization of the interaction strength and implies a reduction of the tensors $\Gamma_{\alpha_1\alpha_{1'},\alpha_2\alpha_{2'}}(\mathbb{K},\Omega_n)$ and $\chi_{\alpha_1\alpha_{1'},\alpha_2\alpha_{2'}}(\mathbb{K},\Omega_n)$ with four indices into matrices $\Gamma_{\alpha_1\alpha_2}(\mathbb{K},\Omega_n)$ and $\chi_{\alpha_1\alpha_2}(\mathbb{K},\Omega_n)$ with only two indices. This reduction is not an approximation, but it is exact in the limit of zero range of the interaction potential. The ultraviolet divergence arises from the particle-particle pair propagator $\chi_{pp}(r,\tau) = \chi_{12,21}(r,\tau) = +[G(r,\tau)]^2$ which is the product of two normal fermion Green's functions with the same direction (in terms of Feynman diagrams: a bubble of two fermion lines with parallel directions). In Fourier representation we separate the following ultraviolet divergence

$$\begin{aligned}\chi_{pp}(\mathbb{K},\Omega_n) &= \int \frac{\mathrm{d}^d k}{(2\pi)^d}\,\frac{1}{\beta}\sum_{\omega_n} G(\tfrac{1}{2}\mathbb{K}-k,\Omega_n-\omega_n)\,G(\tfrac{1}{2}\mathbb{K}+k,\omega_n)\\ &= M_{pp}(\mathbb{K},\Omega_n) + \int \frac{\mathrm{d}^d k}{(2\pi)^d}\,\frac{m}{\hbar^2 k^2}\end{aligned} \tag{3.27}$$

While $M_{pp}(\mathbb{K},\Omega_n)$ is finite, the second term is ultraviolet divergent for $d \geq 2$. On the other hand the particle-hole pair propagator $\chi_{ph}(r,\tau) = \chi_{11,11}(r,\tau) = -G(r,\tau)G(-r,-\tau)$, which is the product of the two normal fermion Green's functions with opposite directions (a bubble of two fermion lines with opposite directions), is finite. The remaining components of $\chi_{\alpha_1\alpha_{1'},\alpha_{2'}\alpha_2}(\mathbb{K},\Omega_n)$ which involve anomalous propagators are finite, too. Thus, for the pair propagator we obtain the decomposition

$$\begin{aligned}\chi_{\alpha_1\alpha_{1'},\alpha_{2'}\alpha_2}(\mathbb{K},\Omega_n) &= M_{\alpha_1\alpha_{1'},\alpha_{2'}\alpha_2}(\mathbb{K},\Omega_n)\\ &\quad + \delta_{\alpha_1\alpha_2}\delta_{\alpha_{1'}\alpha_{2'}}[1-\delta_{\alpha_1\alpha_{1'}}]\int \frac{\mathrm{d}^d k}{(2\pi)^d}\,\frac{m}{\hbar^2 k^2}\end{aligned} \tag{3.28}$$

where $M_{\alpha_1\alpha_{1'},\alpha_{2'}\alpha_2}(\mathbb{K},\Omega_n)$ is finite and the second term is the ultraviolet divergence.

As usual in quantum-field theory, the ultraviolet divergence can be removed by a renormalization of the interaction parameter. Here, in the delta potential (3.2) and hence in the bare interaction vertex Γ_0 the strength of the interaction is described by the parameter V. We define the renormalized interaction parameter T by

$$\frac{1}{T} = \frac{1}{V} + \int \frac{\mathrm{d}^d k}{(2\pi)^d}\,\frac{m}{\hbar^2 k^2} \tag{3.29}$$

If we consider the scattering of two particles by the delta potential (3.2), it turns out that T is the T matrix of scattering theory which is proportional to the scattering amplitude (see e.g. Davydov 1965). The delta potential is the zero-range limit of an interaction potential which implies low-energy s-wave scattering. For this reason the scattering is isotropic. The scattering

amplitude and hence the T matrix do not depend on the scattering angle, so that T is just a constant parameter. For $d = 3$ dimensions the T matrix can be expressed in terms of the s-wave scattering length a_{F} of the fermions by

$$T = \frac{4\pi\hbar^2}{m} a_{\mathrm{F}} \ . \tag{3.30}$$

Now, the renormalization procedure is performed as follows. In the $\boldsymbol{k}$ integrals of (3.27)-(3.29) we introduce an ultraviolet momentum cutoff Λ by requiring $|\boldsymbol{k}| < \Lambda$ so that the separated integral becomes

$$\int_{|\boldsymbol{k}|<\Lambda} \frac{\mathrm{d}^d k}{(2\pi)^d} \frac{m}{\hbar^2 \boldsymbol{k}^2} = \frac{\Omega_d}{(2\pi)^d} \frac{m}{\hbar^2} \frac{\Lambda^{d-2}}{d-2} \tag{3.31}$$

where $\Omega_d = 2\pi^{d/2}/\Gamma(d/2)$ is the surface of the d-dimensional unit spere. This result implies

$$\frac{1}{T} = \frac{1}{V} + \frac{\Omega_d}{(2\pi)^d} \frac{m}{\hbar^2} \frac{\Lambda^{d-2}}{d-2} \ . \tag{3.32}$$

Eventually, we perform the limit $\Lambda \to \infty$ where the renormalized interaction parameter T or equivalently the s-wave scattering length a_{F} is kept constant. One clearly sees that for $d > 2$ the integral (3.31) is divergent for $\Lambda \to \infty$. (For $d = 2$ the ultraviolet divergence is logarithmical, i.e. $\sim \ln \Lambda$, and must be treated in a slightly different way.) To compensate the ultraviolet divergence in (3.32), $1/V$ must tend to $-\infty$. Hence it is $V \to -0$ for $\Lambda \to \infty$. The renormalization in the Feynman diagrams and in the Bethe–Salpeter equation (3.23) is performed by using (3.29) or (3.32) to cancel the ultraviolet divergences of the momentum integrals where V is replaced by T. From inspection of (3.28) we find that only part of the tensor elements of the complete pair propagator $\chi_{\alpha_1\alpha_{1'},\alpha_2\alpha_{2'}}(\boldsymbol{K}, \Omega_n)$ are ultraviolet divergent. Thus, the renormalization will be only partially. The renormalized Bethe–Salpeter equation depends on T and on V. However, because of $V \to -0$ for $\Lambda \to \infty$ a considerable simplification will occur. The renormalized particle-particle pair propagator $M_{pp}(\boldsymbol{K}, \Omega_n)$ defined in (3.27) will be finite for dimensions d in the interval $2 < d < 4$ so that the renormalization procedure will work for $2 < d < 4$.

Since the bare interaction vertex shown in Fig. 3.3c is symmetrized it consists of three elements. However, $-\Gamma_0$ is not just the sum of the three elementary vertices. The Feynman rules imply that for each closed fermion loop there is a factor $(-1)2$, the -1 because the particles are fermions and the 2 for the spin degrees of freedom. For a bare interaction vertex in any Feynman diagram, the number of closed loops in the diagram may be different for the different elementary vertices. Thus, the sum of the elementary vertices in Fig. 3.3c must be modified by weight factors $(-1)2$ if necessary, which will depend on the particular Feynman diagram. For this reason, it is necessary to replace the bare interaction vertex (the open circle) in the Bethe–Salpeter

equation of Fig. 3.5b by the three elementary vertices. Then, by iteration of the Bethe–Salpeter equation we obtain a perturbation series for the vertex function Γ (the black filled circle) where the Feynman diagrams consist of several elements. These elements are bubbles and ladders of fermion lines and combinations of them. Now, in the limit $\Lambda \to \infty$, where $V \to -0$ and T is constant, several of these elements will vanish. Let us assume for the moment that the fermion system is normal fluid. Then, the propagator lines are directed. There will be three elements in the Feynman diagrams: bubbles, particle-hole ladders, and particle-particle ladders. In the perturbation series expansion the first two elements imply terms $V\chi_{ph}(\mathbb{K}, \Omega_n)$ which involve the particle-hole pair propagator, while the third one implies a term $V\chi_{pp}(\mathbb{K}, \Omega_n)$ involving the particle-particle propagator. Now, in the limit $\Lambda \to \infty$ the terms $V\chi_{ph}(\mathbb{K}, \Omega_n)$ will vanish because of $V \to -0$ where $\chi_{ph}(\mathbb{K}, \Omega_n)$ is finite. For this reason bubbles and particle-hole ladders vanish in the limit $\Lambda \to \infty$. Thus, only the particle-particle ladders will remain. By the renormalization $V\chi_{pp}(\mathbb{K}, \Omega_n)$ is replaced by $TM_{pp}(\mathbb{K}, \Omega_n)$ which is finite in the limit $\Lambda \to \infty$.

For a superfluid fermion system the particle-hole and particle-particle ladders are mixed. However, the bubbles never involve a particle-particle pair propagator, so that in the limit $\Lambda \to \infty$ the bubbles can be omitted. This means that in Fig. 3.3c on the right-hand side the first elementary vertex may be omitted. The remaining two elementary vertices in Fig. 3.3c generate only ladder diagrams in the Bethe–Salpeter equation of Fig. 3.5b. Thus, for the vertex function Γ (black filled circle) we obtain a series of ladder diagrams which is shown in Fig. 3.6a. There are two classes of ladder diagrams: direct and exchange diagrams. It is useful to resum these classes separately into the unsymmetrized vertex function which is shown in Fig. 3.6a by the grey squares. Then, for the unsymmetrized vertex function (the grey square) we obtain the Bethe–Salpeter equation shown in Fig. 3.6b with only one elementary interaction vertex (the dashed line), which generates the series of self-consistent ladder diagrams. The grey square may be interpreted as the effective T matrix of two particles scattering each other in the background of a Fermi system with density ϱ. In the zero-density limit $\varrho \to 0$ the grey square exactly is the T matrix of two-particle scattering. The self energy Σ can also be expressed in terms of the unsymmetrized vertex function. Then two diagrams with grey squares are obtained as it is shown in Fig. 3.6c. The first diagram contains a closed fermion loop which implies a weight factor $(-1)2$, while the second diagram does not. Comparing with Fig. 2.8 we find that we have obtained the self energy in self-consistent ladder approximation. The functional $\Phi[G]$ of this conserving approximation is given by Fig. 2.8a where, however, the arrows of the fermion lines must be omitted because here the propagator lines are undirected.

Since the diagrams consist of particle-particle ladders, particle-hole ladders, and more complicated combinations involving the anomalous propagators of the superfluid system, the grey square of Fig. 3.6b identified by

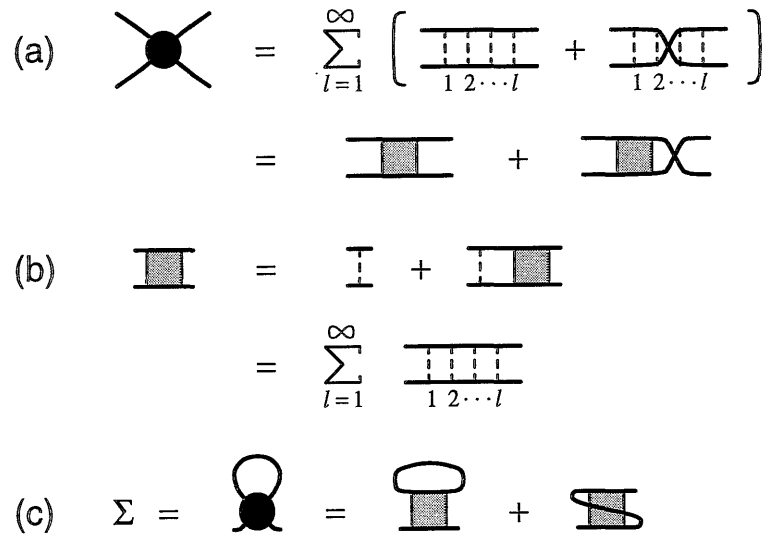

Fig. 3.6. (a) The vertex function $-\Gamma$ as a series of ladder diagrams. There are two types of ladder diagrams: direct and exchange diagrams, which can be resummed separately into the grey squares. (b) The Bethe–Salpeter equation for the unsymmetrized vertex function (grey square), and (c) the self energy expressed in terms of the unsymmetrized vertex function.

the unsymmetrized vertex function still depends on four indices α. Now, in the Bethe–Salpeter equation of Fig. 3.6b we perform the renormalization. The ultraviolet divergence is separated from the pair propagator according to (3.28) and then taken to the renormalized coupling strength T by (3.29). Since the ultraviolet divergence occurs only for the particle-particle ladder but not for the particle-hole ladder, the vertex function depends on the renormalized coupling T and also on the bare coupling V. Now, we perform the limit $\Lambda \to \infty$ so that $V \to -0$ where T is constant. In this limit it turns out that only the particle-particle contribution of the vertex function (grey square) survives, the particle-hole contribution and the mixed contributions become zero. We identify the particle-particle contribution of the unsymmetrized vertex function by the 2×2 matrix $\Gamma_{\alpha_1\alpha_2}(\boldsymbol{K}, \Omega_n)$ and obtain the renormalized Bethe–Salpeter equation

$$\Gamma^{-1}_{\alpha_1\alpha_2}(\boldsymbol{K}, \Omega_n) = T^{-1}\delta_{\alpha_1\alpha_2} + M_{\alpha_1\alpha_2}(\boldsymbol{K}, \Omega_n) \tag{3.33}$$

where

$$M_{\alpha_1\alpha_2}(\boldsymbol{K}, \Omega_n) = \int \frac{\mathrm{d}^d k}{(2\pi)^d}$$
$$\cdot\Big[\frac{1}{\beta}\sum_{\omega_n} G_{\alpha_1\alpha_2}(\tfrac{1}{2}\boldsymbol{K} - \boldsymbol{k}, \Omega_n - \omega_n) G_{\alpha_1\alpha_2}(\tfrac{1}{2}\boldsymbol{K} + \boldsymbol{k}, \omega_n) - \frac{m}{\hbar^2\boldsymbol{k}^2}\,\delta_{\alpha_1\alpha_2}\Big] \tag{3.34}$$

is the regularized pair propagator. Considering the ultraviolet behavior of the k integral in (3.34) we find that $M_{\alpha_1\alpha_2}(K, \Omega_n)$ is finite for dimensions d in the interval $2 < d < 4$. Thus, the renormalization procedure works well for these dimensions. In real space and imaginary time the regularized pair propagator reads

$$M_{\alpha_1\alpha_2}(r, \tau) = [G_{\alpha_1\alpha_2}(r, \tau)]^2 - c\,\delta_{\alpha_1\alpha_2}\delta(r)\,\hbar\,\delta(\tau) \tag{3.35}$$

where c is the infinite constant defined by (3.31) in the limit $\Lambda \to \infty$. Actually, the regularization we have performed is a *dimensional regularization*. This means that while for $d < 2$ the pair propagator $M_{\alpha_1\alpha_2}(K, \Omega_n)$ is finite, for $d > 2$ it is obtained by an analytic continuation in d. As a result of the reduction to the particle-particle contribution, the number of indices of the vertex function and of the pair propagator is reduced from 4 to 2 because now the indices of the two parallel fermion lines in Fig. 3.6b are coupled together. This fact is clearly seen in (3.35): the pair propagator is the product of two identical fermion Green's functions with the same indices.

The grey square is now identified by $-\Gamma_{\alpha_1\alpha_2}(K, \Omega_n)$. Then, from Fig. 3.6c we obtain the particle-particle contribution of the self energy

$$\begin{aligned}\tilde{\Sigma}_{\alpha_1\alpha_2}(r, \tau) &= (-1)2 \cdot G_{\alpha_2\alpha_1}(-r, -\tau)\,[-\Gamma_{\alpha_1\alpha_2}(r, \tau)] \\ &\quad + G_{\alpha_2\alpha_1}(-r, -\tau)\,[-\Gamma_{\alpha_1\alpha_2}(r, \tau)] \\ &= G_{\alpha_2\alpha_1}(-r, -\tau)\,\Gamma_{\alpha_1\alpha_2}(r, \tau)\ .\end{aligned} \tag{3.36}$$

The two diagrams of Fig. 3.6c yield the same analytic expression where the first one has the weight factor $(-1)2$ because of the closed fermion loop. In the limit $V \to 0$ nearly all particle-hole and mixed contributions are zero. However, there is one exception. Let us consider the first order diagrams, i.e. the Hartree and the Fock diagram which are obtained from Fig. 3.6c by replacing the grey squares by the dashed elementary interaction line. Since the interaction is assumed to be local in space and imaginary time, the internal fermion line is identified by a propagator with equal space and imaginary-time arguments, so that we obtain

$$\begin{aligned}\Sigma^{HF}_{\alpha_1\alpha_2}(k, \omega_n) = &- V\,\gamma_{\alpha_1\alpha_2}(-1)2\,\frac{1}{2}\sum_{\alpha_3\alpha_4}\gamma_{\alpha_3\alpha_4}\,G_{\alpha_4\alpha_3}(r = 0, \tau = 0) \\ &- V\sum_{\alpha_3\alpha_4}\gamma_{\alpha_1\alpha_3}\,G_{\alpha_3\alpha_4}(r = 0, \tau = 0)\,\gamma_{\alpha_4\alpha_2}\end{aligned} \tag{3.37}$$

where $\gamma_{\alpha_1\alpha_2}$ is defined in (3.8). The first (Hartree) term and the diagonal part of the second (Fock) term are particle-particle contributions and included already in (3.36). The new term is the nondiagonal part of the second (Fock) term, which according to (3.9) involves the anomalous propagator and which reads

$$(\Sigma^1_{\alpha_1\alpha_2}(k, \omega_n)) = \begin{pmatrix} 0 & V\,F(r = 0, \tau = 0) \\ V\,F^*(r = 0, \tau = 0) & 0 \end{pmatrix}\ . \tag{3.38}$$

In the standard BCS theory with a local interaction,

$$\Delta \;=\; V\,F(\boldsymbol{r}=\boldsymbol{0},\tau=0) \;=\; V\int\frac{\mathrm{d}^d k}{(2\pi)^d}\,F(\boldsymbol{k},\tau=0) \tag{3.39}$$

is defined as the order parameter. Thus, for a superfluid fermion system Δ is expected to be nonzero. However, Eq. (3.32) implies $V\sim -\Lambda^{-(d-2)}\to -0$ for $\Lambda\to\infty$ if $d>2$. Thus, it is not straightforwardly clear if Δ is nonzero. On the other hand, from the BCS theory it is known that $F(\boldsymbol{k},\tau)\sim|\boldsymbol{k}|^{-2}$ for large $\boldsymbol{k}$. Hence, the $\boldsymbol{k}$ integral on the right-hand side of (3.39) is ultraviolet divergent as $\sim\Lambda^{d-2}$, which cancels the factor $V\sim-\Lambda^{-(d-2)}$. Thus, Δ is indeed finite and may be nonzero in the limit $\Lambda\to\infty$. By the use of (3.29) we can replace the bare interaction parameter V by the renormalized interaction parameter T in (3.39). Thus, we obtain

$$\Delta = T\int\frac{\mathrm{d}^d k}{(2\pi)^d}\Big[\,F(\boldsymbol{k},\tau=0)+\Delta\frac{m}{\hbar^2\boldsymbol{k}^2}\,\Big]\,. \tag{3.40}$$

As we shall see below, the integral in (3.40) is indeed finite for large $\boldsymbol{k}$ for dimensions d in the interval $2<d<4$. Hence, Eq. (3.38) yields a nontrivial contribution to the self energy which is related to the order parameter by

$$(\Sigma^1_{\alpha_1\alpha_2}) = \begin{pmatrix} 0 & \Delta \\ \Delta^* & 0 \end{pmatrix}\,. \tag{3.41}$$

Finally, taking both contributions (3.36) and (3.38) together, we obtain the total self energy

$$\Sigma_{\alpha_1\alpha_2}(\boldsymbol{r},\tau) \;=\; \Sigma^1_{\alpha_1\alpha_2}\delta(\boldsymbol{r})\,\hbar\,\delta(\tau) \;+\; G_{\alpha_2\alpha_1}(-\boldsymbol{r},-\tau)\Gamma_{\alpha_1\alpha_2}(\boldsymbol{r},\tau)\,. \tag{3.42}$$

Now, the work is done. We have derived four self-consistent equations given by (3.11) [Dyson equation], (3.42) [self energy], (3.33) [Bethe–Salpeter equation], and (3.35) [dimensionally regularized pair propagator] for the fermion Green's function $G_{\alpha_1\alpha_2}(\boldsymbol{k},\omega_n)$ and the vertex function $\Gamma_{\alpha_1\alpha_2}(\boldsymbol{K},\Omega_n)$ [the effective T matrix]. As an approximation we have replaced the irreducible vertex function (grey circle) by the bare interaction vertex (open circle) as shown in Fig. 3.5. The delta interaction potential (3.2) implies an ultraviolet divergence for $d\geq 2$ which leads to a considerable simplification of the equations: the vertex function $\Gamma_{\alpha_1\alpha_2}(\boldsymbol{r},\tau)$ depends only on the center of mass coordinate and center of mass imaginary time and only on two Nambu indices α. The strength of the interaction is parametrized by the renormalized parameter T (which is the T matrix) or equivalently by the s-wave scattering length a_{F}. It is also possible to write down the functional $\Phi[G]$ which generates the self-consistent equation. We find

$$\begin{aligned}\Phi[G] = {} & -2\,\beta L^d\,V\,F(\boldsymbol{r}=\boldsymbol{0},\tau=0)\,F^*(\boldsymbol{r}=\boldsymbol{0},\tau=0) \\ & -\beta L^d\int\frac{\mathrm{d}^d K}{(2\pi)^d}\,\frac{1}{\beta}\sum_{\Omega_n}\mathrm{Tr}\ln[1+TM(\boldsymbol{K},\Omega_n)]\end{aligned} \tag{3.43}$$

where the expressions in the square brackets are 2×2 matrices with respect to the Nambu indices and Tr is the respective trace. One can convince oneself easily that this functional yields the self energy (3.42) by the functional derivative (3.12).

Previously, the self-consistent equations have been derived in a slightly different way (Haussmann 1993). There the self-consistent ladder approximation for the unsymmetrized vertex function and the Bethe–Salpeter equation has been assumed right from the beginning. The renormalization procedure has been performed following Galitskii (1958) and Gorkov and Melik-Barkhudarov (1961). In this approach the interaction involving the particle-particle ladders is replaced by the T matrix of scattering theory. Then, for the T matrix an approximate form of the scattering amplitude for low-energy s-wave scattering is inserted which depends on two parameters, the s-wave scattering length a_{F} and a second length b_{F} which corresponds to a finite range of the interaction potential. Thus, in principle a more general interaction potential can be described within this approach. However, it turns out that the self-consistent equations represent a conserving approximation only for $b_{\mathrm{F}} = 0$ which corresponds to the delta interaction potential (3.2), but not for nonzero b_{F}. Thus, our theory is reasonable only for a delta interaction potential with zero range, i.e. $b_{\mathrm{F}} = 0$.

Furthermore, the definition of the order parameter Δ in our previous publications (Haussmann 1993 and 1994b) is incorrect. There we have overlooked that the nondiagonal elements of the Fock self energy (3.38) are indeed nonzero after renormalization so that we have taken into account only the second term of (3.42). On the other hand, in the strong-coupling limit the vertex function $\Gamma_{\alpha_1\alpha_2}(r,\tau)$ may be interpreted as the boson Green's function of the bound pairs. For this reason, we have previously defined the order parameter by the limit $\lim_{r\to\infty} \Gamma_{\alpha_1\alpha_2}(r,\tau) = \Gamma^0_{\alpha_1\alpha_2} = -\Delta_{\alpha_1}\Delta^*_{\alpha_2}$ where $(\Delta_\alpha) = (\Delta, \Delta^*)$ in analogy to the order parameter of a superfluid Bose system. However, $\Gamma_{\alpha_1\alpha_2}(r,\tau)$ is given by a series of connected Feynman diagrams so that $\Gamma_{\alpha_1\alpha_2}(r,\tau)$ is proportional to the *connected* boson Green's function. Hence, the limit is necessarily $\lim_{r\to\infty} \Gamma_{\alpha_1\alpha_2}(r,\tau) = 0$ which contradicts our previous definition of the order parameter. Nevertheless, the conclusions in our previous publications (Haussmann 1993 and 1994b) are correct.

3.2 Discussion of the self-consistent equations, weak- and strong-coupling limit

As a model for superfluidity in a dilute fermion system with attractive short-range interaction we have derived four self-consistent equations for the fermion Green's function $G_{\alpha_1\alpha_2}(k,\omega_n)$ and the vertex function $\Gamma_{\alpha_1\alpha_2}(K,\Omega_n)$. These equations are the Dyson equation

$$G^{-1}_{\alpha_1\alpha_2}(k,\omega_n) = -\mathrm{i}\hbar\omega_n\delta_{\alpha_1\alpha_2} + (\varepsilon_k - \mu)\gamma_{\alpha_1\alpha_2} - \Sigma_{\alpha_1\alpha_2}(k,\omega_n) \qquad (3.44)$$

together with the self energy

$$\Sigma_{\alpha_1\alpha_2}(r,\tau) = \Sigma^1_{\alpha_1\alpha_2}\delta(r)\,\hbar\,\delta(\tau) + G_{\alpha_2\alpha_1}(-r,-\tau)\Gamma_{\alpha_1\alpha_2}(r,\tau) \tag{3.45}$$

and the Bethe–Salpeter equation

$$\Gamma^{-1}_{\alpha_1\alpha_2}(\boldsymbol{K},\Omega_n) = \frac{m}{4\pi\hbar^2}\,a_{\rm F}^{-1}\delta_{\alpha_1\alpha_2} + M_{\alpha_1\alpha_2}(\boldsymbol{K},\Omega_n) \tag{3.46}$$

together with the renormalized pair propagator

$$M_{\alpha_1\alpha_2}(r,\tau) = [G_{\alpha_1\alpha_2}(r,\tau)]^2 - c\,\delta_{\alpha_1\alpha_2}\delta(r)\,\hbar\,\delta(\tau)\ . \tag{3.47}$$

Here c is an infinite constant defined by (3.31) in the limit $\Lambda\to\infty$ so that (3.47) is the pair propagator in dimensional regularization. From now on we assume that the dimension of the fermion system is $d=3$. For this reason, in the Bethe–Salpeter equation we have used (3.30) for the T matrix. The order parameter Δ of the superfluid state, defined in (3.40), occurs in the first term of the self energy (3.45) via $\Sigma^1_{\alpha_1\alpha_2}$ defined in (3.41). The kinetic properties of the fermions are described by the quadratic dispersion $\varepsilon_{\boldsymbol{k}} = \hbar^2\boldsymbol{k}^2/2m$ which occurs in the Dyson equation.

A. Scaling invariance

The equations (3.44)-(3.47) contain three parameters which describe the state of the fermion system: the temperature T (hidden in the Matsubara frequencies ω_n and Ω_n), the chemical potential μ in the Dyson equation (3.44), and the inverse s-wave scattering length $a_{\rm F}^{-1}$ for the strength of interaction in the Bethe–Salpeter equation (3.46). Equivalently, the three parameters may be T, $n_{\rm F}$, and $a_{\rm F}^{-1}$ where $n_{\rm F}$ is the fermion density. Because of the quadratic dispersion $\varepsilon_{\boldsymbol{k}}$ and the local interaction (the delta interaction potential (3.2) with zero range) the self-consistent equations (3.44)-(3.47) are scaling invariant. All quantities may be rescaled by the density $n_{\rm F}$. To do this we need the Fermi wave number $k_{\rm F} = (3\pi^2 n_{\rm F})^{1/3}$ for the length scale and the Fermi energy $\varepsilon_{\rm F} = \hbar^2 k_{\rm F}^2/2m$ as energy scale. Thus, the Green's and vertex functions can be written in terms of dimensionless scaling functions depending on the dimensionless variables $k_{\rm F}r$, $\boldsymbol{k}/k_{\rm F}$, $\boldsymbol{K}/k_{\rm F}$, and $\varepsilon_{\rm F}\tau/\hbar$, $\hbar\omega_n/\varepsilon_{\rm F}$, $\hbar\Omega_n/\varepsilon_{\rm F}$:

$$G_{\alpha_1\alpha_2}(\boldsymbol{k},\omega_n) = \varepsilon_{\rm F}^{-1}\cdot g_{\alpha_1\alpha_2}(\boldsymbol{k}/k_{\rm F},\hbar\omega_n/\varepsilon_{\rm F})\ , \tag{3.48}$$

$$\Sigma_{\alpha_1\alpha_2}(r,\tau) = k_{\rm F}^3\varepsilon_{\rm F}^2\cdot\sigma_{\alpha_1\alpha_2}(k_{\rm F}r,\varepsilon_{\rm F}\tau/\hbar)\ , \tag{3.49}$$

$$\Gamma_{\alpha_1\alpha_2}(\boldsymbol{K},\Omega_n) = k_{\rm F}^{-3}\varepsilon_{\rm F}\cdot\gamma_{\alpha_1\alpha_2}(\boldsymbol{K}/k_{\rm F},\hbar\Omega_n/\varepsilon_{\rm F})\ , \tag{3.50}$$

$$M_{\alpha_1\alpha_2}(r,\tau) = k_{\rm F}^6\cdot m_{\alpha_1\alpha_2}(k_{\rm F}r,\varepsilon_{\rm F}\tau/\hbar)\ . \tag{3.51}$$

Inserting (3.48)-(3.51) into (3.44)-(3.47), we obtain four dimensionless self-consistent equations for the scaling functions. The state of the fermion system will be described by only two dimensionless parameters, a dimensionless temperature and a dimensionless renormalized coupling strength which are

$$\theta = k_B T/\varepsilon_F \ , \qquad v = 1/(k_F a_F) \ , \tag{3.52}$$

respectively. Thus, the self-consistent equations (3.44)-(3.47) will imply a phase diagram as shown in Fig. 3.2 with the temperature and the coupling strength as the axes. The phase diagram will not depend on the fermion density n_F if temperature and coupling strength are rescaled to dimensionless variables by (3.52).

The scaling invariance is due to the assumption that the fermion system is very dilute which means that the mean distance between the particles k_F^{-1} is much larger than the range r_0 of the interaction, i.e. $k_F r_0 \ll 1$. Deviations from the scaling and dependences of the phase diagram on n_F will occur for large densities n_F where the mean distance and the range are of the same order so that $k_F r_0 \sim 1$. On the other hand, for very large densities where $k_F r_0 \gg 1$ the effect of the interaction will be strongly reduced by the Pauli blocking. Our self-consistent equations are derived in the dilute limit $k_F r_0 \to 0$. They describe the crossover from BCS superconductivity to Bose–Einstein condensation of bound pairs where the interaction strength $v = 1/(k_F a_F)$ is the relevant parameter which increases from weak to strong coupling. On the other hand, for a constant strong coupling v a crossover from Bose–Einstein condensation to BCS superconductivity may occur as function of an increasing density n_F due to the Pauli blocking. This density dependent crossover has been investigated by Röpke (1994).

The self-consistent equations (3.44)-(3.47) are derived with two assumptions. First, as an approximation in the Bethe–Salpeter equation the irreducible vertex function Γ_1 (the grey circle in the diagrams) is replaced by the bare interaction vertex Γ_0 (the open circle). Secondly, the interaction is assumed to be local in space and (imaginary) time (the interaction potential is a delta function) which leads to considerable simplifications of the vertex function and the Bethe–Salpeter equation: all four equations are just matrix equations, (3.44) and (3.46) in Fourier space and (3.45) and (3.47) in real space and imaginary time. Eventually, the simplifications lead to a self-consistent ladder approximation which is shown in terms of Feynman diagrams in Fig. 3.6. The approximation is conserving because the self energy can be represented as the functional derivative (3.12) with the functional $\Phi[G]$ of (3.43).

B. Ward identity and Thouless criterion

In Sect. 2.4 we have derived the Ward identity (2.57) which implies the Thouless criterion as a consequence: below T_c in the superfluid phase the vertex function Γ has a pole. We now want to figure out if the Thouless criterion is valid also for the vertex function $\Gamma_{\alpha_1\alpha_2}(\mathbb{K}, \Omega_n)$ of our self-consistent equations. If it is valid we expect that the matrix $\Gamma^{-1}_{\alpha_1\alpha_2}(\mathbb{K} = 0, \Omega_n = 0)$ has a zero eigenvalue for $T \leq T_c$. First of all, in our theory we have three kinds of

vertex functions and Bethe–Salpeter equations which are all equivalent because of the local interaction: the black filled circle and the Bethe–Salpeter equation of Fig. 3.5b, the grey square and Fig. 3.6b, and $\Gamma_{\alpha_1\alpha_2}(\boldsymbol{K}, \Omega_n)$ and (3.46). Hence, if the Thouless criterion is valid for the black circle, then it is valid also for $\Gamma_{\alpha_1\alpha_2}(\boldsymbol{K}, \Omega_n)$ and vice versa. Now, let us consider the vertex function Γ identified by the black filled circle. According to Fig. 3.5b this vertex function Γ is defined by the Bethe–Salpeter equation where the irreducible vertex function Γ_1 (grey circle) is approximately replaced by the bare vertex Γ_0 (open circle). Since the irreducible vertex function is defined as the second functional derivative of a functional $\Phi[G]$ by (2.49), here the functional $\Phi_{\mathrm{HF}}[G]$ which generates Γ_0 is given by the first diagram in Fig. 3.5d, i.e. the Hartree–Fock diagram. Thus, the Ward identity (2.55) for Γ of our self-consistent theory will involve the variation of the Hartree–Fock self energy $\delta_\lambda \Sigma_{\mathrm{HF}}$ which will be identified by the order parameter $(\Delta_\alpha) = (\Delta, \Delta^*)$ via $\Sigma^1_{\alpha_1\alpha_2}$ of (3.38) or (3.41). Since the self-consistent equations (3.44)-(3.47) are derived from the functional $\Phi[G]$ in self-consistent ladder approximation which differs from $\Phi_{\mathrm{HF}}[G]$, the right-hand side of (2.55) is not necessarily zero or equivalently $\delta_\lambda A_{\mathrm{HF}} \neq 0$. However, close to T_c where the order parameter Δ is small it is possible to show that $\delta_\lambda A_{\mathrm{HF}} = \mathcal{O}(|\Delta|^3)$. For $H[G]$ in self-consistent ladder approximation Eq. (2.22) reads in short-hand notation

$$\delta H[G]/\delta G = G^{-1} - G_0^{-1} + \Sigma = 0 \,. \tag{3.53}$$

This equation is equivalent to the Dyson equation (3.44). On the other hand for the functional $H_{\mathrm{HF}}[G]$ in Hartree–Fock approximation Eq. (2.21) implies

$$\delta H_{\mathrm{HF}}[G]/\delta G = G^{-1} - G_0^{-1} + \Sigma_{\mathrm{HF}} = -A_{\mathrm{HF}} \,. \tag{3.54}$$

Thus, by combining (3.53) and (3.54) we obtain

$$A_{\mathrm{HF}} = \Sigma - \Sigma_{\mathrm{HF}} \,. \tag{3.55}$$

Since the variation δ_λ is related to a global phase transformation of the fermion field operators $\Psi_X \to \mathrm{e}^{\mathrm{i}\lambda}\Psi_X$, $\delta_\lambda A_{\mathrm{HF}}$ will only possess nondiagonal elements while the diagonal elements are zero. Thus, we must consider the nondiagonal elements of the self energy in (3.45) for small $|\Delta|$. Because of (3.41) the first term in (3.45) is of linear order $\mathcal{O}(|\Delta|)$. In (3.55) this term is canceled by Σ_{HF}. Thus, the order of $\delta_\lambda A_{\mathrm{HF}}$ with respect to $|\Delta|$ is determined by the nondiagonal elements of the second term in (3.45). Let us determine the leading order of this term. Since the leading order of the nondiagonal elements of $\Sigma_{\alpha_1\alpha_2}(\boldsymbol{k}, \omega_n)$ is $\mathcal{O}(|\Delta|)$, the Dyson equation (3.44) implies also $\mathcal{O}(|\Delta|)$ for the nondiagonal elements of $G_{\alpha_1\alpha_2}(\boldsymbol{k}, \omega_n)$ (which is $F(\boldsymbol{k}, \omega_n)$). Then (3.47) implies $\mathcal{O}(|\Delta|^2)$ for the nondiagonal elements of $M_{\alpha_1\alpha_2}(\boldsymbol{K}, \Omega_n)$. Furthermore, (3.46) implies $\mathcal{O}(|\Delta|^2)$ for the nondiagonal elements of $\Gamma_{\alpha_1\alpha_2}(\boldsymbol{K}, \Omega_n)$. Finally, the nondiagonal elements of the second term of the self energy (3.45) are $\mathcal{O}(|\Delta|^3)$. Thus, we find $\delta_\lambda A_{\mathrm{HF}} = \mathcal{O}(|\Delta|^3)$. Inserting this result into (2.55) we eventually obtain the Ward identity

$$\Gamma^{-1}_{\alpha_1\alpha_2}(\mathbb{K}=0,\Omega_n=0)\,\Delta_{\alpha_2}=\mathcal{O}(|\Delta|^3)\ . \tag{3.56}$$

This result implies an important consequence. While the Thouless criterion is not valid for $T<T_c$, it is valid at $T=T_c$. Since $\Gamma^{-1}_{\alpha_1\alpha_2}(\mathbb{K},\Omega)$ is diagonal for $T=T_c$, both eigenvalues are zero in this case so that

$$\Gamma^{-1}_{\alpha_1\alpha_2}(\mathbb{K}=0,\Omega_n=0)=0 \qquad \text{for } T=T_c\ . \tag{3.57}$$

Thus, for our self-consistent theory the Thouless criterion may be used to determine the critical temperature T_c for the superfluid transition. The Ward identity (3.56) guarantees that the Thouless criterion (3.57) yields the same T_c as this one which would be obtained from the order parameter equation (3.40) for $\Delta=0$. Expanding (3.40) in powers of $|\Delta|$ one can show directly that (3.57) is valid in the limit $\Delta\to 0$.

C. Weak coupling limit

From scattering theory it is known that for weak coupling the s-wave scattering length a_F is small. The sign of a_F distinguishes between repulsive and attractive interaction. Since superconductivity with s-wave pairing occurs only for attractive interaction, we assume $a_F<0$. The only length scale in our self-consistent theory is the Fermi wavelength k_F^{-1}. Thus, for the dimensionless coupling parameter v of (3.52) the weak coupling regime is related to the inequality

$$v=1/(k_F a_F)\ll -1\ . \tag{3.58}$$

The weak coupling limit is $a_F\to -0$ or $v\to-\infty$.

In Fig. 3.5 weak coupling means that the bare vertex, i.e. the open circle, is small. Thus, in a lowest order approximation we may replace the vertex function by the bare vertex, i.e. we may replace the black filled circle by the open circle. In this approximation Fig. 3.5c yields the self energy in Hartree–Fock approximation where the anomalous propagators are nonzero. Then, from the Dyson equation (3.11) we obtain the Hartree–Fock equations for the matrix Green's function which turn out to be the well known Gorkov equations for the normal and anomalous Green's functions (see e.g. Abrikosov, Gorkov, and Dzyaloshinskii 1963 or Fetter and Walecka 1971). The Gorkov equations represent the quantum-field theoretic version of the BCS theory, so that in the weak coupling limit the BCS theory is obtained as it should be.

In the self-consistent equations (3.44)-(3.47) for weak coupling $a_F\to -0$ we may approximate the vertex function by the leading term

$$\Gamma_{\alpha_1\alpha_2}(\mathbb{K},\Omega_n)=\frac{4\pi\hbar^2}{m}\,a_F\,\delta_{\alpha_1\alpha_2} \tag{3.59}$$

which is just the scattering amplitude or T matrix of low-energy s-wave scattering. Inserting this vertex function into (3.45) we obtain the Hartree–Fock matrix self energy

$$\left(\Sigma^{\mathrm{HF}}_{\alpha_1\alpha_2}(\boldsymbol{k},\omega_n)\right) = \begin{pmatrix} -(2\pi\hbar^2/m)\cdot n_{\mathrm{F}} a_{\mathrm{F}} & \Delta \\ \Delta^* & +(2\pi\hbar^2/m)\cdot n_{\mathrm{F}} a_{\mathrm{F}} \end{pmatrix} , \tag{3.60}$$

where the fermion density n_{F} is related to the normal Green's function by

$$n_{\mathrm{F}} = -2\,G(\boldsymbol{r}=0,\tau=-0) \; . \tag{3.61}$$

By using the relations $n_{\mathrm{F}} = k_{\mathrm{F}}^3/3\pi^2$ and $\varepsilon_{\mathrm{F}} = \hbar^2 k_{\mathrm{F}}^2/2m$ we can rewrite the self energy matrix as

$$\left(\Sigma^{\mathrm{HF}}_{\alpha_1\alpha_2}(\boldsymbol{k},\omega_n)\right) = \begin{pmatrix} -(4/3\pi)\varepsilon_{\mathrm{F}}\cdot k_{\mathrm{F}} a_{\mathrm{F}} & \Delta \\ \Delta^* & +(4/3\pi)\varepsilon_{\mathrm{F}}\cdot k_{\mathrm{F}} a_{\mathrm{F}} \end{pmatrix} . \tag{3.62}$$

Then, from the Dyson equation (3.44) together with (3.9) we obtain the normal Green's function

$$G(\boldsymbol{k},\omega_n) = u_{\boldsymbol{k}}^2 \frac{1}{-\mathrm{i}\hbar\omega_n + E_{\boldsymbol{k}} - \mu} - v_{\boldsymbol{k}}^2 \frac{1}{\mathrm{i}\hbar\omega_n + E_{\boldsymbol{k}} - \mu} \tag{3.63}$$

and the anomalous Green's function

$$F(\boldsymbol{k},\omega_n) = -\frac{\Delta}{|\Delta|} u_{\boldsymbol{k}} v_{\boldsymbol{k}} \cdot \left[\frac{1}{-\mathrm{i}\hbar\omega_n + E_{\boldsymbol{k}} - \mu} + \frac{1}{\mathrm{i}\hbar\omega_n + E_{\boldsymbol{k}} - \mu}\right] \tag{3.64}$$

which are well known from the BCS theory (see Abrikosov, Gorkov, and Dzyaloshinskii 1963 or Fetter and Walecka 1971). Here $E_{\boldsymbol{k}}$ is the energy dispersion of the fermionic quasiparticles defined by

$$E_{\boldsymbol{k}} - \mu = \sqrt{(\bar{\varepsilon}_{\boldsymbol{k}} - \mu)^2 + |\Delta|^2} \tag{3.65}$$

where

$$\bar{\varepsilon}_{\boldsymbol{k}} = \varepsilon_{\boldsymbol{k}} + (4/3\pi)\varepsilon_{\mathrm{F}}\cdot k_{\mathrm{F}} a_{\mathrm{F}} \tag{3.66}$$

is the dispersion relation of the free particles shifted by the Hartree–Fock energy. Furthermore,

$$u_{\boldsymbol{k}} = \left[\frac{1}{2}\left(1 + \frac{\bar{\varepsilon}_{\boldsymbol{k}} - \mu}{E_{\boldsymbol{k}} - \mu}\right)\right]^{1/2} , \qquad v_{\boldsymbol{k}} = \left[\frac{1}{2}\left(1 - \frac{\bar{\varepsilon}_{\boldsymbol{k}} - \mu}{E_{\boldsymbol{k}} - \mu}\right)\right]^{1/2} \tag{3.67}$$

are the coefficients of the canonical transformation which satisfy the relations $u_{\boldsymbol{k}}^2 + v_{\boldsymbol{k}}^2 = 1$, $u_{\boldsymbol{k}}^2 - v_{\boldsymbol{k}}^2 = (\bar{\varepsilon}_{\boldsymbol{k}} - \mu)/(E_{\boldsymbol{k}} - \mu)$, and $u_{\boldsymbol{k}} v_{\boldsymbol{k}} = |\Delta|/[2(E_{\boldsymbol{k}} - \mu)]$.

The order parameter Δ is determined by (3.40). Inserting the anomalous Green's function (3.64) into this equation and dividing by Δ, after some manipulations we obtain

$$1 = -\frac{4\pi\hbar^2}{m} a_{\mathrm{F}} \int \frac{\mathrm{d}^3 k}{(2\pi)^3} \left[\frac{1}{2(E_{\boldsymbol{k}} - \mu)} \mathrm{th}\left(\tfrac{1}{2}\beta(E_{\boldsymbol{k}} - \mu)\right) - \frac{m}{\hbar^2 \boldsymbol{k}^2}\right] \tag{3.68}$$

which is the well known gap equation of the BCS theory. The chemical potential μ is determined by the density equation (3.61). Inserting the normal Green's function (3.63) after some manipulations we obtain

$$n_{\mathrm{F}} = \int \frac{\mathrm{d}^3k}{(2\pi)^3} \left[1 - \frac{\bar{\varepsilon}_k - \mu}{E_k - \mu} \mathrm{th}\big(\tfrac{1}{2}\beta(E_k - \mu)\big) \right] . \tag{3.69}$$

Because in the BCS theory $k_{\mathrm{B}}T_{\mathrm{c}}$ and Δ are exponentially small compared to the energy scale ε_{F}, Eq. (3.69) is well satisfied by the chemical potential

$$\mu = \varepsilon_{\mathrm{F}}\big[1 + (4/3\pi)k_{\mathrm{F}}a_{\mathrm{F}}\big] . \tag{3.70}$$

The correction term depending on a_{F} arises from the Hartree–Fock contribution of the self energy. With this value for μ the gap equation (3.68) can be solved in the weak coupling regime (3.58). For $T = 0$ we obtain the order parameter (energy gap)

$$\Delta_0 = (8/\mathrm{e}^2) \cdot \varepsilon_{\mathrm{F}} \cdot \exp(\pi/2k_{\mathrm{F}}a_{\mathrm{F}}) , \tag{3.71}$$

and for $\Delta = 0$ we obtain the critical temperature

$$k_{\mathrm{B}}T_{\mathrm{c}} = (\mathrm{e}^{\gamma_{\mathrm{E}}}/\pi) \cdot (8/\mathrm{e}^2) \cdot \varepsilon_{\mathrm{F}} \cdot \exp(\pi/2k_{\mathrm{F}}a_{\mathrm{F}}) \tag{3.72}$$

where $\gamma_{\mathrm{E}} = 0.5772$ is the Euler number. The inequality (3.58) implies that Δ_0 and $k_{\mathrm{B}}T_{\mathrm{c}}$ are indeed exponentially small. Finally we obtain the ratio

$$2\Delta_0/k_{\mathrm{B}}T_{\mathrm{c}} = 2\pi \cdot \mathrm{e}^{-\gamma_{\mathrm{E}}} \approx 3.528 \tag{3.73}$$

which is well known from the BCS theory (Bardeen, Cooper, and Schrieffer 1957). We conclude that in the weak coupling limit $v = 1/(k_{\mathrm{F}}a_{\mathrm{F}}) \to -\infty$ the self-consistent equations (3.44)-(3.47) reproduce the BCS theory correctly. Also, for $T > T_{\mathrm{c}}$ the basic results of the Fermi liquid theory are obtained: in an expansion up to $(k_{\mathrm{F}}a_{\mathrm{F}})^2$ the results of Galitskii (1958) of the energy and damping of the fermionic quasiparticles are recovered.

D. Strong coupling limit

While in the regime of weak attractive interaction it is $-\infty < v \ll -1$, the dimensionless coupling parameter $v = 1/(k_{\mathrm{F}}a_{\mathrm{F}})$ can vary in the hole range $-\infty < v < +\infty$. With increasing v the strength of the interaction increases. As long as v or a_{F}^{-1} is negative there are only unbound scattering states in the two-particle problem. From the theory of low-energy s-wave scattering (see e.g. Landau and Lifshitz vol. 3) it is known that $a_{\mathrm{F}}^{-1} = 0$ is a threshold value of the interaction strength above which the fermions will bind into pairs. A virtual scattering state for $a_{\mathrm{F}}^{-1} < 0$ turns into a bound state for $a_{\mathrm{F}}^{-1} > 0$. Thus, for our many-particle system we expect that bound pairs will form for positive v. The diameter of the pairs is about a_{F} while k_{F}^{-1} is a measure for the average distance between the fermions and hence also a measure for the distance between the pairs. Thus, if we require

$$v = 1/(k_{\mathrm{F}}a_{\mathrm{F}}) \gg +1 \tag{3.74}$$

for the strong coupling regime, the distance between the pairs is much larger than their size so that the pairs are well defined particles which form a weakly interacting Bose gas. For a two-particle system the binding energy of a pair is

$$\varepsilon_{\mathrm{b}} = \hbar^2/ma_{\mathrm{F}}^2 \ . \tag{3.75}$$

The inequality (3.74) implies $\varepsilon_{\mathrm{F}} \ll \varepsilon_{\mathrm{b}}$ so that for low temperatures quantum fluctuations are too small to break pairs into single fermions. For much lower temperatures $k_{\mathrm{B}}T \lesssim 0.2\varepsilon_{\mathrm{F}}$ the system becomes superfluid as we will show below.

In the strong coupling limit $v \to +\infty$ the scattering length a_{F} is small and positive, so that as in the weak coupling limit also for strong couplings an expansion with respect to powers of $k_{\mathrm{F}}a_{\mathrm{F}}$ can be performed. (One should keep in mind that the relation between a_{F} and the interaction strength is not unique. A small positive a_{F} can describe either a Fermi liquid with weak repulsive interactions or a Bose liquid of tightly bound fermion pairs which is considered here.) As in subsection C in lowest order the vertex function $\Gamma_{\alpha_1\alpha_2}(\boldsymbol{K}, \Omega_n)$ is given by (3.59). From the Dyson equation the normal Green's function (3.63) and the anomalous Green's function (3.64) are obtained where the parameters of the canonical transformation are defined in (3.65)-(3.67). These are the Green's functions of the BCS theory which in lowest order are valid also for the strong coupling limit. The expansion in powers of $k_{\mathrm{F}}a_{\mathrm{F}}$ is then obtained by iterating the self-consistent equations (3.44)-(3.47). Inserting the Green's functions (3.63) and (3.64) into (3.47) or (3.34) we obtain the renormalized pair propagator $M_{\alpha_1\alpha_2}(\boldsymbol{K}, \Omega_n)$. The sum over the Matsubara frequencies in (3.34) can be performed exactly. Then, from (3.46) we obtain the inverse vertex function in first iteration. For $\boldsymbol{K} = \boldsymbol{0}$ and $\Omega_n = 0$ we obtain

$$\left(\Gamma^{-1}_{\alpha_1\alpha_2}(\boldsymbol{K} = \boldsymbol{0}, \Omega_n = 0)\right) = \begin{pmatrix} C - A|\Delta|^2 & A\Delta^2 \\ A(\Delta^*)^2 & C - A|\Delta|^2 \end{pmatrix} \tag{3.76}$$

where

$$C = \frac{m}{4\pi\hbar^2}\, a_{\mathrm{F}}^{-1} + \int \frac{\mathrm{d}^3k}{(2\pi)^3} \left[\frac{1}{2(E_{\boldsymbol{k}} - \mu)} \mathrm{th}\left(\tfrac{1}{2}\beta(E_{\boldsymbol{k}} - \mu)\right) - \frac{m}{\hbar^2\boldsymbol{k}^2} \right] \tag{3.77}$$

and

$$A = \int \frac{\mathrm{d}^3k}{(2\pi)^3} \frac{\mathrm{th}\left(\frac{1}{2}\beta(E_{\boldsymbol{k}} - \mu)\right)}{4(E_{\boldsymbol{k}} - \mu)^3} \ . \tag{3.78}$$

The integrals of (3.77) and (3.78) are finite, the ultraviolet divergence in (3.77) is subtracted by the last term. The order-parameter equation (3.40) written in the form (3.68) implies $C = 0$ for $T \leq T_{\mathrm{c}}$. For this reason the matrix (3.76) is singular: one of the eigenvalues is zero. This fact represents the Thouless criterion for $T \leq T_{\mathrm{c}}$ which is a consequence of the Ward identity (2.57). The Green's functions (3.63) and (3.64) are the correct solutions of the

self-consistent equations in Hartree–Fock approximation. The related functional $\Phi_{\mathrm{HF}}[G]$ is given by the first diagram of Fig. 3.5d. Hence the irreducible vertex function Γ_1 is the bare interaction vertex, so that the vertex function Γ which appears in the Ward identity (2.57) is defined by the Bethe–Salpeter equation of Fig. 3.5b where the thick propagator lines are identified by the Hartree–Fock Green's functions (3.63) and (3.64). Thus, Eq. (3.76) represents the Hartree–Fock vertex function which satisfies the Ward identity exactly, i.e. (3.56) with a zero on the right-hand side for all $T \leq T_c$. However, for vertex functions $\Gamma_{\alpha_1\alpha_2}(\boldsymbol{K}, \Omega_n)$ beyond the Hartree–Fock approximation (i.e. in higher order iterations or eventually the solution of the self-consistent equations) the right-hand side of (3.56) will be nonzero.

The $\boldsymbol{K}$ and Ω_n dependence of $\Gamma^{-1}_{\alpha_1\alpha_2}(\boldsymbol{K}, \Omega_n)$ of the first iteration is quite complicated. While in the pair propagator (3.34) the ω_n summation is performed exactly, the $\boldsymbol{k}$ integral cannot be evaluated explicitly in general. However, in the strong coupling limit $v \to +\infty$ the binding energy ε_b is very large so that we may expand in powers of ε_b^{-1}. Supposed $k_B T$, $\hbar\Omega_n$, $\hbar^2\boldsymbol{K}^2/4m$, and $|\Delta|$ are much smaller than ε_b, then the $\boldsymbol{k}$ integrals can be evaluated exactly in an expansion up to the leading order. Thus, for the inverse vertex function we obtain

$$\begin{aligned}\left(\Gamma^{-1}_{\alpha_1\alpha_2}(\boldsymbol{K}, \Omega_n)\right) &= -[8\pi\varepsilon_b^2 a_F^3]^{-1} \\ &\cdot \begin{pmatrix} -\mathrm{i}\hbar\Omega_n + \frac{\hbar^2\boldsymbol{K}^2}{4m} + \frac{|\Delta|^2}{2\varepsilon_b} & -\frac{\Delta^2}{2\varepsilon_b} \\ -\frac{(\Delta^*)^2}{2\varepsilon_b} & \mathrm{i}\hbar\Omega_n + \frac{\hbar^2\boldsymbol{K}^2}{4m} + \frac{|\Delta|^2}{2\varepsilon_b} \end{pmatrix} \end{aligned} \tag{3.79}$$

in the strong coupling limit $v \to +\infty$ up to leading order in ε_b^{-1}. Multiplying by a factor $-8\pi\varepsilon_b^2 a_F^3$ this function precisely looks like the inverse Green's function of a superfluid interacting boson system in Hartree–Fock approximation. For this reason we conclude that the vertex function $\Gamma_{\alpha_1\alpha_2}(\boldsymbol{K}, \Omega_n)$ describes the bosonic degrees of freedom and in the strong coupling limit $v \to +\infty$ it can be identified by a boson Green's function

$$G_{\mathrm{B},\alpha_1\alpha_2}(\boldsymbol{K}, \Omega_n) = -[8\pi\varepsilon_b^2 a_F^3]^{-1} \cdot \Gamma_{\alpha_1\alpha_2}(\boldsymbol{K}, \Omega_n) \,. \tag{3.80}$$

Since the vertex function has necessarily the limit $\lim_{r\to\infty} \Gamma_{\alpha_1\alpha_2}(r, \tau) = 0$ the mean-field term $\Psi_B\Psi_B^*$, where Ψ_B is the order parameter of the bosons, is separated so that (3.80) is the *connected* boson Green's function. For this reason the related boson density

$$n_B^1 = G_{\mathrm{B},11}(r = 0, \tau = -0) = -[8\pi\varepsilon_b^2 a_F^3]^{-1} \cdot \Gamma_{11}(r = 0, \tau = -0) \tag{3.81}$$

only contains the *noncondensed* bosons. The bosons in the condensate have the density

$$n_B^0 = |\Psi_B|^2 \tag{3.82}$$

so that the total boson density is $n_B = n_B^0 + n_B^1$. The identifications of the boson Green's function (3.80) and of the boson density (3.81) are correct

only up to leading order in the strong coupling limit $v \to +\infty$. For finite $v = 1/(k_F a_F)$ there will be corrections. The boson density defined formally in (3.81) is not precisely the density of bound pairs, there is a relative correction of the order $(k_F a_F)^3$ (Haussmann 1993).

Since the bosons are bound pairs of fermions, we expect a relation $n_F = 2n_B$ between the fermion density and the boson density. To establish this relation in the strong coupling limit, we consider n_F defined by (3.61). Inserting the normal Green's function (3.63) of the Hartree–Fock approximation into (3.61), we obtain (3.69) which can be written in the form

$$\begin{aligned} n_F &= 2\int \frac{d^3k}{(2\pi)^3}\left[\frac{1}{2}\left(1-\frac{\bar{\varepsilon}_k-\mu}{E_k-\mu}\right)+\frac{\bar{\varepsilon}_k-\mu}{E_k-\mu}\cdot\frac{1}{e^{\beta(E_k-\mu)}+1}\right] \\ &= n_F^0 + n_F^1 \,. \end{aligned} \tag{3.83}$$

The second term contains a Fermi distribution function so that n_F^1 is the density of the single fermions. On the other hand the first term n_F^0 represents the fermions involved in the superfluidity. For $k_B T \ll \varepsilon_b$ nearly all fermions are bound into pairs so that there are nearly no single fermions. Hence n_F^1 is exponentially small and may be neglected. The integral of n_F^0 can be evaluated up to leading order in ε_b^{-1}. We obtain

$$n_F^0 = 2\,[8\pi\varepsilon_b^2 a_F^3]^{-1}|\Delta|^2 \,. \tag{3.84}$$

Since Δ is the order parameter of the superfluid phase transition which must be proportional to the bosonic order parameter Ψ_B, the density n_F^0 represents the fermions bound into pairs which belong to the bosons in the condensate. Expecting the relation $n_F^0 = 2n_B^0$ we identify the bosonic order parameter

$$\Psi_B = \pm i[8\pi\varepsilon_b^2 a_F^3]^{-1/2}\Delta \,. \tag{3.85}$$

(The factor $\pm i$ is necessary as a convention because of the minus sign of the nondiagonal elements in (3.79)). Now, adding the terms together we obtain the fermion density $n_F = 2|\Psi_B|^2 + n_F^1$ which includes the bound pairs in the condensate and the single fermions. However, the expected contribution $2n_B^1$ of the noncondensed bosons is missing. Thus, we conclude that the Green's functions (3.63) and (3.64) of the Hartree–Fock approximation do not include the noncondensed bound pairs.

To improve this deficiency we must perform one more iteration of the self-consistent equations (3.44)-(3.47). While in the self energy (3.45) the first term $\Sigma^1_{\alpha_1\alpha_2}$ remains unchanged, in the second term we insert the vertex function obtained from (3.79). In the superfluid system the bosonic degrees of freedom are slow modes because of the symmetry breaking. For this reason, $\Gamma_{\alpha_1\alpha_2}(\boldsymbol{r},\tau)$ is a slowly varying function in $\boldsymbol{r}$ and τ. On the other hand, since $\mu \approx -\varepsilon_b/2$ is quite large for strong couplings, the fermion Green's function $G_{\alpha_1\alpha_2}(\boldsymbol{r},\tau)$ is nonzero only in a small area around $(\boldsymbol{r},\tau) = (\boldsymbol{0},0)$. Thus, the second term of the self energy can be approximated by

$$\tilde{\Sigma}_{\alpha_1\alpha_2}(r,\tau) = G_{\alpha_2\alpha_1}(-r,-\tau)\Gamma_{\alpha_1\alpha_2}(0,0) \ . \tag{3.86}$$

(There is a subtlety in choosing either $\tau = +0$ or $\tau = -0$ in the vertex function, because the fermion Green's function and the vertex function are discontinuous at $\tau = 0$.) Since in the strong coupling limit the anomalous Green's function (3.64) is much smaller than the normal Green's function (3.63) by a factor $|\Delta|/\varepsilon_b$, the nondiagonal terms of the self energy (3.86) may be neglected. Then, using (3.81) we obtain

$$\tilde{\Sigma}_{\alpha_1\alpha_2}(r,\tau) = -[8\pi\varepsilon_b^2 a_F^3]\cdot n_B^1\,\delta_{\alpha_1\alpha_2}G_{\alpha_2\alpha_1}(-r,-\tau) \ . \tag{3.87}$$

Adding the first term and performing the Fourier transformation we obtain the self energy

$$\Sigma_{\alpha_1\alpha_2}(k,\omega_n) = \Sigma^1_{\alpha_1\alpha_2} - [8\pi\varepsilon_b^2 a_F^3]\cdot n_B^1\,\delta_{\alpha_1\alpha_2}G_{\alpha_2\alpha_1}(-k,-\omega_n) \ . \tag{3.88}$$

We insert this self energy into the Dyson equation (3.44) to evaluate the normal and anomalous Green's functions. Since the second term of the self energy (3.88) explicitly depends on n_B^1, now the noncondensed bosons are included. Since $n_B^1 a_F^3 \sim (k_F a_F)^3$ is small in the strong coupling limit, we may expand the Green's functions. The first order term yields a correction proportional to n_B^1. Finally, we insert the normal Green's function into (3.61), evaluate the Matsubara frequency sum and the Fourier integral so that eventually we obtain a correction $\Delta n_F = 2n_B^1$ for the fermion density as expected (for more details of the calculation see Sect. 3.B of Haussmann 1993). Thus, together with this correction the fermion density is

$$n_F = 2n_B^0 + n_F^1 + 2n_B^1 = 2n_B + n_F^1 \ . \tag{3.89}$$

For $k_B T \ll \varepsilon_b$ the single fermion contribution n_F^1 can be neglected so that $n_F = 2n_B$. We conclude that for an appropriate treatment of the noncondensed bound pairs the self-consistent equations must be iterated at least once (the Green's functions in Hartree–Fock approximation (3.63) and (3.64) are identified as the zeroth iteration). We can be sure that in the exact solution of the self-consistent equations (which is obtained when the iteration procedure has converged) the bound fermion pairs, condensed and noncondensed, are treated correctly, because the self-consistent equations are derived by a *conserving approximation* so that none of the fermions is lost.

For strong couplings the system is a weakly interacting Bose gas of tightly bound fermion pairs. Thus, it should be possible to eliminate the fermion degrees of freedom and to derive the self-consistent equations for the boson Green's function alone. To do this we consider the self-consistent equations (3.44)-(3.47) and eliminate the fermion Green's function $G_{\alpha_1\alpha_2}(k,\omega_n)$. In the strong coupling limit $v \to +\infty$ the scattering length a_F is small so that the vertex function $\Gamma_{\alpha_1\alpha_2}(K,\Omega_n)$ can be treated as a small quantity for an expansion. We consider the self energy (3.45) and insert the mean-field

Green's functions (3.63) and (3.64) for $G_{\alpha_1\alpha_2}(\boldsymbol{r},\tau)$. Then we insert this self energy into the Dyson equation (3.44) to determine a new Green's function in first iteration. We expand up to first order with respect to the second term of the self energy and obtain a correction $\Delta G_{\alpha_1\alpha_2}(\boldsymbol{k},\omega_n)$ for the Green's function (this correction yields the contribution $2n_{\mathrm{B}}^1$ in the fermion density (3.89) as we have shown above). Next, we insert the new Green's function into (3.47) or (3.34) to determine the correction for the renormalized pair propagator. As a result we obtain

$$\Delta M_{\alpha_1\alpha_2}(\boldsymbol{K},\Omega_n) = \sum_{\alpha_1\alpha_2}\int\frac{\mathrm{d}^3K'}{(2\pi)^3}\,\frac{1}{\beta}\sum_{\Omega_n'} F_{\alpha_1\alpha_2,\alpha_{2'}\alpha_{1'}}(\boldsymbol{K},\Omega_n;\boldsymbol{K}',\Omega_n') \cdot\Gamma_{\alpha_{1'}\alpha_{2'}}(\boldsymbol{K}',\Omega_n') \tag{3.90}$$

where

$$F_{\alpha_1\alpha_2,\alpha_{2'}\alpha_{1'}}(\boldsymbol{K},\Omega_n;\boldsymbol{K}',\Omega_n') = 2\int\frac{\mathrm{d}^3k}{(2\pi)^3}\,\frac{1}{\beta}\sum_{\omega_n} G_{\alpha_1\alpha_2}(\boldsymbol{K}-\boldsymbol{k},\Omega_n-\omega_n) \cdot G_{\alpha_1\alpha_{1'}}(\boldsymbol{k},\omega_n)G_{\alpha_{2'}\alpha_2}(\boldsymbol{k},\omega_n)G_{\alpha_{2'}\alpha_{1'}}(\boldsymbol{K}'-\boldsymbol{k},\Omega_n'-\omega_n)\ . \tag{3.91}$$

Here we insert (3.63) and (3.64) for the fermion Green's function. Then from (3.46) we obtain a self-consistent equation for the vertex function $\Gamma_{\alpha_{1'}\alpha_{2'}}(\boldsymbol{K}',\Omega_n')$ alone. This equation is given by (3.79) where on the right-hand side the correction (3.90) must be added. The resulting equation is similar to the self-consistent equation of a superfluid interacting Bose system in Hartree–Fock approximation. The function (3.91) may be interpreted as the interaction vertex for the interaction between the fermion pairs. In Fig. 3.7 this is shown in terms of Feynman diagrams. The square of propagator lines corresponds to the four fermion Green's functions in (3.91). Here 2, 1′ are the two incoming pairs which scatter and 1, 2′ are the outgoing pairs. During the scattering process each of the two pairs exchanges one fermion with the other pair: while the propagator lines 12 and 2′1′ correspond to the

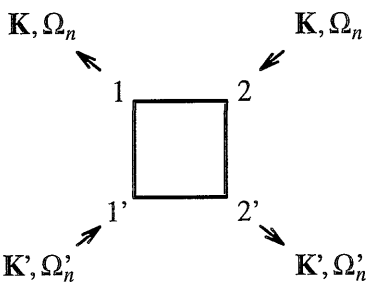

Fig. 3.7. Feynman diagram for the interaction vertex $F_{\alpha_1\alpha_2,\alpha_{2'}\alpha_{1'}}(\boldsymbol{K},\Omega_n;\boldsymbol{K}',\Omega_n')$ for the interaction between the fermion pairs. The four propagator lines of the square represent the four fermion Green's functions in (3.91).

two fermions that remain in the pairs, the lines $11'$ and $2'2$ represent the two fermions that are exchanged. Thus, the leading interaction between the pairs is generated by the exchange of two fermions between the pairs. This interaction is a result of the Pauli exclusion principle for the fermions and hence must be repulsive. In the strong coupling limit $v \to +\infty$ we expand the function (3.91) in powers of $\varepsilon_{\mathrm{b}}^{-1}$. Up to leading order we obtain (Haussmann 1993)

$$F_{\alpha_1\alpha_2,\alpha_{2'}\alpha_{1'}}(\mathbb{K},\Omega_n;\mathbb{K}',\Omega_n') = \delta_{\alpha_1\alpha_2}\delta_{\alpha_{1'}\alpha_{2'}}\delta_{\alpha_1\alpha_{1'}}F_0 \tag{3.92}$$

where

$$F_0 = [8\pi\varepsilon_{\mathrm{b}}^2 a_{\mathrm{F}}^3]^{-1}\cdot\varepsilon_{\mathrm{b}}^{-1}\ . \tag{3.93}$$

Inserting this result into (3.90) we obtain

$$\begin{aligned}\Delta M_{\alpha_1\alpha_2}(\mathbb{K},\Omega_n) &= [8\pi\varepsilon_{\mathrm{b}}^2 a_{\mathrm{F}}^3]^{-1}\varepsilon_{\mathrm{b}}^{-1}\cdot\Gamma_{11}(r=0,\tau=0)\,\delta_{\alpha_1\alpha_2}\\ &= -\varepsilon_{\mathrm{b}}^{-1}n_{\mathrm{B}}^1\,\delta_{\alpha_1\alpha_2}\ .\end{aligned} \tag{3.94}$$

Now, adding this correction to the right-hand side of (3.79) we obtain the self-consistent equation for the boson Green's function defined in (3.80) which reads after some manipulations

$$\begin{aligned}&\left(G^{-1}_{\mathrm{B},\alpha_1\alpha_2}(\mathbb{K},\Omega_n)\right) =\\ &\quad=\begin{pmatrix} -\mathrm{i}\hbar\Omega_n + \frac{\hbar^2\boldsymbol{K}^2}{4m} + 2T_{\mathrm{B}}n_{\mathrm{B}} - \mu_{\mathrm{B}} & T_{\mathrm{B}}\Psi_{\mathrm{B}}^2\\ T_{\mathrm{B}}(\Psi_{\mathrm{B}}^*)^2 & \mathrm{i}\hbar\Omega_n + \frac{\hbar^2\boldsymbol{K}^2}{4m} + 2T_{\mathrm{B}}n_{\mathrm{B}} - \mu_{\mathrm{B}}\end{pmatrix}\end{aligned} \tag{3.95}$$

where $n_{\mathrm{B}} = |\Psi_{\mathrm{B}}|^2 + n_{\mathrm{B}}^1$ and

$$T_{\mathrm{B}} = [8\pi\varepsilon_{\mathrm{b}}^2 a_{\mathrm{F}}^3]\cdot(2\varepsilon_{\mathrm{b}})^{-1} = \frac{4\pi\hbar^2}{2m}\cdot 2a_{\mathrm{F}}\ . \tag{3.96}$$

While in (3.79) $C = 0$ has been assumed, here we evaluate the k integral of (3.77) and obtain $C = -[8\pi\varepsilon_{\mathrm{b}}^2 a_{\mathrm{F}}^3]^{-1}(-\mu_{\mathrm{B}} + |\Delta|^2/2\varepsilon_{\mathrm{b}})$ where $\mu_{\mathrm{B}} = 2\mu + \varepsilon_{\mathrm{b}}$ is the chemical potential of the pairs. A boson Green's function $G_{\mathrm{B},\alpha_1\alpha_2}(\mathbb{K},\Omega_n)$ with the same structure as (3.95) can be obtained directly for the interacting Bose system in Hartree–Fock approximation. Thus, a comparison of our Fermi system in the strong coupling limit with a weakly interacting Bose system is possible. The order parameter Ψ_{B} is defined by the quantum average of a boson field operator and is related to Δ by (3.85). In (3.95) T_{B} is identified as the T matrix or scattering amplitude of the bosons. In analogy to (3.30) the T matrix can be expressed in terms of the s-wave scattering length of the bosons a_{B} by

$$T_{\mathrm{B}} = \frac{4\pi\hbar^2}{2m}\cdot a_{\mathrm{B}} \tag{3.97}$$

where $2m$ is the mass of the fermion pairs. Hence, from (3.96) and (3.97) we obtain the relation (Haussmann 1993)

$$a_B = 2a_F \tag{3.98}$$

(which has been obtained independently also by Sá de Melo et al. 1993). Thus, we explicitly find an effective interaction between the pairs which is related to the original attractive interaction between the fermions by (3.98). The inequality for strong coupling (3.74) implies $0 < k_F a_F \ll 1$ so that a_B is small and positive. Hence, the interaction between the pairs is *weak* and *repulsive*. In (3.95) we clearly see that the interaction of the condensed and also of the noncondensed pairs is included: the terms with T_B and Ψ_B represent the interaction between the condensed pairs while the terms with T_B and n_B^1 represent the interaction between the noncondensed pairs.

Since for strong couplings the Fermi system is a weakly interacting Bose gas of bound pairs, we expect that the system becomes superfluid below a critical temperature T_c which is approximately the temperature $T_{c,BE}$ for Bose–Einstein condensation of an ideal Bose gas. For $d = 3$ dimensions this temperature is

$$T_{c,BE} = \frac{2\pi\hbar^2}{2mk_B} \cdot \left(\frac{n_F/2}{\zeta(3/2)}\right)^{2/3} = 0.2180 \cdot \varepsilon_F/k_B \tag{3.99}$$

where $n_B = n_F/2$ is the density and $m_B^* = 2m$ the mass of the bosons. Here $\zeta(z)$ is the Riemann zeta function. For $d = 3$ dimensions, in the strong coupling limit the system becomes a weakly interacting Bose gas where the interaction strength tends to zero. Hence it is $\lim_{v\to+\infty} T_c = T_{c,BE}$. Since (3.79) and (3.95) are mean-field boson Green's functions, in leading order our theory yields $T_c = T_{c,BE}$ for strong couplings. However, for finite v there will be a correction of order $v^{-3} = (k_F a_F)^3$ which is caused by a correction to the effective boson mass m_B^* in (3.99) (Haussmann 1993). For a weakly interacting boson system in perturbation theory it is well known (Fetter and Walecka 1971) that the effective boson mass m_B^* increases if the interaction has a finite range. For our system of interacting fermion pairs we obtain (Haussmann 1993)

$$m_B^* = 2m \cdot [1 + (3\pi)^{-1}(k_F a_F)^3] \,. \tag{3.100}$$

To derive this result we need a correction of the coefficients of the terms $\hbar\Omega_n$ and $\hbar^2\boldsymbol{K}^2/4m$ in (3.95). Since (3.92) does not yield such a correction, we must expand the boson interaction vertex (3.91) up to one order higher in ε_b^{-1}. Now, replacing $2m$ in (3.99) by the effective mass (3.100) we obtain (Haussmann 1993)

$$T_c = T_{c,BE} \cdot [1 - (3\pi)^{-1}(k_F a_F)^3] \,. \tag{3.101}$$

Thus, the leading effect of the interaction between the fermion pairs is a depression of the critical temperature for the superfluid transition. The previous theories for the crossover which approximate the fermionic degrees of

freedom by the mean-field Green's functions (3.63) and (3.64) (Nozières and Schmitt-Rink 1985, Drechsler and Zwerger 1992, and Sá de Melo et al. 1993) do not include the interaction between the noncondensed pairs and hence do not obtain the correction term of (3.101) which would lead to a depression of T_c. However, in the extension of the Ginzburg–Landau theory beyond the mean-field approximation the interaction between the noncondensed pairs is included so that the asymptotic formulas of the effective mass (3.100) and of the critical temperature (3.101) for strong couplings have been obtained also within this approach (Stintzing 1996).

In a recent numerical investigation of the hard sphere Bose gas Grüter, Ceperley, and Laloë (1997) have found an enhancement of T_c for low densities where the system is dilute, while for higher densities T_c is depressed which agrees with our asymptotic formula (3.101). Furthermore, also in analytical calculations an enhancement of T_c has been found (Stoof 1992, Bijlsma and Stoof 1996). If this observation is correct, then for very strong couplings, where the system is a dilute interacting Bose gas, our asymptotic formula (3.101) would be incorrect. The correction should be proportional to $+k_F a_F$ with positive sign. Thus, the correct form of the asymptotic formula for T_c for very strong couplings remains as an open question.

E. The crossover region

We have shown above that in the weak coupling limit and in the strong coupling limit the self-consistent equations (3.44)-(3.47) can be solved approximately by an expansion in powers of $k_F a_F$ starting with the mean-field fermion Green's functions (3.63) and (3.64). However, in the crossover region

$$-1 \lesssim v \lesssim +1 \tag{3.102}$$

$v^{-1} = k_F a_F$ is no longer a small parameter so that the mean-field approximation is invalid there and a full self-consistent treatment becomes necessary. For this reason, the previous theories (Leggett 1980, Nozières and Schmitt-Rink 1985, Drechsler and Zwerger 1992, and Sá de Melo et al. 1993) which are based on a mean-field approximation yield only crude interpolations in the crossover region between the two limiting cases.

It is possible to rederive the previous theories from our self-consistent equations. Leggett's theory (Leggett 1980) is based on the BCS gap equation (3.68) and the fermion density equation (3.69). Since (3.69) does not include the contribution $2n_B^1$ of the noncondensed fermion pairs, this theory is valid only for $T = 0$. The critical temperature T_c of Nozières and Schmitt-Rink (1985) is obtained from the Thouless criterion (3.57) by calculating the vertex function via (3.46) and (3.47) where the free fermion Green's function is inserted into (3.47). The Ginzburg–Landau theory of Drechsler and Zwerger (Drechsler 1991, Drechsler and Zwerger 1992) can be derived from the

Ward identity (3.56) where the vertex function is determined in Hartree–Fock approximation so that the right-hand side of (3.56) is exactly zero. This means that we calculate the vertex function by (3.46) and (3.47) where the mean-field fermion Green's functions (3.63) and (3.64) are inserted into (3.47). Then the inverse vertex function $\Gamma^{-1}_{\alpha_1\alpha_2}(\boldsymbol{K}, \Omega_n)$ is expanded up to first order in $\hbar\Omega_n$, $\hbar^2\boldsymbol{K}^2/4m$, and $|\Delta|^2$, so that from (3.56) we obtain the Ginzburg–Landau equation after a Fourier back transformation.

It is also possible to derive the *time-dependent* Ginzburg–Landau equation of Sá de Melo et al. (1993). To do this we perform an analytical continuation to complex frequencies $\mathrm{i}\Omega_n \to z$ in the inverse vertex function, expand up to first order in $\hbar z$, $\hbar^2\boldsymbol{K}^2/2m$, and $|\Delta|^2$, set the frequency real by $z = \omega + \mathrm{i}0$, and perform a Fourier back transformation to real space and real time. Thus we obtain the time-dependent Ginzburg–Landau equation

$$d\,\mathrm{i}\hbar\frac{\partial\Delta(\boldsymbol{r},\tau)}{\partial t} = \left[-c\frac{\hbar^2}{2m}\boldsymbol{\nabla}^2 + a + b|\Delta(\boldsymbol{r},t)|^2\right]\Delta(\boldsymbol{r},t) \tag{3.103}$$

where a, b, c, and $d = d' + \mathrm{i}d''$ are the parameters of the equation which can be expressed in terms of some $\boldsymbol{k}$ integrals similar to (3.77) and (3.78). The analytical continuation implies that $d = d' + \mathrm{i}d''$ is complex while the other parameters a, b, and c are real. The imaginary part $d'' > 0$ implies a damping in the Ginzburg–Landau equation. Requiring the similarity of (3.103) with a Schrödinger equation we define the effective boson mass

$$m^*_{\mathrm{B}} = m\,(d' + \mathrm{i}d'')/c\,. \tag{3.104}$$

While in the strong coupling limit we obtain (3.100), for weak couplings the effective mass can be evaluated explicitly, too (Haussmann 1994a). By definition m^*_{B} may be complex and thus may have an imaginary part which corresponds to a damping in the system.

3.3 Numerical results for $T = T_c$ and discussion

In the limits of weak and strong coupling $k_{\mathrm{F}}a_{\mathrm{F}}$ is a small parameter so that it is possible to solve the self-consistent equations approximately. Thus, we have recovered the BCS theory in the weak coupling limit and the weakly interacting superfluid Bose gas in the strong coupling limit. The approximation works because the relevant quasiparticles, the fermions and the bosons, are well defined and have long life times. However, for intermediate couplings $-1 \lesssim v = 1/(k_{\mathrm{F}}a_{\mathrm{F}}) \lesssim +1$ in the crossover region the fermionic and bosonic quasiparticles are short-living. Here the self consistency of the equations (3.44)-(3.47) is essential to deal with the nontrivial spectra of the quasiparticles. Thus the self-consistent equations must be solved numerically, which can be done by the following iteration procedure. We start by inserting the mean-field Green's functions (3.63) and (3.64) into (3.47) and (3.45) and

then determine Γ and G in first order by (3.46) and (3.44), respectively. The next iteration step is done by inserting the first-order G into (3.47) and (3.45) again. The iteration procedure is repeated until convergence is achieved. In practice it turns out that 13 iterations are sufficient. While in (3.44) and (3.46) the functions are represented in Fourier space, in (3.45) and (3.47) the functions are represented in real space. Thus, we need a numerical procedure for the Fourier transformations (3.10) and (3.20) to perform the iteration procedure. The functions G and Γ have rather nontrivial singularities. We must transform functions which vary characteristically on a *logarithmic scale* over 6 to 10 decades. Since a standard fast Fourier transformation (see e.g. Stoer 1983) cannot be used because it assumes a constant step width, we have invented a special slow Fourier transformation (Haussmann 1994a). We discretize the functions on a logarithmic scale over 6 to 10 decades with only 100 points in each dimension, interpolate the functions in between by cubic spline polynomials, and evaluate the Fourier integrals exactly. Since the physical system is spherically symmetric and the Fourier transformations can be reduced to two dimensions, the numerical effort is comparatively moderate so that a high-performance computer is not necessary.

We have performed the numerical calculations for $T = T_c$. In this case it is $\Delta = 0$ so that the fermion Green's function $G_{\alpha_1\alpha_2}(\mathbb{k}, \omega_n)$ and the vertex function $\Gamma_{\alpha_1\alpha_2}(\mathbb{K}, \Omega_n)$ are diagonal. Thus, the matrix structure with respect to the indices α disappears. The self-consistent equations (3.44)-(3.47) reduce to equations for the normal fermion Green's function $G(\mathbb{k}, \omega_n)$ and the normal vertex function $\Gamma(\mathbb{K}, \Omega_n)$ (Haussmann 1994a). The critical temperature T_c of the superfluid transition is determined by the Thouless criterion $[\Gamma(\mathbb{K} = 0, \Omega_n = 0)]^{-1} = 0$. Since the dilute fermion system with short-range interaction is scaling invariant, we calculate the dimensionless temperature $\theta_c = k_B T_c/\varepsilon_F$ as a function of the dimensionless coupling strength $v = 1/(k_F a_F)$. The result is shown in Fig. 3.8 as full line. One clearly sees that $\theta_c(v)$ is a continuous function which increases monotonically with increasing v. Thus, the crossover from BCS superconductivity to Bose–Einstein condensation of fermion pairs is *continuous*, which agrees with all previous theories. In the weak coupling limit $v \to -\infty$ the BCS transition temperature (3.72) is approached asymptotically which is shown as dashed line on the left-hand side and which tends to zero exponentially. On the other hand, in the strong coupling limit $v \to +\infty$ the Bose–Einstein condensation temperature $\theta_{c,BE} = 0.2180$ is approached from below. The asymptotic formula (3.101) including the correction term due to the interaction between the pairs is shown as dashed line on the right-hand side. For comparison we have determined $\theta_c(v)$ neglecting self consistency, which is shown as dotted line in Fig. 3.8. To do this we have inserted the free fermion Green's function into (3.47) and (3.45) and then determined Γ and G by (3.46) and (3.44). This approximation does not include the repulsive interaction between the (noncondensed) pairs and is equivalent to the theory of Nozières and Schmitt-Rink (1985)

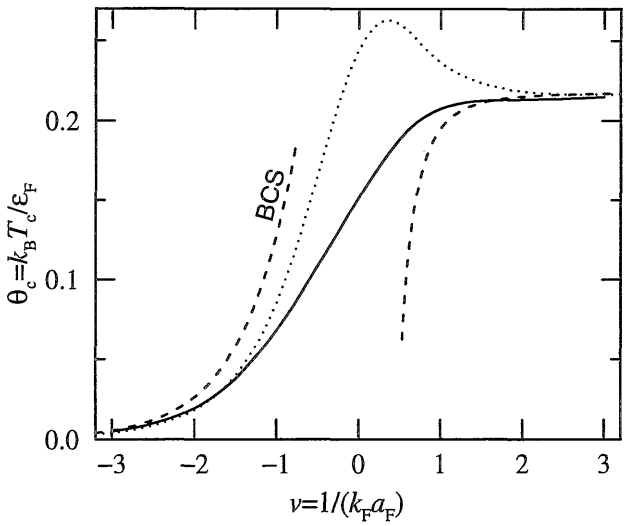

Fig. 3.8. The superfluid transition temperature $\theta_c = k_B T_c/\varepsilon_F$ as function of the dimensionless coupling strength $v = 1/(k_F a_F)$. The full line represents the numerical result of our self-consistent theory. The dotted line is obtained by neglecting self consistency and is similar to the results of the previous theories. The left-hand dashed line corresponds to the BCS theory, (3.72). The right-hand dashed line corresponds to our first-order asymptotic formula (3.101) including the interaction between the fermion pairs.

and to the mean-field theories (Drechsler and Zwerger 1992, Sá de Melo et al. 1993). The main feature of these previous theories is the maximum of $\theta_c(v)$ in the crossover region which is clearly seen for the dotted curve in Fig. 3.8 as a considerable effect. While Nozières and Schmitt-Rink have pointed out that this maximum should be unphysical and presumably due to the approximations, we have found that the maximum is caused by the deficiency of the interaction between the (noncondensed) fermion pairs in the mean-field approximation (first iteration). In the next iteration the maximum disappears and $\theta_c(v)$ is monotonic because then the interaction between the pairs is included. Also, in the extended version of the Ginzburg–Landau theory beyond mean-field approximation the maximum of $\theta_c(v)$ disappears (Stintzing 1996).

In Fig. 3.9 the chemical potential μ_c at the superfluid transition is shown in units of the Fermi energy $\varepsilon_F = \hbar^2 k_F^2/2m$ as a function of $v = 1/(k_F a_F)$. The full line represents our numerical result. In the weak coupling limit $v \to -\infty$ we find $\mu_c \to \varepsilon_F$ as expected for an ideal Fermi gas. For finite weak couplings we have calculated the chemical potential (3.70) in Hartree–Fock approximation which includes a correction term representing the interaction between the fermions. This asymptotic chemical potential is shown in Fig. 3.9 as the left dashed line. Since the interaction is attractive, it is $\mu_c < \varepsilon_F$. In the strong coupling limit $v \to +\infty$ the fermions are bound into pairs with

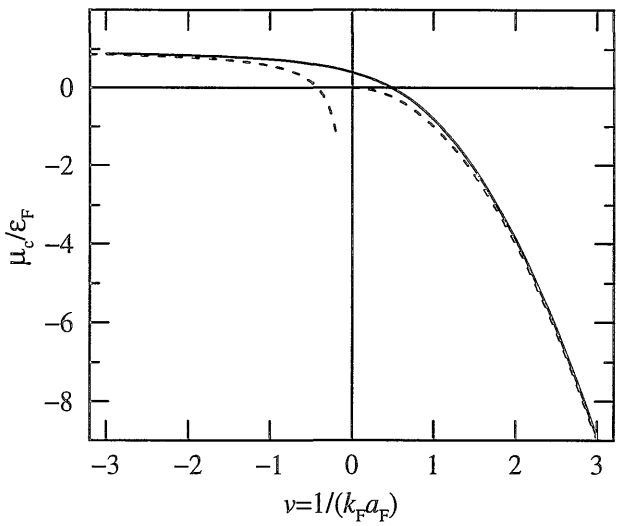

Fig. 3.9. The chemical potential μ_c at the superfluid transition as a function of $v = 1/(k_F a_F)$. The full line represents our numerical result. The asymptotic result for the weakly interacting Fermi gas (3.70) is shown as dashed line on the left-hand side. The dashed line on the right-hand side corresponds to the binding energy of the fermion pairs divided by 2.

binding energy $\varepsilon_b = \hbar^2/ma_F^2 = \varepsilon_F 2v^2$. Hence we expect $\mu_c \to -\varepsilon_b/2 = -\varepsilon_F v^2$ for $v \to +\infty$. In Fig. 3.9 the right dashed line represents $-\varepsilon_b/2$. The full line approaches the right dashed line from above for $v \to +\infty$. The difference $\mu + \varepsilon_b/2$ is positive and represents an energy due to the repulsive interaction between the pairs. One clearly sees that our numerical result (full line) interpolates well between the two limiting cases.

For strong couplings $v \gtrsim +1$ it is $\mu \lesssim -\varepsilon_F$ so that more than a Fermi energy ε_F is necessary to break a pair into two fermions. Thus, in this case the quantum fluctuations are too weak for breaking the pairs. We conclude that for $v \gtrsim +1$ and $k_B T \lesssim k_B T_{diss} \sim \varepsilon_b$ the system is a Bose liquid: nearly all fermions are bound into pairs so that there are nearly no single fermions. In the crossover region $-1 \lesssim v \lesssim +1$ single fermions and bound pairs coexist so that the system is a mixture of bosons and fermions. For weak couplings $v \lesssim -1$ bound pairs are very rare, the system is a Fermi liquid. Only below T_c there will be a few Cooper pairs. Turning back to the qualitative phase diagram shown in Fig. 3.2 the grey area corresponds to the region where composite bosons and single fermions coexist. On the left-hand side of this area nearly all particles are fermions while on the right-hand side nearly all particles are bound pairs.

Until now we have considered the *macroscopic* quantities T and μ, which determine the thermodynamic state of the system for a given coupling strength v. However, the functions $G(k, \omega_n)$ and $\Gamma(K, \Omega_n)$ we have calcu-

lated numerically contain also information about the *microscopic* details of the system. Since the bosonic degrees of freedom are described by the vertex function, we obtain the effective mass m_B^* of the fermion pairs from $\Gamma(\boldsymbol{K}, \Omega_n)$. More precisely, by an analytic continuation $i\Omega_n \to z$ of $[\Gamma(\boldsymbol{K}, \Omega_n)]^{-1}$ and expansion up to first order in $\hbar z$ and $\hbar^2 \boldsymbol{K}^2/2m$ we determine the coefficients $d = d' + id''$ and c of the time-dependent Ginzburg–Landau equation (3.103) and then by (3.104) the effective boson mass m_B^*. We note that the Ginzburg–Landau equation (3.103) is derived from the Ward identity (3.56) where the right-hand side is assumed to be zero. Since here it is $T = T_c$ and $\Delta = 0$, this assumption is satisfied. In Fig. 3.10 our numerical result for the effective boson mass m_B^* is shown as full line. Since m_B^* is complex we must distinguish between real part $\mathrm{Re}(m_B^*)$ and imaginary part $\mathrm{Im}(m_B^*)$ which are shown in Fig. 3.10a and Fig. 3.10b versus the coupling strength $v = 1/(k_F a_F)$, respectively.

For strong couplings $v \gtrsim +1$ where nearly all fermions are bound into pairs and nearly no single fermions are present, the effective boson mass is real and about $m_B^* \approx 2m$. The value $2m$ is expected because the bosons are pairs of fermions of mass m. More precisely, the effective boson mass m_B^* is slightly larger than $2m$. From the weakly interacting Bose gas it is known (Fetter and Walecka 1971) that this enhancement of the effective boson mass is due to the repulsive interaction between the pairs with a finite range. For the leading correction we have derived the asymptotic formula (3.100) which is shown as dashed line on the right-hand side of Fig. 3.10a. For $v \gtrsim 2$ the full line (numerical result for $\mathrm{Re}(m_B^*)$) converges quite well to the asymptotic dashed line. On the other hand, the imaginary part $\mathrm{Im}(m_B^*)$ is nearly zero for $v \gtrsim 1$ because here damping by pair breaking is negligible. We find that $\mathrm{Im}(m_B^*)$ becomes exponentially small with increasing v. We expect $\mathrm{Im}(m_B^*) \sim \exp(-\varepsilon_0/k_B T_c)$ where $k_B T_c \approx 0.22\varepsilon_F$ and ε_0 is a characteristic energy of the order of the pair-binding energy $\varepsilon_b = 2\varepsilon_F \cdot v^2$. However, because of the uncertainties of the numerical analytical continuation, it is hard to extract a certain exponential behavior of $\mathrm{Im}(m_B^*)$ reliably from our numerical results shown in Fig. 3.10b. We note that our theory includes the interaction between the pairs only in first order (Hartree–Fock approximation, see (3.95)). From the weakly interacting Bose gas it is known that the repulsive interaction between the pairs in higher orders of the perturbation theory will cause damping effects which result in a nonzero $\mathrm{Im}(m_B^*)$. Thus, the exponential decrease of $\mathrm{Im}(m_B^*)$ for strong couplings v shown in Fig. 3.10b might be an artifact of our approximation. In the exact theory $\mathrm{Im}(m_B^*)$ probably decreases much slower with increasing coupling strength v in the strong coupling limit. For intermediate couplings $-1 \lesssim v \lesssim +1$ the quantum fluctuations are sufficiently strong to break a considerable fraction of the pairs into single fermions. This causes a finite lifetime of the bosons which is reflected by a nonzero damping d'' in the time-dependent Ginzburg–Landau equation (3.103). Thus, Eq. (3.104) implies a positive imaginary part of the

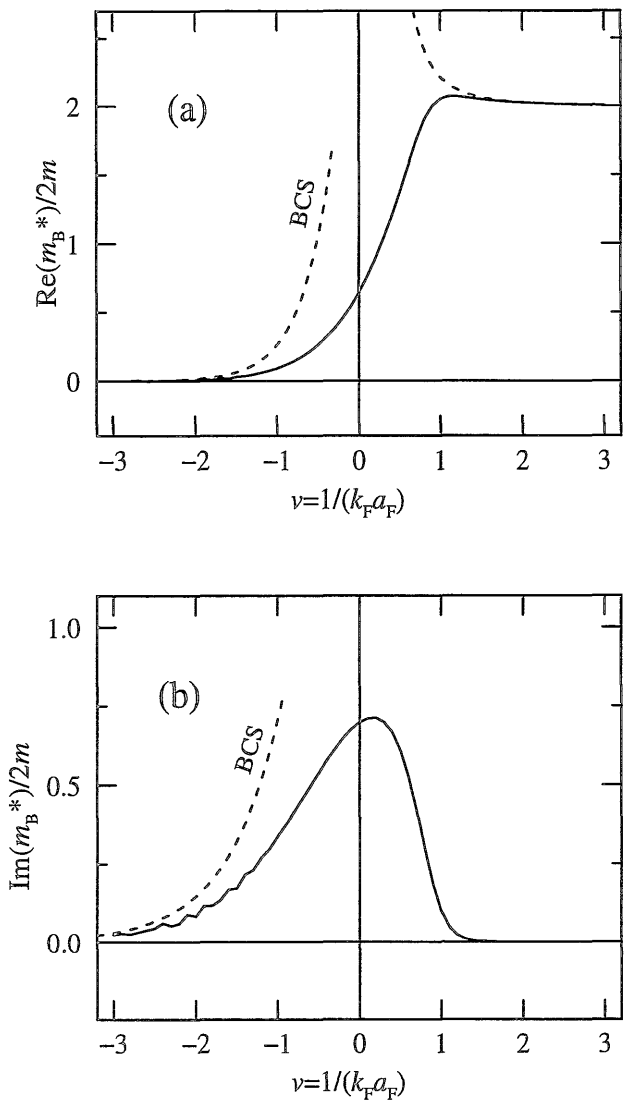

Fig. 3.10. The real part (a) and the imaginary part (b) of the effective boson mass m_B^* versus the dimensionless coupling strength v. The full lines represent our numerical result. The left-hand dashed lines correspond to the BCS theory. The right-hand dashed line in the figure for the real part represents the asymptotic strong-coupling result (3.100).

boson mass for $v \lesssim +1$ which is clearly seen in Fig. 3.10b. The interaction of the bosons with the single fermions causes a decrease of the real part $\mathrm{Re}(m_B^*)$ with decreasing coupling strength v. Near $v \approx +1$ the real part has a maximum, which is, however, rather tiny. At $v = 0$ real and imaginary part are nearly equal. For $v < 0$ the imaginary part becomes dominant while for $v > 0$ the real part is dominant. Finally, for weak couplings $v \lesssim -1$ the imaginary part is much larger than the real part, which means that the system is overdamped. In the weak coupling limit $v \to -\infty$ the effective boson mass m_B^* can be evaluated asymptotically (Haussmann 1993). This asymptotic result is shown as dashed lines on the left-hand sides of Figs. 3.10 a and b. Our numerical result for m_B^* (full line) interpolates between the asymptotic results (dashed lines) for weak and strong couplings.

From the fermion Green's function we obtain the fermion occupation number $n(\boldsymbol{k}) = -G(\boldsymbol{k}, \tau = -0)$. The result for $n(k) = n(\boldsymbol{k})$ of our numerical calculation for $T = T_c$ is shown in Fig. 3.11 for several couplings $v = 1/(k_F a_F)$. For weak couplings (here $v = -1$) a rather sharp Fermi surface is seen at $k \approx k_F$. Most of the fermions are single fermions, which occupy the states of momenta $\hbar\boldsymbol{k}$ within the Fermi sphere $0 \leq |\boldsymbol{k}| \lesssim k_F$. The Fermi surface is smeared out by the finite temperature $T = T_c$ and by the weak interaction between the fermions. For increasing v the Fermi surface is smeared out more and more until it disappears for $v \gtrsim 1$. For strong couplings (here $v = +1$ and $v = +2$) the fermion occupation number $n(k)$ is small compared to 1

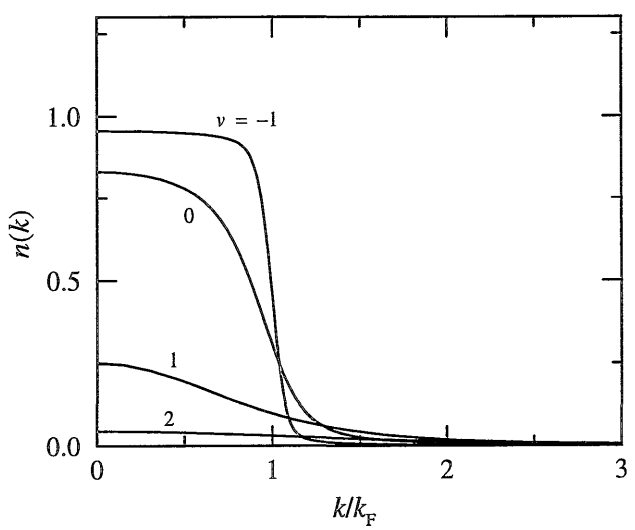

Fig. 3.11. The fermion occupation number $n(k)$ for various coupling strengths $v = -1$, 0, $+1$, $+2$ at $T = T_c$. While for weak coupling $v = -1$ the discontinuity of a Fermi surface at $k = k_F$ is indicated, $n(k)$ is small compared to 1 and similar to a classical distribution function for strong coupling $v = +2$.

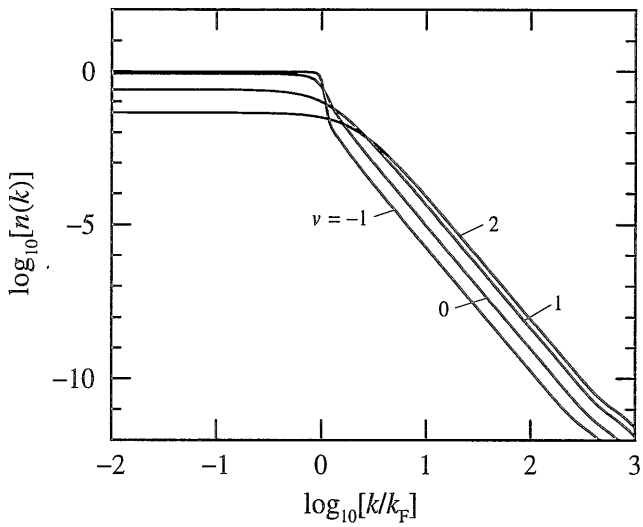

Fig. 3.12. Double-logarithmic plot of the fermion occupation number $n(k)$ versus k. For large k the power law tails $n(k) \sim k^{-4}$ caused by the delta interaction potential is clearly seen as straight lines for all couplings $v = -1, 0, +1, +2$.

and looks like a classical distribution function. While for an ideal Fermi gas $n(k)$ would decay to zero exponentially for large k, in the present case we observe a power law tail $n(k) \sim k^{-4}$ for $k \gg k_F$, which is clearly seen as the straight lines in the double logarithmic plot of Fig. 3.12 for *all* coupling strengths v. In the strong coupling limit $v \to +\infty$ we obtain the asymptotic formula (Haussmann 1993 and 1994a)

$$n(k) = 8\pi n_B a_F^3/(1 + k^2 a_F^2)^2 \tag{3.105}$$

where $n_B = n_F/2$ is the density of fermion pairs. This result can be written in the form $n(k) = n_B|\varphi_0(k)|^2$ where $\varphi_0(k)$ is the Fourier transform of the wave function $\varphi_0(r)$ for the relative motion of the fermions in a pair. Thus, (3.105) is the distribution function for fermions bound into pairs. The delta interaction potential (3.2) implies a singularity of $\varphi_0(r)$ for $r = 0$. In the Fourier transform this singularity is reflected by a power-law decay $\varphi_0(k) \sim k^{-2}$ for $k \to \infty$. Hence, we conclude that the power-law tail $n(k) \sim k^{-4}$ for $k \to \infty$, which is seen in Fig. 3.12 as the straight lines, is caused by the delta interaction potential. An interaction with finite range r_0 would smoothen the singularity of $\varphi_0(r)$ at $r = 0$ which would cause an exponential cutoff of the power law tails in $\varphi_0(k)$ and $n(k)$ for $k \gtrsim r_0^{-1}$.

The spectrum of the fermionic quasiparticles $A(\mathbb{k}, \varepsilon)$ is related to the fermion Green's function by

$$G(\mathbb{k}, \omega_n) = \int \mathrm{d}\varepsilon \, \frac{A(\mathbb{k}, \varepsilon)}{-\mathrm{i}\hbar\omega_n + \varepsilon - \mu} \tag{3.106}$$

(see e.g. Fetter and Walecka 1971). This integral can be inverted by an analytic continuation $i\omega_n \to z$ of the fermion Green's function to complex frequencies z. The spectral function $A(\boldsymbol{k}, \varepsilon)$ is then obtained by inserting $z = (\varepsilon - \mu)/\hbar \pm i0$ and taking the imaginary part. In practice the analytic continuation is known to be problematic: small numerical deviations of $G(\boldsymbol{k}, \omega_n)$ can cause big differences in $A(\boldsymbol{k}, \varepsilon)$. Thus, our numerical result for $A(\boldsymbol{k}, \varepsilon)$ is not always reliable and may have numerical errors. For medium-weak couplings $v \lesssim 0$ we obtain spectral functions $A(\boldsymbol{k}, \varepsilon)$ which seem to be qualitatively correct. In Fig. 3.13a the spectral function is shown for the weak coupling $v = -1$. The several curves correspond to wave numbers $k = 0$, $0.5k_F$, $1.0k_F$, $1.5k_F$, $2.0k_F$, etc.. We find peaks at positions $\varepsilon \approx \varepsilon_{\boldsymbol{k}} = \hbar^2\boldsymbol{k}^2/2m$ with a small width which correspond to the fermionic quasiparticles with a finite lifetime. As expected for a Fermi liquid, the sharpest peaks are found at $k \approx k_F$ which corresponds to relatively long-living quasiparticles close to the Fermi surface. From the Hartree–Fock approximation we obtain

$$A(\boldsymbol{k}, \varepsilon) = \delta(-\varepsilon + \varepsilon_{\boldsymbol{k}} + \tfrac{4}{3\pi}\varepsilon_F(k_F a_F)) \tag{3.107}$$

in the weak coupling limit $v \to -\infty$. For increasing v the width of the peaks increases and the life-time of the quasiparticles decreases. In Fig. 3.13b the spectral function is shown for $v = 0$ and several values of the wave number k. Here the peaks are quite broad so that the fermionic quasiparticles are short-living. While in the crossover region $0 \lesssim v \lesssim 1.2$ our numerical analytical continuation fails, for strong couplings $v \gtrsim 1.2$ we again obtain good results. In Figs. 3.13c and d the spectral function is shown for $v = 1.2$ and 1.7, respectively. Again we find broad peaks located at the energies $\varepsilon \approx \varepsilon_{\boldsymbol{k}} = \hbar^2\boldsymbol{k}^2/2m$ which represent the main spectral weight and correspond to single fermion states. However, there are small second peaks shifted to lower energies by a pair-binding energy $-\varepsilon_b$ which correspond to the states of the fermions bound into pairs. These second peaks occur for small wave numbers k, they decrease and broaden with increasing k. In Figs. 3.13 c and d the second peaks are clearly seen for $k = 0$, $0.5k_F$, and $1.0k_F$. The chemical potential $\mu \approx -\varepsilon_b/2$ is located in between the two peaks, so that the single fermion states are nearly empty while the states corresponding to the fermions bound into pairs are nearly filled. From the asymptotic expression of the fermion Green's function in the strong coupling limit (see (3.21) of Haussmann 1993) we obtain the spectral function

$$A(\boldsymbol{k}, \varepsilon) = [1 - n(k)]\,\delta(-\varepsilon + \varepsilon_{\boldsymbol{k}}) + n(k)\,\delta(-\varepsilon + [-\varepsilon_b - \varepsilon_{\boldsymbol{k}}]) \tag{3.108}$$

for $v \to +\infty$ where $n(k)$ is the fermion distribution function (3.105). The asymptotic formula (3.108) agrees with our numerical results in Figs. 3.13c and d. For very large positive v, pair breaking becomes very difficult and recombination of single fermions into pairs becomes very rare because of the large binding energy and the small scattering length. Thus, for $v \to +\infty$ the lifetime of the single fermions and also of the fermions bound into pairs

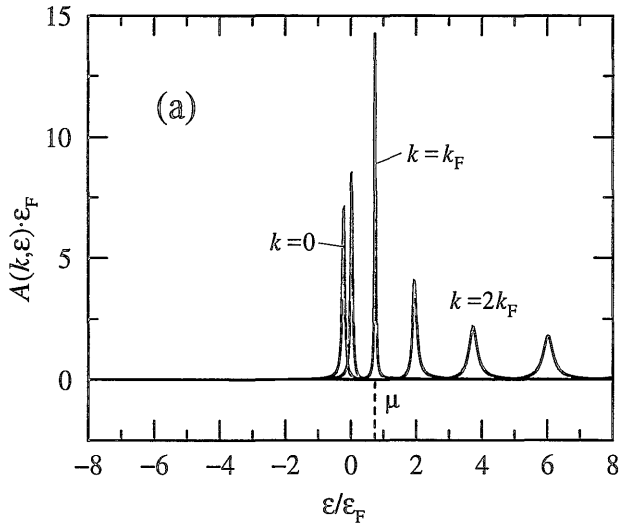
15
10
5
0
(a)
$k=k_F$
$k=0$
$k=2k_F$
μ
$A(k,\varepsilon)\cdot\varepsilon_F$
−8 −6 −4 −2 0 2 4 6 8
$\varepsilon/\varepsilon_F$

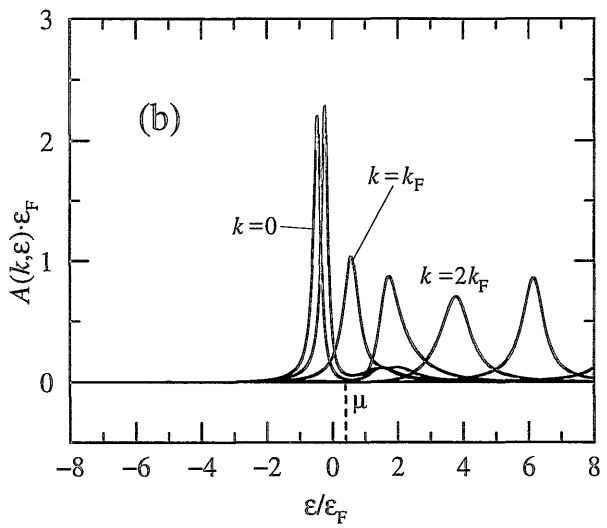
3
2
1
0
(b)
$k=k_F$
$k=0$
$k=2k_F$
μ
$A(k,\varepsilon)\cdot\varepsilon_F$
−8 −6 −4 −2 0 2 4 6 8
$\varepsilon/\varepsilon_F$

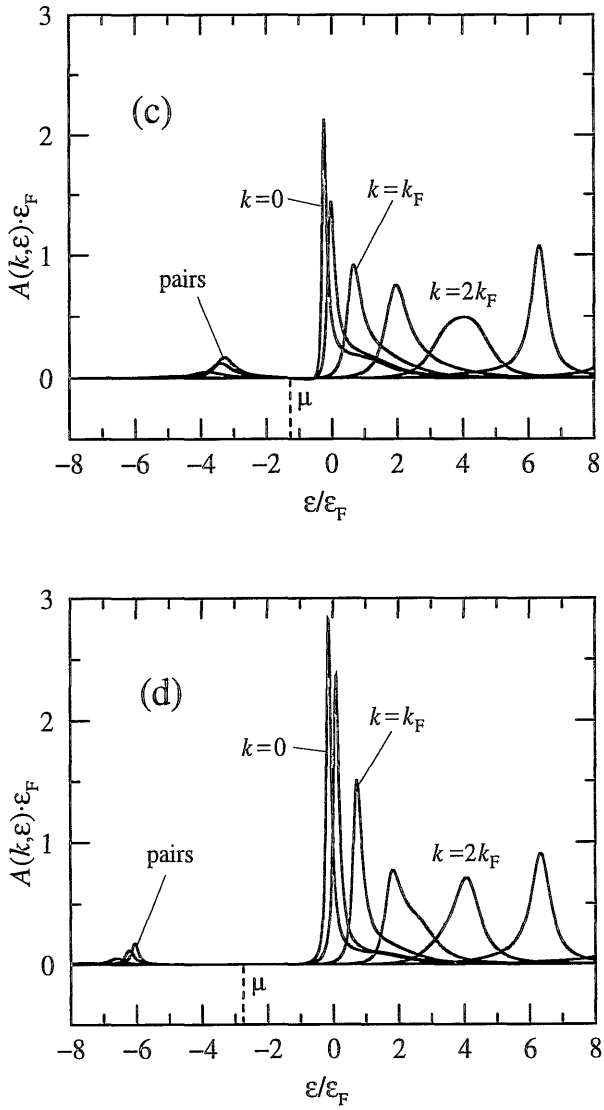

Fig. 3.13. The spectral function $A(k,\varepsilon)$ of the fermions for couplings (a) $v = -1$, (b) $v = 0$, (c) $v = 1.2$, and (d) $v = 1.7$. The several curves correspond to wave numbers $k = 0$, $0.5k_F$, $1.0k_F$, $1.5k_F$, $2.0k_F$, etc.. The large peaks located at $\varepsilon \approx \varepsilon_k$ for all v with finite witdths correspond to the single fermions with finite lifetimes. In (c) and (d) there are small second peaks at energies $\varepsilon \approx -\varepsilon_b - \varepsilon_k$ which decrease with increasing k and which corresponds to the fermions bound into pairs. The vertical dashed lines below the curves indicate the value of the chemical potential μ.

will become infinite which is indicated by the delta functions in (3.108). We conclude that the fermionic quasiparticles have long lifetimes for weak couplings $v \ll -1$ and for strong couplings $v \gg +1$, while in the crossover region $-1 \lesssim v \lesssim +1$ the lifetimes are short.

Since the vertex function describes the bosonic degrees of freedom, we obtain the spectral function of the bound pairs from $\Gamma(\mathbb{K}, \Omega_n)$ by an analytical continuation to complex frequencies $\mathrm{i}\Omega_n \to z$. In the strong coupling limit $v \to +\infty$ we have found that $\Gamma(\mathbb{K}, \Omega_n)$ is proportional to a free boson Green's function (Haussmann 1993). Thus, since for $v \gtrsim +1$ nearly all fermions are bound into pairs, we expect that the bosons are well defined pairs with a long lifetime for $v \gtrsim +1$. For $v \lesssim +1$, the system is a mixture of bound pairs and single fermions which are in thermal equilibrium with each other by pair breaking and recombination. Thus, for $v \lesssim +1$ the bosons have short lifetimes. For weak couplings $v \lesssim -1$ the few Cooper pairs are in equilibrium with the huge bath of single fermions, so that the life-time of the Cooper pairs is very short. This fact is also represented in Fig. 3.10 by the large imaginary part of the effective boson mass compared to the real part.

Our numerical calculations have been restricted to the critical temperature $T = T_c(v)$ of the superfluid transition. However, it is possible to generalize the numerical procedure also to arbitrary temperatures T. This should be done in future investigations. While $T > T_c$ does not need much changes, for $T < T_c$ the numerical effort increases, because in the superfluid phase the fermion Green's function and the vertex function are matrices so that also the anomalous fermion Green's function and the anomalous vertex function must be included. Once G and Γ are determined as solutions of the self-consistent equations, we can calculate the value of the functional $\Phi[G]$ by (3.43). Then from (2.17), (2.19), and (2.24) we obtain the grand-canonical thermodynamic potential $\Omega(T, \mu)$. It is also possible to determine the entropy $S(T, n_F)$ in an analogous way (De Dominicis and Martin 1964). Thermodynamic quantities like the specific heat $C_V(T)$ and the compressibility $\kappa_T(T)$ are obtained by derivatives from the thermodynamic potential and the entropy. Furthermore, the functions G and Γ can be used to derive the linearized hydrodynamic equations and to determine transport coefficients like the thermal conductivity $\lambda(T)$ and the shear viscosity $\eta(T)$. This must be done by analytical continuations $\mathrm{i}\Omega_n \to z$ of the respective correlation functions to complex frequencies and by expansion up to lowest order in z and $\mathbb{K}^2$ in a similar way as we have derived the time-dependent Ginzburg–Landau equation (3.103). Of special interest will be the dependences of $C_V(T)$, $\kappa_T(T)$, $\lambda(T)$, and $\eta(T)$ on the coupling strength $v = 1/(k_F a_F)$.

4. Gauge transformation and bosonization

Standard perturbation theory fails for quantum systems with degeneracies. Here one has quantum systems in mind for which the ground state is degenerate if the interaction is zero. A nonzero interaction then implies a complete or partial removal of the degeneracy so that the ground state is considerably changed. For this reason the interaction cannot be treated perturbatively. An important example of this kind is the two-dimensional electron system in a perpendicular magnetic field which exhibits the fractional quantum Hall effect (FQHE). The motion of the electrons in the homogeneous magnetic field is quantized into Landau levels which are degenerate. Thus, for a noninteger filling factor ν one of the Landau levels is partially filled which implies a degenerate ground state of the noninteracting system. The Coulomb interaction between the electrons removes the degeneracy and implies a strongly correlated ground state for the electrons. For noninteger filling factors ν rather exotic behaviors of the electron system have been observed due to the FQHE, which are related to rather unusual strongly correlated ground states (see e.g. Prange and Girvin 1987). The quantum-field theory, which is represented by an infinite series of Feynman diagrams, is a standard perturbation theory for the many-particle systems. It fails for electron systems in the regime of the FQHE at zero temperatures because the degeneracies of the Landau levels imply zero energy denominators in the terms of the perturbation series. At finite temperatures T the Feynman diagrams of the Matsubara formalism are finite. The degeneracies imply that a Feynman diagram of order n has a factor $\beta^n = 1/(k_B T)^n$ which becomes infinite in the zero-temperature limit indicating the zero energy denominators.

In quantum mechanics the perturbation theory for degenerate levels is performed by solving the problem in the subspace of the degenerate degrees of freedom exactly and treating the remaining degrees of freedom perturbatively (see e.g. Landau and Lifshitz vol. 3). For quantum-field theory of many-particle systems this approach is not useful because after the exact treatment of the problem in the subspace the Wick theorem, which generates the perturbation series of Feynman diagrams, is no more valid. Instead, one should resum the Feynman diagrams of the standard perturbation series to achieve a similar effect as the exact treatment of the subspace and an improvement of the perturbation theory.

In Chap. 2 we have described the resummation of the self-energy subdiagrams which leads to the self-consistent quantum-field theory. This resummation goes beyond perturbation theory to some extent and is essential for the description of superfluid fermion systems as we have shown in Chap. 3. It might be useful also for systems with degeneracies. The self-consistent quantum-field theory is a perturbation-series expansion in terms of the dressed Green's function G which incorporates the complete spectrum of the fermionic quasiparticles. Since the spectrum is broadened, the energies in the energy denominators of the perturbation series are smeared out. For this reason, the Feynman diagrams of the self-consistent theory are finite for $T = 0$. This fact appears to be a considerable achievement to deal with degenerate systems. Thus, the self-consistent random-phase approximation (SC-RPA) of Sect. 2.3 which incorporates the screening of the Coulomb interaction, may be a candidate to describe the two-dimensional electron system in the FQHE regime. However, it turns out that in this case the SC-RPA fails, too (Haussmann 1996). Let us consider the self-energy diagram in Fig. 2.7b. The thick dashed line corresponds to the effective screened interaction $U_{\text{eff}}(\boldsymbol{k}, \Omega_n) = V(\boldsymbol{k}) - [V(\boldsymbol{k})]^2 \chi_{\varrho\varrho}(\boldsymbol{k}, \Omega_n)$ which includes collective excitations via the density-density correlation function $\chi_{\varrho\varrho}(\boldsymbol{k}, \Omega_n)$. Hence, we interpret the self-energy diagrams as follows: the electron (thick full line) emits and absorbs one collective-excitation quantum (thick dashed line). The approximation works as long as the characteristic energy of the collective excitations is larger than the characteristic energy of the fermionic quasiparticles, so that only one quantum of the collective excitations is involved. However, this assumption is not satisfied here. For FQHE systems the important collective excitations are the magnetorotons which turn out to have energies about 5 times smaller than the characteristic energy of the fermionic quasiparticles (Haussmann 1996). Thus, several magnetorotons (5 on average) may be emitted and absorbed, so that in the self energy the diagrams for multi-collective-excitation processes must be included. We conclude that for a successful theory of FQHE systems the SC-RPA must be modified by a resummation procedure which properly takes the most important contributions of diagrams of multi-collective-excitation processes into account.

Other systems for which conventional methods of the quantum-field theory fail are the one-dimensional fermion systems. Here it turns out that the fundamental excitations of the ground state are bosons but not fermions. While the particle-number conservation implies a linear dispersion relation $\omega = uk$ for the collective excitations (charge-density fluctuations), the lifetime of the collective excitations is $\tau_{\text{B}} \sim k^{-2}$. Thus, in the limit of small k and large wave lengths the collective excitations related to charge-density fluctuations become free bosons. Furthermore, collective excitations related to spin-density fluctuations become free bosons in this limit, too. On the other hand, the fermionic quasiparticles do not become free fermions in the limit $k \to k_{\text{F}}$. In contrast, the self-consistent quantum-field theory always yields

nearly free fermionic quasiparticles close to the Fermi surface with lifetimes $\tau_F \sim (k - k_F)^{-2}$ (as expected for conventional Fermi liquids in two or three dimensions) while the collective excitations are always damped, even for long wavelengths. Thus, conventional methods of the quantum-field theory do not describe the low-energy physics of the collective excitations properly. To construct a successful theory for one-dimensional fermion systems one may start with a system of bosons, which represents the collective excitations, and figure out how the fermionic degrees of freedom can be expressed in terms of the bosons. This idea leads to the well known concept of *bosonization* (see e.g. Chap. 4 of Mahan 1990) which we describe in the next chapter.

There exist a few models of interacting many-particle systems which can be solved exactly (see e.g. Chap. 4 of Mahan 1990). The Luttinger model describes an idealized one-dimensional fermion system. The independent-boson model describes fermions on one localized site which interact with the bosonic excitations of the surroundings. The independent-boson model turns out to be useful for the spectrum of the electronic excitations in FQHE systems (Johansson and Kinaret 1993 and 1994, Haussmann 1996). Exactly solvable models can describe certain properties of quantum many-particle systems which are not accessible by perturbation theory. As an advantage, the interesting physical quantities can be calculated exactly. On the other hand, these models are considerably idealized and simplified. Thus, as a disadvantage it is unclear if the results of the exactly solvable models can be applied to more realistic systems and how large the deviations are. Nevertheless, the exactly solvable models may serve as guides for constructing new resummation procedures for the quantum-field theory to go beyond perturbation theory. One may figure out which terms are zero and how the Feynman diagrams must be summed to obtain the exact solution of such a model. Then one may apply this method to more general and more realistic systems to derive an approximation which in lowest order yields the solution of the ideal exactly solvable model and in higher orders the corrections.

In this chapter we present a quantum-field theoretic approach for bosonization. The basic idea is a gauge transformation of the fermion field operators $\Psi_X = e^{i\Lambda_X}\tilde{\Psi}_X$ where the phase Λ_X is a real bosonic field operator which is identified by the collective excitations. In analogy to quantum electrodynamics, local particle number conservation implies that a gauge transformation may not lead to new physical effects. While new interactions are created by the gauge transformation which couple to the density ϱ and the current $\boldsymbol{j}$ of the particles, the continuity equation $\partial_t \varrho + \boldsymbol{\nabla} \boldsymbol{j} = 0$ implies that these new interactions must drop out again. Thus, in the perturbation series of Feynman diagrams all terms which depend on the gauge field Λ_X must cancel. However, a single Feynman diagram which involves gauge fields Λ_X is usually nonzero. The cancellation is achieved only if certain subclasses of Feynman diagrams are resummed. (For the cancellation of the longitudinal part of the photon propagator in quantum electrodynamics this problem is discussed in

Bjorken and Drell 1965.) The classes of diagrams which are resummed to obtain the self-consistent quantum-field theory do not coincide with the classes needed to resum to cancel the gauge field Λ_X. For this reason the "enthalpy" functional $H[G]$ defined in Chap. 2, which is the generating functional of the self-consistent quantum-field theory, will not be invariant under gauge transformations if the self-consistent perturbation series in (2.29) is truncated. $H[G]$ is invariant only if all Feynman diagrams of (2.29) are included because the exact theory is gauge invariant. Actually, the self-consistent perturbation series of the "enthalpy" functional $H[G]$ is resummed by the gauge transformation. Thus, we have found a method to go beyond perturbation theory once more. While the gauge transformation can be applied always to any many-particle system which satisfies local particle conservation, the success of the method will depend on the choice of the dynamics of the boson field Λ_X, so that the transformed perturbation series is improved. We will then apply this method to the Luttinger model and to the independent-boson model and show how the exact solutions of these models are obtained very easily. In Chap. 5 we apply the bosonization by gauge transformation to the FQHE system as a realistic many-particle system to obtain physically relevant results.

4.1 Conventional bosonization for one- and higher-dimensional fermion systems

Before we present our approach, here we describe briefly how bosonization is performed usually until now. The one-dimensional interacting fermion system can be mapped approximately to a system of noninteracting bosons under certain assumptions (Tomonaga 1950). The interaction should be long ranged and restricted to small momentum transfers (forward scattering) so that the relevant physical processes happen only close to the Fermi points $k = \pm k_{\mathrm{F}}$. The dispersion relation is assumed to be linear $\varepsilon_k = \varepsilon_0 + \hbar v_{\mathrm{F}}|k|$ which is a good approximation close to the Fermi points, where $v_{\mathrm{F}} = \hbar k_{\mathrm{F}}/m$ is the Fermi velocity. An exactly solvable model of an one-dimensional fermion system has been proposed by Luttinger (1963) which is defined by the Hamiltonian

$$H = \sum_{\alpha\sigma} -\mathrm{i}\alpha\hbar v_{\mathrm{F}} \int \mathrm{d}x\, \Psi^{+}_{\alpha\sigma}(x)\partial_x \Psi_{\alpha\sigma}(x) + \frac{1}{2}\sum_{\alpha_1\alpha_2} \int \mathrm{d}x_1 \int \mathrm{d}x_2 \,:\varrho_{\alpha_1}(x_1) V_{\alpha_1\alpha_2}(x_1 - x_2)\varrho_{\alpha_2}(x_2): \qquad (4.1)$$

where $\varrho_\alpha(x) = \sum_\sigma \Psi^{+}_{\alpha\sigma}(x)\Psi_{\alpha\sigma}(x)$. Here two branches of fermions are considered with linear dispersion relations $\varepsilon_{k\alpha} = \varepsilon_0 + \alpha\hbar v_{\mathrm{F}} k$ where $\alpha = \pm 1$ is the index of the branches. The spin degree of freedom is denoted by the index σ. For simplicity we assume that the interaction does not depend on

the spin. The Luttinger model defined by (4.1) can be solved exactly. Mattis and Lieb (1965) have shown that the Luttinger model can be mapped exactly to a system of noninteracting bosons. The densities $\varrho_\alpha(k)$ are identified as Bose operators up to a factor $(k/2\pi)^{1/2}$. A Hamiltonian in terms of the Bose operators can be found which determines the dynamics of the collective excitations related to $\varrho_\alpha(k)$. The density correlation functions are evaluated easily because they can be related to free boson Green's functions. The fermion distribution function $n(k)$ has been found to be continuous at the Fermi points $k = \pm k_\mathrm{F}$ (Mattis and Lieb 1965) in contrast to normal Fermi liquids. It is also possible to evaluate the fermion Green's functions exactly. To do this the Fermi operators $\Psi_{\alpha\sigma}(x)$ are expressed in terms of the Bose operators (Luther and Peschel 1974 and Haldane 1981) so that the fermion Green's functions are obtained by evaluating expectation values or averages of Bose operators.

To summarize we note that the concept of bosonization is performed always in two steps. First, the fermion system is mapped to a noninteracting boson system where a Hamiltonian is obtained which is quadratic in the Bose operators and which determines the dynamics of the system. The bosons are identified by collective excitations. Secondly, the fermion operators are expressed in terms of the boson operators (as exponential functions) so that eventually all fermionic correlation functions can be calculated by evaluating expectation values or averages of boson operators.

The Luttinger model (4.1) is an idealized model system which differs clearly from more realistic one-dimensional fermion systems. The linear dispersion relations $\varepsilon_{k\alpha} = \varepsilon_0 + \alpha\hbar v_\mathrm{F} k$ for the two branches are not bounded below. There is an infinite number of single-particle states present with negative energies. This fact seems to be an unphysical artifact of the theory. However, for interactions with only small momentum transfers, the relevant physics is located close to the Fermi points $k = \pm k_\mathrm{F}$, so that the negative energy states are irrelevant. For k values farther away from the Fermi points the fermion distribution function $n(k)$ is either 0 or 1. The related single-particle states are either empty of fully occupied so that they do not yield a contribution to physical quantities. For more realistic one-dimensional fermion systems there will be deviations from the Luttinger model. There will be corrections due to the curvature of the energy dispersion ε_k. If the interaction has contributions with higher momentum transfers, then $n(k)$ will differ from 0 or 1 also for k values farther away from the Fermi points, so that the physical properties of one-dimensional fermion systems are not described by the Luttinger model alone. Nevertheless, the Luttinger model seems to describe the low energy physics correctly. By renormalization-group theory it has been shown, that the Luttinger model is an infrared fixed point (Sólyom 1979 and Metzner and Di Castro 1993). Correction terms arising from interactions with high-momentum transfer have shown to be irrelevant in the infrared (low-energy) limit. Thus, the notion of a "Luttinger liquid" for one-

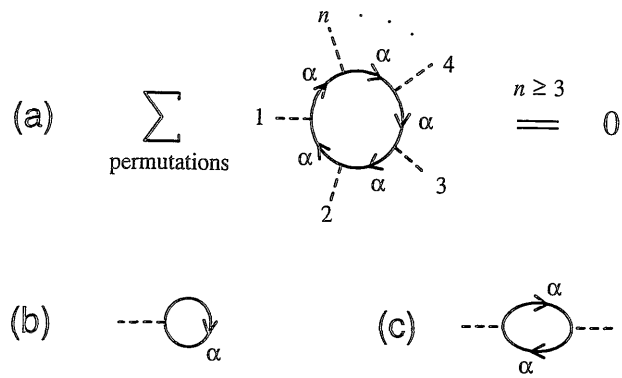

Fig. 4.1. (a) Fermion loops with $n \geq 3$ vertices cancel, where the sum is taken over all $n!$ permutations of the n vertex points. (b) $n = 1$ corresponds to the Hartree diagram. (c) $n = 2$ is the bubble diagram which represents the RPA polarization. The linear energy dispersion $\varepsilon_{k\alpha} = \varepsilon_0 + \alpha\hbar v_F k$ implies that the bubble diagram is proportional to a free boson Green's function.

dimensional fermion systems (Haldane 1981) in contrast to the "Fermi liquid" for higher-dimensional fermion systems appears to be useful.

Usually, the bosonization is performed in the operator formalism we have described above. However, it is also possible to solve the Luttinger model in terms of the quantum-field theory. This has been done first by Dzyaloshinskii and Larkin (1974). A considerable simplification occurs by the closed-loop theorem which is shown in Fig. 4.1a and which implies that most of the Feynman diagrams cancel. In a Feynman diagram there may be closed loops of fermion lines (full directed lines). A certain number n of dashed interaction lines may be attached to a loop by three vertices. While a single loop diagram is nonzero, the closed loop theorem states that for $n \geq 3$ the diagrams cancel if the sum is taken over all $n!$ permutations of the three vertices. Thus, since in the perturbation series the sum is taken over all possibilities and hence also over all permutations of the vertices, all Feynman diagrams which contain fermion loops with $n \geq 3$ cancel. Only loops with $n = 1$ and $n = 2$ remain, which are shown in Fig. 4.1b and c, respectively. For the proof of the closed loop theorem the following assumptions are necessary. The fermion lines are thin lines which are identified by the free fermion Green's function. The energy dispersion $\varepsilon_{k\alpha} = \varepsilon_0 + \alpha\hbar v_F k$ is linear. The interaction couples to the fermion lines via the densities $\varrho_\alpha(x)$ as it is in (4.1) so that the three vertices are identified by 1 and that the fermion Green's functions of a loop all have the same branch index α. The $n = 1$ loop can be discarded because it is identified as the bare Hartree diagram which leads to an energy shift which can be absorbed by a redefinition of ε_0 in the energy dispersion. (Actually, the Hartree diagram is an infinite constant, because it is proportional to the particle number N_α in branch α which is infinite because there is an infinite

number of negative energy states.) The $n = 2$ loop is the bubble diagram which can be evaluated easily. The result is proportional to a free boson Green's function.

Thus, we come to the following conclusion. The only nontrivial fermion loops, which may occur in a Feynman diagram, are the bubble diagrams of Fig. 4.1c, which are proportional to free boson Green's functions. This fact corresponds to the first step of bosonization: the fermion system is mapped onto a boson system. For the density-density correlation function and for the effective screened potential $U_{\mathrm{eff},\alpha_1\alpha_2}(k, \Omega_n)$ it turns out that the random-phase approximation (RPA) is exact: the polarization function is exactly given by the bubble diagram of Fig. 4.1c. (Note that the fermion lines are thin. Here the RPA is not self consistent.) In Fig. 4.2a the RPA series of the effective screened interaction is shown. Since two dashed lines are attached to a bubble diagram, the $n = 2$ fermion loops form chains which can be resummed by the geometric series. The thick dashed line on the left-hand side is identified by $-U_{\mathrm{eff},\alpha_1\alpha_2}(k, \Omega_n)$.

Furthermore, the fermion Green's function $G_\alpha(k, \omega_n)$ can be calculated exactly (Dzyaloshinskii and Larkin 1974). From the equation of motion for the fermion operators the Dyson equation is derived where the self energy is expressed in terms of the fermion Green's function and in terms of a three-vertex function. The structure of the interaction of the Luttinger model (4.1) implies that the particle number is locally conserved independently for each branch α. This conservation law implies a Ward identity which relates the three-vertex function exactly to the single-particle Green's function. Hence, a closed expression for the self energy $\Sigma_\alpha(k, \omega_n)$ in terms of the fermion Green's function $G_\alpha(k, \omega_n)$ is found. With this self energy the Dyson equation is an integral equation for $G_\alpha(x, \tau)$ which can be solved exactly to obtain the fermion Green's function (Dzyaloshinskii and Larkin 1974). Conservation laws and Ward identities have turned out to be an important tool for the quantum-field-theoretic approach of bosonization (Sólyom 1979 and Metzner and Di Castro 1993). It is also possible to calculate the fermion Green's function $G_\alpha(x, \tau)$ by a direct summation of the Feynman diagrams. A typical Feynman diagram of the one-particle Green's function is shown in Fig. 2.3: it

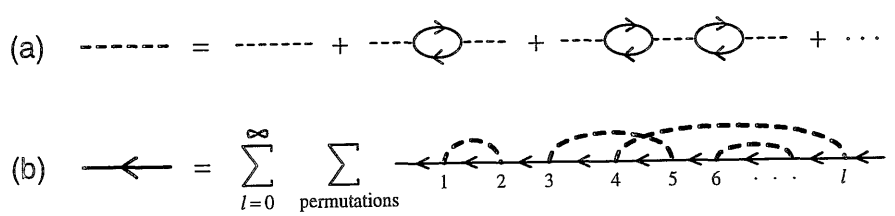

Fig. 4.2. (a) The effective screened interaction (thick dashed line) is exactly given by the RPA series. (b) The perturbation series of the fermion Green's function (thick full line). All $n = 2$ loops can be resummed and are included in the thick dashed lines.

consists of one open propagator line and a certain number of closed fermion loops. Because of the closed loop theorem only $n = 2$ loops occur which form chains. For this reason, the loops can be resummed by the series of Fig. 4.2a. Thus, the fermion Green's function is the sum of diagrams which are shown in Fig. 4.2b. The thick dashed lines are identified by the effective screened interaction and include all $n = 2$ closed fermion loops. The sum over the number l and the sum over all permutations of the three vertices are taken so that the interaction can be separated by an exponential factor. Eventually, the fermion Green's function can be written in the form

$$G_\alpha(x,\tau) = \exp\{\Phi_\alpha(x,\tau)\} \cdot G_{0\alpha}(x,\tau) \tag{4.2}$$

where $G_{0\alpha}(x,\tau)$ is the free fermion Green's function and $\Phi_\alpha(x,\tau)$ is related to the effective screened interaction.

The bosonization has been extended also to higher dimensional fermion systems, i.e. $d > 1$. After Luther's pioneering attempt (Luther 1979), further progress has been made by several authors (Haldane 1992, Houghton et al. 1993, 1994a, and 1994b, and Castro Neto and Fradkin 1994 and 1995). Also, the field theoretic approach of bosonization using conservation laws and Ward identities has been considered for $d > 1$ (Metzner and Di Castro 1993 and Castellani, Di Castro, and Metzner 1994). Motivated by experimental observations in the normal state of high-temperature superconductors, the question is investigated if fermion systems for $d > 1$ may have non-Fermi-liquid behavior.

An alternative approach starts with the functional integral of the one-dimensional fermion system. By two succeeding Hubbard-Stratonovich transformations an effective action functional for the density fluctuations can be derived where the fermion degrees of freedom have been integrated out (Fogedby 1976 and Lee and Chen 1988). For the Luttinger model the action of a noninteracting boson system has been obtained as expected. Since this approach can be applied also to more realistic one-dimensional fermion systems, for the bosonic degrees of freedom corrections beyond the Luttinger model can be derived systematically. The functional integral approach has been extended also to fermion systems in higher dimensions to develop an alternative bosonization method for $d > 1$ (Kopietz and Schönhammer 1996 and Kopietz et al. 1995). While in the Gaussian approximation a bosonized Hamiltonian is found, in one-loop order corrections are obtained which correspond to an effective interaction between the bosons (Kopietz et al. 1995). Also, the fermion Green's function can be calculated within this method by considering the Dyson equation (Fogedby 1976, Lee and Chen 1988, and Kopietz and Schönhammer 1996). Because of the Hubbard-Stratonovich transformation the Dyson equation of a free fermion system in an external potential is found where the external potential is related to the Hubbard-Stratonovich field. Supposed the energy dispersion of the fermions is linear as in the case of the Luttinger model, the Dyson equation is a first-order differential equation

which can be solved by integration. Thus, a fermion Green's function depending on the Hubbard-Stratonovich field is obtained. Eventually, the physical relevant fermion Green's function is obtained by performing the functional integral over the Hubbard-Stratonovich field. In this way, for the Luttinger model the exact fermion Green's function is recovered. For a nonlinear energy dispersion Kopietz and Castilla (1996) have solved the Dyson equation approximately by a suitable ansatz and obtained a nonperturbative formula for the fermion Green's function which includes corrections beyond the Luttinger model. The resulting nonperturbative formula for the fermion Green's function may be useful for dimensions $d > 1$ to investigate the question if an interacting fermion system is a "Fermi liquid" or a "Luttinger liquid". More details of the functional-integral approach of bosonization for interacting fermion systems for dimensions $d > 1$ are described in the textbook by Kopietz (1997).

4.2 Modification of the self-consistent quantum-field theory by gauge transformation

A quantum liquid is invariant under local gauge transformations $\Psi_X = \mathrm{e}^{\mathrm{i}\Lambda_X}\tilde{\Psi}_X$ if the particle number is conserved locally, so that the continuity equation $\partial_t \varrho + \boldsymbol{\nabla} \boldsymbol{j} = 0$ is valid for the particle density operator and the current density operator. As a concrete system we consider bosons or fermions in d dimensions which interact by a two-particle potential $V(\boldsymbol{r} - \boldsymbol{r}')$ which only depends on the distance between the particles. In second-quantization representation the Hamiltonian is

$$H = \int \mathrm{d}^d r \sum_\sigma \frac{\hbar^2}{2m} [\boldsymbol{\nabla}\Psi_\sigma^+(\boldsymbol{r})][\boldsymbol{\nabla}\Psi_\sigma(\boldsymbol{r})] + \frac{1}{2}\int \mathrm{d}^d r \int \mathrm{d}^d r' : \varrho(\boldsymbol{r}) V(\boldsymbol{r}-\boldsymbol{r}')\varrho(\boldsymbol{r}') : \tag{4.3}$$

where $\Psi_\sigma(\boldsymbol{r})$ and $\Psi_\sigma^+(\boldsymbol{r})$ are the field operators of the particles and $\varrho(\boldsymbol{r}) = \sum_\sigma \Psi_\sigma^+(\boldsymbol{r})\Psi_\sigma(\boldsymbol{r})$ is the density operator. The two colons : : mean that the product of field operators in between is normal ordered. The grand-canonical partition function for the many-particle system at finite temperatures is defined by $Z = \mathrm{Tr}\,\mathrm{e}^{-\beta K}$ where $\beta = 1/k_\mathrm{B}T$ and $K = H - \mu N$. The particle number operator is given by

$$N = \int \mathrm{d}^d r\, \varrho(\boldsymbol{r}) = \int \mathrm{d}^d r \sum_\sigma \Psi_\sigma^+(\boldsymbol{r})\Psi_\sigma(\boldsymbol{r}) \; . \tag{4.4}$$

To develop the quantum-field theory we use the formalism of functional integrals (Negele and Orland 1988). The grand-canonical partition function can be written as the functional integral

$$Z = \mathcal{N} \int \mathcal{D}\Psi \; \mathrm{e}^{-S[\Psi]} \tag{4.5}$$

with the action functional

$$S[\Psi] = \frac{1}{\hbar}\int_0^{\hbar\beta} \mathrm{d}\tau \Big[\int \mathrm{d}^d r \frac{\hbar}{2} \Big(\Psi_\sigma^*(r,\tau) \frac{\partial \Psi_\sigma(r,\tau)}{\partial \tau} - \frac{\partial \Psi_\sigma^*(r,\tau)}{\partial \tau} \Psi_\sigma(r,\tau) \Big) + K(\tau) \Big] . \tag{4.6}$$

Here $K(\tau) = H(\tau) - \mu N(\tau)$ is obtained from (4.3) and (4.4) by replacing the field operators by the field variables $\Psi_\sigma(r,\tau)$ and $\Psi_\sigma^*(r,\tau)$ which according to the Matsubara formalism depend on the imaginary times. For bosons the field variables are just scalar functions, while for fermions they are Grassmann variables. In (4.5) $\mathcal{N}$ is a normalization constant which must be chosen properly. It can be determined by considering the many-particle system without interaction ($V(r) = 0$) for which the partition function and the functional integral can be evaluated explicitly.

The elements and rules for the construction of the Feynman diagrams are obtained by inspection of the several terms of the action functional (4.6) together with (4.3) and (4.4). The resulting Feynman rules for the interacting boson or fermion system are shown in Fig. 4.3. From the terms quadratic in the field variables we obtain the free Green's function, which is identified by a thin directed line in Fig. 4.3a. Since the many-particle system described by the Hamiltonian (4.3) is homogeneous in space and time and since the interaction is spin independent, the structure of the free Green's function (and also of the dressed Green's function) simplifies as

$$G_{0,\sigma\sigma'}(r,\tau;r',\tau') = \delta_{\sigma\sigma'} G_0(r-r',\tau-\tau') \tag{4.7}$$

where the Fourier transform of the free Green's function on the right-hand side is given by

$$G_0(k,\omega_n) = 1/[-\mathrm{i}\hbar\omega_n + \varepsilon_k - \mu] . \tag{4.8}$$

Here ω_n are either bosonic or fermionic Matsubara frequencies and $\varepsilon_k = \hbar^2 k^2/2m$ is the kinetic energy dispersion. From the interaction term (which

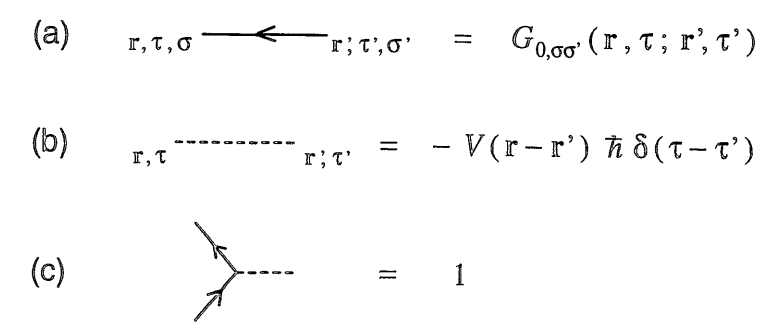

Fig. 4.3. Feynman rules for interacting bosons or fermions: (a) propagator line identified by the free Green's function, (b) dashed interaction line identified by the two-particle potential, and (c) three vertex which couples the interaction line to the fermion lines.

corresponds to the last term of (4.3)) a four vertex is obtained. We decompose this four vertex into a dashed interaction line, which is shown in Fig. 4.3b and identified by minus the interaction potential, and two three vertices, one of which is shown in Fig. 4.3c. By the three vertex the dashed interaction line is attached to the fermion lines. Since in (4.3) the interaction potential couples to the density $\varrho(\boldsymbol{r})$, the three vertex is just identified by a factor 1. The space and time variables $\boldsymbol{r}$, τ and the spin indices σ of the three attached lines are equal. Furthermore, the integrals over $\boldsymbol{r}$, τ and the sum over σ are taken for each three vertex.

A. Gauge transformation

Now we perform a local and imaginary-time dependent gauge transformation of the field operators

$$\Psi_\sigma(\boldsymbol{r},\tau) = \mathrm{e}^{\mathrm{i}\Lambda(\boldsymbol{r},\tau)}\tilde{\Psi}_\sigma(\boldsymbol{r},\tau)\ , \qquad \Psi^*_\sigma(\boldsymbol{r},\tau) = \mathrm{e}^{-\mathrm{i}\Lambda(\boldsymbol{r},\tau)}\tilde{\Psi}^*_\sigma(\boldsymbol{r},\tau)\ . \tag{4.9}$$

The phase of the gauge transformation $\Lambda(\boldsymbol{r},\tau)$ is assumed to be an arbitrary real function of space and imaginary time which does not depend on the spin index σ. The measure

$$\mathcal{D}\Psi = \prod_{\boldsymbol{r},\tau,\sigma} \mathrm{d}\Psi_\sigma(\boldsymbol{r},\tau)\cdot\mathrm{d}\Psi^*_\sigma(\boldsymbol{r},\tau) \tag{4.10}$$

remains unchanged under the gauge transformation because the exponential factors of (4.9) just cancel. Hence it is

$$\mathcal{D}\Psi = \mathcal{D}\tilde{\Psi}\ . \tag{4.11}$$

Inserting the transformation (4.9) into the action functional (4.6) we obtain

$$S[\Psi] = S[\tilde{\Psi}] + \Delta S[\tilde{\Psi},\Lambda] \tag{4.12}$$

where

$$\Delta S[\tilde{\Psi},\Lambda] = \frac{1}{\hbar}\int_0^{\hbar\beta}\mathrm{d}\tau\int\mathrm{d}^d r\Big[\mathrm{i}\hbar(\partial_\tau\Lambda)\tilde{\varrho} + \hbar(\boldsymbol{\nabla}\Lambda)\,\tilde{\boldsymbol{j}} + \frac{\hbar^2}{2m}(\boldsymbol{\nabla}\Lambda)^2\tilde{\varrho}^2\Big]\ . \tag{4.13}$$

Here

$$\tilde{\varrho} = \tilde{\varrho}(\boldsymbol{r},\tau) = \sum_\sigma \tilde{\Psi}^*_\sigma(\boldsymbol{r},\tau)\tilde{\Psi}_\sigma(\boldsymbol{r},\tau) \tag{4.14}$$

is the density and

$$\tilde{\boldsymbol{j}} = \tilde{\boldsymbol{j}}(\boldsymbol{r},\tau) = \sum_\sigma \frac{\hbar}{2m\mathrm{i}}\Big(\tilde{\Psi}^*_\sigma(\boldsymbol{r},\tau)[\boldsymbol{\nabla}\tilde{\Psi}_\sigma(\boldsymbol{r},\tau)] - [\boldsymbol{\nabla}\tilde{\Psi}^*_\sigma(\boldsymbol{r},\tau)]\,\tilde{\Psi}_\sigma(\boldsymbol{r},\tau)\Big) \tag{4.15}$$

is the current density of the "gauge-transformed particles". Then, by (4.9), (4.11), and (4.12) the functional integral of the grand-canonical partition function is transformed into

$$Z = \mathcal{N} \int \mathcal{D}\tilde{\Psi}\, \mathrm{e}^{-(S[\tilde{\Psi}]+\Delta S[\tilde{\Psi},A])} \,. \tag{4.16}$$

The value of Z may not change by the gauge transformation. For this reason, the functional integral (4.16) may not depend on the gauge field $A(\mathbf{r},\tau)$, i.e. it must be gauge invariant. By the perturbation theory in terms of Feynman diagrams the partition function (4.16) is expanded in powers of A. Clearly the terms of order A^n must be zero for $n \geq 1$. This means that the sum of all Feynman diagrams with a certain number $n \geq 1$ of gauge fields $A(\mathbf{r},\tau)$ must cancel.

For the gauge-transformed particles the elements and rules for the Feynman diagrams are obtained from the action functional (4.12). The first term $S[\tilde{\Psi}]$ is given by (4.6) where the fields are replaced by the gauge-transformed fields $\tilde{\Psi}_\sigma(\mathbf{r},\tau)$ and $\tilde{\Psi}^*_\sigma(\mathbf{r},\tau)$. The gauge-transformed particles have the kinetic energy dispersion $\varepsilon_k = \hbar^2 k^2/2m$ and interact by the two-particle potential $V(\mathbf{r}-\mathbf{r}')$ as it is for the original particles. Thus, the Feynman rules shown in Fig. 4.3 remain valid also for the gauge-transformed particles. The second contribution $\Delta S[\tilde{\Psi},A]$ in the action functional (4.12) implies an additional interaction of the particles with the gauge field $A(\mathbf{r},\tau)$. From (4.13) we obtain the related vertices which are shown in Fig. 4.4. The gauge field is denoted by a wavy line. We find a three vertex (Fig. 4.4a) and a four vertex (Fig. 4.4b) by which wavy lines can be attached to the particle lines (the full directed lines). In the three vertex the gauge field couples to the particles via the density (4.14) and the current density (4.15). The operators ∂_τ^A and ∇^A act on the gauge field, while $\overleftrightarrow{\nabla}$ acts left and right on the particle fields (the full directed lines) according to

$$f\overleftrightarrow{\nabla}g = f(\nabla g) - (\nabla f)g \,. \tag{4.17}$$

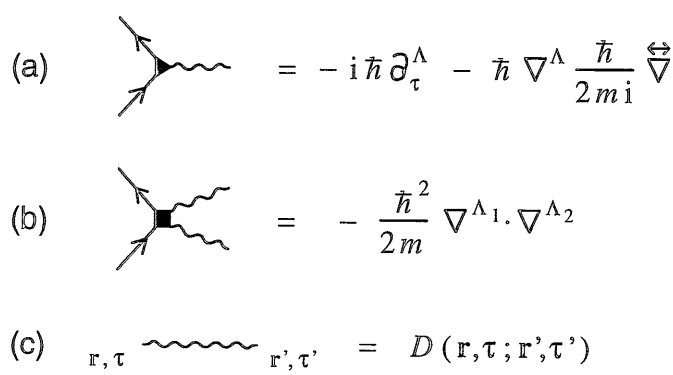

Fig. 4.4. (a) Three vertex and (b) four vertex by which the gauge field (wavy line) couples to the particles (directed full lines). The differential operators ∂_τ^A and ∇^A act on the gauge field while $\overleftrightarrow{\nabla}$ acts left and right on the particle fields according to (4.17). (c) The wavy line is identified by the gauge-field propagator D.

In the four vertex two gauge fields couple to the particles by two densities. For this reason the differential operators ∇^{Λ_1} and ∇^{Λ_2} act on the two gauge fields, respectively.

We want the gauge field $\Lambda(\boldsymbol{r},\tau)$ to be a real boson field, where later the bosons should be identified by or related to the collective excitations of the system. For this reason we should rewrite the partition function (4.16) as a functional integral also with respect to the gauge field $\Lambda(\boldsymbol{r},\tau)$. To do this we just take the average of (4.16) with respect to the gauge field with a weight factor $\mathrm{e}^{-S_\Lambda[\Lambda]}$ so that we obtain

$$Z = \mathcal{M} \int \mathcal{D}\Lambda \, \mathrm{e}^{-S_\Lambda[\Lambda]} \left[\int \mathcal{D}\tilde{\Psi} \, \mathrm{e}^{-(S[\tilde{\Psi}]+\Delta S[\tilde{\Psi},\Lambda])} \right] . \tag{4.18}$$

By construction the expression in the square brackets is independent of $\Lambda(\boldsymbol{r},\tau)$. Hence the new normalization constant $\mathcal{M}$ is determined by

$$\mathcal{M} \int \mathcal{D}\Lambda \, \mathrm{e}^{-S_\Lambda[\Lambda]} = \mathcal{N} . \tag{4.19}$$

Eventually, we write the functional integral in the symmetric form

$$Z = \mathcal{M} \int \mathcal{D}\tilde{\Psi} \int \mathcal{D}\Lambda \, \mathrm{e}^{-(S_\Lambda[\Lambda]+S[\tilde{\Psi}]+\Delta S[\tilde{\Psi},\Lambda])} . \tag{4.20}$$

Until now the action functional of the gauge bosons $S_\Lambda[\Lambda]$ is arbitrary. For simplicity, we assume $S_\Lambda[\Lambda]$ to be quadratic in the gauge field $\Lambda(\boldsymbol{r},\tau)$ so that it can be written as

$$S_\Lambda[\Lambda] = \frac{1}{2}\frac{1}{\hbar}\int_0^{\hbar\beta} \mathrm{d}\tau \int \mathrm{d}^d r \, \frac{1}{\hbar}\int_0^{\hbar\beta} \mathrm{d}\tau' \int \mathrm{d}^d r' \cdot\Lambda(\boldsymbol{r},\tau)\, D^{-1}(\boldsymbol{r},\tau;\boldsymbol{r}',\tau')\, \Lambda(\boldsymbol{r}',\tau') . \tag{4.21}$$

As a consequence

$$D(\boldsymbol{r},\tau;\boldsymbol{r}',\tau') = \langle T[\Lambda(\boldsymbol{r},\tau)\,\Lambda(\boldsymbol{r}',\tau')]\rangle \tag{4.22}$$

is the propagator of the gauge field which in terms of Feynman diagrams is identified by a wavy line as it is shown in Fig. 4.4c. The quadratic form (4.21) implies that the Wick theorem is valid for the gauge field. There will be no direct interactions between the gauge field so that there are no vertices which involve only wavy lines.

The functional integral (4.20) defines the series of Feynman diagrams of the grand-canonical partition function. The elements for the construction of the Feynman diagrams are shown in Figs. 4.3 and 4.4. The degrees of freedom of the gauge transformation are included by the real boson field $\Lambda(\boldsymbol{r},\tau)$ with the propagator (4.22) where $D(\boldsymbol{r},\tau;\boldsymbol{r}',\tau')$ is an arbitrary function until now. Because of the gauge transformation there will be two single-particle Green's functions, the physical Green's function of the particles (bosons or fermions)

$$G_{\sigma\sigma'}(\mathbf{r},\tau;\mathbf{r}',\tau') = \langle T[\Psi_\sigma(\mathbf{r},\tau)\,\Psi^+_{\sigma'}(\mathbf{r}',\tau')]\rangle \tag{4.23}$$

and the Green's function of the gauge-transformed particles

$$\tilde{G}_{\sigma\sigma'}(\mathbf{r},\tau;\mathbf{r}',\tau') = \langle T[\tilde{\Psi}_\sigma(\mathbf{r},\tau)\,\tilde{\Psi}^+_{\sigma'}(\mathbf{r}',\tau')]\rangle\ . \tag{4.24}$$

These two Green's functions can be related to each other. We write (4.24) in terms of the functional integral

$$\tilde{G}_{\sigma\sigma'}(\mathbf{r},\tau;\mathbf{r}',\tau') = Z^{-1}\,\mathcal{M}\int\mathcal{D}\tilde{\Psi}\int\mathcal{D}\Lambda\,\tilde{\Psi}_\sigma(\mathbf{r},\tau)\,\tilde{\Psi}^*_{\sigma'}(\mathbf{r}',\tau')\,\mathrm{e}^{-(S_\Lambda[\Lambda]+S[\tilde{\Psi}]+\Delta S[\tilde{\Psi},\Lambda])}\ . \tag{4.25}$$

By using (4.9) we replace the gauge transformed fields by the original fields. Furthermore, we use (4.11) and (4.12) and the obtain

$$\tilde{G}_{\sigma\sigma'}(\mathbf{r},\tau;\mathbf{r}',\tau') = Z^{-1}\,\mathcal{M}\int\mathcal{D}\Psi\int\mathcal{D}\Lambda \cdot\mathrm{e}^{-\mathrm{i}\Lambda(\mathbf{r},\tau)}\Psi_\sigma(\mathbf{r},\tau)\,\mathrm{e}^{\mathrm{i}\Lambda(\mathbf{r}',\tau')}\Psi^*_{\sigma'}(\mathbf{r}',\tau')\,\mathrm{e}^{-(S_\Lambda[\Lambda]+S[\Psi])}\ . \tag{4.26}$$

The gauge field $\Lambda(\mathbf{r},\tau)$ and the particle fields $\Psi_\sigma(\mathbf{r},\tau)$, $\Psi^+_\sigma(\mathbf{r},\tau)$ are independent from and do not interact with each other. For this reason the functional integral in (4.26) factorizes so that

$$\begin{aligned}\tilde{G}_{\sigma\sigma'}(\mathbf{r},\tau;\mathbf{r}',\tau') &= Z^{-1}\,\mathcal{M}\int\mathcal{D}\Lambda\,\mathrm{e}^{-\mathrm{i}[\Lambda(\mathbf{r},\tau)-\Lambda(\mathbf{r}',\tau')]}\,\mathrm{e}^{-S_\Lambda[\Lambda]}\\ &\quad\cdot\int\mathcal{D}\Psi\;\Psi_\sigma(\mathbf{r},\tau)\Psi^*_{\sigma'}(\mathbf{r}',\tau')\,\mathrm{e}^{-S[\Psi]}\\ &= \langle T[\mathrm{e}^{-\mathrm{i}[\Lambda(\mathbf{r},\tau)-\Lambda(\mathbf{r}',\tau')]}]\rangle\;G_{\sigma\sigma'}(\mathbf{r},\tau;\mathbf{r}',\tau')\ .\end{aligned} \tag{4.27}$$

Because of the quadratic action (4.21) the expectation value of the exponential functions of the gauge field can be evaluated by the Wick theorem so that

$$\langle T[\mathrm{e}^{-\mathrm{i}[\Lambda(\mathbf{r},\tau)-\Lambda(\mathbf{r}',\tau')]}]\rangle = \exp\{-\tfrac{1}{2}\langle T[(\Lambda(\mathbf{r},\tau)-\Lambda(\mathbf{r}',\tau'))^2]\rangle\}\ . \tag{4.28}$$

Thus, for the Green's function we obtain the transformation formula

$$G_{\sigma\sigma'}(\mathbf{r},\tau;\mathbf{r}',\tau') = \exp\{\Phi(\mathbf{r},\tau;\mathbf{r}',\tau')\}\cdot\tilde{G}_{\sigma\sigma'}(\mathbf{r},\tau;\mathbf{r}',\tau') \tag{4.29}$$

where

$$\Phi(\mathbf{r},\tau;\mathbf{r}',\tau') = \tfrac{1}{2}\langle T[(\Lambda(\mathbf{r},\tau)-\Lambda(\mathbf{r}',\tau'))^2]\rangle \tag{4.30}$$

is related to the gauge-field propagator (4.22).

The transformation formula (4.29) is the central relation of our theory. It enables a resummation of the perturbation series. Since the physical Green's

function G is given by the standard perturbation series with Feynman diagrams which are constructed by the elements shown in Fig. 4.3, the transformed Green's function $\tilde{G}$ is given by the modified perturbation series with Feynman diagrams which are constructed by the elements shown in Figs. 4.3 and 4.4. The modified perturbation series involves the gauge-field propagator D (wavy line) as an additional degree of freedom, which in general may be an arbitrary function. Eventually, the gauge-field propagator D will be chosen so that the modified perturbation series for $\tilde{G}$ is improved and may be truncated. Thus, in practice we calculate $\tilde{G}$ perturbatively and then obtain a nonperturbative result for the physical Green's function G by (4.29). In some cases, i.e. the Luttinger model and the independent-boson model, the perturbation series of $\tilde{G}$ truncates exactly so that we obtain the exact physical Green's function G by (4.29). For more realistic and more general systems we may derive approximations which are guided by the method for the two exactly solvable models.

B. Theorems for partial resummations of Feynman diagrams

To understand the structure of the resummation we now prove some theorems for the Feynman diagrams. We consider a system of bosons or fermions without interaction, i.e. $V(\boldsymbol{r}-\boldsymbol{r}')=0$. The Green's function of this system is the free Green's function G_0 given by (4.7) and (4.8). We perform the gauge transformation where, however, the gauge field $\Lambda(\boldsymbol{r},\tau)$ is assumed to be an external field. We do not integrate over $\Lambda(\boldsymbol{r},\tau)$ so that (4.16) is the functional integral of the grand-canonical partition function. The Green's function of the gauge-transformed particles $\tilde{G}_0$ is then obtained by (4.27) without taking the expectation value with respect to the gauge field. Thus, it is

$$\tilde{G}_{0,\sigma\sigma'}(\boldsymbol{r},\tau;\boldsymbol{r}',\tau') = T[\mathrm{e}^{-\mathrm{i}[\Lambda(\boldsymbol{r},\tau)-\Lambda(\boldsymbol{r}',\tau')]}\cdot G_{0,\sigma\sigma'}(\boldsymbol{r},\tau;\boldsymbol{r}',\tau') \ . \qquad (4.31)$$

The gauge-transformed Green's function $\tilde{G}_0$ on the left-hand side can be calculated directly by the perturbation series. The Feynman diagrams are constructed by the elements shown in Figs. 4.3a (propagator line), 4.4a, and 4.4b (vertices) where the wavy lines are external lines. Thus, we obtain a theorem which is shown in Fig. 4.5. On the left-hand side the perturbation series of $\tilde{G}_0$ is shown. The Feynman diagrams consist of a long open propagator line (directed full line) with l wavy lines attached to it by three and four vertices. The sum is taken over all possibilities of using three and four vertices to attach the wavy lines. Furthermore, the sum is taken over the $l!$ permutations to distribute the wavy lines. Finally, the sum is taken over l. The right-hand side in Fig. 4.5 corresponds to the right-hand side of (4.31). While we have proven Theorem 1 by considering a noninteracting many-particle system, the theorem is valid generally as a resummation of Feynman diagrams. For this reason, Theorem 1 can be used also for the diagrams of an interacting many-particle system to resum the subdiagrams with wavy lines partially.

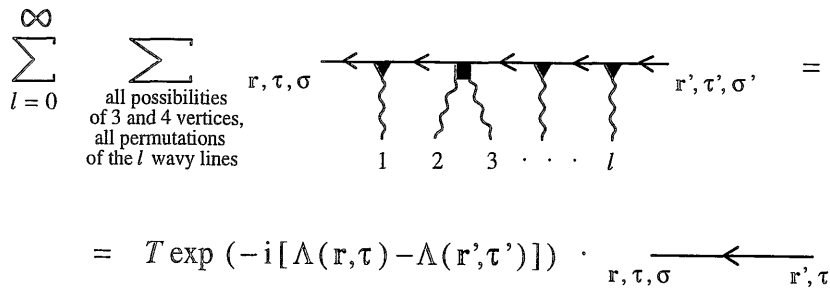

Fig. 4.5. *Theorem 1*: Resummation of the perturbation series of $\tilde{G}_0$. The Feynman diagrams on the left-hand side consist of one open propagator line with l wavy lines attached to it by three and four vertices. The sum is taken over l, all possibilities of three and four vertices, and all permutations of the l wavy lines.

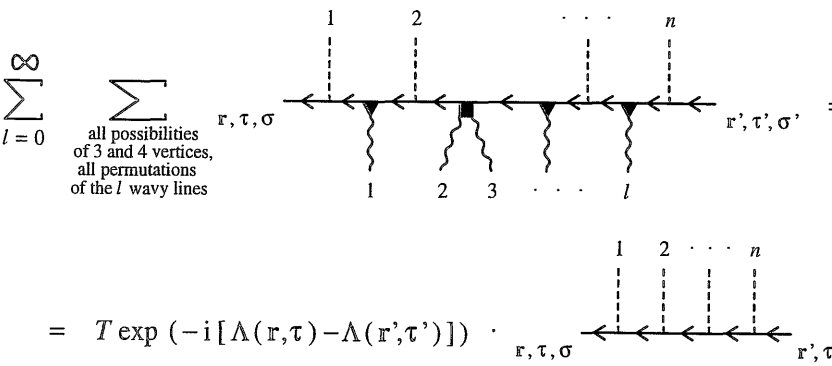

Fig. 4.6. *Theorem 2*: A certain number n of dashed interaction lines is attached to the open propagator line (directed full line) by the respective three vertices. The order of the dashed lines and three vertices is kept fixed. On the left-hand side additionally wavy lines are attached to the propagator line by three and four vertices in all possible ways. The sum is taken over all possibilities to distribute these three and four vertices, over all permutations of the l wavy lines, and over l.

Next, we prove a generalized theorem where also dashed interaction lines corresponding to the two-particle potential $V(r - r')$ are attached to the open propagator line. This theorem is shown in Fig. 4.6. A certain number of dashed interaction lines is attached to the propagator line by the three vertices of Fig. 4.3c. The order of the dashed lines and three vertices is assumed to be kept fixed. On the left-hand side of Fig. 4.6 additionally l wavy lines are attached to the propagator line by the three and four vertices of Figs. 4.4a and b. We take the sum over all possibilities to distribute these three and four vertices. Furthermore, we take the sum over l and over all $l!$ permutations of the wavy lines. For the propagator line in between two neighboring three vertices with dashed lines we can apply Theorem 1. Thus, the propagator lines between the dashed lines can be identified by $\tilde{G}_0$ or by

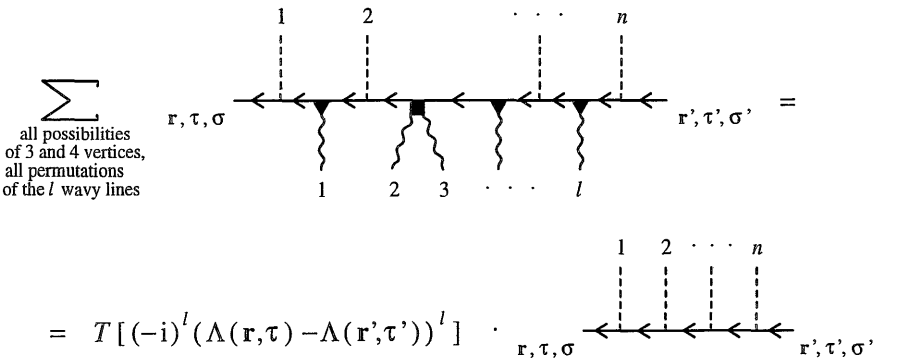

Fig. 4.7. *Theorem 3*: On the left-hand side the sum is taken as in Theorem 2 (Fig. 4.6) where, however, the number l of the wavy lines is kept constant. This theorem is valid for $l \geq 0$.

the right-hand side of Fig. 4.5 which corresponds to a propagator line and an exponential factor of gauge fields. Since the interaction (dashed line) couples to the particles (full line) via the density $\varrho(\boldsymbol{r}, \tau)$, the exponential factors with gauge fields cancel at the three vertices with dashed lines. Thus, we obtain the right-hand side of Fig. 4.6 and Theorem 2 is proven. Next, we expand in powers of the gauge field $\Lambda(\boldsymbol{r}, \tau)$ and obtain Theorem 3 which is shown in Fig. 4.7. On the left-hand side the sum is taken as in Theorem 2 where, however, the number of wavy lines l is kept constant. Theorem 3 is valid for $l \geq 0$.

Now, we bend the propagator line (full directed line), set $\boldsymbol{r}' = \boldsymbol{r}$, $\tau' = \tau$, $\sigma' = \sigma$ and close it by another three vertex with a dashed interaction line. Then we obtain Theorem 4 which is shown in Fig. 4.8. The right-hand side is zero because of

$$\lim_{\boldsymbol{r}' \to \boldsymbol{r}} \lim_{\tau' \to \tau} T[(-\mathrm{i})^l (\Lambda(\boldsymbol{r}, \tau) - \Lambda(\boldsymbol{r}', \tau'))^l] = 0 \tag{4.32}$$

for $l \geq 1$. This theorem is the closed-loop theorem which is equivalent to the closed-loop theorem of the Luttinger model (Dzyaloshinskii and Larkin 1974). While for the Luttinger model the closed-loop theorem is based on the linear energy dispersion of the fermions, here it relies on the local gauge invariance of the system and is valid for all interacting many-particle systems with local particle conservation. In quantum electrodynamics the closed-loop theorem is known since a long time where the wavy lines represent the longitudinal part of the photon propagator (Bjorken and Drell 1965). In this case the closed loop-theorem guarantees that only the transverse photons couple to the matter.

We have proven the theorems with the assumption that $\Lambda(\boldsymbol{r}, \tau)$ is an external field. However, the theorems are valid also if $\Lambda(\boldsymbol{r}, \tau)$ is a boson field operator so that the wavy lines are identified by the gauge-field propagator D according to Fig. 4.4c. Then, the wavy lines have two ends, by which

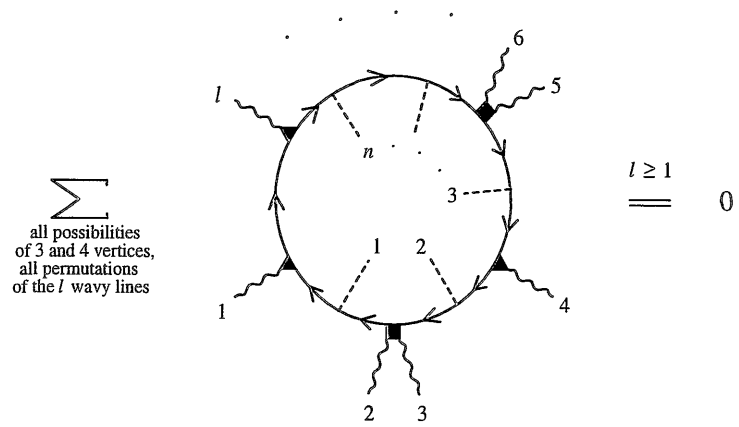

Fig. 4.8. *Theorem 4* (closed-loop theorem): A certain number n of dashed interaction lines is attached to a closed propagator loop (full line) by respective three vertices. The order of these three vertices and dashed lines is kept fixed. Additionally a fixed number l of wavy lines is attached to the propagator loop by three and four vertices. The sum is taken over all possibilities to distribute these three and four vertices and over the $l!$ permutations of the wavy lines. While the single diagrams are nonzero, the sum cancels for $l \geq 1$.

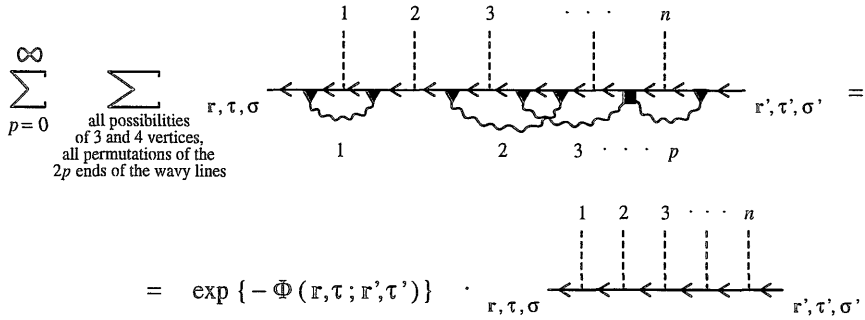

Fig. 4.9. *Theorem 2'*: A certain number n of dashed interaction lines is attached to the open propagator line (full line) where the order of the respective three vertices is kept fixed. On the left-hand side additionally wavy lines, which represent the gauge-field propagator D, are attached with both ends to the propagator line by three and four vertices in all possible ways. The sum is taken over all possibilities to distribute these three and four vertices, over all permutations of the $2p$ ends of the wavy lines, and over the number p of wavy lines (propagators D).

they can be attached to the particle lines. Thus, in Figs. 4.5-4.8 the wavy lines are attached to the open propagator line either with both ends or only with one end. Important for the proof of the theorems is that the sum is taken over all permutations of the ends of the wavy lines which are attached to the open propagator line. As an example we average Theorem 2 with respect to the gauge field $A(r, \tau)$ with the weight factor $e^{-S_A[A]}$. The resulting

Theorem 2′ is shown in Fig. 4.9. Here on the left-hand side all wavy lines are attached with both ends to the propagator lines. The exponential factor on the right-hand side results from (4.28) and (4.30). The diagrammatic equation of Fig. 4.9 looks very similar like the gauge-transformation formula for the Green's function (4.29) with the same exponential factor. In fact it turns out that Theorem 2′ is the fundamental theorem which is needed for the explicit representation of the gauge transformation for the Green's function in terms of Feynman diagrams. Theorem 2′ tells us which kinds of diagrams are resummed by the gauge transformation.

Now, we apply the theorems to the grand-canonical partition function Z and the Green's function $\tilde{G}$ defined by the functional integrals (4.20) and (4.25), respectively. First we consider Z. A typical Feynman diagram of Z is shown in Fig. 4.10. It consists of a certain number of closed propagator loops (loops of directed full lines) which are connected with each other by dashed interaction lines and by wavy lines in all possible ways. Since the perturbation series is the sum of all possible diagrams, Theorem 4 (the closed-loop theorem) can be applied to each propagator loop. If we consider a certain propagator loop of a diagram, the sum over all possibilities to distribute the three and four vertices and to permute the attached wavy lines is included in the perturbation series. Thus, Theorem 4 implies that diagrams with wavy lines attached to the closed propagator loops cancel. Since in the diagrams of Z all propagator lines are closed loops, all diagrams which contain wavy lines cancel so that only diagrams without wavy lines remain. This result proves a statement in all orders of the perturbation theory which we have derived earlier for the functional integral: the grand-canonical partition function (4.20) does not depend on the gauge field, which here means that Z does not depend on the gauge-field propagator D (wavy line). Thus, for the evaluation of Z we need not take diagrams with wavy lines into account.

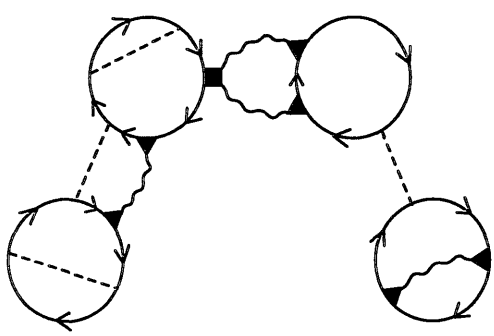

Fig. 4.10. A typical Feynman diagram of the grand-canonical partition function Z defined by (4.20). It consists of a certain number of propagator loops which are connected with each other by dashed interaction lines and by wavy lines.

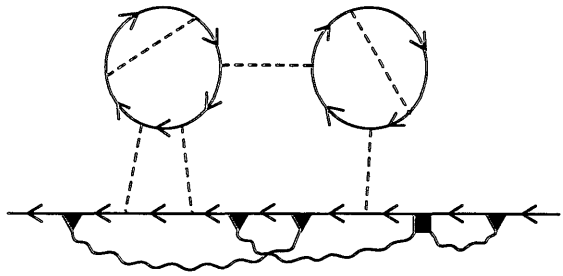

Fig. 4.11. A typical Feynman diagram of the gauge-transformed Green's function $\tilde{G}$ defined by (4.25). It consists of one open propagator line and a certain number of closed propagator loops which are connected with each other by dashed interaction lines and by wavy lines. Because of the closed loop theorem (Fig. 4.8) only those diagrams are relevant for which all wavy lines are connected with both ends to the open propagator line.

Next we consider the perturbation series of $\tilde{G}$. A typical Feynman diagram of $\tilde{G}$ is shown in Fig. 4.11. It consists of one open propagator line and a certain number of propagator loops which are connected with each other by dashed interaction lines and by wavy lines. Again the closed loop theorem (Theorem 4) implies that diagrams with wavy lines attached to propagator loops cancel. For this reason, in diagrams which do not cancel and which yield nontrivial contributions, all wavy lines must be attached with both ends to the open propagator line. A diagram of this kind is shown in Fig. 4.11. Eventually, the diagrams can be resummed by Theorem 2′ (Fig. 4.9) so that all wavy lines disappear and the transformation formula (4.29) is obtained.

We come to the conclusion, that for performing the gauge transformation it is sufficient to take only those diagrams into account for which all wavy lines are attached with both ends to the open propagator line. These diagrams are sufficient to reproduce the transformation formula (4.29). All diagrams with at least one wavy line attached to a propagator loop may be discarded. However, it is not necessary to discard all diagrams of this kind. In the following we will include also diagrams with wavy lines which are connected with both ends to the same propagator loop. (Of course these diagrams cancel.) In this way we obtain a symmetric rule for constructing the Feynman diagrams which does not distinguish between open propagator lines and closed propagator loops:

Feynman rule W: *Wavy lines must be attached with both ends to the same propagator line.*

In the following we always assume that the Feynman diagrams of Z and $\tilde{G}$ are constructed with this rule. The closed-loop theorem (Fig. 4.8) guarantees that diagrams which are not included by Feynman rule W cancel. Theorem 2′

(Fig. 4.9) implies that the gauge-transformation formula (4.29) is valid for the Green's function. We note, however, that Feynman rule W would not be applicable if we would consider higher-order Green's functions as e.g. the two-particle Green's function. In this case there would be several open propagator lines so that there would exist diagrams with wavy lines connecting two different open propagator lines which are not included by Feynman rule W and which do not cancel.

C. Modified self-consistent quantum-field theory

We have established the elements and rules for constructing the Feynman diagrams for the gauge-transformed many-particle system by Figs. 4.3 and 4.4. The Feynman rule W is of special importance and implies a considerable simplification of the perturbation series involving wavy lines because a large number of Feynman diagrams, which cancel either, is omitted right from the beginning. We now want to evaluate the gauge-transformed Green's function $\tilde{G}$ explicitly by the perturbation series. (The physical Green's function G is obtained eventually by the transformation formula (4.29).) For this purpose we perform the same resummations and develop the self-consistent quantum-field theory as we have done in Chap. 2 for the original many-particle system. The Feynman rule W is sufficiently general so that it does not lead to artificial contradictions and difficulties during the resummation. The main change compared to Chap. 2 is that now for the interaction of the particles besides the dashed lines (the two-particle potential) now also the wavy lines are taken into account which represent the interaction with the gauge field. Until now, the gauge-field propagator D identified by the wavy line is an arbitrary function which only must satisfy the usual boundary conditions for a bosonic Green's function. Eventually, D should be chosen so that the convergence behavior of the perturbation series is improved.

In the liquid state the many-particle system described by the Hamiltonian (4.3) is homogeneous in space and time. For this reason, the Green's and correlation functions depend only on the differences of the space coordinates and imaginary times. Thus, it is

$$G_{\sigma\sigma'}(\boldsymbol{r},\tau;\boldsymbol{r}',\tau') = \delta_{\sigma\sigma'} G(\boldsymbol{r}-\boldsymbol{r}',\tau-\tau') \;, \tag{4.33}$$

$$\tilde{G}_{\sigma\sigma'}(\boldsymbol{r},\tau;\boldsymbol{r}',\tau') = \delta_{\sigma\sigma'} \tilde{G}(\boldsymbol{r}-\boldsymbol{r}',\tau-\tau') \;, \tag{4.34}$$

$$D(\boldsymbol{r},\tau;\boldsymbol{r}',\tau') = D(\boldsymbol{r}-\boldsymbol{r}',\tau-\tau') \;, \tag{4.35}$$

$$\Phi(\boldsymbol{r},\tau;\boldsymbol{r}',\tau') = \Phi(\boldsymbol{r}-\boldsymbol{r}',\tau-\tau') \;. \tag{4.36}$$

Since the interaction of the particles by the two-particle potential is spin independent, the Green's functions G and $\tilde{G}$ are proportional to $\delta_{\sigma\sigma'}$. Thus, in the Feynman diagrams the spin indices need not be considered explicitly. The spin degrees of freedom are taken into account sufficiently if we multiply the respective terms of the perturbation series for each closed propagator loop by a factor

$$g_s = (2s+1) \cdot (-1)^{2s} \tag{4.37}$$

where $2s+1$ is the multiplicity of the spin state and $(-1)^{2s}$ is a sign which is positive for bosons and negative for fermions. (For electrons it is $g_s = -2$.) Now, the gauge-transformation formula (4.29) can be written in the form

$$G(\mathbf{r}, \tau) = \mathrm{e}^{\Phi(\mathbf{r},\tau)} \cdot \tilde{G}(\mathbf{r}, \tau) \tag{4.38}$$

for the Green's function of the homogeneous system. From (4.30) and (4.22) we obtain the relation

$$\Phi(\mathbf{r}, \tau) = D(0, 0) - D(\mathbf{r}, \tau) \ . \tag{4.39}$$

The homogeneous Green's functions can be Fourier transformed into $G(\mathbf{k}, \omega_n)$, $\tilde{G}(\mathbf{k}, \omega_n)$, and $D(\mathbf{k}, \Omega_n)$, where $\mathbf{k}$ is the wave vector, ω_n are either bosonic or fermionic Matsubara frequencies depending on the kind of particles, and Ω_n are the bosonic Matsubara frequencies for the gauge bosons. The Green's function $\tilde{G}(\mathbf{k}, \omega_n)$ can be expressed via the Dyson equation

$$\tilde{G}(\mathbf{k}, \omega_n) = 1 \,/\, [-\mathrm{i}\hbar\omega_n + \varepsilon_{\mathbf{k}} - \mu - \tilde{\Sigma}(\mathbf{k}, \omega_n)] \tag{4.40}$$

in terms of the self energy $\tilde{\Sigma}(\mathbf{k}, \omega_n)$ which is given by an infinite sum of one-particle irreducible Feynman diagrams. These diagrams are constructed by the usual rules and by the elements of Figs. 4.3 and 4.4 where Feynman rule W is applied. As described in Chap. 2, in the Feynman diagrams we resum all self-energy subdiagrams so that the propagator lines become thick and are identified by the dressed gauge-transformed Green's function $\tilde{G}$, which is shown in Fig. 4.12a. Then, for $\tilde{\Sigma}$ we obtain an infinite series of irreducible skeleton diagrams with thick propagator lines, thin dashed interaction lines, and thin wavy lines. The skeleton diagrams are irreducible in the sense that they do not contain self-energy subdiagrams or more precisely that they do not fall into pieces if the thick propagator lines are cut twice at any two points. In this way the self energy $\tilde{\Sigma}$ becomes a functional of $\tilde{G}$ so that it can be written as the functional derivative

$$\tilde{\Sigma}(\mathbf{k}, \omega_n) = \frac{1}{\beta L^d g_s} \frac{\delta \tilde{\Phi}[\tilde{G}]}{\delta \tilde{G}(\mathbf{k}, \omega_n)} \tag{4.41}$$

of a functional $\tilde{\Phi}[\tilde{G}]$ which is the sum of all vacuum skeleton diagrams with thick propagator lines identified by $\tilde{G}$ (Fig. 4.12a), thin interaction lines identified by $-V$ (Fig. 4.3b), and thin wavy lines identified by D (Fig. 4.4c). The factor $1/(\beta L^d g_s)$ is needed for a proper normalization of the functional derivative.

A further resummation can be performed for the interaction with respect to polarization insertions so that the dashed interaction lines become thick. In Fig. 4.12b the corrections to the interaction due to polarization effects are

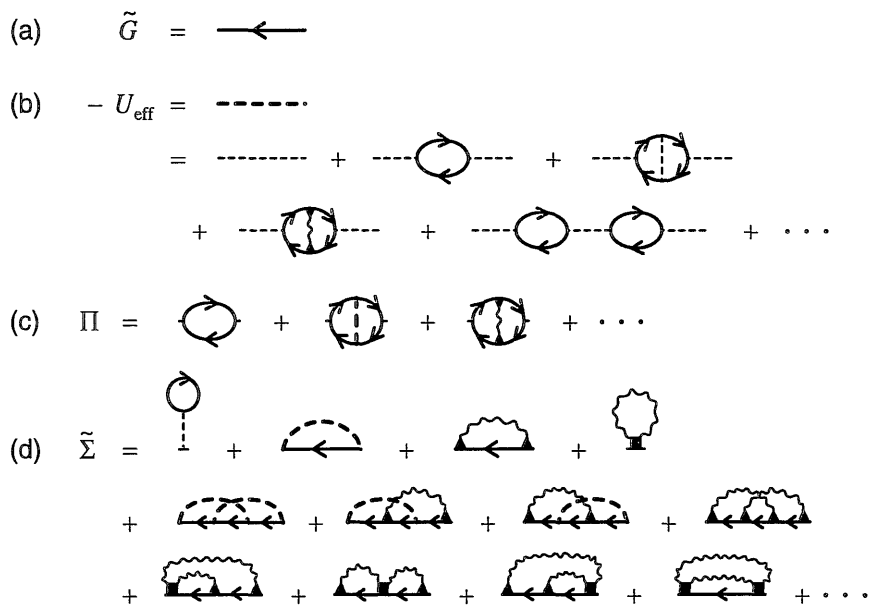

Fig. 4.12. (a) The thick propagator line (directed thick full line) is identified by the dressed gauge transformed Green's function $\tilde{G}$. (b) Minus the effective screened interaction $-U_{\text{eff}}$, identified by a thick dashed line, is obtained by resumming all diagrams with polarization insertions. (c) The polarization function Π and (d) the self energy $\tilde{\Sigma}$ up to second order in terms of irreducible skeleton diagrams with thick propagator lines and thick dashed lines. The wavy lines stay thin because of Feynman rule W.

shown up to second order. The thick dashed interaction line is then identified by $-U_{\text{eff}}$ where $U_{\text{eff}}(\boldsymbol{k}, \Omega_n)$ is the effective screened interaction. A first resummation is performed by expressing $U_{\text{eff}}(\boldsymbol{k}, \Omega_n)$ via the equation

$$U_{\text{eff}}(\boldsymbol{k}, \Omega_n) = V(\boldsymbol{k}) \,/\, [1 + V(\boldsymbol{k}) \Pi(\boldsymbol{k}, \Omega_n)] \tag{4.42}$$

in terms of the polarization function $\Pi(\boldsymbol{k}, \Omega_n)$, where $V(\boldsymbol{k})$ is the Fourier transform of the bare two-particle interaction potential. (This equation may be interpreted as a Dyson equation with Π as the self energy if the interaction is mediated by some bosons so that the dashed lines may be identified by the respective boson Green's function.) The polarization Π is then given by a series of skeleton diagrams, which are additionally one-particle irreducible with respect to the dashed interaction lines (they do not fall into pieces if a dashed line is cut). In a second step in the diagrams of Π the partial resummation with respect to the polarization insertions is performed so that the dashed interaction lines become thick, too. The same partial resummation is also performed in the diagrams of $\tilde{\Sigma}$. On the other hand, Feynman rule W implies that there are no polarization insertions for the gauge-field propagator D so that the wavy lines stay thin. As an example we consider the diagrams

shown in Fig. 4.12b where the dashed lines are replaced by wavy lines. In all diagrams with polarization insertions (which are all diagrams except the first one) the two external wavy lines are connected with only one end to propagator loops. Diagrams of this kind are excluded by Feynman rule W. Hence, only the first diagram without polarization insertions remains which is a thin wavy line.

Thus, we find that the self energy $\tilde{\Sigma}$ and the polarization Π are given by series' of irreducible skeleton diagrams with thick propagator lines, thick dashed interaction lines, and thin wavy lines. The skeleton diagrams are irreducible in the sense that they do not contain any self-energy subdiagrams and polarization insertions. More precisely, the diagrams do not fall into pieces if either the thick propagator lines or the thick dashed lines are cut twice at any two points. Furthermore, because of Feynman rule W there are also no polarization insertions for the wavy lines, so that the diagrams do also not fall into pieces if the wavy lines are cut twice at any two points. In Fig. 4.12 c and d, respectively, the Feynman diagrams of Π and $\tilde{\Sigma}$ are shown up to second order. An exception is the Hartree diagram, which is the first diagram of the self energy $\tilde{\Sigma}$ in Fig. 4.12d: in this diagram the dashed interaction line is thin. The Hartree diagram represents minus the average single-particle potential caused by the average density $\varrho_0 = \langle \varrho \rangle$ of the particles via the bare interaction potential. For electrically charged systems the Hartree diagram is canceled by the neutralizing positively charged background.

It is possible to find a functional $\tilde{\Xi}[\tilde{G}, U_{\text{eff}}]$ so that the self energy and the polarization function can be written as functional derivatives

$$\tilde{\Sigma}(k, \omega_n) = \frac{1}{\beta L^d g_s} \left(\frac{\delta \tilde{\Xi}[\tilde{G}, U_{\text{eff}}]}{\delta \tilde{G}(k, \omega_n)} \right)_{U_{\text{eff}}, D}, \tag{4.43}$$

$$\Pi(k, \Omega_n) = -\frac{2}{\beta L^d} \left(\frac{\delta \tilde{\Xi}[\tilde{G}, U_{\text{eff}}]}{\delta U_{\text{eff}}(k, \Omega_n)} \right)_{\tilde{G}, D}, \tag{4.44}$$

respectively. In (4.43) the functional derivative is performed at constant U_{eff} and constant D, while in (4.44) the functional derivative is performed at constant $\tilde{G}$ and constant D. The factors $1/(\beta L^d g_s)$ and $-2/(\beta L^d)$, respectively, are needed for proper normalization of the functional derivatives. In (4.44) the minus sign is due to the fact that the thick dashed lines are identified by $-U_{\text{eff}}$, while the factor 2 is needed to cancel a symmetry factor 1/2 which occurs because the thick dashed lines are undirected. In Fig. 4.13 the Feynman diagrams of the functional $\tilde{\Xi}[\tilde{G}, U_{\text{eff}}]$ are shown up to second order. The first diagram which is the Hartree diagram is an exception: here the dashed interaction line is thin and identified by the bare interaction. All the other diagrams are irreducible vacuum skeleton diagrams with thick propagator lines, thick dashed lines, and thin wavy lines. These diagrams are irreducible in the sense that they do not fall into pieces if either the thick propagator lines or the thick dashed lines are cut twice at any two points. The diagrams do also not fall into pieces if the wavy lines are cut twice at any two points.

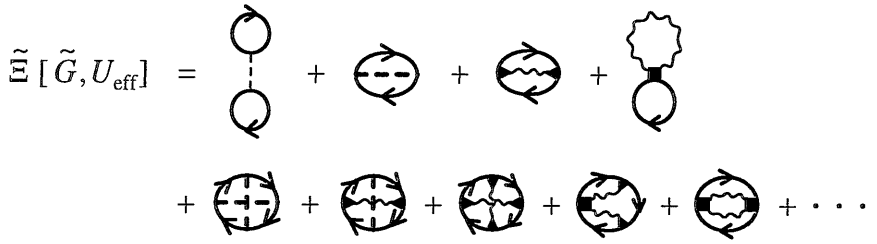

Fig. 4.13. The Feynman diagrams of the functional $\tilde{\Xi}[\tilde{G}, U_{\text{eff}}]$ up to second order. The thick propagator lines are identified by $\tilde{G}$, the thick dashed lines by $-U_{\text{eff}}$. The wavy lines are thin and represent the gauge-field propagator D. The Hartree diagram (first diagram) is an exception: here the dashed interaction line is thin and identified by minus the bare interaction $-V$.

Thus, the full perturbation series of $\tilde{\Xi}[\tilde{G}, U_{\text{eff}}]$ is given by

$$\tilde{\Xi}[\tilde{G}, U_{\text{eff}}] = \text{Hartree diagram} + \left\{ \begin{array}{c} \text{sum of all vacuum skeleton diagrams with} \\ \text{thick propagator lines identified by } \tilde{G}, \\ \text{thick dashed lines identified by } -U_{\text{eff}}, \\ \text{and thin wavy lines identified by } D \end{array} \right\} . \tag{4.45}$$

Because of (4.42) together with Fig. 4.12c the effective screened interaction $U_{\text{eff}}(\boldsymbol{k}, \Omega_n)$ is a functional of $\tilde{G}(\boldsymbol{k}, \omega_n)$. Determining the self energy $\tilde{\Sigma}(\boldsymbol{k}, \omega_n)$, in (4.43) the functional derivative with respect to $\tilde{G}$ is performed at constant U_{eff} while on the other hand in (4.41) the effective screened interaction U_{eff} does not occur at all. For this reason, $\tilde{\Xi}[\tilde{G}, U_{\text{eff}}]$ is different from $\tilde{\Phi}[\tilde{G}]$. To determine the functional $\tilde{\Phi}[\tilde{G}]$ we consider (4.44) together with (4.42). Eliminating the polarization function we obtain the equation

$$U_{\text{eff}}^{-1}(\boldsymbol{k}, \Omega_n) - V^{-1}(\boldsymbol{k}) = -\frac{2}{\beta L^d} \left(\frac{\delta \tilde{\Xi}[\tilde{G}, U_{\text{eff}}]}{\delta U_{\text{eff}}(\boldsymbol{k}, \Omega_n)} \right)_{\tilde{G}, D} . \tag{4.46}$$

This equation can be put into the form

$$\left(\frac{\delta}{\delta U_{\text{eff}}(\boldsymbol{k}, \Omega_n)} \left[\frac{1}{2} \beta L^d \int \frac{\mathrm{d}^d k}{(2\pi)^d} \frac{1}{\beta} \sum_{\Omega_n} \left\{ \ln \frac{U_{\text{eff}}(\boldsymbol{k}, \Omega_n)}{V(\boldsymbol{k})} - \left[\frac{U_{\text{eff}}(\boldsymbol{k}, \Omega_n)}{V(\boldsymbol{k})} - 1 \right] \right\} + \tilde{\Xi}[\tilde{G}, U_{\text{eff}}] \right] \right)_{\tilde{G}, D} = 0 . \tag{4.47}$$

Thus, a candidate for the functional $\tilde{\Phi}[\tilde{G}]$ is

$$\tilde{\Phi}[\tilde{G}] = \tfrac{1}{2} \mathrm{Tr} \{ \ln(V^{-1} U_{\text{eff}}) - [V^{-1} U_{\text{eff}} - 1] \} + \tilde{\Xi}[\tilde{G}, U_{\text{eff}}] \tag{4.48}$$

because Eq. (4.47) implies that this functional satisfies the condition

$$\left(\frac{\delta\tilde{\Phi}[\tilde{G}]}{\delta U_{\text{eff}}(k,\Omega_n)}\right)_{\tilde{G},D} = 0 \tag{4.49}$$

so that (4.41) yields the correct self energy even though $U_{\text{eff}}(k,\Omega_n)$ is itself a functional of $\tilde{G}$. By considering the perturbation series of Feynman diagrams order by order one can convince oneself that (4.48) is indeed the correct functional $\tilde{\Phi}[\tilde{G}]$.

Finally, from (2.19) we obtain the "enthalpy" functional

$$\begin{aligned} H[\tilde{G},U_{\text{eff}}] &= \pm\text{Tr}\{-\ln\tilde{G}+[G_0^{-1}\tilde{G}-1]\} \\ &\quad + \tfrac{1}{2}\text{Tr}\{-\ln(V^{-1}U_{\text{eff}})+[V^{-1}U_{\text{eff}}-1]\} - \tilde{\Xi}[\tilde{G},U_{\text{eff}}] \,. \end{aligned} \tag{4.50}$$

This "enthalpy" functional can be viewed as the fundamental functional of the modified self-consistent quantum-field theory. The fact that $H[\tilde{G},U_{\text{eff}}]$ depends explicitly on $\tilde{G}$ and U_{eff} is related to the resummation of the self-energy subdiagrams and the polarization insertions so that the propagator lines and dashed lines in the Feynman diagrams are thick and identified by $\tilde{G}$ and U_{eff}, respectively. The gauge-transformed Green's function $\tilde{G}(k,\omega_n)$ and the effective screened interaction $U_{\text{eff}}(k,\Omega_n)$ are obtained by extremizing the "enthalpy" functional $H[\tilde{G},U_{\text{eff}}]$ (in the weak sense of a saddle point). For this purpose the necessary conditions are

$$\left(\frac{\delta H[\tilde{G},U_{\text{eff}}]}{\delta\tilde{G}(k,\omega_n)}\right)_{U_{\text{eff}},D} = 0 \,, \qquad \left(\frac{\delta H[\tilde{G},U_{\text{eff}}]}{\delta U_{\text{eff}}(k,\Omega_n)}\right)_{\tilde{G},D} = 0 \,. \tag{4.51}$$

These two equations are equivalent to the Dyson equation for $\tilde{G}$ (4.40) together with the self energy (4.43) and the Dyson equation for U_{eff} (4.42) together with the polarization function (4.44), respectively. Eventually, the grand-canonical thermodynamic potential $\Omega(T,\mu)$ is obtained from $H[\tilde{G},U_{\text{eff}}]$ by inserting $\tilde{G}$ and U_{eff} so that

$$\Omega(T,\mu) = k_{\text{B}}T\cdot\text{extr}\{H[\tilde{G},U_{\text{eff}}]\} \,. \tag{4.52}$$

The nontrivial contributions of the interaction in the "enthalpy" are included in the functional $\tilde{\Xi}[\tilde{G},U_{\text{eff}}]$ which is given by the infinite perturbation series of irreducible vacuum skeleton diagrams (4.45). In general, this perturbation series cannot be handled so that an approximation must be introduced by truncating the functional $\tilde{\Xi}[\tilde{G},U_{\text{eff}}]$ at a finite order. The conventional self-consistent quantum-field theory is modified by the gauge-transformation. For this reason the functional $\tilde{\Xi}[\tilde{G},U_{\text{eff}}]$ additionally depends explicitly on the gauge-field propagator $D(k,\Omega_n)$ which in the Feynman diagrams is represented by the wavy lines and which may be an arbitrary function with bosonic character. Now, the basic idea is to choose $D(k,\Omega_n)$ so that part of the diagrams are canceled and hence the properties of the perturbation series are improved. In Fig. 4.13 the second and third diagram have the same topological structure. While in the second diagram the interaction is a thick dashed

line identified by $-U_{\text{eff}}$, in the third diagram the interaction is a wavy line identified by D. Since the wavy line is an arbitrary function, it may be chosen so that the two diagrams cancel each other at least partially. Cancellations of the same kind occur also for higher order diagrams. In Fig. 4.13 second order diagrams with the same topological structure are the fifth, sixth, and seventh diagram. These diagrams will cancel at least partially, too. For any diagram with a thick dashed line there can always be found a diagram with the same topological structure and with a wavy line, so that the sum of the two diagrams leads to cancellations. Thus, we conclude that for an improvement of the perturbation theory by partial cancellations of diagrams the wavy line will be related in some way to the thick dashed line. Hence, the gauge-field propagator D will be related to the effective screened interaction U_{eff}. Effects of collective excitations are included in $U_{\text{eff}}(\boldsymbol{k}, \Omega_n)$ via the polarization function $\Pi(\boldsymbol{k}, \Omega_n)$. Equation (4.42) can be written in the form

$$U_{\text{eff}}(\boldsymbol{k}, \Omega_n) = V(\boldsymbol{k}) - [V(\boldsymbol{k})]^2 \chi_{\varrho\varrho}(\boldsymbol{k}, \Omega_n) \tag{4.53}$$

where

$$\chi_{\varrho\varrho}(\boldsymbol{k}, \Omega_n) = \Pi(\boldsymbol{k}, \Omega_n)/[1 + V(\boldsymbol{k})\Pi(\boldsymbol{k}, \Omega_n)] \tag{4.54}$$

is the density-density correlation function. Thus, the gauge-field propagator $D(\boldsymbol{k}, \Omega_n)$ will be related to the collective excitations via the density-density correlation function $\chi_{\varrho\varrho}(\boldsymbol{k}, \Omega_n)$.

D. Modified SC-RPA

The modified self-consistent random-phase approximation (modified SC-RPA) is obtained by considering only the first-order diagrams in $\tilde{\Xi}[\tilde{G}, U_{\text{eff}}]$. In Fig. 4.13 these are the first four diagrams. The corresponding self energy $\tilde{\Sigma}(\boldsymbol{r}, \tau)$ is given by the first four diagrams in Fig. 4.12d. The first diagram (Hartree diagram) implies a constant shift of the energy which for electron systems is canceled by the neutralizing background. Thus, the first diagram may be omitted. We obtain three contributions for the self energy

$$\tilde{\Sigma}(\boldsymbol{r}, \tau) = \tilde{\Sigma}_1(\boldsymbol{r}, \tau) + \tilde{\Sigma}_2(\boldsymbol{r}, \tau) + \tilde{\Sigma}_3(\boldsymbol{r}, \tau) \ . \tag{4.55}$$

The first contribution arises from the second diagram of Fig. 4.12d which is given by

$$\tilde{\Sigma}_1(\boldsymbol{r}, \tau) = -U_{\text{eff}}(\boldsymbol{r}, \tau)\tilde{G}(\boldsymbol{r}, \tau) \ . \tag{4.56}$$

This is the known self energy (2.31) of the conventional SC-RPA theory. The other two contributions represent the interaction of the particles with the gauge field. Because of the derivatives in the three vertex shown in Fig. 4.4a, the second contribution arising from the third diagram is quite complicated. This contribution can be written in the form

$$\tilde{\Sigma}_2(r,\tau) = \tilde{G}(r,\tau)\cdot\Big(\Big[\hbar\partial_\tau + \frac{\hbar^2}{2m}\nabla^2\Big]^2 D(r,\tau)\Big) + \nabla\Big\{-4\frac{\hbar^2}{2m}\tilde{G}(r,\tau)\Big(\nabla\Big[\hbar\partial_\tau + \frac{\hbar^2}{2m}\nabla^2\Big]D(r,\tau)\Big)\Big\} + \sum_{kl}\partial_k\partial_l\Big\{4\Big(\frac{\hbar^2}{2m}\Big)^2\tilde{G}(r,\tau)\big(\partial_k\partial_l D(r,\tau)\big)\Big\}\,. \tag{4.57}$$

which is quite convenient for numerical calculations. Finally, the fourth diagram yields

$$\tilde{\Sigma}_3(r,\tau) = -\int\frac{\mathrm{d}^d k}{(2\pi)^d}\,\frac{\hbar^2 k^2}{2m}\,D(k,\tau'=0)\cdot\delta(r)\;\hbar\,\delta(\tau) \tag{4.58}$$

which leads to a constant shift of the energy in a similar way as the Hartree diagram. For this reason, the third contribution is not very important. The polarization function is given by the first diagram of Fig. 4.12c. Thus, we obtain

$$\Pi(r,\tau) = g_s[\tilde{G}(r,\tau)]^2\,. \tag{4.59}$$

Now, we have all equations for the modified SC-RPA theory. These equations are the Dyson equation for the gauge-transformed Green's function (4.40) together with the self energy given by (4.55)-(4.58) and the Dyson equation for the effective screened interaction (4.42) together with the polarization function (4.59). As usual in self-consistent theories, the equations are written partly in Fourier and partly in real-space representation. Thus, if a proper and efficient numerical Fourier transformation procedure is available, the self-consistent equations can be solved by an iteration on the computer so that the gauge-transformed Green's function $\tilde{G}(k,\omega_n)$, the effective screened interaction $U_{\mathrm{eff}}(k,\Omega_n)$, and related quantities can be calculated explicitly. Finally, the physical relevant Green's function $G(k,\omega_n)$ is obtained from the transformation formula (4.38) together with (4.39).

The "modification" of the SC-RPA theory is represented by the occurrence of the gauge-field propagator $D(r,\tau)$ in (4.39), (4.57), and (4.58), which is an arbitrary bosonic function and must be chosen properly. Clearly, by the choice $D(r,\tau) = 0$ we recover the conventional SC-RPA theory. Because of the self-consistency the SC-RPA self energy (4.56) has a nontrivial imaginary-time dependence which after Fourier transformation implies a nontrivial frequency dependence and a nontrivial spectral function. This nontrivial behavior of the first contribution should be canceled by the second contribution (4.57), at least partially. Especially, the "low energetic" contributions should be canceled, because these contributions would imply small energy denominators in the perturbation series. For this purpose, the gauge-field propagator $D(r,\tau)$ must be chosen appropriately. Clearly, by inspection of (4.56) and (4.57) we find that $D(r,\tau)$ must be related somehow to the effective screened interaction $U_{\mathrm{eff}}(r,\tau)$. However, because of the complicated structure of (4.57) with respect to the spatial derivatives it is unclear in

general, if a proper cancellation can be achieved at all. Nevertheless, in the next sections and chapters we will consider many-particle systems for which the cancellation works quite well and for which the modified SC-RPA theory yields good results.

4.3 Application to the Luttinger model

The Luttinger model for a one-dimensional interacting fermion system is defined by the Hamiltonian (4.1). The Feynman rules for the quantum-field theory are obtained from the related action functional which can be constructed from the Hamiltonian by (4.6). Since (4.1) does not contain terms which imply exchange of fermions between the two branches, the particle number is conserved locally for each branch separately. Thus, continuity equations

$$\mathrm{i}\partial_\tau \varrho_\alpha(x,\tau) + \partial_x j_\alpha(x,\tau) = 0 \tag{4.60}$$

are valid for $\alpha = \pm 1$. Consequently, the gauge transformation of the fermion fields can be performed for each branch separately. The transformation formulas read

$$\Psi_{\alpha\sigma}(x,\tau) = \mathrm{e}^{\mathrm{i}\Lambda_\alpha(x,\tau)}\tilde{\Psi}_{\alpha\sigma}(x,\tau)\ , \quad \Psi^*_{\alpha\sigma}(x,\tau) = \mathrm{e}^{-\mathrm{i}\Lambda_\alpha(x,\tau)}\tilde{\Psi}^*_{\alpha\sigma}(x,\tau) \tag{4.61}$$

where the gauge field $\Lambda_\alpha(x,\tau)$ depends on the branch index α. The linear energy dispersion $\varepsilon_{k\alpha} = \varepsilon_0 + \alpha\hbar v_\mathrm{F} k$ implies that the fermions of branch α all move with the same velocity αv_F so that the related current is simply

$$j_\alpha(x,\tau) = \alpha v_\mathrm{F} \cdot \varrho_\alpha(x,\tau)\ . \tag{4.62}$$

This fact implies a considerable simplification of the Feynman rules involving the gauge field. In Fig. 4.14 the elements for constructing the Feynman diagrams are summarized. The thin propagator line identified by the free Green's function (Fig. 4.14a) depends on the branch index α. By definition in (4.1) the interaction identified by the dashed line (Fig. 4.14b) is a matrix with respect to the branch index. Since the gauge field $\Lambda_\alpha(x,\tau)$ depends on the branch index, the gauge-field propagator

$$\langle T[\Lambda_\alpha(x,\tau)\Lambda_{\alpha'}(x',\tau')]\rangle = D_{\alpha\alpha'}(x-x',\tau-\tau') \tag{4.63}$$

identified by the wavy line (Fig. 4.14c) is a matrix with respect to the branch indices, too. The interaction is assumed to be spin independent so that spin indices do not appear explicitly. The spin degrees of freedom are taken into account sufficiently by multiplying the respective term by a factor $g_s = -2$ for each closed fermion loop in a Feynman diagram. The dashed lines are attached to the fermion lines by the three vertex shown in Fig. 4.14d as usual. The linear energy dispersion of the Luttinger model implies that the

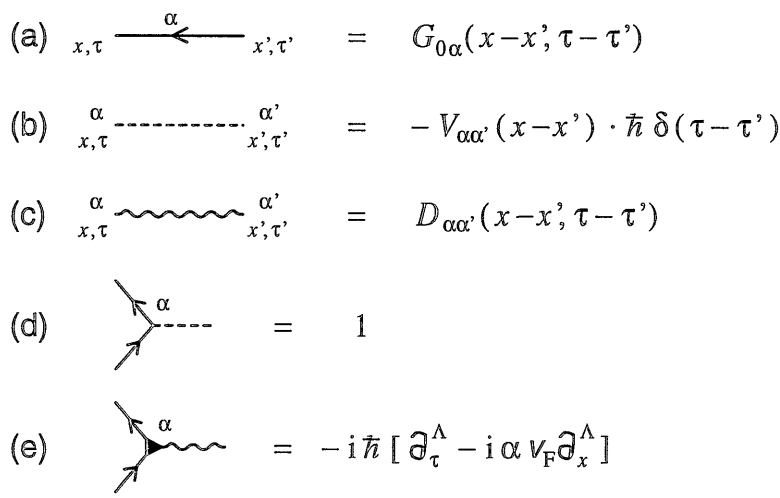

Fig. 4.14. The elements for constructing the Feynman diagrams of the gauge transformed Luttinger model. While the fermion propagator (a) is diagonal in the branch index, the interaction (b) and the gauge-field propagator (c) are matrices with nonzero nondiagonal elements. In the three vertices (d) and (e) the branch indices of the three incoming lines must be equal.

wavy lines are attached to the fermion lines only by a three vertex as shown in Fig. 4.14e. (A four vertex as this one in Fig. 4.4b is not present here.) Because of the simple structure of the current (4.62), the differential operators on the right-hand side of Fig. 4.14e act only on the gauge field (wavy line). There are no differential operators present that act on the fermion fields (propagator lines) as it is in Fig. 4.4a. It will turn out below that the simple structure of the three vertex in Fig. 4.14e with respect to the differential operators and the absence of higher-order vertices with more than one wavy line eventually allows a complete cancellation of the interaction so that the Luttinger model can be solved exactly.

The absence of particle exchange between the branches is reflected by the fact that in the three vertices in Fig. 4.14d and Fig. 4.14e the branch indices of the three incoming lines must be equal. As a consequence the free fermion Green's functions $G_{0\alpha}$ in a long propagator line with dashed and wavy lines attached to it (which might be either an open line or a closed loop) all have the same branch index α. This fact is indicated by the α's in Fig. 4.1 and is an important assumption for proving the closed loop theorem (Fig. 4.1a) and the theorems with wavy lines (Figs. 4.5-4.9) for the Luttinger model. As a further consequence, by inspection of the Feynman diagrams we find that the gauge-transformed fermion Green's function is diagonal with respect to the branch indices so that

$$\langle T[\tilde{\Psi}_{\alpha\sigma}(x,\tau)\tilde{\Psi}^{+}_{\alpha'\sigma'}(x',\tau')]\rangle = \delta_{\alpha\alpha'}\delta_{\sigma\sigma'}\tilde{G}_{\alpha}(x-x',\tau-\tau') \; . \tag{4.64}$$

The same is true also for the original fermion Green's function so that

$$\langle T[\Psi_{\alpha\sigma}(x,\tau)\Psi^{+}_{\alpha'\sigma'}(x',\tau')]\rangle = \delta_{\alpha\alpha'}\delta_{\sigma\sigma'}G_{\alpha}(x-x',\tau-\tau') \ . \tag{4.65}$$

Thus, there will be two Green's functions $G_{\alpha}(x,\tau)$ and $\tilde{G}_{\alpha}(x,\tau)$. In analogy to (4.38) and (4.39) we find the transformation formula

$$G_{\alpha}(x,\tau) = \mathrm{e}^{\Phi_{\alpha}(x,\tau)} \cdot \tilde{G}_{\alpha}(x,\tau) \tag{4.66}$$

where

$$\Phi_{\alpha}(x,\tau) = D_{\alpha\alpha}(0,0) - D_{\alpha\alpha}(x,\tau) \ . \tag{4.67}$$

Now, we evaluate the gauge-transformed Green's function $\tilde{G}_{\alpha}(x,\tau)$ by considering the perturbation series. In Fourier representation the Green's function $\tilde{G}_{\alpha}(k,\omega_n)$ can be expressed via the Dyson equation

$$\tilde{G}_{\alpha}(k,\omega_n) = 1\,/\,[-\mathrm{i}\hbar\omega_n + \varepsilon_{k\alpha} - \mu - \tilde{\Sigma}_{\alpha}(k,\omega_n)] \tag{4.68}$$

in terms of the self energy $\tilde{\Sigma}_{\alpha}(k,\omega_n)$, where the self energy is given by an infinite series of Feynman diagrams. A typical self-energy diagram is shown in Fig. 4.15a. The diagram consists of one open fermion line and a certain number of closed fermion loops which are connected with each other by dashed and wavy lines. The self-energy diagram must be one-particle irreducible which means that it does not fall into pieces if any fermion line is cut at any

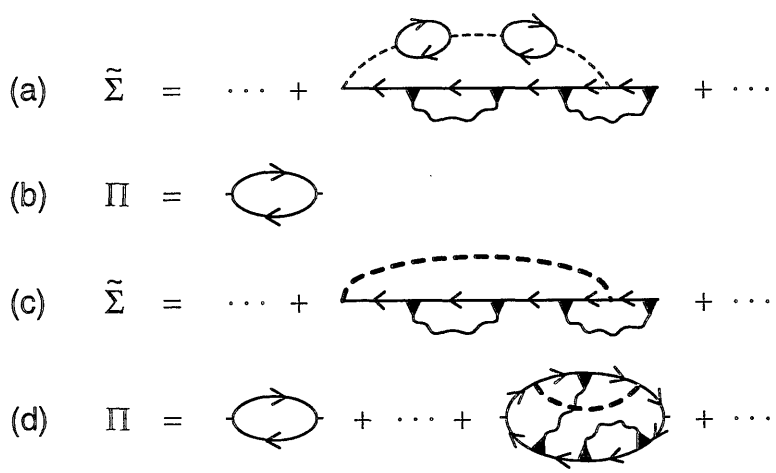

Fig. 4.15. (a) Feynman diagrams of the self energy $\tilde{\Sigma}$ for the Luttinger model. (b) The polarization function Π is exactly given by the bubble. (c) The self energy $\tilde{\Sigma}$ after resummation of the polarization subdiagrams. (d) Because of the closed loop theorem we may add further bubble diagrams to the polarization function Π with thick dashed and wavy lines attached to the fermion loop with both ends. These additional diagrams cancel if the sum is taken over all permutations of the three vertices.

point. According to Theorem 2′ in Fig. 4.9 the transformation formula (4.66) requires that wavy lines are attached with both ends to the open fermion line in all possible ways and numbers. However, wavy lines attached to the closed fermion loops are not needed. Only dashed interaction lines may be attached to the closed loops. The closed-loop theorem of the Luttinger model (Dzyaloshinskii and Larkin 1974) implies that the number of three vertices with dashed lines must be $n \leq 2$ in a loop, otherwise the Feynman diagrams cancel in the perturbation series. The $n = 1$ loops are resummed into the Hartree diagram which implies an average single-particle potential which is canceled by the potential of the positively charged neutralizing background. Thus, only the $n = 2$ loops remain, i.e. the bubbles.

To obtain the self-consistent representation of the self energy we perform partial resummations so that the propagator lines and the dashed interaction lines become thick. First, we perform the resummation with respect to the polarization subdiagrams. By inspection of the diagrams we find that the bubble is the only polarization diagram. Thus, the polarization function $\Pi_{\alpha\alpha'}(k, \Omega_n)$ is exactly given by the bubble diagram shown in Fig. 4.15b. Now, the resummation of the bubbles is performed according to Fig. 4.2a. As a result, we obtain the effective interaction $U_{\mathrm{eff},\alpha\alpha'}(k, \Omega_n)$ which is related to the polarization function by the Dyson equation

$$U^{-1}_{\mathrm{eff},\alpha\alpha'}(k, \Omega_n) = V^{-1}_{\alpha\alpha'}(k) + \Pi_{\alpha\alpha'}(k, \Omega_n) \tag{4.69}$$

and which is identified by a thick dashed line. We note that this equation together with the polarization function in Fig. 4.15b means that here for the effective potential and for the collective excitations the random-phase approximation (RPA) is exact. Now, the self energy $\tilde{\Sigma}$ is given by a series of diagrams which consist of one open thin fermion line with thick dashed lines and wavy lines attached to it as it is shown in Fig. 4.15c. The polarization function Π is given only by the bubble diagram. However, we may add diagrams consisting of one fermion loop and any number of thick dashed lines and wavy lines attached to the loop with both ends as it is shown in Fig. 4.15d. The closed loop theorems guarantee that these additional diagrams cancel if the sum over all permutations of the three vertices is taken. The polarization diagrams in Fig. 4.15d have an analogous structure as the self-energy diagrams in Fig. 4.15c. For this reason, now in a second step the resummation of the self-energy subdiagrams can be performed straightforwardly for the self energy $\tilde{\Sigma}$ and also for the polarization function Π. As a result, $\tilde{\Sigma}$ and Π are given by series' of irreducible skeleton diagrams which consist of thick fermion lines, thick dashed lines, and thin wavy lines. As usual, the skeleton diagrams are irreducible in the sense that they do not fall into pieces if either the thick fermion lines or the thick dashed lines are cut twice at any two points. In Figs. 4.16 a and b the skeleton diagrams of $\tilde{\Sigma}$ and of Π are shown up to second order, respectively. Furthermore, a functional $\tilde{\Xi}[\tilde{G}, U_{\mathrm{eff}}]$ can be found so that $\tilde{\Sigma}$ and Π can be written as the functional

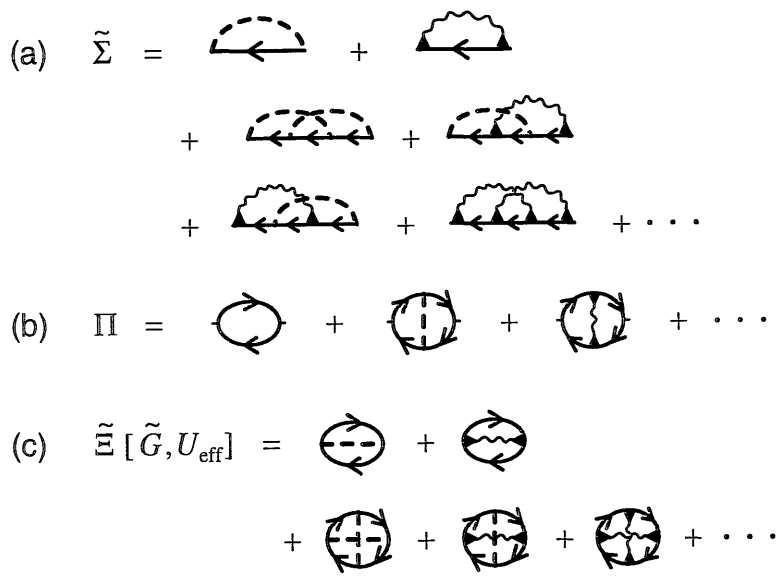

Fig. 4.16. The irreducible skeleton diagrams with thick fermion lines and thick dashed lines up to second order for (a) the self energy $\tilde{\Sigma}$, (b) the polarization function $\tilde{\Pi}$, and (c) the functional $\tilde{\Xi}[\tilde{G}, U_{\text{eff}}]$.

derivatives (4.43) and (4.44), respectively (where the branch index must be added appropriately). We find that this functional is given by a series of all possible vacuum skeleton diagrams which consist of one thick fermion loop and any number of thick dashed lines and wavy lines which are attached to the loop with both ends in all possible ways. In Fig. 4.16c the functional $\tilde{\Xi}[\tilde{G}, U_{\text{eff}}]$ is shown up to second order.

By the series' of skeleton diagrams shown in Fig. 4.16 we have established the modified self-consistent quantum-field theory for the Luttinger model. Now we must choose the gauge-field propagator $D_{\alpha\alpha'}(x,\tau)$ so that the major parts of the diagrams cancel. Combining the thick dashed line and also the thin wavy line with two respective three vertices, we obtain two kinds of composite four vertices which are shown in Fig. 4.17. We claim that the sum of these two four vertices is zero. Since the three vertices (defined in Fig. 4.14) do not contain differential operators acting on the fermion fields, we can amputate the four external thick fermion lines in Fig. 4.17. Thus, by applying the Feynman rules, from Fig. 4.17 we obtain the equation

$$-U_{\text{eff},\alpha\alpha'}(x-x',\tau-\tau') + (-\mathrm{i}\hbar)^2[\partial_\tau - \mathrm{i}\alpha v_{\text{F}}\partial_x]\,[\partial_{\tau'} - \mathrm{i}\alpha' v_{\text{F}}\partial_{x'}] \cdot D_{\alpha\alpha'}(x-x',\tau-\tau') = 0\,. \quad (4.70)$$

This equation can be written in the simpler form

$$\hbar^2[\partial_\tau - \mathrm{i}\alpha v_{\text{F}}\partial_x]\,[\partial_\tau - \mathrm{i}\alpha' v_{\text{F}}\partial_x]\,D_{\alpha\alpha'}(x,\tau) = U_{\text{eff},\alpha\alpha'}(x,\tau)\,. \quad (4.71)$$

Fig. 4.17. Two composite four vertices are obtained by combining the thick dashed line and the wavy line with the respective three vertices. The gauge-field propagator D (wavy line) is chosen so that the sum of the two composite four vertices is zero.

After a Fourier transformation we obtain the gauge-field propagator explicitly as

$$D_{\alpha\alpha'}(k,\Omega_n) = \frac{U_{\mathrm{eff},\alpha\alpha'}(k,\Omega_n)}{(-\mathrm{i}\hbar\Omega_n + \alpha\hbar v_\mathrm{F} k)\,(-\mathrm{i}\hbar\Omega_n + \alpha'\hbar v_\mathrm{F} k)} \,. \tag{4.72}$$

By construction this choice of the gauge-field propagator guarantees that the sum of the two composite four vertices shown in Fig. 4.17 cancels explicitly.

Now, we apply the cancellation of the thick dashed and thin wavy lines to $\tilde{\Sigma}$ and Π. In Fig. 4.16a one clearly sees that the two first-order diagrams and also the four second-order diagrams of $\tilde{\Sigma}$ cancel. In Fig. 4.16b the two second-order diagrams of Π cancel, while the first-order diagram (the bubble) remains. It turns out that all diagrams cancel which contain at least one interaction line, because the interaction lines may be either thick dashed or thin wavy so that the sum of the respective diagrams is zero according to Fig. 4.17. Thus, as a result we find the self energy

$$\tilde{\Sigma}_\alpha(x,\tau) = 0 \tag{4.73}$$

and the polarization function

$$\Pi_{\alpha\alpha'}(x,\tau) = -2\,\delta_{\alpha\alpha'}[\tilde{G}_\alpha(x,\tau)]^2 \,. \tag{4.74}$$

For $\tilde{\Sigma}$ all diagrams cancel while for Π the bubble (the first diagram in Fig. 4.16b) remains. Equations (4.68) and (4.69) together with (4.73) and (4.74) represent the exact self-consistent equations for the Luttinger model. These equations can be solved easily. Inserting the self energy (4.73) into the Dyson equation (4.68) we find that the gauge-transformed fermion Green's function is just the free Green's function, i.e.

$$\tilde{G}_\alpha(k,\omega_n) = G_{0\alpha}(k,\omega_n) = 1\,/\,[-\mathrm{i}\hbar\omega_n + \alpha\hbar v_\mathrm{F} k + \varepsilon_0 - \mu] \tag{4.75}$$

where $\varepsilon_{k\alpha} = \varepsilon_0 + \alpha\hbar v_\mathrm{F} k$ is the linear energy dispersion of the two branches. Next, we insert this Green's function into (4.74) and obtain the polarization function

$$\Pi_{\alpha\alpha'}(k,\Omega_n) = 2\cdot\frac{\alpha k}{2\pi}\,\frac{1}{-\mathrm{i}\hbar\Omega_n + \alpha\hbar v_\mathrm{F} k}\cdot\delta_{\alpha\alpha'} \,. \tag{4.76}$$

Eventually, the effective screened interaction $U_{\mathrm{eff},\alpha\alpha'}(k,\Omega_n)$ is obtained from (4.69). Thus, $\tilde{G}$ and U_eff are determined exactly.

The collective excitations are described by the density-density correlation function

$$\chi_{\alpha\alpha'}(x-x',\tau-\tau') = \langle T[\varrho_\alpha(x,\tau)\varrho_{\alpha'}(x',\tau')]\rangle \ . \tag{4.77}$$

The Fourier transform of this function can be expressed in terms of the polarization function by

$$\chi^{-1}_{\alpha\alpha'}(k,\Omega_n) = \Pi^{-1}_{\alpha\alpha'}(k,\Omega_n) + V_{\alpha\alpha'}(k) \ . \tag{4.78}$$

Thus, for a noninteracting system where $V_{\alpha\alpha'}(k) = 0$ the density-density correlation function is just the polarization function. Equation (4.76) implies that Π is proportional to a free boson Green's function. This observation means that the Fourier transformed densities $\varrho_\alpha(k)$ are proportional to Bose operators or equivalently that the densities satisfy Bose commutation relations

$$[\varrho_\alpha(k), \varrho_{\alpha'}(k')] = (\alpha k/\pi)\,\delta_{\alpha\alpha'} 2\pi\,\delta(k+k') \tag{4.79}$$

modified by a factor $\alpha k/\pi$ which are well known from the operator formalism of bosonization (Mahan 1990). Moreover, Eq. (4.78) implies that for the interacting system the collective excitations are free bosons, too, where the energy dispersion is modified by the interaction. The bosons are modified by a Bogolyubov transformation if the interaction matrix $V_{\alpha\alpha'}(k)$ has nondiagonal elements.

The properties of the fermionic excitations are described by the one-particle Green's function $G_\alpha(k,\omega_n)$. Inserting the gauge-transformed Green's function (4.75) into the transformation formula (4.66) we obtain

$$G_\alpha(x,\tau) = \mathrm{e}^{\Phi_\alpha(x,\tau)} \cdot G_{0\alpha}(x,\tau) \tag{4.80}$$

where $G_{0\alpha}$ is the free Green's function. This result for the fermion Green's function is well known from the operator formalism of bosonization (Mahan 1990). The nontrivial properties of the fermions are included in the exponential factor, where the function $\Phi_\alpha(x,\tau)$ is related to the bosonic degrees of freedom by (4.67), (4.72), (4.69), and (4.76). We conclude that the fermion Green's function can be evaluated explicitly and exactly for the Luttinger model, it remains to perform some Fourier transformations.

The grand-canonical thermodynamic potential $\Omega(T,\mu)$ defined in (4.52) can be calculated by (4.50) where $\tilde{G}$ and U_{eff} are assumed to be solutions of the self-consistent equations (4.51) or equivalently (4.40) and (4.42)-(4.44). For the Luttinger model this means that $\tilde{G}$ and U_{eff} are assumed to be determined by (4.68), (4.69), (4.73), and (4.74) and that D is defined by (4.72). Then, the thick dashed lines and the thin wavy lines cancel according to Fig. 4.17. Consequently, in Fig. 4.16c all diagrams of the functional $\tilde{\Xi}[\tilde{G}, U_{\mathrm{eff}}]$ cancel except the two first order diagrams which must be considered carefully because of a certain subtlety. While for higher order diagrams bubbles are excluded by the resummation of the polarization subdiagrams, the first order diagrams both contain a bubble or $n = 2$ loop. Because of (4.75) the thick

fermion lines may be replaced by thin fermion lines. Thus, the closed-loop theorems may be applied to the first-order diagrams. (Permutations of the diagrams do not appear here.) By construction of the gauge transformation the closed loop theorem involving wavy lines shown in Fig. 4.8 is valid for all numbers $l \geq 1$ of wavy lines where the number of dashed lines may be $n = 0$. For this reason, the second diagram in Fig. 4.16c must be zero. For the Luttinger model, the closed loop theorem shown in Fig. 4.1 is valid also for loops without wavy lines. However, here the $n = 2$ loop is an exception and nonzero so that the first diagram in Fig. 4.16c is nonzero. Thus, we find that in Fig. 4.16c all diagrams cancel except the first one. As a result we obtain the functional

$$\tilde{\Xi}[\tilde{G}, U_{\text{eff}}] = -\frac{\beta L}{2} \int \frac{\mathrm{d}k}{2\pi} \frac{1}{\beta} \sum_{\Omega_n} \mathrm{Tr}\{\Pi(k, \Omega_n) U_{\text{eff}}(k, \Omega_n)\} \tag{4.81}$$

if the respective functions $\tilde{G}$ and U_{eff} are inserted. Now, from (4.52) and (4.50) we obtain a quite simple result for the thermodynamic potential which is

$$\begin{aligned} \Omega(T, \mu) = &-L \int \frac{\mathrm{d}k}{2\pi} \frac{1}{\beta} \sum_{\omega_n} \sum_{\alpha} 2\{-\ln[G_{0\alpha}(k, \omega_n)]\} \\ &+ \frac{L}{2} \int \frac{\mathrm{d}k}{2\pi} \frac{1}{\beta} \sum_{\Omega_n} \mathrm{Tr}\{-\ln[V^{-1}(k) U_{\text{eff}}(k, \Omega_n)]\} \ . \end{aligned} \tag{4.82}$$

Here the trace is defined with respect to the branch indices, because $V(k) = (V_{\alpha\alpha'}(k))$ and $U_{\text{eff}}(k, \Omega_n) = (U_{\text{eff},\alpha\alpha'}(k, \Omega_n))$ are matrices. The length L of the one-dimensional system is assumed to be infinite in the thermodynamic limit. We note that in (4.50) the functional (4.81) cancels the term linear in U_{eff} so that only the logarithmic terms remain. The first term in (4.82) is the thermodynamic potential of the free fermions because the sum over the Matsubara frequencies ω_n yields

$$\Omega_0(T, \mu) = -\frac{L}{\beta} \int \frac{\mathrm{d}k}{2\pi} \sum_{\alpha} 2 \ln(1 + \mathrm{e}^{-\beta(\varepsilon_{k\alpha} - \mu)}) \ . \tag{4.83}$$

The second term in (4.82) contains the contributions of the interaction and the collective excitations (i.e. the bosons). The sum over the Matsubara frequencies Ω_n can also be evaluated explicitly. We obtain

$$\Omega(T, \mu) = \Omega_0(T, \mu) + \frac{L}{\beta} \int \frac{\mathrm{d}k}{2\pi} \ln\Big(\frac{\mathrm{sh}[\frac{1}{2}\beta E_k]}{\mathrm{sh}[\frac{1}{2}\beta E_{0k}]} \Big) \tag{4.84}$$

where

$$E_k = E_{0k} \cdot \Big[1 + \frac{\mathrm{Tr}[V(k)]}{\hbar v_{\mathrm{F}} \pi} + \frac{\det[V(k)]}{(\hbar v_{\mathrm{F}} \pi)^2} \Big]^{1/2} \tag{4.85}$$

is the energy dispersion of the collective excitations and $E_{0k} = \hbar v_{\mathrm{F}} k$. The second term of (4.84) is just the difference of the thermodynamic potentials

of free bosons with energy dispersion E_k and of free bosons with E_{0k}. For the Luttinger model the free energy has been first calculated by Mattis and Lieb (1965). Our result (4.84) agrees with Mattis and Lieb.

Now, we have some comments on the structure of our theory for the Luttinger model. To establish the self-consistent quantum-field theory for an interacting many-particle system $\tilde{\Xi}[\tilde{G}, U_{\text{eff}}]$ is the essential functional which must be known. In this section we have derived the perturbation series of this functional in terms of irreducible skeleton diagrams for the Luttinger model by application of the two closed-loop theorems which are shown in Fig. 4.1 and Fig. 4.8, respectively. Up to second order the resulting Feynman diagrams are shown in Fig. 4.16c. In all orders the functional is given by

$$\tilde{\Xi}[\tilde{G}, U_{\text{eff}}] = \left\{ \begin{array}{c} \text{sum of all vacuum skeleton diagrams which} \\ \text{consist of one closed fermion loop and any} \\ \text{number of thick dashed lines and thin wavy} \\ \text{lines attached to the loop with both ends} \end{array} \right\} . \quad (4.86)$$

The self energy $\tilde{\Sigma}$ and the polarization function $\tilde{\Pi}$ are obtained from this functional by the functional derivatives (4.43) and (4.44). It turns out that for the self-consistent equations (4.68), (4.69), (4.73), and (4.74) and for the thermodynamic potential (4.82) only the first-order diagrams yield a non-trivial contribution while the higher-order diagrams cancel. Thus, for the Luttinger model only the first-order diagrams are needed. An arbitrariness with respect to the higher-order diagrams is possible whenever these diagrams cancel. There may be different functionals $\tilde{\Xi}[\tilde{G}, U_{\text{eff}}]$ which yield the same results.

On the other hand, in Sect. 4.2 we have derived the functional $\tilde{\Xi}[\tilde{G}, U_{\text{eff}}]$ for the general interacting many-particle system which is given by (4.45) and shown in Fig. 4.13 up to second order. We can use these formulas also for the Luttinger model to construct the functional $\tilde{\Xi}[\tilde{G}, U_{\text{eff}}]$. To do this we note that for the Luttinger model the four vertex with two wavy lines (Fig. 4.4b) is zero and the three vertex with one wavy line (Fig. 4.4a) is identified by the differential operators as shown in Fig. 4.14e. Thus, in Fig. 4.13 and also in Figs. 4.12 c and d the diagrams with four vertices must be omitted. (Furthermore, the Hartree diagram must be omitted because it is canceled by the neutralizing background.) In this way we recover the diagrams shown in Fig. 4.16. Thus, we conclude that for the Luttinger model the functional $\tilde{\Xi}[\tilde{G}, U_{\text{eff}}]$ defined in (4.45) is equal to the functional (4.86) up to second order. (The same is true also for $\tilde{\Sigma}$ and $\tilde{\Pi}$.) However, in higher orders there are differences. First of all we realize that all diagrams of (4.86) are contained in the more general functional (4.45). However, the functional (4.45) includes more diagrams: while (4.86) is restricted to diagrams with only one fermion loop, (4.45) also contains diagrams with several loops. Clearly, for the Luttinger model all these additional diagrams must cancel. Nevertheless, for applicability of the modified self-consistent perturbation theory, the cancellation should be order by order according to Fig. 4.17.

Let us consider a vacuum skeleton diagram which consists of two closed fermion loops which are connected with each other by a thick dashed line. (There may be further thick dashed and thin wavy lines.) Feynman rule W prohibits that another diagram exists where the thick dashed line is replaced by a thin wavy line. Thus, this particular vacuum skeleton diagram cannot be canceled according to Fig. 4.17. (In the derivation of (4.86) we have argued that this diagram must be excluded because of the closed-loop theorem of the Luttinger model (Fig. 4.1).) We conclude that there exist many higher-order diagrams which do not cancel according to Fig. 4.17. This missing cancellation is caused by the Feynman rule W. While this rule is easy for practical use, it appears to exclude too many diagrams. To remove the problem we must generalize the rule. The main purpose of Feynman rule W is that there are no polarization subdiagrams for the wavy lines so that the wavy lines stay thin. Thus, we just state the most general rule which exhibits this property.

Feynman rule W2: *All those Feynman diagrams are excluded, which contain polarization subdiagrams which are connected with the remaining part of the diagram by at least one wavy line.*

Clearly, this rule guarantees that the wavy lines stay thin if the polarization subdiagrams are resummed, where only the minimum number of diagrams is excluded. The rule can be stated also in the following equivalent form: all those Feynman diagrams are excluded which fall into pieces if either two wavy lines are cut or one dashed line and one wavy line are cut. Clearly, this topological criterion for distinction between excluded and included diagrams is invariant with respect to permutations of three and four vertices by which the dashed and wavy lines are attached to the propagator lines. This means, if a diagram is excluded, then the new diagram obtained by permutation of vertices is excluded, too. As a consequence, if we consider the bare perturbation series where all lines in the diagrams are thin, the sum of all diagrams excluded by Feynman rule W2 contains the sum of all permutations of the vertices. By definition, these diagrams have at least one wavy line attached to a closed propagator loop. Thus, by the closed-loop theorem shown in Fig. 4.8 we conclude, that the sum of all excluded diagrams of the bare perturbation series with thin lines is zero. For this reason, Feynman rule W2 is proven to be consistent and does not lead to contradictions. We can perform the resummations with respect to self-energy subdiagrams and polarization insertions where no conflicts occur. Thus, Feynman rule W2 can be applied directly to the perturbation series' of $\tilde{\Xi}[\tilde{G}, U_{\text{eff}}]$, $\tilde{\Sigma}$, and Π. We find that the functional $\tilde{\Xi}[\tilde{G}, U_{\text{eff}}]$ is given by the series of (4.45). No diagrams are excluded except that the diagrams in (4.45) must be irreducible in the sense that there are no self-energy subdiagrams and no polarization subdiagrams with respect to both dashed and wavy lines. Feynman rule W2 guarantees that the wavy lines stay thin, but it has no further effect.

Now, in the present form we can apply our general theory directly to the Luttinger model and determine the functional $\tilde{\Xi}[\tilde{G}, U_{\text{eff}}]$ directly by (4.45). The four vertices with two wavy lines (Fig. 4.4b) are zero because of the linear energy dispersion. Feynman rule W2 does not exclude irreducible diagrams, so that in all orders of perturbation theory the diagrams are symmetric with respect to thick dashed lines and thin wavy lines. This means, if we consider any diagram of $\tilde{\Xi}[\tilde{G}, U_{\text{eff}}]$ and construct a new diagram by replacing thick dashed lines by thin wavy lines and vice versa in any possible ways, then the new diagram is also included in the perturbation series of $\tilde{\Xi}[\tilde{G}, U_{\text{eff}}]$. Consequently, in all orders of perturbation theory all thick dashed lines and thin wavy lines can be resummed according to Fig. 4.17 so that all higher-order diagrams cancel. The only exception are the two first-order diagrams which must be treated more carefully as discussed above.

Our theory is suited for applications to more general fermion systems beyond the Luttinger model. For example we may consider a one-dimensional fermion system with two branches $\alpha = \pm 1$, where the energy dispersions $\varepsilon_{k\alpha}$ are nonlinear. If the system is not too far away from the Luttinger model, the diagrams of $\tilde{\Xi}[\tilde{G}, U_{\text{eff}}]$ will cancel partially, so that corrections beyond the Luttinger model can be calculated. Furthermore, our theory can be applied also to study bosonization in higher dimensional fermion systems with $d > 1$ and to investigate Fermi liquid versus Luttinger liquid behavior. We conclude that our modified self-consistent quantum-field theory is a well suited approach for any kind of bosonization. Our method combines bosonization with the self-consistent perturbation theory so that corrections beyond the exactly solvable models can be obtained.

4.4 Application to the independent-boson model

Another exactly solvable model is the independent-boson model, which is defined by the Hamiltonian (Mahan 1990)

$$H = \varepsilon_0 c^+ c + \sum_q \hbar\omega_q a_q^+ a_q + \sum_q M_q (a_q + a_q^+) c^+ c \,. \tag{4.87}$$

This model describes one fermion of energy ε_0 interacting with a set of bosons of energies $\hbar\omega_q$ where q is an index which counts the bosons. Here c and c^+ are fermion operators, while a_q and a_q^+ are boson operators. The bosons are called independent because they do not interact directly with each other. The interaction between the one fermion and the many bosons is described by the parameters M_q. The independent-boson model is important in many-particle physics. It can be used to describe relaxation phenomena (Mahan 1990). For example, the fermion might be a particular electron in a many-particle system where the interaction with the surroundings is approximated by an interaction with collective excitations which are assumed to be independent bosons.

In the next chapter we will approximately derive an independent-boson model from the microscopic theory which describes the electronic spectrum and the magnetization curve of a two-dimensional electron system in the regime of the fractional quantum Hall effect (FQHE).

The independent-boson model cannot be treated by conventional quantum-field theoretic methods because it describes phenomena beyond the perturbation theory. Usually, the independent-boson model is considered in the operator formalism and solved exactly by a canonical transformation (Mahan 1990). Here, we apply our quantum-field theoretical approach modified by a gauge transformation and show that this is a very natural method to solve the independent-boson model and to calculate the fermion Green's function $G(\tau-\tau') = \langle T[c(\tau)c^+(\tau')]\rangle$ exactly. First, we derive the Feynman rules. To do this we consider the action functional of the functional integral which is defined by

$$S = \frac{1}{\hbar}\int_0^{\hbar\beta} \mathrm{d}\tau \Big[\frac{\hbar}{2}\Big(c^*(\tau)\frac{\partial c(\tau)}{\partial\tau} - \frac{\partial c^*(\tau)}{\partial\tau}c(\tau)\Big) + \sum_q \frac{\hbar}{2}\Big(a_q^*(\tau)\frac{\partial a_q(\tau)}{\partial\tau} - \frac{\partial a_q^*(\tau)}{\partial\tau}a_q(\tau)\Big) + K(\tau)\Big] \tag{4.88}$$

where $K(\tau) = H(\tau) - \mu N(\tau)$ is obtained from the Hamiltonian (4.87) and the fermion number operator $N = c^+c$ where the field operators are replaced by the Grassmann variables $c(\tau)$, $c^*(\tau)$ and the scalar boson fields $a_q(\tau)$, $a_q^*(\tau)$. From the quadratic terms we obtain the free fermion Green's function

$$G_0(\omega_n) = 1\,/\,[-\mathrm{i}\hbar\omega_n + \varepsilon_0 - \mu] \tag{4.89}$$

which is identified by a directed full line as shown in Fig. 4.18a and the free boson Green's functions

$$b_q(\omega_n) = 1\,/\,[-\mathrm{i}\hbar\Omega_n + \hbar\omega_q] \tag{4.90}$$

for each q which are identified by a directed dashed line. The interaction between the one fermion and the bosons is described by three vertices which are identified by M_q and consist of one incoming fermion line, one outgoing fermion line, and either an incoming or an outgoing dashed boson line.

Now, we combine two three vertices and one dashed line into a composite four vertex. We sum over all q and also over both directions of the dashed boson line. Since in the three vertices the fermion lines are not affected by the index q and the direction of the dashed line, we may amputate the four external fermion lines from the composite four vertex. As a result we obtain

$$B(\tau-\tau') = \sum_q M_q^2\,[\,b_q(\tau-\tau') + b_q(\tau'-\tau)\,] \tag{4.91}$$

for the amputated four vertex. It turns out that the boson Green's functions (4.90) appear in the Feynman diagrams only in the combination of (4.91).

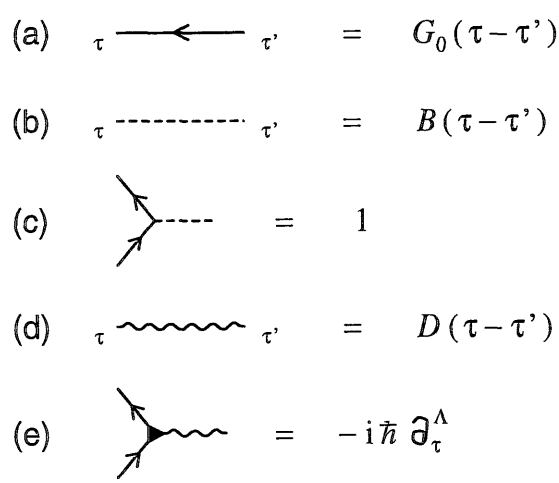

Fig. 4.18. The elements for constructing the Feynman diagrams for the independent-boson model: (a) the free fermion Green's function, (b) the boson Green's function including all the independent bosons, and (c) the respective three vertex. The gauge transformation requires two further elements: (d) the gauge-field propagator and (e) the respective three vertex.

For this reason it is useful to redefine the Feynman rules so that the elements for constructing the Feynman diagrams have a simpler structure. We define an undirected dashed line which is identified by $B(\tau-\tau')$ as it is shown in Fig. 4.18b. To obtain the correct composite four vertex we must identify the respective three vertices by unity as it is shown in Fig. 4.18c. We conclude that Fig. 4.18a-c represent all elements which are needed to construct all the Feynman diagrams for the independent-boson model. Now, we perform the gauge transformation

$$c(\tau) = e^{i\Lambda(\tau)}\tilde{c}(\tau)\ , \qquad c^+(\tau) = e^{-i\Lambda(\tau)}\tilde{c}^+(\tau) \tag{4.92}$$

where the phase $\Lambda(\tau)$ is a real boson field operator. The related gauge-field propagator

$$\langle T[\Lambda(\tau)\Lambda(\tau')]\rangle = D(\tau-\tau') \tag{4.93}$$

is an arbitrary function which must be chosen appropriately. For constructing the Feynman diagrams of the gauge-transformed independent-boson model we obtain two more elements which are shown in Figs. 4.18 d and e, the wavy line identified by the gauge-field propagator D and the respective three vertex. Since here the gauge-transformation is only imaginary-time dependent, the three vertex in Fig. 4.18e contains only a derivative ∂_τ^Λ. (There are no spatial variables and no spatial derivatives).

The interaction of the gauge-transformed fermion consists of two contributions. The first contribution is mediated by the independent bosons (dashed line) while the second contribution is mediated by the gauge field (wavy

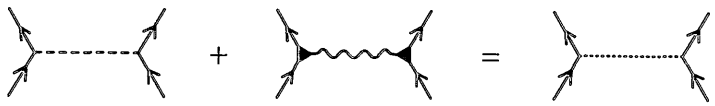

Fig. 4.19. The two composite four vertices for the interaction of the gauge-transformed fermion mediated by the independent bosons (dashed line) and by the gauge field (wavy line) are resummed into an effective interaction (dotted line). We choose the gauge-field propagator D so that the effective interaction is instantaneous in the (imaginary) time.

line). In the perturbation series of any observable quantity like the gauge-transformed Green's function $\tilde{G}(\tau)$ the Feynman diagrams can be resummed so that the two contributions of the interaction is combined into an effective interaction identified as dotted line as it is shown in Fig. 4.19. Amputating the four external lines, from Fig. 4.19 we obtain the equation

$$B(\tau - \tau') + (-\mathrm{i}\hbar)^2 \partial_\tau \partial_{\tau'} D(\tau - \tau') = -V \cdot \hbar\, \delta(\tau - \tau') \; . \tag{4.94}$$

The right-hand side of this equation is written in a form which assumes that the effective interaction of the gauge-transformed fermion is instantaneous in the (imaginary) time. This assumption for the effective interaction implies that the gauge-field propagator D is determined uniquely. For $D(\tau)$ we obtain the differential equation

$$B(\tau) + \hbar^2 \partial_\tau^2 D(\tau) = -V \cdot \hbar\, \delta(\tau) \; . \tag{4.95}$$

After a Fourier transformation this equation becomes

$$B(\Omega_n) - (\hbar\Omega_n)^2 D(\Omega_n) = -V \tag{4.96}$$

which can be solved easily with respect to $D(\Omega_n)$. For $\Omega_n \neq 0$ we obtain the gauge-field propagator

$$D(\Omega_n) = [B(\Omega_n) - B(0)]/(\hbar\Omega_n)^2 \tag{4.97}$$

while for $\Omega_n = 0$ the value of $D(\Omega_n)$ may be arbitrary so that we choose $D(0) = 0$. As an input we need the boson Green's function $B(\Omega_n)$ which is given by

$$B(\Omega_n) = \sum_q M_q^2 [b_q(\Omega_n) + b_q(-\Omega_n)] = \sum_q M_q^2 \frac{2\hbar\omega_q}{(\hbar\Omega_n)^2 + (\hbar\omega_q)^2} \; . \tag{4.98}$$

For $\Omega_n = 0$ Eq. (4.96) yields the strength of the effective interaction

$$V = -B(\Omega_n = 0) = -2 \sum_q M_q^2 / \hbar\omega_q \; . \tag{4.99}$$

Clearly V is negative which means that the effective interaction is attractive.

Since the effective interaction is instantaneous there exists a Hamiltonian which describes the interacting gauge-transformed fermion system. This Hamiltonian is given by

$$\tilde{H} = \varepsilon_0 \tilde{c}^+ \tilde{c} + \tfrac{1}{2} V (\tilde{c}^+ \tilde{c})(\tilde{c}^+ \tilde{c}) \; . \tag{4.100}$$

In the interaction term the fermion operators are not normal ordered because the instantaneous interaction originates from bosons. By using the anticommutation relations for $\tilde{c}$ and $\tilde{c}^+$ we rewrite the Hamiltonian in the normal ordered form

$$\tilde{H} = (\varepsilon_0 + \tfrac{1}{2} V) c^+ \tilde{c} + \tfrac{1}{2} V \tilde{c}^+ \tilde{c}^+ \tilde{c} \tilde{c} \; . \tag{4.101}$$

Now, a considerable simplification occurs because there is only one fermion degree of freedom. The interaction term in (4.101) cancels because of $\tilde{c}\tilde{c} = 0$ and $\tilde{c}^+ \tilde{c}^+ = 0$. Thus, there is no interaction for the gauge-transformed fermion. The only effect of the interaction is a shift of the single-particle energy by $\frac{1}{2} V$. Consequently, for the gauge-transformed fermion Green's function $\tilde{G}(\omega_n)$ we obtain a free Green's function with a shifted energy which reads

$$\tilde{G}(\omega_n) = 1 \,/\, [-\mathrm{i}\hbar\omega_n + \varepsilon_0 + \tfrac{1}{2} V - \mu] \; . \tag{4.102}$$

In the imaginary-time representation this Green's function reads

$$\tilde{G}(\tau) = [\theta(\tau) - n] \exp\{-\hbar^{-1} (\varepsilon_0 + \tfrac{1}{2} V - \mu)\tau\} \tag{4.103}$$

where

$$n = \langle \tilde{c}^+ \tilde{c} \rangle = 1 \,/\, [\exp\{\beta(\varepsilon_0 + \tfrac{1}{2} V - \mu)\} + 1] \tag{4.104}$$

is the average fermion occupation number.

The physical relevant fermion Green's function $G(\tau)$ is obtained from the gauge-transformation formula (4.38) which here reads

$$G(\tau) = \mathrm{e}^{\Phi(\tau)} \cdot \tilde{G}(\tau) \tag{4.105}$$

where

$$\Phi(\tau) = D(0) - D(\tau) \; . \tag{4.106}$$

Thus, we obtain

$$G(\tau) = [\theta(\tau) - n] \exp\{-\hbar^{-1} (\varepsilon_0 + \tfrac{1}{2} V - \mu)\tau + \Phi(\tau)\} \; . \tag{4.107}$$

This is the exact result for the fermion Green's function for the independent-boson model. The same result has been obtained also by the operator formalism (Mahan 1990). The nontrivial effects of the interaction of the fermion with the independent bosons is included in the function $\Phi(\tau)$ which is related to the boson Green's function $B(\tau)$ by (4.106) and (4.97). In the imaginary-time representation this relation can be written as

$$\Phi(\tau) = \hbar^{-1} \tfrac{1}{2} V |\tau| + \hbar^{-2} \int_0^{\tau} \mathrm{d}\tau' \int_0^{\tau'} \mathrm{d}\tau'' B(\tau'') \; . \tag{4.108}$$

The independent-boson model can be solved also if c and c^+ are boson operators. The gauge transformation (4.92) is performed in the same way and the same formulas are obtained as above up to (4.101). However, by writing the Hamiltonian in the normal-ordered form (4.101) it is not possible to cancel the interaction term because in this case $\tilde{c}$ and $\tilde{c}^+$ are boson operators. Thus, $\tilde{G}(\tau)$ is not a free Green's function. Nevertheless, for the Hamiltonian (4.100) the quantum statistical average $\langle T[\tilde{c}(\tau)\tilde{c}^+(\tau)]\rangle = \tilde{G}(\tau - \tau')$ can be evaluated directly to determine the gauge-transformed boson Green's function $\tilde{G}(\tau)$ exactly. Eventually, the physical relevant boson Green's function $G(\tau)$ is obtained from (4.105) and (4.106). In the same way also more general independent-boson models including several fermion operators c_i and c_i^+ (Mahan 1990) can be solved exactly. We note that for all independent-boson models the gauge-transformed Green's function $\tilde{G}(\tau)$ cannot be calculated by the self-consistent perturbation theory because the Feynman diagrams with thick propagator lines do not cancel order by order. In Fig. 4.19 the gauge-field propagator (wavy line) does not cancel the interaction mediated by the independent bosons (dashed line) completely, it only cancels the nontrivial frequency dependent part so that an instantaneous effective interaction (dotted line) remains. Nevertheless, the success of our method to solve the independent-boson model relies on the assumption that the effective interaction is sufficiently simple so that $\tilde{G}(\tau)$ can be calculated exactly in any possible way.

5. Two-dimensional electron systems in the FQHE regime

Since the experimental discovery of the integral quantum Hall effect (IQHE) (von Klitzing et al. 1980) and later of the fractional quantum Hall effect (FQHE) (Tsui et al. 1982 and Störmer et al. 1983) it is well known that two-dimensional electron systems in a strong magnetic field show rather complex and unusual behaviors at very low temperatures where quantum effects come into play (Prange and Girvin 1987). The quantum Hall effects are caused by the interplay of quantization of the electrons into Landau levels by the magnetic field, disorder by impurities, and the repulsive Coulomb interaction between the electrons, where the thermal energy $k_{\mathrm{B}}T$ must be smaller than the relevant energy scales. The IQHE can be explained by the single-particle motion alone where the electrons move in a homogeneous magnetic field and in the disorder potential of the impurities. Here the Coulomb interaction plays a minor role and is not needed for the explanation of the effect. For this reason, the IQHE is observed in relatively dirty samples at temperatures $T \lesssim 5\,\mathrm{K}$. On the other hand the FQHE is observed only in very clean samples at much lower temperatures $T \lesssim 1\,\mathrm{K}$ where disorder plays a minor role. The FQHE is believed to be explained by a strongly correlated electronic state which is caused by the Coulomb interaction and the Landau-level quantization of the electrons in a magnetic field.

In this chapter we investigate the two-dimensional system of interacting electrons in a perpendicular magnetic field $\boldsymbol{B}$. We focus on interaction effects and strong correlations of the electrons related to the FQHE. For this reason we neglect disorder by impurities completely and consider idealized systems which are absolutely clean. In second-quantization representation the system is described by the Hamiltonian

$$H = \int \mathrm{d}^2 r \left\{ \sum_\sigma \frac{1}{2m^*} \left| \left(\boldsymbol{p} + \frac{e}{c}\boldsymbol{A} \right) \Psi_\sigma(\boldsymbol{r}) \right|^2 + g\mu_{\mathrm{B}} \boldsymbol{B} \cdot \boldsymbol{s}(\boldsymbol{r})/\hbar \right\} + \frac{1}{2} \int \mathrm{d}^2 r \int \mathrm{d}^2 r' : [\varrho(\boldsymbol{r}) - \varrho_{\mathrm{b}}] V(\boldsymbol{r} - \boldsymbol{r}') [\varrho(\boldsymbol{r}') - \varrho_{\mathrm{b}}] : \tag{5.1}$$

where $\boldsymbol{r}$, $\boldsymbol{p}$, and $\boldsymbol{A}$ are two-dimensional vectors in the xy plane and $\mathrm{curl}\,\boldsymbol{A} = \boldsymbol{B} = B\boldsymbol{e}_z$ is the perpendicular magnetic field. Here $\Psi_\sigma(\boldsymbol{r})$ and $\Psi_\sigma^+(\boldsymbol{r})$ are the fermion field operators, $\varrho(\boldsymbol{r}) = \sum_\sigma \Psi_\sigma^+(\boldsymbol{r})\Psi_\sigma(\boldsymbol{r})$ is the operator of the electron density, and $\boldsymbol{s}(\boldsymbol{r}) = (\hbar/2)\sum_{\sigma\sigma'} \Psi_\sigma^+(\boldsymbol{r})\boldsymbol{\sigma}_{\sigma\sigma'}\Psi_{\sigma'}(\boldsymbol{r})$ is the operator of

the spin density. The first term describes the motion of the electrons in the magnetic field $\mathcal{B}$ which results in the quantization into Landau levels. In circular gauge the vector potential is given by $A_x = -\frac{1}{2}By$ and $A_y = \frac{1}{2}Bx$. The second term represents the Zeeman splitting where $\mu_B = e\hbar/2mc$ is the Bohr magneton. The last term describes the Coulomb interaction between the electrons with the potential $V(r) = e^2/\varepsilon|r|$. Here ϱ_b is the density of the homogeneous positively charged background which neutralizes the system. The two colons : : mean that the product in between is normal ordered with respect to the fermion operators. In particular we assume that the electrons are moving in $GaAs$ so that we have the effective electron mass $m^* = 0.07\,m$, the Landé factor $g = 0.44$, and the dielectric constant $\varepsilon = 13$.

In experiments two-dimensional electron systems can be realized by an inversion layer close to an interface in semiconductor devices like MOSFET's and $GaAs-Al_xGa_{1-x}As$ heterostructures (see e.g. Prange and Girvin 1987). The charge carriers need not be electrons, two-dimensional systems of positively charged holes are possible, too. Furthermore, two-dimensional electron or hole systems can be realized also by a quantum well in a semiconductor heterostructure. For the observation of the FQHE very clean samples with very high mobilities are needed. Thus, a $GaAs$ quantum well with electronic mobility $\mu = 10^6\,\mathrm{cm}^2/\mathrm{Vs}$ at low temperatures will be a good candidate for a two-dimensional electron system to observe the FQHE. For this reason we assume that the electrons are moving in a $GaAs$ quantum well so that in the Hamiltonian (5.1) we have $m^* = 0.07\,m$, $g = 0.44$, and $\varepsilon = 13$. The electron system is two-dimensional in the sense that the motion in the perpendicular direction is quantized where only the lowest subband is occupied. Nevertheless, the charge distribution has a certain thickness d in the perpendicular direction which is related to the wave function of the lowest subband. Consequently, the Coulomb interaction is reduced effectively for short distances for the two-dimensional motion of the electrons. To include finite thickness effects, in the Hamiltonian (5.1) we must replace the bare Coulomb interaction $V(r) = e^2/\varepsilon|r|$ by an effective potential $V_d(r)$ which is smeared out by the subband wave function and which depends on the thickness d.

5.1 Theory of the FQHE

The many-particle system described by the Hamiltonian (5.1) is quite complicate. It turns out to be hard to calculate physical quantities and to explain the physical properties of the system. Here we briefly describe several theoretical approaches which are more or less successful to explain the FQHE and related effects. First we consider the two-dimensional electron system without interaction so that $V(r) = 0$. Here the electrons are moving independently from each other in the xy plane in the magnetic field $\mathcal{B} = Be_z$. Thus, the motion of the electrons is described by the single-particle wave functions $\varphi_{nq}(r)$ which are solutions of the one-particle Schrödinger equation

$$\left[\frac{1}{2m^*}\left(\boldsymbol{p}+\frac{e}{c}\boldsymbol{A}\right)^2+g\mu_{\mathrm{B}}B\sigma\right]\varphi_{nq}(\boldsymbol{r})=\varepsilon_{n\sigma}\,\varphi_{nq}(\boldsymbol{r}) \tag{5.2}$$

with the energy eigenvalues

$$\varepsilon_{n\sigma}=\hbar\omega_c(\tfrac{1}{2}+n)+g\mu_{\mathrm{B}}B\sigma\ . \tag{5.3}$$

The first term of (5.3) represents the quantization into Landau levels where $\omega_c = eB/m^*c$ is the cyclotron frequency and $n = 0, 1, 2, \ldots$ is the Landau-level index. The second term describes the Zeeman splitting of the Landau levels with respect to the spin of the electrons where $\sigma = \pm 1/2$ is the spin index. The Landau levels are known to be highly degenerate which is described by a further index q. Thus, a single-particle state of an electron in the xy plane in a magnetic field $\boldsymbol{B} = B\boldsymbol{e}_z$ is uniquely labeled by the three quantum numbers n, q, and σ. Assuming that $\varphi_{nq}(\boldsymbol{r})$ represent a complete and orthonormalized set of single-particle wave functions we can write the fermion field operators as

$$\Psi_\sigma(\boldsymbol{r})=\sum_{nq}\varphi_{nq}(\boldsymbol{r})c_{nq\sigma}\ ,\qquad \Psi_\sigma^+(\boldsymbol{r})=\sum_{nq}\varphi_{nq}^*(\boldsymbol{r})c_{nq\sigma}^+ \tag{5.4}$$

where $c_{nq\sigma}^+$ and $c_{nq\sigma}$ are the creation and annihilation operators of the electrons in the Landau levels. Inserting (5.4) into (5.1) the noninteracting part of the Hamiltonian (the first line of (5.1)) is diagonalized so that we obtain

$$H_0=\sum_{nq\sigma}\varepsilon_{n\sigma}\,c_{nq\sigma}^+c_{nq\sigma}\ . \tag{5.5}$$

In Fig. 5.1 the Landau levels are shown schematically. The horizontal lines represent the spin-splitted Landau levels with energies $\varepsilon_{n\sigma}$ given by (5.3). The number of degenerate single-particle states in one of these levels is given by the number N_Φ of magnetic flux quanta which penetrate the two-dimensional electron system. (We may count the degenerate states by $q = 1, 2, 3, \ldots, N_\Phi$.) Depending on the total number N of electrons the levels are filled more or less with electrons. An important number for characterizing the system is the filling factor $\nu = N/N_\Phi$ which indicates how many of the spin-polarized Landau levels are filled. For integer ν in the ground state (temperature $T = 0$) there are ν levels completely filled with electrons. For noninteger ν, there exists at least one level which is partially filled. For convenience it is useful to assume that the electrons are moving in a finite geometry of area F as e.g. a parallelogram with periodic boundary conditions, so that N and N_Φ are finite numbers. Eventually, the thermodynamic limit $F \to \infty$ is considered where N and N_Φ become infinite and $\nu = N/N_\Phi$ is kept finite.

The levels of the noninteracting system are characterized by two energies, the cyclotron energy $\hbar\omega_c$, which describes the separation of the Landau levels, and the Zeeman energy $g\mu_{\mathrm{B}}B$ which describes the spin splitting of the Landau levels. For interacting systems there is a third characteristic energy which describes the strength of the interaction. This energy is given by

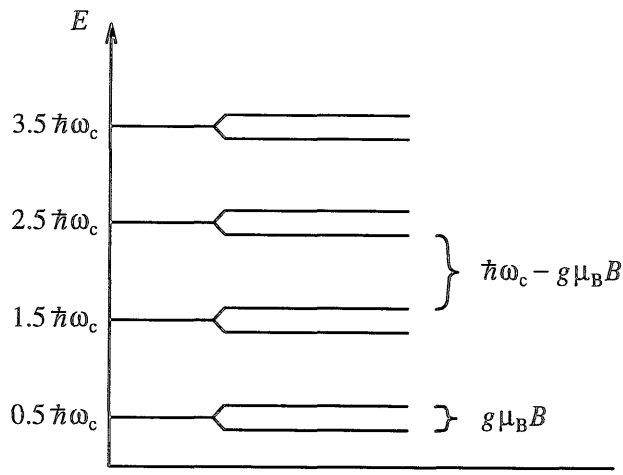

Fig. 5.1. The spin-splitted Landau levels of the noninteracting two-dimensional electron system in a homogeneous magnetic field B. Because of (5.7) the Zeeman energy $g\mu_B B$, which describes the spin splitting of the Landau levels, is much smaller than the cyclotron energy $\hbar\omega_c$ which describes the distance between the Landau levels.

$e^2/\varepsilon a$ where a is the mean distance between the electrons, which is related to the two-dimensional electron density by $\varrho_0 = 1/\pi a^2$. The values of the three characteristic energies depend on the material in which the electrons are moving. It turns out that for two-dimensional electron systems which are realized in *GaAs* samples to observe the FQHE (Tsui et al. 1982 and Störmer et al. 1983) the three characteristic energies satisfy the inequality

$$g\mu_B B \ll e^2/\varepsilon a \lesssim \hbar\omega_c \ . \tag{5.6}$$

First of all for the Zeeman energy we find the ratio

$$\frac{g\mu_B B}{\hbar\omega_c} = \frac{g}{2}\frac{m^*}{m} = 0.015 \tag{5.7}$$

which means that in *GaAs* the Zeeman energy is quite small because of the small effective mass of the electrons. Secondly, for the characteristic interaction energy we find the ratio

$$\frac{e^2/\varepsilon a}{\hbar\omega_c} = \frac{\nu}{2} r_s \sim 0.4 \tag{5.8}$$

where ν is the filling factor and $r_s = a/a_0$ is a dimensionless parameter which represents the mean distance between the particles in units of the Bohr radius a_0 which here is given by $a_0 = \hbar^2\varepsilon/m^* e^2 = 98$ Å. For Coulomb plasmas r_s is an important parameter which describes the relation between quantum and interaction effects. For $r_s < 1$ quantum effects are dominating

while for $r_s > 1$ interaction effects are dominating. In *GaAs* samples in which the FQHE is observed (Tsui et al. 1982 and Störmer et al. 1983), the charge carrier density is usually about $\varrho_0 \sim 10^{11}\,\mathrm{cm}^{-2}$ which implies $r_s \sim 1.5$. Thus, quantum and interaction effects will be of the same order of magnitude. Inserting $\nu \sim 0.5$ into (5.8) we obtain the ratio 0.4 which means that the characteristic interaction energy $e^2/\varepsilon a$ is nearly of the same order of magnitude as and slightly smaller than the cyclotron energy $\hbar\omega_c$. Consequently, from (5.7) and (5.8) we find that the interaction energy $e^2/\varepsilon a$ is much larger than the Zeeman energy as stated in the inequality (5.6). The related ratio is

$$\frac{e^2/\varepsilon a}{g\mu_B B} = \frac{\nu}{g}\frac{m}{m^*} r_s \sim 26 \,. \tag{5.9}$$

For the applicability of perturbation theory the inequality (5.6) together with the ratios (5.7)-(5.9) of the energy scales is important.

The IQHE corresponds to integer filling factors ν. In this case in the ground state of the noninteracting system the ν lowest levels of the spin splitted Landau levels (Fig. 5.1) are completely filled while all higher levels are completely empty. As a consequence the noninteracting ground state is unique so that for integer ν the standard perturbation theory as e.g. the quantum-field theory with Feynman diagrams can be developed to describe the interacting system. The lowest excitations of the noninteracting ground state are particle-hole pairs: one electron of the highest occupied level jumps into the lowest empty level leaving a hole in the filled level. The energy of the excitation depends on the value of ν. In Fig. 5.1 we clearly see that for even ν the excitation energy is $\hbar\omega_c - g\mu_B B \approx \hbar\omega_c$ while for odd ν it is $g\mu_B B$. The expansion parameter of the perturbation theory at zero temperature is the ratio of the characteristic interaction energy $e^2/\varepsilon a$ and the lowest excitation energy. Thus, for even ν the expansion parameter is given by the ratio (5.8). For $r_s \sim 1.5$ the value of this parameter is of order unity which is not quite small as needed for the perturbation theory. However, we have found that the self-consistent quantum-field theory (see Chap. 2) works quite well for even $\nu = 2, 4, 6, \ldots$ for all temperatures T whenever $r_s \lesssim 2$. For odd filling factors ν the expansion parameter is given by the ratio (5.9) which is quite large because of the small Zeeman energy for *GaAs* systems. Consequently, spin-polarization effects and magnetic properties of two-dimensional electron systems are nonperturbative for odd integer ν. It turns out that the Zeeman energy is effectively enhanced for low temperatures which enhances the spin-polarization of the system. The IQHE is observed only for low temperatures $T \lesssim 5\,\mathrm{K}$. These temperatures are sufficiently low so that for odd integer ν the system is completely spin polarized. In this case the Hartree–Fock approximation is valid in lowest order which yields the effective Zeeman energy $g\mu_B B + (\pi/2)^{1/2} e^2/\varepsilon\ell \approx (\pi/2)^{1/2} e^2/\varepsilon\ell$. As a consequence, the expansion parameter of the perturbation theory now is $(\nu/\pi)^{1/2}$ which is of order unity. We find that for low temperatures, for which the IQHE is observed and the

system is nearly completely spin polarized, the self-consistent quantum-field theory works quite well also for odd integer ν if $r_s \lesssim 2$. This fact agrees with the common statement that the IQHE is affected by the Coulomb interaction of the electrons only as a perturbation. For increasing temperature T when the system is no more completely spin polarized, interaction effects become nonperturbative and the IQHE disappears.

The FQHE is observed for certain fractions $\nu = p/q$ where p and q are integers which do not have a common divisor (Prange and Girvin 1987). Usually q is odd. The filling factor ν is noninteger so that always at least one Landau level with certain spin direction is partially occupied. The ground state of the noninteracting system is degenerate so that standard perturbation theory and conventional quantum-field theory cannot be applied here for low temperatures. The repulsive Coulomb interaction implies a rearrangement of the electrons within the partially occupied level so that in the ground state the energy has a minimum value. The interaction together with the degeneracy of the Landau levels causes a strong correlation of the electrons. For a proper treatment of the interacting quantum many-particle system a perturbation theory for degenerate levels must be developed (see e.g. Landau and Lifshitz vol. 3). To do this first in the subspace, where the motion of the electrons is restricted to the partially filled level, the system is treated exactly e.g. by solving the corresponding restricted many-particle Schrödinger equation. Then, the interaction with the other levels is treated perturbatively.

Most commonly the FQHE is observed for filling factors ν in the interval $0 < \nu < 1$. Thus, the partially occupied level is the lowest spin-polarized Landau level. Usually, in theories for the FQHE only the first step of the perturbation theory for degenerate levels is considered: the motion of the electrons is restricted to the lowest spin-polarized Landau level. The higher levels are neglected because they do not lead to qualitative changes but only imply small perturbations. The fundamental problem to be solved is the restricted Schrödinger equation to determine the many-particle wave function for the electrons in the lowest spin-polarized Landau level. The number of dimensions of the restricted Hilbert space is

$$D = \binom{N_\Phi}{N} = \frac{N_\Phi!}{N!(N_\Phi - N)!} \tag{5.10}$$

which becomes extremely large for large systems where $\nu = N/N_\Phi$ is fixed. For $N_\Phi = 20$ the dimension might be up to $D = 184\,756$. Thus, it turns out that the Schrödinger equation can be solved exactly only for small systems with $N_\Phi \lesssim 20$ by using the best computers. For many-particle systems this task becomes impossible because the number of degrees of freedom D is much too large. However, there exist some proposals for approximate many-particle wave functions which exhibit interesting structures and which describe strongly correlated electron systems.

Laughlin (1983) has proposed a variational wave function for the ground state at filling factors $\nu = 1/m$, where $m = 1, 3, 5, \ldots$ is an odd integer

number. This wave function is a product of Jastrow functions, each of which describes the relative motion of two electrons with angular momentum $\hbar m$. The related radial distribution function (density-density correlation function) shows a power law decay $g(r) \sim r^{2m}$ for small distances $r \to 0$, which leads to a minimization of the short-range repulsive part of the interaction. Though the Laughlin wave function is not an exact solution of the Schrödinger equation in general, except for some short-range interaction potentials (Trugman and Kivelson 1985), it describes the true FQHE ground state rather well. This has been shown by comparison with numerical calculations, where the Schrödinger equation has been solved exactly for a small number of particles $N \leq 9$ (see Laughlin and Haldane in Prange and Girvin 1987). The Laughlin wave function describes a strongly correlated electron system with the correct properties of the FQHE ground state. Following Laughlin (1983) also wave functions for excited states can be constructed. The elementary excitations are quasielectrons and quasiholes, which are anomalous collective excitations localized within a magnetic length $\ell = (\hbar c/eB)^{1/2}$ with fractional charges $\mp e/m$ and fractional statistics (Laughlin 1983, Prange and Girvin 1987). For the excitation of a quasielectron-quasihole pair a finite energy is necessary. It turns out that for the observation of the FQHE the main feature of the ground state is *incompressibility* which is related to the existence of a finite energy gap for the elementary excitations. Indeed, the ground state based on the Laughlin wave function shows these properties. While originally the Laughlin wave function has been constructed for a droplet of N particles (Laughlin 1983), this wave function can be constructed also for electrons in spherical geometry (Haldane 1983) and for electrons in planar geometry with periodic boundary conditions (Haldane and Rezayi 1985a).

The Laughlin wave function explains the FQHE for the fractions $\nu = 1/m$ and by particle-hole conjugation also for $\nu = 1 - 1/m$. However, the FQHE is observed also for some other fractions $\nu = p/q$ as e.g. 2/5 and 3/7 (see Chang in Prange and Girvin 1987). In the last fourteen years there have been several attempts to describe the FQHE ground state for fractions ν beyond those of the Laughlin theory. Haldane (1983), Laughlin (1984), and Halperin (1984) have proposed a procedure on how to construct a hierarchy of ground states with more complicate rational ν. This theory is based on the idea that the quasielectrons or quasiholes condense into a Laughlin state by their own, which can be excited by quasiquasiparticles again, and so on. The resulting ν is represented by a continued fraction (Haldane 1984). However, the hierarchy theory produces more fractions $\nu = p/q$ than observed in experiments. Moreover, it is not clear why for a given order of the hierarchy some fractions are observed and others not. Furthermore, it seems to be difficult to find appropriate many-particle wave functions for the electronic system. A procedure to construct wave functions in spherical geometry for the fractions of the hierarchy theory has been proposed by Greiter (1994) and by

Yang (1994). However, it remains unclear if these wave functions describe the FQHE ground states properly.

Jain (1989) has proposed to consider the FQHE as an integral quantum Hall effect (IQHE) of composite fermions, which are bound objects of one electron and a thin magnetic flux line of an even number of flux quanta. In mean-field approximation the composite fermions are moving in the effective magnetic field $\Delta B = B - B_0$, where B_0 is the average field of the magnetic flux lines. This leads to effective Landau levels with filling fractions $\nu = n/[(m-1)n+1]$ where $n = 1, 2, 3, \ldots$ and $m - 1 = 2, 4, 6, \ldots$ which is the even number of flux quanta. In experiments these fractions and the related particle-hole conjugated fractions have been observed for $m - 1 = 2$ and 4. Jain has also proposed wave functions for the ground states with these fractions (Jain 1990 and 1992), which for $n = 1$ are identical to the Laughlin wave function. Jain's wave functions are products of IQHE wave functions so that for $n \geq 2$ they are not restricted to the lowest Landau level but mix with higher levels. This may lead to problems in the limit of high magnetic fields. For this reason, in practice the wave functions are projected to the lowest Landau level (Jain 1992). While the hierarchy theory has some deficiencies, at present the composite fermion theory of Jain appears to be the best available theory for the FQHE ground states (and also excited states) for fractions ν beyond the Laughlin fractions.

Recently, we have proposed a generalization of the Laughlin wave function (Haussmann 1995) which can be constructed for the fractions ν of the composite-fermion theory and also for the fractions of the hierarchy theory. In contrast to Jain's wave functions, in our approach the motion of the electrons is restricted to the lowest Landau level right from the beginning. The idea for constructing the wave functions is the following. In the conventional Laughlin wave function the Jastrow functions imply that the N electrons move with angular momentum $\hbar m$ with respect to each other so that the number of magnetic flux quanta is $N_\Phi = Nm$. Hence it is $\nu = N/N_\Phi = 1/m$. To obtain fractions $\nu = p/q$ beyond those of the Laughlin theory we must change the angular momentum of the Jastrow functions so that numbers of magnetic flux quanta N_Φ are possible, which are not not just multiples of N. To do this, we divide the N particles into n groups of N/n particles (n must be a divisor of N). The electrons within one group are correlated by a Jastrow function with relative angular momentum $\hbar m$ as in the Laughlin wave function. However, two electrons of two different groups are correlated by another Jastrow function with relative angular momentum $\hbar(m-1)$. Eventually, the wave functions are antisymmetrized. As a result the number of magnetic flux quanta is $N_\Phi = (N/n) \cdot [(m-1)n+1]$ so that $\nu = n/[(m-1)n+1]$ which are the fractions of the composite fermion theory. The detailed form of the wave functions and its construction is found in the paper by Haussmann (1995). While we have constructed the wave functions for electrons in planar geometry with periodic boundary conditions, the wave functions can be

transformed also into other geometries. Wave functions for excited states with quasielectrons and quasiholes are obtained by introducing quasiholes into the groups. Thus, the groups may be partially filled. While a nearly filled group corresponds to the excitation of a few quasiholes, a nearly empty group corresponds to the excitation of a few quasielectrons. It turns out that there exists an analogy and a correspondence between our approach (Haussmann 1995) and the composite fermion theory (Jain 1992). First, the fractions ν are identical. Secondly, the groups of our approach correspond to the Landau levels of the composite fermions in the effective magnetic field ΔB. The groups are filled with electrons as the Landau levels are filled with composite fermions. Our approach allows a further generalization of the wave functions. The numbers $m_1, \ldots, m_n$, which describe the relative angular momenta of the Laughlin like correlations of the electrons within the groups, may have different values. The resulting wave functions describe correlated electron states for the fractions ν of the hierarchy theory (Haussmann 1995). Here, the composite fermion theory may be viewed as a special case of the hierarchy theory for equal numbers $m_1 = \cdots = m_n$. By a qualitative handwaving argument (Haussmann 1995) we believe that the energy gap of the elementary excitations is largest for equal numbers $m_1 = \cdots = m_n$, while the gap may be very small if the numbers are not equal. As a consequence, the fractions ν of the composite fermion theory should be observed preferably while the more complicate fractions of the hierarchy theory should be nearly invisible. At least, this statement agrees with the experimental findings.

In the literature there exist some more proposals of wave functions for FQHE states which we will not discuss here. All many-particle wave functions which have been considered until now do not solve the Schrödinger equation. They are more or less good approximations of the exact wave function. The quality of the proposed wave functions is estimated by considering small systems with $N \leq 10$ particles for which the exact wave function can be calculated. The ground-state and excitation energies are calculated for the proposed and the exact wave function and compared with each other. Furthermore, the overlap between the two wave functions is calculated. For the fractions $\nu = 1/m$ it has been found that the Laughlin wave function represents the FQHE ground state very well. Overlaps very close to unity around 0.99 are found (Laughlin 1983, Haldane and Rezayi 1985b, Fano, Ortolani, and Colombo 1986). For the more complicate fractions $\nu = p/q$ there exist several wave functions, those of Jain (1990 and 1992), of Greiter (1994) and Yang (1994), of Haussmann (1995) and some others. All those wave functions yield reasonable energy values and overlaps close to unity, around 0.97 to 0.99. Thus, for the fractions beyond the Laughlin theory the question which of the wave functions are the best and correct ones appears to be hard and not uniquely answered. It remains to be unclear if one of these wave functions describes the correlations of the electrons in the FQHE states correctly. Nevertheless, according to the numerical work for small system sizes of Dev and

Jain (1992) the wave functions of the composite fermion theory (Jain 1990 and 1992) appear to be the best ones. Our wave functions (Haussmann 1995) have not been tested by numerical calculations for small system sizes so that until now the quality of our wave functions related to those of Jain is not known. This test must be done in the future. We conclude that for $\nu = 1/m$ the Laughlin wave function describes the FQHE states quite well while for more complicate fractions the wave functions are less uniquely known. In the latter case there remain several open questions.

Most of the current understanding of the ground states and the excited states of FQHE systems arises from the wave functions which we have discussed above and from numerical calculations for small system sizes. Besides the quasielectrons and quasiholes as the elementary excitations there are also collective excitations which may be viewed as combinations of quasielectron-quasihole pairs. Girvin, MacDonald, and Platzman (1985 and 1986) have developed an approach which is called the single-mode approximation to investigate the essential properties of collective excitations. This approach is constructed for FQHE systems analogously as the Feynman theory for the low-lying collective excitations in superfluid ^{4}He (Feynman 1972). The spectrum of the collective excitations is described by the dynamic structure factor $S(k, \varepsilon)$ which is related to the density-density correlation function. In single-mode approximation the dynamic structure factor is approximated by a single delta peak

$$S(k, \varepsilon) = S(k) \cdot \delta(\varepsilon - \Delta(k)) \tag{5.11}$$

where $\Delta(k)$ is the energy of the collective excitation with wave vector k. This energy can be related to the integrals $S(k) = \int_0^\infty \mathrm{d}\varepsilon\, S(k, \varepsilon)$ and $f(k) = \int_0^\infty \mathrm{d}\varepsilon\, \varepsilon \cdot S(k, \varepsilon)$ by $\Delta(k) = f(k)/S(k)$. A sum rule implies that the oscillator strength $f(k)$ can be related to the static structure factor $S(k)$ so that the energies of the collective excitations can be calculated if $S(k)$ is known. Girvin, MacDonald, and Platzman (1985 and 1986) have calculated $\Delta(k)$ for the fractions $\nu = 1/m$ by relating the static structure factor $S(k)$ to the pair correlation function $g(r)$ which is determined from the Laughlin wave function. For the success of the single-mode approximation for FQHE systems the assumption is important that the density operator $\varrho(r)$, for which the structure factors are defined, is restricted to the lowest Landau level. More precisely this means that in $\varrho(r)$ only those fermion operators are taken into account which describe electrons in the lowest Landau level. As a result, Girvin, MacDonald, and Platzman (1985 and 1986) obtain a dispersion relation $\Delta(k)$ for $\nu = 1/m$, $m = 3, 5, 7$, which exhibits a finite energy gap. While $\Delta(k)$ is finite for $k = 0$, for wave numbers $k \approx \ell^{-1}$ where ℓ is the magnetic length the energy $\Delta(k)$ has a minimum. In analogy to the collective excitations in superfluid ^{4}He, in the FQHE system the collective excitations for wave numbers k close to the minimum are called *magnetorotons*. It turns out that $S(k)$ has a maximum around $k \sim \ell^{-1}$ so that the main spectral weight of the collective excitations in FQHE systems arises from the

magnetorotons. The characteristic energies of the magnetorotons are about $0.1\,e^2/\varepsilon\ell$ for $\nu = 1/3$ (Girvin, MacDonald, and Platzman 1985 and 1986). For $\nu = 1/5$ and $1/7$ the characteristic magnetoroton energies are smaller. The most important feature of the collective excitations is the finite energy gap which is required for FQHE states.

The quantum many-particle problem of the two-dimensional electron system in the homogeneous magnetic field described by the Hamiltonian (5.1) can be transformed exactly into a Chern–Simons field theory. Via a singular gauge transformation an infinitesimal thin magnetic flux line with a certain number p of magnetic flux quanta can be attached formally to each electron. In general, the transformed particles are anyons. Chern–Simons field theories imply approximation schemes beyond the conventional perturbation theory of the many-particle quantum-field theory. In mean-field approximation the particles are assumed to move in the effective magnetic field $\Delta B = B - B_0$ where B_0 is the average field of the magnetic flux lines attached to the electrons. Zhang, Hansson, and Kivelson (1989) performed the transformation for odd integer p so that the transformed particles are *bosons* moving in a Chern–Simons field. For the Laughlin fractions $\nu = 1/m$ and $p = m$ it turns out that the effective magnetic field is $\Delta B = 0$. The effective boson system with Chern–Simons fields appears to have some similarities with a conventional interacting boson system at low temperatures: off-diagonal long-range order (Girvin and MacDonald 1987). More details of the Chern–Simons field theory with bosons for the FQHE are found in the review by Zhang (1992). Lopez and Fradkin (1991) have performed the singular gauge transformation for even integer p so that the transformed particles are *fermions* moving in the Chern–Simons field. This Chern–Simons field theory appears to be a field theoretic version of Jain's composite fermion theory. The fermions are moving in the effective magnetic field $\Delta B = B - B_0$. If n of the respective Landau levels are filled, then the filling factor is $\nu = n/[(m-1)n+1]$ where $m - 1 = p$, which is known from the composite fermion theory. The Chern–Simons field theory has been developed further by Halperin, Lee, and Read (1993) to describe the correlated electron system at the even denominator fractions $\nu = 1/(m-1) = 1/p$, especially $\nu = \frac{1}{2}$, which are obtained from the fractions of the composite fermion theory in the limit $n \to \infty$. In this limit the effective magnetic field for the composite fermions is $\Delta B = 0$. Consequently, there is no energy gap for the elementary excitations. The system appears to have some unusual properties as may be a Fermi surface for the composite fermions. In an experiment with high-frequency acoustic waves an unusual enhancement of the longitudinal dynamic conductivity $\sigma_{xx}(k,\omega)$ has been observed for even-denominator fractions $\nu = \frac{1}{2}$, $\frac{3}{2}$, $\frac{1}{4}$, and $\frac{3}{4}$ (Willett et al. 1993). The theory of Halperin, Lee, and Read (1993) can explain these experimental observations.

5.2 General properties of the spectral functions for FQHE systems

The theories we have discussed above are more or less successful to explain the FQHE and related properties of the strongly correlated electron system. However, until now none of these theories is complete and satisfactory. There exist several approaches each of which addresses another aspect of the problem and which are hard to compare with each other. Nevertheless, there is a unique requirement for the correlated ground state of the electron system to observe the FQHE: for the respective fractions $\nu = p/q$ the ground state must be *incompressible* which means that there must be a finite energy gap for all elementary excitations, for the single-particle excitations as the quasi-electrons and the quasiholes and also for the collective excitations.

In the next sections we consider the many-particle quantum-field theory for the correlated electron system in the FQHE regime. To overcome the problem of the perturbation theory for systems with degeneracies we apply the approach which we have developed in Chap. 4. The basic quantities which are calculated by the quantum-field theory are the fermion Green's function $G_{n\sigma}(\omega_l)$ for the Landau levels with certain spin polarization and the density-density correlation function $\chi_{\varrho\varrho}(\Bbbk, \Omega_l)$. These functions are defined by

$$\langle T[c_{nq\sigma}(\tau)c^{+}_{n'q'\sigma'}(\tau')]\rangle = \delta_{nn'}\delta_{qq'}\delta_{\sigma\sigma'} \cdot G_{n\sigma}(\tau - \tau') \tag{5.12}$$

and by

$$\langle T[\varrho(\mathbb{r}, \tau)\varrho(\mathbb{r}', \tau')]\rangle = \chi_{\varrho\varrho}(\mathbb{r} - \mathbb{r}', \tau - \tau') \; . \tag{5.13}$$

The fermion Green's function in Matsubara representation $G_{n\sigma}(\omega_l)$ is related to the spectral function $A_{n\sigma}(\varepsilon)$ of the single-particle excitations by

$$G_{n\sigma}(\omega_l) = \int \mathrm{d}\varepsilon \, \frac{A_{n\sigma}(\varepsilon)}{-\mathrm{i}\hbar\omega_l + \varepsilon - \mu} \; . \tag{5.14}$$

The density-density correlation function $\chi_{\varrho\varrho}(\Bbbk, \Omega_l)$ in Matsubara representation is related to the spectral function $\chi''_{\varrho\varrho}(\Bbbk, \varepsilon)$ of the collective excitations by

$$\chi_{\varrho\varrho}(\Bbbk, \Omega_l) = \int \mathrm{d}\varepsilon \, \frac{\chi''_{\varrho\varrho}(\Bbbk, \varepsilon)}{-\mathrm{i}\hbar\Omega_l + \varepsilon} \; . \tag{5.15}$$

Eqs. (5.14) and (5.15) can be inverted by an analytical continuation with respect to the frequencies. Thus, the spectral functions $A_{n\sigma}(\varepsilon)$ and $\chi''_{\varrho\varrho}(\Bbbk, \varepsilon)$ are eventually determined by analytical continuation. In this chapter we denote the Matsubara frequencies by ω_l and Ω_l with index l to avoid confusion with the Landau-level index n.

From the normalization conditions and from the requirement of incompressibility it is possible to figure out how the spectral functions must look like qualitatively for the correlated electron system at low temperatures in a FQHE state. By

$$A(\varepsilon) = A_{0\downarrow}(\varepsilon) \tag{5.16}$$

we denote the electronic spectral function of the lowest spin-polarized Landau level with $n = 0$ and $\sigma = -\frac{1}{2} = \downarrow$. This spectral function is normalized by

$$\int \mathrm{d}\varepsilon\, A(\varepsilon) = 1\,. \tag{5.17}$$

Supposed the motion of the electrons is restricted to the lowest spin-polarized Landau level, then

$$\int \mathrm{d}\varepsilon\, n(\varepsilon) A(\varepsilon) = \nu \tag{5.18}$$

is the filling factor where $n(\varepsilon)$ is the fermion distribution function. For zero temperature $T = 0$ it is $n(\varepsilon) = \theta(\mu - \varepsilon)$ so that in this case from (5.17) and (5.18) we obtain

$$\int_{-\infty}^{\mu} \mathrm{d}\varepsilon\, A(\varepsilon) = \nu\,, \qquad \int_{\mu}^{+\infty} \mathrm{d}\varepsilon\, A(\varepsilon) = 1 - \nu\,. \tag{5.19}$$

The incompressibility of the FQHE states implies that at $T = 0$ the spectral function $A(\varepsilon)$ has a finite gap at the Fermi energy $\varepsilon = \mu$ which means that $A(\varepsilon) = 0$ in a finite interval around $\varepsilon = \mu$. As a consequence the electronic spectral function $A(\varepsilon)$ must have a double-peak structure as it is shown in Fig. 5.2. For $0 < \nu < 1$ the lowest spin-polarized Landau level splits into two peaks separated by a finite energy gap. The left peak for $\varepsilon < \mu$ is called the hole peak because it represents the spectrum of the hole excitations. The right peak for $\varepsilon > \mu$ is the electron peak because it represents the spectrum

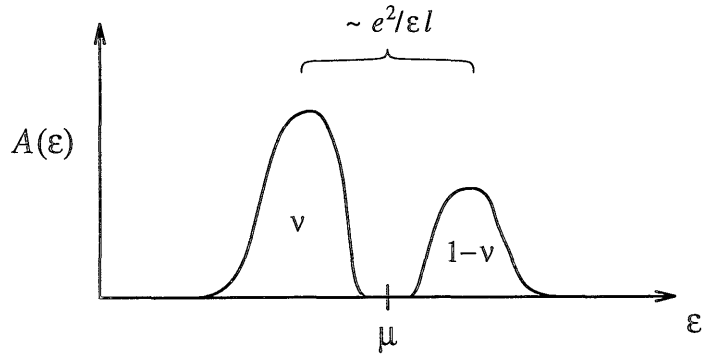

Fig. 5.2. The electronic spectral function $A(\varepsilon) = A_{0\downarrow}(\varepsilon)$ of the lowest spin-polarized Landau level for a FQHE state at $T = 0$ with $\nu = p/q$ in the interval $0 < \nu < 1$. The Landau level splits into two peaks, the hole peak on the left-hand side with spectral weight ν and the electron peak on the right-hand side with spectral weight $1 - \nu$. The two peaks are separated by a finite energy gap around the Fermi energy $\varepsilon = \mu$.

of the electron excitations. According to (5.19) the spectral weight of the hole peak is ν while the spectral weight of the electron peak is $1-\nu$. Since the splitting of the Landau level into two peaks is caused by the Coulomb interaction, the distance between the maxima of the two peaks is of order $e^2/\varepsilon\ell$, i.e. the characteristic interaction energy. The spectral function $A(\varepsilon)$ need not be smooth as it is shown in Fig. 5.2. Since the FQHE exhibits a fractal structure, the spectral function $A(\varepsilon)$ may have a fractal structure, too. The smooth spectral function in Fig. 5.2 should be understood to be averaged over small energy intervals to smear out the fractal structure.

By the definition (5.13) the density-density correlation function is symmetric, $\chi_{\varrho\varrho}(r,\tau)=\chi_{\varrho\varrho}(-r,-\tau)$, which implies that the related spectral function is antisymmetric, $\chi''_{\varrho\varrho}(k,\varepsilon)=-\chi''_{\varrho\varrho}(-k,-\varepsilon)$. Because of the isotropy of the FQHE states, the spectral function only depends on the wavenumber $k=|k|$ but not on the direction of k. Thus, $\chi''_{\varrho\varrho}(k,\varepsilon)$ is positive for $\varepsilon>0$ and negative for $\varepsilon<0$. We define the integrated spectral function $\chi''_{\varrho\varrho}(\varepsilon)$ by

$$\chi''_{\varrho\varrho}(\varepsilon)=\int\frac{\mathrm{d}^2k}{(2\pi)^2}\,\chi''_{\varrho\varrho}(k,\varepsilon)\;, \tag{5.20}$$

which represents the spectrum of all collective excitations together. In Fig. 5.3 this spectral function is shown qualitatively. The incompressibility of the FQHE states implies that there is a finite energy gap around $\varepsilon=0$ which means that $\chi''_{\varrho\varrho}(\varepsilon)=0$ in a finite interval around $\varepsilon=0$. Then, there is a peak located around the energy $\varepsilon=\varepsilon_{\mathrm{mr}}$ which represents the spectrum of the magnetorotons. Because of antisymmetry there is a negative peak of the same structure around $\varepsilon=-\varepsilon_{\mathrm{mr}}$. The mean energy $\varepsilon_{\mathrm{mr}}$ of the magnetorotons can be estimated by the single-mode approximation (Girvin, MacDonald, and

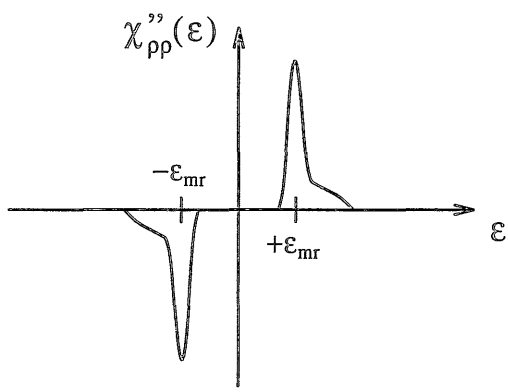

Fig. 5.3. The spectral function $\chi''_{\varrho\varrho}(\varepsilon)$ related to the density-density correlation function integrated over all wave vectors k. The peaks around $\varepsilon=\pm\varepsilon_{\mathrm{mr}}$ represent the spectrum of the magnetorotons, while the energy gap around $\varepsilon=0$ represents the incompressibility of the FQHE states.

Platzman 1985 and 1986). For $\nu = 1/3$ it is $\varepsilon_{\rm mr} \approx 0.1\, e^2/\varepsilon\ell$. It turns out that $\varepsilon_{\rm mr}$ is much smaller (by about a factor 10) than the characteristic energy for the splitting of the Landau levels, i.e. the distance between the two maxima of $A(\varepsilon)$ in Fig. 5.2. The spectral function $\chi''_{\varrho\varrho}(\varepsilon)$ has no peaks at higher energies because we assume that the motion of the electrons is restricted to the lowest spin-polarized Landau level so that $\varrho(\boldsymbol{r})$ is the density projected to this lowest level. Again, the spectral function $\chi''_{\varrho\varrho}(\varepsilon)$ need not be smooth because of the fractal structure of the FQHE. In Fig. 5.3 the spectral function is shown smooth where we assume a finite resolution of the energy scale.

The spectral function $\chi''_{\varrho\varrho}(\boldsymbol{k},\varepsilon)$ of the collective excitations can be tested by optical measurements and by conductivity experiments because the dielectric function $\varepsilon_{ij}(\boldsymbol{k},\omega)$ and the dynamic conductivity $\sigma_{ij}(\boldsymbol{k},\omega)$ can be expressed in terms of the density-density correlation function. The zero spectral weight $\chi''_{\varrho\varrho}(\boldsymbol{k},\varepsilon)$ for small energies $\varepsilon \sim 0$, which is related to the energy gap of the collective excitations, implies that at zero temperature $T = 0$ the longitudinal conductivity is $\sigma_{xx} = 0$. This fact agrees with the experimental observations of the FQHE: the longitudinal conductivity σ_{xx} is found to be zero for the fractions $\nu = p/q$ of the FQHE at low temperatures.

The spectral function $A(\varepsilon)$ of the single-particle excitations can be measured by tunneling experiments because $A(\varepsilon)$ may be interpreted as the generalized density of states for interacting electron systems. An experiment considering the tunneling between two two-dimensional electron systems in a strong magnetic field has been performed by Eisenstein et al. (1992 and 1994) and by Brown, Turner, et al. (1994) (see also Turner et al. 1996). The two two-dimensional electron systems are realized in a $GaAs$–$Al_xGa_{1-x}As$ heterostructure by a double quantum well. The two electron layers are separated by a sufficiently large barrier so that tunneling of electrons between the layers is sufficiently small. Supposed the two electron layers in the FQHE regime interact with each other only by the tunneling matrix element t and supposed the system is symmetric which means that the filling factors ν are equal in both layers, the tunneling current between the layers can be written as

$$I(V) = -e\,\frac{t^2 F}{\hbar\ell^2}\int \mathrm{d}\varepsilon\,[A_-(\varepsilon)A_+(\varepsilon - eV) - A_+(\varepsilon + eV)A_-(\varepsilon)] \qquad (5.21)$$

where

$$A_-(\varepsilon) = n(\varepsilon)A(\varepsilon)\ , \qquad A_+(\varepsilon) = [1 - n(\varepsilon)]A(\varepsilon) \qquad (5.22)$$

are the spectral functions of the hole excitations and of the electron excitations, respectively. Here F is the area of the tunneling contact and ℓ is the magnetic length. The first term in (5.21) represents the tunneling of the electrons from the left layer into the right layer. This term is the convolution integral of the hole spectrum $A_-(\varepsilon)$ in the left layer and the electron spectrum $A_+(\varepsilon)$ in the right layer. Analogously, the second term in (5.21) represents the tunneling of the electrons from the right layer into the left layer, where this term is the convolution integral of the hole spectrum $A_-(\varepsilon)$

in the right layer and the electron spectrum $A_+(\varepsilon)$ in the left layer. (The spectral functions of the left layer and the right layer are equal because of the assumed symmetry.)

In the experiment (Eisenstein et al. 1992 and 1994 and Brown et al. 1994) the following tunneling current $I(V)$ has been observed as function of the applied voltage V for low temperatures. For small voltages V the tunneling current $I(V)$ is strongly suppressed and hence nearly zero. For larger voltages a broad peak has been observed. For voltages beyond this peak the tunneling current $I(V)$ is zero again. (For even higher voltages some more peaks are observed, which involve higher Landau or spin levels, and thus are not relevant here.) Inserting the electronic spectral function $A(\varepsilon)$ of Fig. 5.2 into (5.21) we obtain a current voltage characteristic of precisely the same qualitative form as it is observed in the tunneling experiment. The suppression of $I(V)$ for small voltages is directly related to the gap of $A(\varepsilon)$ around $\varepsilon = \mu$. The peak of $I(V)$ is the convolution of the hole peak and the electron peak of $A(\varepsilon)$ in Fig. 5.2. We conclude that the double-peak structure of the spectral function $A(\varepsilon)$ of the lowest spin-polarized Landau level shown in Fig. 5.2 is strongly supported by the observed form of the current-voltage characteristic $I(V)$ in the tunneling experiment (Eisenstein et al. 1992 and 1994 and Brown et al. 1994).

A similar experiment (Ashoori et al. 1990 and 1993), which concerns the tunneling between a two-dimensional electron layer and a n^+ doped substrate, has also reported a strong suppression of the zero-voltage tunneling conductance for strong magnetic fields and low temperatures. This latter experiment also supports the double-peak structure of $A(\varepsilon)$ with a gap at $\varepsilon = \mu$. In the tunneling current (5.21) the interaction of the electrons within each layer is taken into account via the spectral function $A(\varepsilon)$. However, the Coulomb interaction of the electrons *between* the layers is neglected. Eisenstein et al. (1995) have investigated the effect of the Coulomb interaction between the layers in the tunneling experiment by varying the thickness of the barrier between the quantum wells. They find that the interlayer interaction leads to a small shift of the peak in $I(V)$ to lower voltages which may be interpreted as the evidence for the existence for an interlayer exciton. However, there are no qualitative changes, so that in leading approximation the neglection of the interlayer interaction in (5.21) is justified.

The tunneling experiment has been performed for continuous filling factors ν in the interval $0 < \nu < 1$, not too close to $\nu = 0$ and 1. It turns out that the current-voltage characteristic $I(V)$ depends only weakly on ν. While the FQHE strongly depends on ν, i.e. if $\nu = p/q$ is a certain fraction or not, in $I(V)$ no dramatic qualitative changes are observed. Eisenstein et al. (1992 and 1994) have found only a slight shift and modification of the peak at the fraction $\nu = \frac{2}{3}$. Thus, we conclude that the electronic spectral function $A(\varepsilon)$ depends only weakly on ν so that it has the double-peak structure shown in Fig. 5.2 over a wide range of ν, not too close to $\nu = 0$ and 1. While the

spectral function $A(\varepsilon)$ describes the single-particle excitations over a larger energy scale, the FQHE is a low energy effect because it is observed in the conductivity at zero voltage. Thus, the FQHE is influenced by the spectrum $A(\varepsilon)$ very close to the Fermi energy $\varepsilon = \mu$. While for the fractions $\nu = p/q$ of the FQHE the spectrum $A(\varepsilon)$ must be zero in a finite interval around $\varepsilon = \mu$, for other filling factors $A(\varepsilon)$ may be nonzero close to $\varepsilon = \mu$. Nevertheless, near the Fermi energy $\varepsilon = \mu$ the spectrum $A(\varepsilon)$ will be at least small compared to the size of the hole peak and the size of the electron peak. Thus, the distinction between FQHE and non-FQHE states is a small detail in the spectral function $A(\varepsilon)$. In the next section we apply the modified SC-RPA theory, which we have developed in Chap. 4, to the two-dimensional electron system in a strong magnetic field. We calculate the electron Green's function $G(\omega_l)$ and obtain a spectral function $A(\varepsilon)$ with the double-peak structure as expected and shown in Fig. 5.2. Our approach does not resolve the small details of the FQHE in $A(\varepsilon)$ so that our theory does not explain the FQHE. However, we obtain a tunneling current $I(V)$ which agrees with the tunneling experiments (Eisenstein et al. 1992 and 1994, Brown et al. 1994, and Turner et al. 1996).

5.3 Modified SC-RPA theory for the two-dimensional electron system in a homogeneous magnetic field

The two-dimensional electron system in a perpendicular homogeneous magnetic field is described by the Hamiltonian (5.1) in second quantization representation. We now develop the self-consistent quantum-field theory modified by the gauge transformation for this system according to the general theory which is described in Chap. 4. First we consider the structure of the fermion Green's function

$$G_{\sigma\sigma'}(\boldsymbol{r}, \tau; \boldsymbol{r}', \tau') = \langle T[\Psi_\sigma(\boldsymbol{r}, \tau)\Psi^+_{\sigma'}(\boldsymbol{r}', \tau')]\rangle \ . \tag{5.23}$$

Expanding the fermion field operators $\Psi_\sigma(\boldsymbol{r})$ and $\Psi^+_\sigma(\boldsymbol{r})$ in terms of the fermion operators of the spin-polarized Landau levels $c_{nq\sigma}$ and $c^+_{nq\sigma}$ according to (5.4) we obtain

$$G_{\sigma\sigma'}(\boldsymbol{r}, \tau; \boldsymbol{r}', \tau') = \sum_{nn'} \sum_{qq'} \varphi_{nq}(\boldsymbol{r}) \, \langle T[c_{nq\sigma}(\tau) c^+_{n'q'\sigma'}(\tau')]\rangle \, \varphi^*_{n'q'}(\boldsymbol{r}') \ . \tag{5.24}$$

The Green's function in Landau-level representation (5.12) is diagonal in the spin indices σ, σ' because the Coulomb interaction $V(\boldsymbol{r} - \boldsymbol{r}')$ is spin independent, proportional to the unit matrix $\delta_{qq'}$ because of translational invariance of the system in the homogeneous magnetic field, and furthermore diagonal in the Landau-level indices n, n' because of momentum conservation. Thus, the fermion Green's function can be represented in the form

$$G_{\sigma\sigma'}(\mathbf{r},\tau;\mathbf{r}',\tau') = \sum_{nq} \varphi_{nq}(\mathbf{r})\, G_{n\sigma}(\tau-\tau')\, \varphi^*_{nq}(\mathbf{r}') \cdot \delta_{\sigma\sigma'} \ . \tag{5.25}$$

Consequently, the electron system is described uniquely by the fermion Green's function $G_{n\sigma}(\tau)$ which depends on the Landau-level index n and the spin index σ. More precisely $G_{n\sigma}(\tau)$ describes the electrons in the spin-polarized Landau level characterized by n and σ.

The gauge transformation is performed by

$$\Psi_\sigma(\mathbf{r},\tau) = \mathrm{e}^{\mathrm{i}\Lambda(\tau)}\, \tilde{\Psi}_\sigma(\mathbf{r},\tau) \ , \qquad \Psi^+_\sigma(\mathbf{r},\tau) = \mathrm{e}^{-\mathrm{i}\Lambda(\tau)}\, \tilde{\Psi}^+_\sigma(\mathbf{r},\tau) \tag{5.26}$$

where the phase $\Lambda(\tau)$ is a real boson field which only depends on the imaginary time τ but does not depend on the space variable $\mathbf{r}$. The propagator of the gauge field is defined by

$$\langle T[\Lambda(\tau)\Lambda(\tau')]\rangle = D(\tau-\tau') \tag{5.27}$$

where $D(\tau)$ is an arbitrary bosonic function which will be determined later. The space independence of the gauge transformation implies that the structure of the fermion Green's function (5.25) is preserved under the transformation so that

$$\tilde{G}_{\sigma\sigma'}(\mathbf{r},\tau;\mathbf{r}',\tau') = \sum_{nq} \varphi_{nq}(\mathbf{r})\, \tilde{G}_{n\sigma}(\tau-\tau')\, \varphi^*_{nq}(\mathbf{r}') \cdot \delta_{\sigma\sigma'} \tag{5.28}$$

where $\tilde{G}_{n\sigma}(\tau)$ is the Green's function of the transformed fermions in the spin-polarized Landau level n,σ. In space and imaginary-time representation the gauge transformation of the fermion Green's function is defined by (4.29) and (4.30). However, because of (5.25) and (5.28) and because of the space independence of the gauge field, the gauge transformation formula can be written for the fermion Green's functions of the spin-polarized Landau levels separately in the form

$$G_{n\sigma}(\tau) = \mathrm{e}^{\Phi(\tau)} \cdot \tilde{G}_{n\sigma}(\tau) \tag{5.29}$$

where

$$\Phi(\tau) = D(0) - D(\tau) \ . \tag{5.30}$$

The elements and rules for constructing the Feynman diagrams are obtained from the action functional $S[\Psi]$ which is defined in (4.6) where the Hamiltonian (5.1) must be inserted. For the gauge-transformed fermion system we must add the functionals $\Delta S[\tilde{\Psi},\Lambda]$ and $S_\Lambda[\Lambda]$ defined by (4.13) and (4.21), respectively. (Because of the space independence of the gauge transformation the gradient terms in (4.13) are zero.) For the noninteracting system we obtain the free fermion Green's function

$$G_{0,n\sigma}(\omega_l) = 1\,/\,[-\mathrm{i}\hbar\omega_l + \varepsilon_{n\sigma} - \mu] \tag{5.31}$$

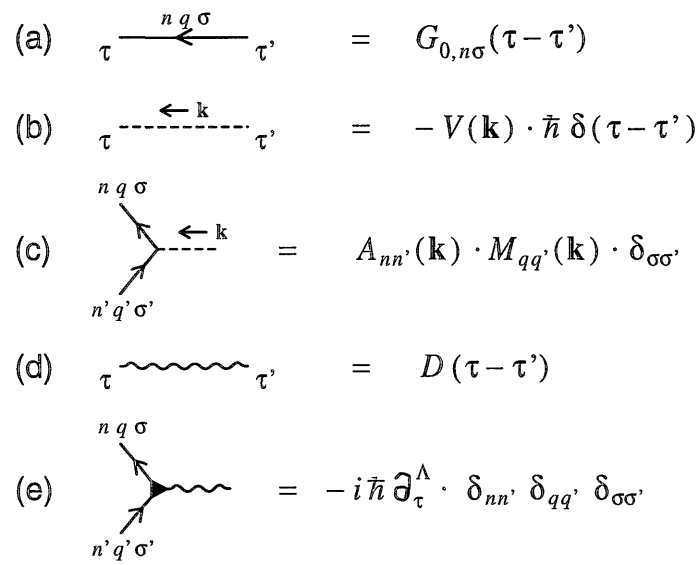

Fig. 5.4. The elements for constructing the Feynman diagrams for the two-dimensional electron system in a perpendicular homogeneous magnetic field: (a) The free fermion Green's function, (b) the Coulomb interaction, and (c) the three vertex by which the Coulomb interaction couples to the fermions. For the gauge-transformed fermion system additional elements are (d) the gauge-field propagator and (e) the three vertex by which the gauge field couples to the fermions.

where $\varepsilon_{n\sigma}$ are the energy eigenvalues (5.3) of the spin-polarized Landau levels. In Fig. 5.4 the elements for constructing the Feynman diagrams are shown. According to Fig. 5.4a the directed full propagator line is identified by the free fermion Green's function. As usual, in Fig. 5.4b the dashed interaction line is identified by minus the interaction potential. Here for convenience we use the Fourier representation for the space variables so that the Coulomb interaction potential $V(\boldsymbol{k}) = 2\pi e^2/\varepsilon|\boldsymbol{k}|$ depends on the wave vector $\boldsymbol{k}$. The Coulomb interaction potential couples to the fermions by the three vertex shown in Fig. 5.4c which is identified by the matrix element

$$\int \mathrm{d}^2 r\; \varphi^*_{nq}(\boldsymbol{r})\, \mathrm{e}^{\mathrm{i}\boldsymbol{k}\boldsymbol{r}}\, \varphi_{n'q'}(\boldsymbol{r}) = A_{nn'}(\boldsymbol{k})\cdot M_{qq'}(\boldsymbol{k}) \tag{5.32}$$

times the unit matrix $\delta_{\sigma\sigma'}$ in the spin indices.

Evaluating the integral with the single-particle wave functions $\varphi_{nq}(\boldsymbol{r})$ of the Landau levels we find that the matrix element decomposes into the product of two matrices $A_{nn'}(\boldsymbol{k})$ and $M_{qq'}(\boldsymbol{k})$ so that the Landau-level degrees of freedom and the degenerate degrees of freedom are separated. We choose the normalization $A_{00}(\boldsymbol{k}) = 1$ so that $M_{qq'}(\boldsymbol{k})$ is the matrix element of the lowest Landau level while $A_{nn'}(\boldsymbol{k})$ is the additional contribution for the higher Landau levels. The explicit form of $M_{qq'}(\boldsymbol{k})$ depends on the particular representation of the degenerate degrees of freedom which, however, is irrelevant

because of the translational invariance of the system. All we need are some formulas which define the algebra of these matrices. From any particular representation we derive (Haussmann 1996)

$$\sum_{q'} M_{qq'}(k_1)\, M_{q'q''}(k_2) = \exp(\tfrac{1}{2}\kappa_1^*\kappa_2\ell^2)\, M_{qq''}(k_1+k_2)\ , \tag{5.33}$$

$$M_{qq'}(0) = \delta_{qq'}\ , \tag{5.34}$$

$$\sum_{q} M_{qq}(k) = [2\pi\ell^2]^{-1}\,(2\pi)^2\delta(k)\ , \tag{5.35}$$

where $\kappa = k_x - ik_y$ is the complex representation of the wave vector k and ℓ is the magnetic length. The matrix $A_{nn'}(k)$ for the Landau-level degrees of freedom is unique. It does not depend on the gauge and on the representation of the degenerate degrees of freedom. We obtain

$$A_{nn'}(\mathbb{k}) = \begin{cases} \sqrt{\frac{n'!}{n!}}\left(-\frac{\mathrm{i}}{\sqrt{2}}\kappa\ell\right)^{n-n'} L_{n'}^{(n-n')}\left(\frac{1}{2}\mathbb{k}^2\ell^2\right)\ , & \text{for } n > n' \\ L_n\left(\frac{1}{2}\mathbb{k}^2\ell^2\right)\ , & \text{for } n = n' \\ \sqrt{\frac{n!}{n'!}}\left(-\frac{\mathrm{i}}{\sqrt{2}}\kappa^*\ell\right)^{n'-n} L_n^{(n'-n)}\left(\frac{1}{2}\mathbb{k}^2\ell^2\right)\ , & \text{for } n < n' \end{cases} \tag{5.36}$$

where $L_n(x)$ are the Laguerre polynomials and $L_n^{(\alpha)}(x)$ are the generalized Laguerre polynomials (Abramowitz and Stegun 1972). For convenience of our calculations we define the matrix elements

$$Q_{nn'}(k) = |A_{nn'}(k)|^2 \exp(-\tfrac{1}{2}k^2\ell^2) \tag{5.37}$$

which can be written in the form

$$Q_{nn'}(k) = (-1)^{n-n'} L_{n'}^{(n-n')}(\tfrac{1}{2}k^2\ell^2)\, L_n^{(n'-n)}(\tfrac{1}{2}k^2\ell^2)\cdot\exp(-\tfrac{1}{2}k^2\ell^2) \tag{5.38}$$

for all $n, n' = 0, 1, 2, \ldots$.

For the gauge-transformed fermion system there are two more elements for constructing the Feynman diagrams: the gauge-field propagator shown in Fig. 5.4d and the three vertex shown in Fig. 5.4e by which the gauge field couples to the fermions. The structure of the three vertex with respect to the indices n, q, and σ is given by the matrix element (5.32) times $\delta_{\sigma\sigma'}$ for $k = 0$ which is just $\delta_{nn'}\delta_{qq'}\delta_{\sigma\sigma'}$. Since the gauge transformation does not depend on the space variables, there is only an imaginary-time derivative ∂_τ^A but no gradient ∇^A (compare with Fig. 4.4a). Furthermore, there is no four vertex (like this one shown in Fig. 4.4b). For evaluating a given Feynman diagram, there are some further rules. As usual, for each three vertex an integration over τ is performed according to $\hbar^{-1}\int_0^{\hbar\beta}\mathrm{d}\tau$. For each full propagator line the sum over n, q, and σ is taken, i.e. $\sum_{nq\sigma}$. For each dashed interaction line an integral over k is performed according to $(2\pi)^{-2}\int \mathrm{d}^2k$.

Now we derive the self-consistent equations to determine the gauge-transformed fermion Green's function $\tilde{G}_{n\sigma}(\omega_l)$ and the effective screened interaction potential $U_{\mathrm{eff}}(k, \Omega_l)$. To do this we apply the modified self-consistent

quantum-field theory of Sect. 4.2. The Green's function $\tilde{G}_{n\sigma}(\omega_l)$ is expressed via the Dyson equation

$$\tilde{G}_{n\sigma}(\omega_l) = 1 / [-\mathrm{i}\hbar\omega_l + \varepsilon_{n\sigma} - \mu - \tilde{\Sigma}_{n\sigma}(\omega_l)] \tag{5.39}$$

in terms of the self energy $\tilde{\Sigma}_{n\sigma}(\omega_l)$, while the effective screened interaction is expressed via

$$U_{\mathrm{eff}}(\boldsymbol{k}, \Omega_l) = V(\boldsymbol{k}) / [1 + V(\boldsymbol{k}) \Pi(\boldsymbol{k}, \Omega_l)] \tag{5.40}$$

in terms of the polarization function $\Pi(\boldsymbol{k}, \Omega_l)$. The self energy $\tilde{\Sigma}_{n\sigma}(\omega_l)$ and the polarization $\Pi(\boldsymbol{k}, \Omega_l)$ are given by infinite series' of irreducible Feynman diagrams with thick propagator lines identified by $\tilde{G}_{n\sigma}$ and thick dashed interaction lines identified by $-U_{\mathrm{eff}}$. In Fig. 4.16 these series' are shown up to second order. (Note that no four vertices with wavy lines are present here and in Sect. 4.3. The Hartree diagram is omitted because it is canceled by the positively charged neutralizing background.) For the self-consistent equations in the modified SC-RPA theory we only need the first-order diagrams. In Fig. 4.16a there are two first-order diagrams which yield the self energy

$$\begin{aligned}
\tilde{\Sigma}_{n\sigma}(\tau - \tau') \cdot \delta_{nn'}\delta_{qq'}\delta_{\sigma\sigma'} = \\
&- \sum_{n''q''\sigma''} \int \frac{\mathrm{d}^2k}{(2\pi)^2} A_{nn''}(\boldsymbol{k}) M_{qq''}(\boldsymbol{k}) \delta_{\sigma\sigma''} U_{\mathrm{eff}}(\boldsymbol{k}, \tau - \tau') \\
&\qquad \cdot \tilde{G}_{n''\sigma''}(\tau - \tau')\, \delta_{\sigma''\sigma'} M_{q''q'}(-\boldsymbol{k}) A_{n'n''}(-\boldsymbol{k}) \\
&+ \sum_{n''q''\sigma''} \delta_{nn''}\delta_{qq''}\delta_{\sigma\sigma''} [(-\mathrm{i}\hbar\partial_\tau)(-\mathrm{i}\hbar\partial_{\tau'}) D(\tau - \tau')] \\
&\qquad \cdot \tilde{G}_{n''\sigma''}(\tau - \tau')\, \delta_{\sigma''\sigma'}\delta_{q''q'}\delta_{n''n'}
\end{aligned} \tag{5.41}$$

In the first term the sum over q'' is evaluated by (5.33) and (5.34). The integral over the angle of $\boldsymbol{k}$ implies that the first term is diagonal in the Landau-level indices. Thus, the self energy is diagonal with respect to all three indices n, q, and σ. Eventually we obtain

$$\begin{aligned}
\tilde{\Sigma}_{n\sigma}(\tau) = &- \sum_{n'} \int \frac{\mathrm{d}^2k}{(2\pi)^2} Q_{nn'}(\boldsymbol{k})\, U_{\mathrm{eff}}(\boldsymbol{k}, \tau)\, \tilde{G}_{n'\sigma}(\tau) \\
&+ [(\hbar\partial_\tau)^2 D(\tau)]\, \tilde{G}_{n\sigma}(\tau)
\end{aligned} \tag{5.42}$$

where $Q_{nn'}(\boldsymbol{k})$ is defined in (5.37) and (5.38). In Fig. 4.16b there is one first-order diagram which yields the polarization function

$$\begin{aligned}
\Pi(\boldsymbol{k}, \tau - \tau')\, (2\pi)^2 \delta(\boldsymbol{k} - \boldsymbol{k}') = &- \sum_{nq\sigma} \sum_{n'q'\sigma'} A_{n'n}(-\boldsymbol{k}) M_{q'q}(-\boldsymbol{k}) \delta_{\sigma'\sigma} \\
&\cdot \tilde{G}_{n\sigma}(\tau - \tau') \tilde{G}_{n'\sigma'}(\tau' - \tau)\, \delta_{\sigma\sigma'} M_{qq'}(\boldsymbol{k}') A_{nn'}(\boldsymbol{k}') \,.
\end{aligned} \tag{5.43}$$

The sum over q and q' is performed by (5.33) and (5.35). The delta function in (5.35) implies a factor $(2\pi)^2\delta(\mathbb{k}-\mathbb{k}')$ which represents momentum conservation. Thus, we obtain

$$\Pi(\mathbb{k},\tau) = -[2\pi\ell^2]^{-1}\sum_{nn'}\sum_{\sigma} Q_{nn'}(\mathbb{k})\tilde{G}_{n\sigma}(\tau)\tilde{G}_{n'\sigma}(-\tau)\ . \tag{5.44}$$

Eqs. (5.39) and (5.40) together with (5.42) and (5.44) are the self-consistent equations of the modified SC-RPA theory. To solve these equations numerically a Fourier transformation between the imaginary-time representation and the Matsubara-frequency representation is needed.

Until now the gauge-field propagator $D(\tau)$ is an arbitrary bosonic function. We must choose $D(\tau)$ so that the modified self-consistent quantum-field theory is a perturbation theory for degenerate levels, at least up to the first-order diagrams which we consider here. For a given filling factor ν the integer n_0, which is defined by the inequality $n_0 < \nu/2 < n_0+1$, is the index of the partially filled Landau level. (Note that the Landau level n_0 has two spin polarizations $\sigma =\uparrow$ and $\sigma =\downarrow$ so that strictly speaking one of the spin-polarized Landau levels may be completely filled or completely empty while the other one is partially filled.) Since the degeneracies of the noninteracting system are related to the partially filled Landau level n_0, in the Feynman diagrams the gauge-field propagator $D(\tau)$ must cancel all those terms which correspond to the interaction of the electrons within the partially filled Landau level n_0 with small energy transfers. For the modified SC-RPA theory the gauge-field propagator $D(\tau)$ appears only in the self energy (5.42) but not in the polarization (5.44). Thus, the cancellations occur only in the self energy $\tilde{\Sigma}_{n\sigma}(\tau)$ but not in the polarization $\Pi(\mathbb{k},\tau)$.

First of all we separate the Fock term from the self energy (5.42), because in the Dyson equation (5.39) this term is frequency independent and only implies a shift of the energies. We write the effective interaction (5.40) in the form

$$U_{\text{eff}}(\mathbb{k},\Omega_l) = V(\mathbb{k}) - [V(\mathbb{k})]^2\chi_{\varrho\varrho}(\mathbb{k},\Omega_l) \tag{5.45}$$

where

$$\chi_{\varrho\varrho}(\mathbb{k},\Omega_l) = \Pi(\mathbb{k},\Omega_l)/[1+V(\mathbb{k})\Pi(\mathbb{k},\Omega_l)] \tag{5.46}$$

is the density-density correlation function. Inserting (5.45) into the self energy (5.42) we obtain

$$\begin{aligned}\tilde{\Sigma}_{n\sigma}(\tau) = &-\Delta\varepsilon^{\text{F}}_{n\sigma}\cdot\hbar\delta(\tau)\\ &+\sum_{n'}\int\frac{\mathrm{d}^2k}{(2\pi)^2}\,Q_{nn'}(\mathbb{k})\,[V(\mathbb{k})]^2\,\chi_{\varrho\varrho}(\mathbb{k},\tau)\,\tilde{G}_{n'\sigma}(\tau)\\ &+[(\hbar\partial_\tau)^2D(\tau)]\,\tilde{G}_{n\sigma}(\tau)\end{aligned} \tag{5.47}$$

where

$$\Delta\varepsilon^{\mathrm{F}}_{n\sigma} = -\sum_{n'} \int \frac{\mathrm{d}^2k}{(2\pi)^2}\, Q_{nn'}(\boldsymbol{k})\, V(\boldsymbol{k}) \cdot \nu_{n'\sigma} \tag{5.48}$$

are the Fock energies and $\nu_{n\sigma} = -\tilde{G}_{n\sigma}(\tau = -0)$. Supposed the motion of the electrons is restricted to the partially filled Landau level so that $n = n_0$ and $n' = n_0$ in all terms of (5.47), then the last term must cancel all nontrivial frequency dependences of the second term so that

$$\int \frac{\mathrm{d}^2k}{(2\pi)^2}\, Q_{n_0n_0}(\boldsymbol{k})\, [V(\boldsymbol{k})]^2\, \chi_{\varrho\varrho}(\boldsymbol{k}, \tau) + (\hbar\partial_\tau)^2 D(\tau) = -V \cdot \hbar\delta(\tau)\ . \tag{5.49}$$

Because of certain properties of the bosonic function $D(\tau)$ the right-hand side cannot be zero but must be an instantaneous interaction with a certain constant V. Via a Fourier transformation we obtain

$$\int \frac{\mathrm{d}^2k}{(2\pi)^2}\, Q_{n_0n_0}(\boldsymbol{k})\, [V(\boldsymbol{k})]^2\, \chi_{\varrho\varrho}(\boldsymbol{k}, \Omega_l) - (\hbar\Omega_l)^2 D(\Omega_l) = -V\ . \tag{5.50}$$

Inserting $\Omega_l = 0$, from this equation we obtain

$$V = -\int \frac{\mathrm{d}^2k}{(2\pi)^2}\, Q_{n_0n_0}(\boldsymbol{k})\, [V(\boldsymbol{k})]^2\, \chi_{\varrho\varrho}(\boldsymbol{k}, \Omega_l = 0)\ . \tag{5.51}$$

We solve (5.49) for $(\hbar\partial_\tau)^2 D(\tau)$ and insert the resulting term into (5.47). Then, eventually we obtain the self energy

$$\begin{aligned}\tilde{\Sigma}_{n\sigma}(\tau) = &-\left(\Delta\varepsilon^{\mathrm{F}}_{n\sigma} + \Delta\varepsilon^{\mathrm{D}}_{n\sigma}\right) \cdot \hbar\delta(\tau) \\ &+ \sum_{n'} \int \frac{\mathrm{d}^2k}{(2\pi)^2} \left[Q_{nn'}(\boldsymbol{k}) - \delta_{nn'} Q_{n_0n_0}(\boldsymbol{k})\right] [V(\boldsymbol{k})]^2\, \chi_{\varrho\varrho}(\boldsymbol{k}, \tau)\, \tilde{G}_{n'\sigma}(\tau)\end{aligned} \tag{5.52}$$

where

$$\begin{aligned}\Delta\varepsilon^{\mathrm{D}}_{n\sigma} &= -V \cdot (\nu_{n\sigma} - \tfrac{1}{2}) \\ &= \int \frac{\mathrm{d}^2k}{(2\pi)^2}\, Q_{n_0n_0}(\boldsymbol{k})\, [V(\boldsymbol{k})]^2 \chi_{\varrho\varrho}(\boldsymbol{k}, \Omega_l = 0) \cdot (\nu_{n\sigma} - \tfrac{1}{2})\end{aligned} \tag{5.53}$$

is another energy shift.

Equation (5.52) represents the final form of the self energy where the gauge-field propagator $D(\tau)$ has been eliminated. One clearly sees that the second term does not include contributions with $n = n' = n_0$ in agreement with the perturbation theory for degenerate levels. Now, the self-consistent equations, which determine the gauge-transformed fermion Green's function $\tilde{G}_{n\sigma}(\tau)$ and the density-density correlation function $\chi_{\varrho\varrho}(\boldsymbol{k}, \tau)$ within the modified SC-RPA theory, are given by (5.39) and (5.46) together with the self energy (5.52) and the polarization function (5.44). These equations can be solved numerically by iteration and Fourier transformation to calculate

$\tilde{G}_{n\sigma}(\tau)$ and $\chi_{\varrho\varrho}(k,\tau)$ explicitly. The physical relevant electron Green's function $G_{n\sigma}(\tau)$ is then obtained from the gauge-transformation formula (5.29) together with (5.30). Finally we need the explicit form of the gauge-field propagator $D(\tau)$. From (5.50) we obtain

$$D(\Omega_l) = [B(\Omega_l) - B(0)]/(\hbar\Omega_l)^2 \tag{5.54}$$

for $\Omega_l \neq 0$ where

$$B(\Omega_l) = \int \frac{\mathrm{d}^2k}{(2\pi)^2} Q_{n_0 n_0}(k)\,[V(k)]^2\,\chi_{\varrho\varrho}(k,\Omega_l)\ . \tag{5.55}$$

For $\Omega_l = 0$ the value of $D(\Omega_l)$ may be arbitrary, because in the difference $\Phi(\tau) = D(0) - D(\tau)$ this value cancels so that it is irrelevant. For definiteness we choose $D(\Omega_l = 0) = 0$. We may use (4.108) to calculate the function $\Phi(\tau)$ by integrations.

Comparing (5.49)-(5.51) and (5.54)-(5.55) with (4.95)-(4.99) of Chap. 4 we find close analogies of our modified SC-RPA theory for the two-dimensional electron system in a strong magnetic field with the independent-boson model. While for the independent-boson model the bosonic function $B(\Omega_l)$ is given by the sum of free boson Green's functions (4.98), in the present case the bosonic function is given by (5.55). We note that both formulas (4.48) and (5.55) have a similar structure: the Coulomb interaction potential $V(k)$ corresponds to the interaction vertex M_q, while $\chi_{\varrho\varrho}(k,\Omega_l)$ corresponds to the Green's functions of the independent bosons. If we restrict the motion of the electrons to the partially filled Landau level and neglect the other Landau levels so that $n = n' = n_0$ in all formulas, then indeed we obtain an independent-boson model *exactly*, because in this case the second term of the self energy (5.52) is zero so that the resulting transformed fermion Green's function $\tilde{G}_{n_0\sigma}(\omega_l)$ is a free Green's function with a shifted energy in agreement with (4.102). (More precisely we obtain two independent-boson models for both spin polarizations $\sigma = \uparrow$ and $\sigma = \downarrow$ which are decoupled from each other.) We conclude that here our modified SC-RPA theory acts as a perturbation theory for degenerate levels: the degenerate degrees of freedom, which are related to the partially filled Landau level n_0, are treated by the independent-boson model, while the other Landau levels $n \neq n_0$ are treated perturbatively in SC-RPA.

The spectral functions $A_{n\sigma}(\varepsilon)$ of the spin-polarized Landau levels, which are defined in (5.14), are obtained from the electronic Green's functions $G_{n\sigma}(\omega_l)$ by analytic continuation. From our numerical calculations we obtain the following results. We assume that the spin-polarized Landau level with indices n_0 and σ_0 is partially filled so that the filling factor $\nu_{n_0\sigma_0}$ of this level is in the interval $0 < \nu_{n_0\sigma_0} < 1$ no too close to 0 and 1. Then, for low temperatures we find that the spectral function of this level $A_{n_0\sigma_0}(\varepsilon)$ splits into two peaks separated by a minimum or pseudogap at the Fermi energy $\varepsilon = \mu$. For this level we find a double-peak structure which is shown qualitatively in Fig. 5.2. On the other hand, for the spectral functions $A_{n\sigma}(\varepsilon)$ of

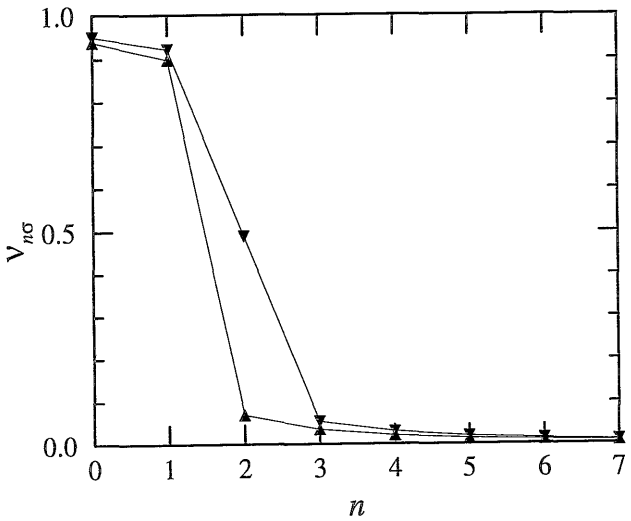

Fig. 5.5. The filling factors $\nu_{n\sigma}$ of the spin-polarized Landau levels versus n for temperature $k_B T = 0.01\,\hbar\omega_c$ and $r_s = 1.5$. The total filling factor is $\nu = \sum_{n\sigma} \nu_{n\sigma} = 4.5$. The triangles up correspond to $\sigma = \uparrow$, wile the triangles down correspond to $\sigma = \downarrow$. The thin lines are guides to the eyes. Note that $\nu_{n\uparrow} < \nu_{n\downarrow}$. The level with $n_0 = 2$ and $\sigma_0 = \downarrow$ is half filled. The other levels are either nearly filled or nearly empty.

the other levels, which are either nearly filled or nearly empty, we find single peaks with a certain width. Thus, for the electronic spectral function $A_{n\sigma}(\varepsilon)$ our modified SC-RPA theory yields a result which is qualitatively expected.

As an example we have performed the numerical calculations for $\nu = 4.5$. Assuming that the two-dimensional electron system is realized in a *GaAs* quantum well, in the Hamiltonian (5.1) we use the effective electron mass $m^* = 0.07\,m$, the Landé factor $g = 0.44$, and the dielectric constant $\varepsilon = 13$. The plasma parameter is assumed to be $r_s = 1.5$ which corresponds to electron densities realized usually in experiments. We choose the temperature $k_B T = 0.01\,\hbar\omega_c$ which is quite low. In Fig. 5.5 the filling factors $\nu_{n\sigma}$ of the several spin-polarized Landau levels are shown versus n. The triangles up correspond to $\sigma = \uparrow$, while the triangles down correspond to $\sigma = \downarrow$. Clearly we find $\nu_{n_0\sigma_0} \approx 0.5$ for $n_0 = 2$ and $\sigma_0 = \downarrow$, so that here the partially filled spin-polarized Landau level with indices $n_0 = 2$ and $\sigma_0 = \downarrow$ is half filled. The other levels are either nearly filled, $\nu_{n\sigma} > 0.9$ for $n \leq 1$, or nearly empty, $\nu_{n\sigma} < 0.1$ for $n \geq 3$ and for $n = 2$ and $\sigma = \uparrow$. For this reason, the other levels imply only small perturbations, while the main properties of the system are determined by the correlations of the electrons in the half-filled level with $n_0 = 2$ and $\sigma_0 = \downarrow$. The sum of all filling factors $\nu_{n\sigma}$ is the total filling factor $\sum_{n\sigma} \nu_{n\sigma} = \nu = 4.5$. We may define the sum of the filling factors with a certain spin direction σ by $\nu_\sigma = \sum_n \nu_{n\sigma}$. In the zero-temperature

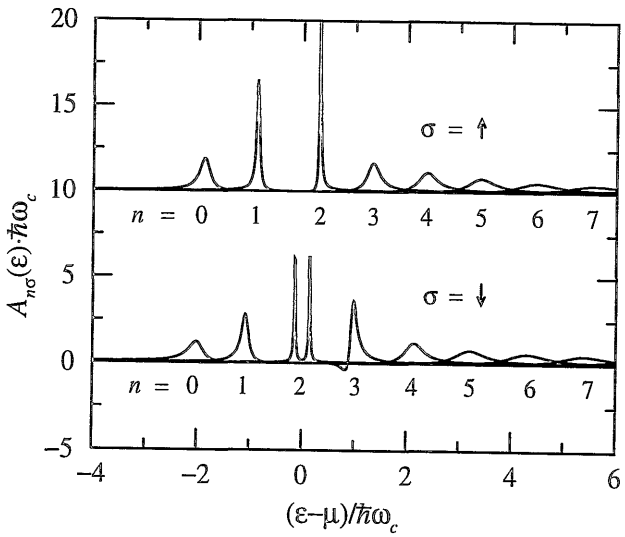

Fig. 5.6. The spectral functions $A_{n\sigma}(\varepsilon)$ of the spin-polarized Landau levels versus the energy ε for temperature $k_BT = 0.01\,\hbar\omega_c$ and total filling factor $\nu = 4.5$ where $r_s = 1.5$. Each peak corresponds to a level with certain n and σ. For distinction between the two spin-directions σ, the curves for $\sigma =\uparrow$ are shifted upwards. Clearly, for $n = 2$ and $\sigma =\downarrow$ the double-peak like spectral function of the half-filled level is seen around the Fermi energy $\varepsilon = \mu$.

limit we find $\nu_\downarrow = 2.5$ and $\nu_\uparrow = 2.0$, where $\nu_\uparrow + \nu_\downarrow = \nu = 4.5$. Since the temperature $k_BT = 0.01\,\hbar\omega_c$ is quite low, the values for $\nu_\downarrow$ and $\nu_\uparrow$ of our numerical calculation are quite close to the zero-temperature limit. In Fig. 5.6 the spectral functions $A_{n\sigma}(\varepsilon)$ of the several spin-polarized Landau levels are shown versus the energy ε. For convenience we choose the Landau level spacing $\hbar\omega_c$ (the cyclotron energy) as the energy scale. Each peak in Fig. 5.6 corresponds to a certain level with indices n and σ. For clarity of the figure we have shifted the curves for $\sigma =\uparrow$ upwards. As expected for the half-filled level with $n_0 = 2$ and $\sigma =\downarrow$ we find a spectral function $A_{n_0\sigma_0}(\varepsilon)$ with a double-peak structure, where the minimum or pseudogap between the two peaks is located at the Fermi energy $\varepsilon = \mu$. The spectral functions $A_{n\sigma}(\varepsilon)$ of the other levels are single peaks with certain widths. The small negative spectral weight on the left-hand side of the peak for $n = 3$ and $\sigma =\downarrow$ is a numerical error, which is caused by the analytical continuation of the Matsubara Green's function to determine the spectral function.

In the following we apply our theory to the two-dimensional electron system in the FQHE regime for strong magnetic fields where $0 < \nu < 2$. We compare our results with experimental observations. For $\nu < 2$ only the lowest Landau level $n_0 = 0$ is partially occupied. Whenever the plasma parameter r_s is small, the higher Landau levels are nearly empty. For $r_s < 2$ we find $\nu_{n\sigma} < 0.1$ for $n \geq 1$. Thus, the higher Landau levels imply only

small perturbations but do not lead to qualitative changes. Hence, in leading approximation we may neglect the higher Landau levels so that the motion of the electrons is restricted to the lowest Landau level. Then, we obtain an independent-boson model for the interacting electrons in the lowest Landau level.

5.4 Electronic excitation spectrum of the partially filled lowest Landau level

A first qualitative explanation of the double-peak structure of the spectral function $A(\varepsilon) = A_{0\downarrow}(\varepsilon)$ shown in Fig. 5.2 has been given by Eisenstein et al. (1992 and 1994). For filling factors ν in the interval $0 < \nu < 1$ the lowest spin-polarized Landau level is partially filled. At low temperatures $T \lesssim 1\,\mathrm{K}$ the two-dimensional electron system is in a strongly correlated state which is liquid-like and which shows the FQHE at certain fractions $\nu = p/q$. The strong correlations imply a near ordering of the electrons which is somewhat similar like in a Wigner crystal. Thus, for the tunneling process realized in the experiment one electron is taken out from a "lattice place" of one layer and then put into an "interstitial place" of the other layer. First, the electron is taken out leaving a hole behind which needs a certain amount of energy Δ. For this reason, in Fig. 5.2 the hole peak of $A(\varepsilon)$ is shifted to lower energies by Δ. Secondly, the electron is put onto an interstitial place which also needs an energy Δ, so that in Fig. 5.2 the electron peak of $A(\varepsilon)$ is shifted to higher energies by Δ. The empty lattice place and the filled interstitial place will relax by reordering the electrons in the surroundings, which leads to emission of collective excitations, i.e. magnetorotons. This relaxation process implies a finite width of the two peaks in $A(\varepsilon)$. To obtain two well defined peaks separated by a pseudogap as shown in Fig. 5.2 the relaxation process must be sufficiently slowly. For this reason the characteristic energy $\varepsilon_{\mathrm{mr}}$ of the magnetorotons must be much smaller than the energy Δ of the single-particle excitations, so that the relaxation time is sufficiently long and the width of the two peaks is smaller than their distance. The double-peak structure of $A(\varepsilon)$ which is indirectly inferred from the tunneling experiments (Eisenstein et al. 1992 and 1994, Brown et al. 1994) implies the ratio $\Delta/\varepsilon_{\mathrm{mr}} \approx 5$, which means that the magnetoroton energies are five times smaller than the energies of the single-particle excitations.

In order to bring these ideas to a quantitative level, Johansson and Kinaret (1993 and 1994) have developed a theory based on an independent-boson model. They consider the tunneling process of a single electron from one layer into the other layer while the interaction with the other electrons is modeled by an interaction with collective excitations which are treated as independent bosons. Using the spectrum of the magnetophonons in a Wigner crystal as an input for the collective excitations, Johansson and Kinaret calculated the

current-voltage characteristic $I(V)$ and obtained a quite good qualitative and quantitative agreement with the experiments. While the model of Johansson and Kinaret seems to be an easy explanation and yields good results, it looks like somewhat artificially constructed and adjusted to the particular physical problem. Thus, a justification of this model within the framework of a microscopic description is desirable.

There are some other theoretical approaches to explain the observation of the tunneling experiment. Efros and Pikus (1993) have applied a model of a classical electron liquid on a two-dimensional lattice to calculate the spectral function $A(\varepsilon)$. They find the double-peak structure of $A(\varepsilon)$ and the tunneling pseudogap of $I(V)$, and their results agree with the experiments. Aleiner, Baranger, and Glazman (1995) have considered the spectral function $A(\varepsilon)$ of a two-dimensional electron liquid in a weak magnetic field. Approximating the collective excitations by a hydrodynamic model, they find a pseudogap of $A(\varepsilon)$ even for $\nu \gg 1$. Alternatively the spectral function $A(\varepsilon)$ has been calculated by numerical exact diagonalization of the Schrödinger equation for finite particle numbers $N \leq 9$ in spherical geometry (Hatsugai et al. 1993 and He et al. 1993) and in planar geometry with periodic boundary conditions (Haussmann et al. 1996). Our recent more extensive numerical calculations (Haussmann et al. 1996) have shown that by this approach the double-peak structure of $A(\varepsilon)$ with a pseudogap at the Fermi energy $\varepsilon = \mu$ is not found convincingly, probably because the particle number is too small. The existence of a well defined double-peak structure requires collective excitations with small energies $\varepsilon_{\mathrm{mr}}$. For small system sizes the energies $\varepsilon_{\mathrm{mr}}$ are not sufficiently small.

From our modified SC-RPA theory we obtain an independent-boson model if we neglect the higher Landau levels and restrict the motion of the electrons to the lowest Landau level. To do this, in all equations we replace the Landau-level indices by $n = n' = 0$. Thus, in (5.52) the second term cancels so that the resulting self energy $\tilde{\Sigma}_{0\sigma}(\omega_l) = -(\Delta\varepsilon^{\mathrm{F}}_{0\sigma} + \Delta\varepsilon^{\mathrm{D}}_{0\sigma})$ is frequency independent. From the Dyson equation (5.39) we obtain the gauge-transformed fermion Green's function

$$\tilde{G}_{0\sigma}(\omega_l) = 1 \,/\, [-\mathrm{i}\hbar\omega_l + \bar{\varepsilon}_{0\sigma} - \mu] \tag{5.56}$$

which is a free Green's function with shifted energy

$$\bar{\varepsilon}_{0\sigma} = \varepsilon_{0\sigma} + \Delta\varepsilon^{\mathrm{F}}_{0\sigma} + \Delta\varepsilon^{\mathrm{D}}_{0\sigma} \,. \tag{5.57}$$

The Fock energy $\Delta\varepsilon^{\mathrm{F}}_{0\sigma}$ and the correlation energy $\Delta\varepsilon^{\mathrm{D}}_{0\sigma}$ are obtained from (5.48) and (5.53) by inserting $Q_{00}(\mathbb{k}) = \mathrm{e}^{-\mathbb{k}^2\ell^2/2}$. By a Fourier back transformation from (5.56) we obtain the gauge-transformed fermion Green's function in imaginary-time representation

$$\tilde{G}_{0\sigma}(\tau) = [\theta(\tau) - \nu_{0\sigma}] \cdot \exp\{-\hbar^{-1}(\bar{\varepsilon}_{0\sigma} - \mu)\tau\} \tag{5.58}$$

where

$$\nu_{0\sigma} = n(\bar{\varepsilon}_{0\sigma}) = 1/[\exp\{\beta(\bar{\varepsilon}_{0\sigma} - \mu)\} + 1] \tag{5.59}$$

are the filling factors of the lowest Landau levels with spin polarization σ. The total filling factor is $\nu = \nu_{0\downarrow} + \nu_{0\uparrow}$. From the gauge transformation formula (5.29) we obtain the physical relevant electron Green's function

$$G_{0\sigma}(\tau) = [\theta(\tau) - \nu_{0\sigma}] \cdot \exp\{-\hbar^{-1}(\bar{\varepsilon}_{0\sigma} - \mu)\tau + \Phi(\tau)\} \; . \tag{5.60}$$

Clearly, all nontrivial imaginary-time and frequency dependences are contained in the function $\Phi(\tau)$ which is related to the density-density correlation function $\chi_{\varrho\varrho}(\boldsymbol{k}, \tau)$ by (5.54) and (5.55). The fermion Green's function (5.60) has exactly the form of the solution of the independent-boson model (see Mahan 1990). Thus, by our modified SC-RPA theory we have derived an independent-boson model from the microscopic quantum-field theory of the two-dimensional electron system in the FQHE regime. Consequently, our theory supports the approach of Johansson and Kinaret (1993 and 1994) on a microscopic level.

The density-density correlation function $\chi_{\varrho\varrho}(\boldsymbol{k}, \tau)$ and hence the function $\Phi(\tau)$ can be calculated within the modified SC-RPA theory. To do this we insert the gauge-transformed fermion Green's function (5.58) into (5.44) to determine the polarization function and then by (5.46) the density-density correlation function. From (5.55) we obtain the bosonic function

$$B(\tau) = 2\Delta/\beta \tag{5.61}$$

which in the imaginary-time representation is constant. Here $\Delta = -V/2$ is a positive energy value which is related to the interaction constant V defined in (5.51). Defining the dimensionless interaction potential

$$u(\boldsymbol{k}) = \lambda\beta\, V(\boldsymbol{k}) \cdot [2\pi\ell^2]^{-1} \mathrm{e}^{-k^2\ell^2/2} \tag{5.62}$$

where

$$\lambda = \sum_{\sigma} \nu_{0\sigma}(1 - \nu_{0\sigma}) \tag{5.63}$$

is a dimensionless parameter, we write the energy value Δ in the form

$$\Delta = \frac{\pi\ell^2}{\lambda\beta} \int \frac{\mathrm{d}^2k}{(2\pi)^2} \, \frac{[u(\boldsymbol{k})]^2}{1 + u(\boldsymbol{k})} \; . \tag{5.64}$$

Finally, inserting (5.61) into (4.108) we obtain

$$\Phi(\tau) = -\hbar^{-1}\Delta|\tau| + \hbar^{-2}(\Delta/\beta)\tau^2 \; . \tag{5.65}$$

This function is a particular simple result, so that from (5.60) we obtain a simple explicit expression for the electron Green's function $G_{0\sigma}(\tau)$. The spectral function $A_{0\sigma}(\varepsilon)$ related to this Green's function can be determined exactly. We find (Haussmann 1996 and 1997)

$$A_{0\sigma}(\varepsilon) = \nu_{0\sigma} \cdot [2\pi\delta^2]^{-1/2} \exp\{-(\varepsilon - [\bar{\varepsilon}_{0\sigma} - \Delta])^2/2\delta^2\} + (1 - \nu_{0\sigma}) \cdot [2\pi\delta^2]^{-1/2} \exp\{-(\varepsilon - [\bar{\varepsilon}_{0\sigma} + \Delta])^2/2\delta^2\} \tag{5.66}$$

which is just the sum of two Gaussian peaks of width $\delta = (2k_BT\Delta)^{1/2}$ for the holes and the electrons. The hole peak of weight $\nu_{0\sigma}$ is located at the energy $\varepsilon = \bar{\varepsilon}_{0\sigma} - \Delta$ while the electron peak of weight $1 - \nu_{0\sigma}$ is located at the energy $\varepsilon = \bar{\varepsilon}_{0\sigma} + \Delta$.

Until now we have included both spin polarizations of the lowest Landau level. However, for filling factors ν in the interval $0 < \nu < 1$ and for low temperatures $k_BT \ll e^2/\varepsilon\ell$ the lowest level with spin polarization $\sigma = \downarrow$ is partially filled by $\nu_{0\downarrow} \approx \nu$ while the higher level with $\sigma = \uparrow$ is nearly empty where $\nu_{0\uparrow}$ is exponentially small. Consequently, the level with $\sigma = \uparrow$ may be neglected so that in the above formulas we may replace the spin index σ by $\downarrow$. Thus, from (5.66) we obtain the spectral function $A(\varepsilon) = A_{0\downarrow}(\varepsilon)$ of the lowest spin-polarized Landau level which reads (Haussmann 1996)

$$A(\varepsilon) = \nu \cdot [2\pi\delta^2]^{-1/2} \exp\{-(\varepsilon - [\bar{\varepsilon}_{0\downarrow} - \Delta])^2/2\delta^2\} + (1 - \nu) \cdot [2\pi\delta^2]^{-1/2} \exp\{-(\varepsilon - [\bar{\varepsilon}_{0\downarrow} + \Delta])^2/2\delta^2\} \tag{5.67}$$

where Δ is defined by (5.64) with $\lambda = \nu(1-\nu)$. The partial filling of the lowest level by $\nu_{0\downarrow} = n(\bar{\varepsilon}_{0\downarrow}) \approx \nu$ requires the Fermi energy to be $\mu = \bar{\varepsilon}_{0\downarrow}$. Clearly, the spectral function $A(\varepsilon)$ defined in (5.67) has the expected double-peak structure as shown qualitatively in Fig. 5.2. For low temperatures $k_BT \ll e^2/\varepsilon\ell$ the two Gaussian peaks are well separated by a pseudogap at the Fermi energy $\varepsilon = \mu$ because the width of the peaks $\delta = (2k_BT\Delta)^{1/2}$ is smaller than the distance $2\Delta \sim e^2/\varepsilon\ell$ between the two peaks.

In the zero-temperature limit $T \to 0$ the width of the peaks $\delta \to 0$ is infinitesimally small while $2\Delta \to (\pi/2)^{1/2}e^2/\varepsilon\ell$ remains constant (Haussmann 1996). Thus, for $T = 0$ the spectral function

$$A(\varepsilon) = \nu \cdot \delta(\varepsilon - [\mu - \Delta]) + (1 - \nu) \cdot \delta(\varepsilon - [\mu + \Delta]) \tag{5.68}$$

is the sum of two delta peaks. However, the experiments performed at very low temperatures (Eisenstein et al. 1992 and 1994 and Brown et al. 1994) indicate that the width of the peaks δ remains finite even in the zero-temperature limit. Thus, our modified SC-RPA theory fails for very low temperatures. The reason of this failure is related to the fact that the modified SC-RPA theory does not yield the correct spectrum for the collective excitations. We obtain a density-density correlation function $\chi_{\varrho\varrho}(k, \tau)$ and hence a bosonic function $B(\tau)$ which are constant in the imaginary time. Consequently, the energies of the collective excitations are $\varepsilon_{\mathrm{mr}} = 0$ which is incorrect. Eq. (5.61) implies the related spectral function

$$B''(\varepsilon) = \lim_{\varepsilon_{\mathrm{mr}} \to 0} \Delta \cdot \varepsilon_{\mathrm{mr}}[\delta(\varepsilon - \varepsilon_{\mathrm{mr}}) - \delta(\varepsilon + \varepsilon_{\mathrm{mr}})] \tag{5.69}$$

which does not agree with the expected spectral function shown in Fig. 5.3. Correctly, the characteristic energies of the collective excitations are expected to be $\varepsilon_{\mathrm{mr}} \approx 0.1\, e^2/\varepsilon\ell$. For temperatures $k_{\mathrm{B}}T \gtrsim 0.1\, e^2/\varepsilon\ell$ the energies are smeared out sufficiently, so that in this case the precise location of the spectral weight of the collective excitations does not influence $A(\varepsilon)$ essentially so that the SC-RPA theory yields a reasonable result. However, for very low temperatures $k_{\mathrm{B}}T \lesssim 0.1\, e^2/\varepsilon\ell$ the precise spectrum of the collective excitations is needed to obtain the correct electronic spectral function $A(\varepsilon)$.

The single-mode approximation developed by Girvin, MacDonald, and Platzman (1985 and 1986) is known to describe the essential properties of the collective excitations in FQHE systems. This method can be used to determine the density-density correlation function approximately. For the spectrum of the collective excitations the ansatz

$$\chi''_{\varrho\varrho}(\boldsymbol{k},\varepsilon) = a(\boldsymbol{k})\,[\delta(\varepsilon - E(\boldsymbol{k})) - \delta(\varepsilon + E(\boldsymbol{k}))] \tag{5.70}$$

is used where the energy dispersion $E(\boldsymbol{k})$ of the collective excitations and the related spectral weight $a(\boldsymbol{k})$ are determined by sum rules. Details of these calculations are described in Sect. 6 of our previous paper (Haussmann 1996). From (5.55) we obtain the integrated spectrum of the collective excitations

$$B''(\varepsilon) = \int \frac{\mathrm{d}^2k}{(2\pi)^2}\, \mathrm{e}^{-k^2\ell^2/2}\, [V(\boldsymbol{k})]^2\, \chi''_{\varrho\varrho}(\boldsymbol{k},\varepsilon) \tag{5.71}$$

which we need to determine the function $\Phi(\tau)$. For $\nu = 1/2$ and $T = 0$ the resulting spectral function $B''(\varepsilon)$ is shown in Fig. 5.7 as full line. Clearly, the main spectral weight of the collective excitations is located at the energy $0.1\, e^2/\varepsilon\ell$ and arises from the magnetorotons. We may define the characteristic energy $\varepsilon_{\mathrm{mr}}$ of the collective excitations precisely by the average

$$\varepsilon_{\mathrm{mr}} = \int_0^\infty \mathrm{d}\varepsilon\; \varepsilon\, B''(\varepsilon) \;\Big/\; \int_0^\infty \mathrm{d}\varepsilon\; B''(\varepsilon) \tag{5.72}$$

and obtain $\varepsilon_{\mathrm{mr}} = 0.099\, e^2/\varepsilon\ell$ (Haussmann 1996). The ansatz of the collective-excitation spectrum (5.70) with delta peaks is an oversimplification. In reality the collective excitations have a finite lifetime so that the peaks of $\chi''_{\varrho\varrho}(\boldsymbol{k},\varepsilon)$ have finite widths. For this reason, alternatively in the ansatz (5.70) we have replaced the delta peaks by Gaussian peaks of width $\Delta\varepsilon = 0.02\, e^2/\varepsilon\ell$. The related spectral function $B''(\varepsilon)$ is shown as dashed line in Fig. 5.7. While the average energy $\varepsilon_{\mathrm{mr}} = 0.099\, e^2/\varepsilon\ell$ of the collective excitations remains unchanged, now the spectral weight is smeared out over a larger range of energies. We believe that the correct spectral function $B''(\varepsilon)$ is somewhere in between the full line and the dashed line of Fig. 5.7.

From the spectral function $B''(\varepsilon)$ of Fig. 5.7 we obtain the bosonic function $B(\tau)$. Then we calculate the electron Green's function $G(\tau) = G_{0\downarrow}(\tau)$ by (5.60) and (4.108) and obtain the electronic spectral function $A(\varepsilon) = A_{0\downarrow}(\varepsilon)$

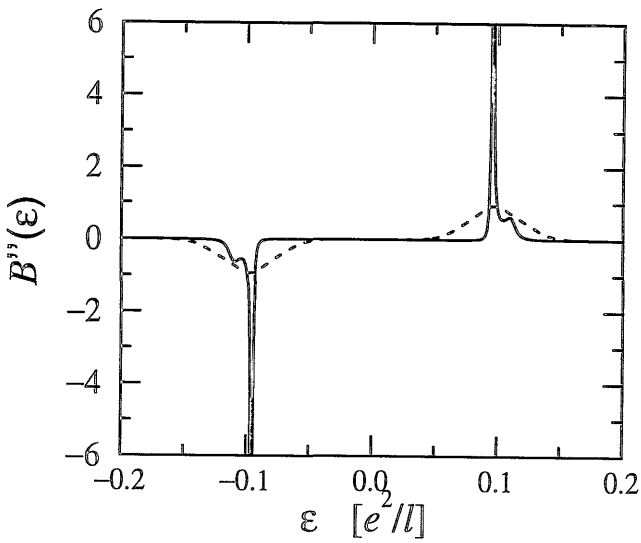

Fig. 5.7. The spectral function $B''(\varepsilon)$ of the k integrated collective excitations, defined by (5.71), in single-mode approximation for $\nu = 1/2$ and $T = 0$. The dashed line is the same but with the delta functions in (5.70) replaced by Gaussian peaks of width $\Delta\varepsilon = 0.02\, e^2/\varepsilon\ell$. The main spectral weight arises from the magnetorotons and is located at the average energy $\varepsilon_{\rm mr} = 0.099\, e^2/\varepsilon\ell$.

by analytic continuation. We have performed the calculations for the filling factor $\nu = 1/2$ and temperature $k_{\rm B}T = 0.01\, e^2/\varepsilon\ell$. The result is shown in Fig. 5.8 where the full line and the dashed line correspond to those in Fig. 5.7. As expected, for $A(\varepsilon)$ we find two peaks separated by a pseudogap at $\varepsilon = \mu$. We may define the distance between the two peaks precisely by the difference of two average energies as

$$2\Delta = \frac{\int \mathrm{d}\varepsilon\, \varepsilon A_+(\varepsilon)}{\int \mathrm{d}\varepsilon\, A_+(\varepsilon)} - \frac{\int \mathrm{d}\varepsilon\, \varepsilon A_-(\varepsilon)}{\int \mathrm{d}\varepsilon\, A_-(\varepsilon)} \tag{5.73}$$

where $A_+(\varepsilon) = [1 - n(\varepsilon)]A(\varepsilon)$ is the spectrum of the electron peak and $A_-(\varepsilon) = n(\varepsilon)A(\varepsilon)$ is the spectrum of the hole peak. Equivalently, we may interpret Δ as the characteristic energy of the single-particle excitations. Inserting the spectral function $A(\varepsilon)$ obtained from the Green's function (5.60) together with (4.108), this characteristic energy can be written as an integral of the bosonic spectrum $B''(\varepsilon)$ according to

$$2\Delta = B(\Omega_l = 0) = \int \mathrm{d}\varepsilon\, B''(\varepsilon)/\varepsilon\ . \tag{5.74}$$

Consequently, from the bosonic spectral function shown in Fig. 5.7 we obtain $2\Delta = 0.96\, e^2/\varepsilon\ell$ for the full line and $2\Delta = 1.01\, e^2/\varepsilon\ell$ for the dashed line (Haussmann 1996).

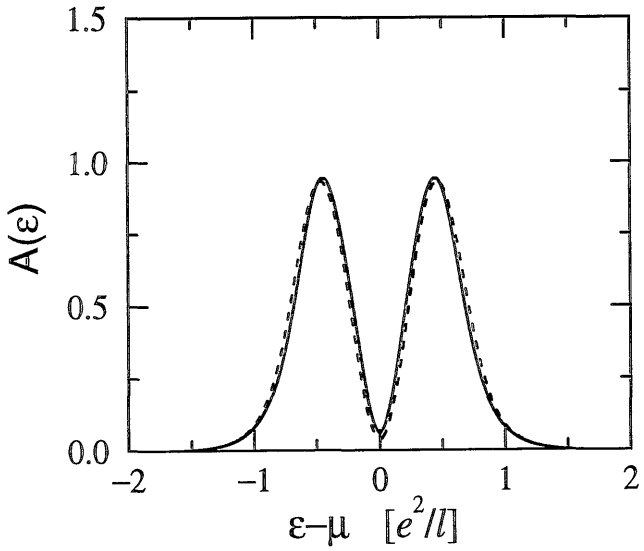

Fig. 5.8. The electronic spectral function $A(\varepsilon)$ of the lowest spin-polarized Landau level for $\nu = 1/2$ and $k_B T = 0.01\, e^2/\varepsilon\ell$ obtained from (5.60), (4.108), and analytic continuation using $B''(\varepsilon)$ of Fig. 5.7 as input for the collective excitations. Full and dashed line correspond to those in Fig. 5.7. One clearly sees the double-peak structure with the pseudogap at $\varepsilon = \mu$. The symmetry of $A(\varepsilon)$ around $\varepsilon = \mu$ is a speciality of the occupation fraction $\nu = 1/2$ and reflects particle-hole symmetry.

We conclude that the system is described by three characteristic energies, the thermal energy $k_B T$, the magnetoroton energy $\varepsilon_{\rm mr}$, and the single-particle energy Δ. Neglecting the last digits these energies have the values

$$k_B T = 0.01\, e^2/\varepsilon\ell\ , \qquad \varepsilon_{\rm mr} = 0.1\, e^2/\varepsilon\ell\ , \qquad \Delta = 0.5\, e^2/\varepsilon\ell\ . \tag{5.75}$$

First of all, the experiments (Eisenstein et al. 1992 and 1994 and Brown et al. 1994) were performed at the temperature $k_B T \approx 0.01\, e^2/\varepsilon\ell$ which is close to the temperature of our calculation. The related thermal energy is considerably smaller than the relevant characteristic energies $\varepsilon_{\rm mr}$ and Δ. Thus, the system is close to the zero temperature limit. Consequently, the spectral function $A(\varepsilon)$ does not depend significantly on the temperature for $0 < k_B T < 0.01\, e^2/\varepsilon\ell$ so that the curves shown in Fig. 5.8 are very close to the zero-temperature limit. For these low temperatures the width of the two peaks remains finite and is not small compared to the distance 2Δ between the two peaks.

While in Fig. 5.7 for $B''(\varepsilon)$ the full line and the dashed line differ considerably from each other, in Fig. 5.8 for $A(\varepsilon)$ the full line and the dashed line nearly coincide. Since the energies $\varepsilon_{\rm mr}$ and Δ are nearly the same in both cases, we conclude that the shape of the electronic spectral function $A(\varepsilon)$ does not depend significantly on the shape of the bosonic spectral function $B''(\varepsilon)$

but only on the average energy $\varepsilon_{\rm mr}$ and the total spectral weight (which is related to Δ) of the collective excitations. More precisely, the main features of the shapes of the two peaks of $A(\varepsilon)$, i.e. the width of the peaks compared to the distance between the peaks, is mainly determined by the ratio of the two characteristic energies which here for the FQHE system is

$$\Delta/\varepsilon_{\rm mr} = 5 \; . \tag{5.76}$$

The width of the peaks decreases for increasing $\Delta/\varepsilon_{\rm mr}$ while it increases for decreasing $\Delta/\varepsilon_{\rm mr}$. For $\Delta/\varepsilon_{\rm mr} \lesssim 1$ the two peaks merge into one peak so that in this case there will be no double-peak structure at all. On the other hand in the limit $\Delta/\varepsilon_{\rm mr} \to \infty$, where $\varepsilon_{\rm mr} \to 0$ and Δ is constant, the two peaks are delta peaks which correspond to the spectral function (5.68) of the modified SC-RPA theory at $T = 0$. In Fig. 5.8 the spectral function $A(\varepsilon)$ is symmetric with respect to the Fermi energy $\varepsilon = \mu$. This fact is a speciality of the filling factor $\nu = 1/2$ and reflects particle-hole symmetry. For other values of ν the spectral function $A(\varepsilon)$ is not symmetric. In this case the two peaks have different sizes characterized by the spectral weights ν and $1-\nu$ respectively. Nevertheless, the double-peak structure with a pseudogap at $\varepsilon = \mu$ remains.

For the tunneling of electrons between two FQHE layers with equal properties the current-voltage characteristic $I(V)$ is obtained from the spectral function $A(\varepsilon)$ by (5.21) and (5.22). It turns out that we need not calculate the convolution integral in (5.21) explicitly. We define the pair propagator $\chi(\tau)$ by

$$\chi(\tau) = -G(\tau)G(-\tau) \; , \tag{5.77}$$

obtain $\chi(\Omega_l)$ by a Fourier transformation, and determine the related spectral function $\chi''(\varepsilon)$ by analytical continuation with respect to the frequency. The convolution theorem of the Fourier transformation implies that $\chi''(\varepsilon)$ is just the convolution integral in (5.21) so that the tunneling current can be written as

$$I(V) = e\,\frac{t^2 F}{\hbar \ell^2}\,\chi''(eV) \; . \tag{5.78}$$

Thus, the spectral function $\chi''(\varepsilon)$ can be compared directly with the current-voltage characteristic $I(V)$ found in the tunneling experiment (Eisenstein et al. 1992 and 1994 and Brown et al. 1994) by rescaling the two axes. While the voltage V is identified uniquely by $\varepsilon = eV$, the amplitude of the current I depends on the tunneling matrix element t and on the area of the tunneling contact F, which are parameters to be adjusted. In Fig. 5.9 the spectral function $\chi''(\varepsilon)$ is shown for $\nu = 1/2$ and $k_{\rm B}T = 0.01\, e^2/\varepsilon\ell$ which is obtained from our numerical calculations. The full line and the dashed line correspond to the respective lines in Figs. 5.7 and 5.8 and again nearly coincide. Thus, in agreement with $A(\varepsilon)$, the shape of the spectral function $\chi''(\varepsilon)$ is determined mainly by the ratio $\Delta/\varepsilon_{\rm mr}$ while the precise shape of the bosonic spectral function $B''(\varepsilon)$ in Fig. 5.7 is irrelevant. The curves shown in Fig. 5.9 qualitatively agree quite well with the experimentally observed shape

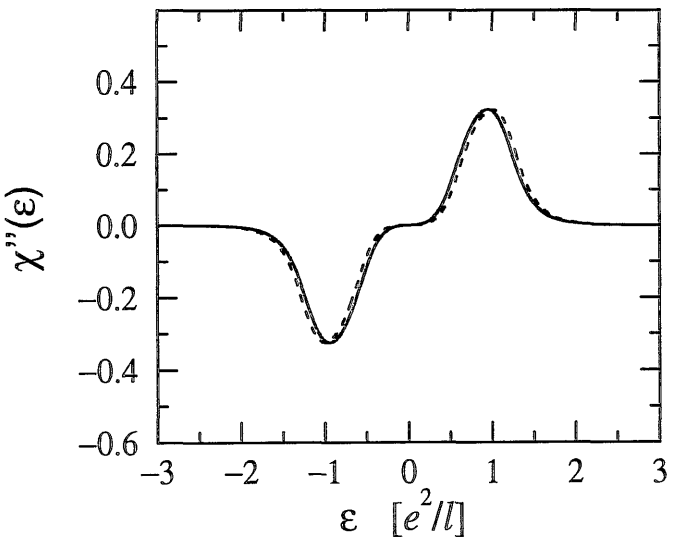

Fig. 5.9. The spectral function of the pair propagator $\chi''(\varepsilon)$ for $\nu = 1/2$ and $k_B T = 0.01\, e^2/\varepsilon\ell$ obtained from (5.77) and analytic continuation. Full and dashed line correspond to those in Figs. 5.7 and 5.8. Equation (5.78) allows to compare the curve directly with the current-voltage characteristic $I(V)$ by proper rescaling of both axes. Qualitatively our curve agrees quite well with the experimental results of Eisenstein et al. (1992 and 1994) and Brown et al. (1994).

of the current-voltage characteristic $I(V)$. We find a strong suppression of the tunneling current $I(V)$ for small voltages and a peak with a maximum at a certain position, which corresponds to the tunneling of the electrons involving only the lowest spin-polarized Landau level. We may define the peak position precisely by the average

$$\begin{aligned} 2\Delta &= \int_0^\infty \mathrm{d}V\; eV\, I(V) \;\Big/\; \int_0^\infty \mathrm{d}V\; I(V) \\ &= \int_0^\infty \mathrm{d}\varepsilon\; \varepsilon\, \chi''(\varepsilon) \;\Big/\; \int_0^\infty \mathrm{d}\varepsilon\; \chi''(\varepsilon)\;. \end{aligned} \tag{5.79}$$

Inserting the tunneling current (5.21) into (5.79) we obtain (5.73), so that the 2Δ defined by (5.79) and this one defined by (5.73) are equal.

By considering the values of 2Δ we can compare the position of the peak of $I(V)$ between theory and experiment quantitatively. Our theory yields the value $2\Delta = 0.96\, e^2/\varepsilon\ell$ (corresponding to the full lines in the figures). On the other hand, in the experiment the peak is located at a voltage which corresponds to $2\Delta_{\mathrm{exp}} \approx 0.5\, e^2/\varepsilon\ell$ for $\nu = 1/2$. In a recent paper (Haussmann et al. 1996) the average peak position 2Δ defined by (5.79) or by (5.73) has been related exactly to the ground-state energy via a sum rule. Using an interpolation formula for the ground-state energy the value $2\Delta_{\mathrm{exact}} \approx 0.6\, e^2/\varepsilon\ell$ has

been found for $\nu = 1/2$ which is very accurate and can be viewed as nearly exact. Thus it turns out that the value 2Δ of our theory is by a factor of 1.9 or 1.6 too large compared to the measured or the exact value, respectively. Since our theory contains a lot of approximations which imply that the original microscopic theory is drastically reduced to an independent-boson model, we cannot expect that our theory yields a quantitatively correct value for 2Δ. In our calculations we have assumed that the electron system is perfectly two-dimensional. However, in the real systems (Eisenstein et al. 1992 and 1994 and Brown et al. 1994) the electrons are confined in $GaAs$ quantum wells of finite thickness which is about 200 Å. The Coulomb interaction is reduced effectively for short distances by the finite layer thickness. Thus, eventually 2Δ will be reduced by finite-thickness corrections so that it is closer to the experimental value $2\Delta_{\text{exp}}$. Consequently, finite-thickness corrections will reduce the discrepancy between our theory and the experiment.

While we have calculated $\chi''(\varepsilon)$ only for $\nu = 1/2$, it turns out that this spectral function depends only weakly on the filling factor ν, as long as ν is not too close to 0 or 1. This fact agrees with the experimental observation, because the current-voltage characteristic $I(V)$ does not change significantly if ν is varied. The position of the peak is shifted only slightly which means that in theory and experiment the average peak position 2Δ also depends only weakly on ν.

Until now we have considered only very low temperatures close to the zero-temperature limit. Turner et al. (1996) have measured the differential tunneling conductance $G(V) = dI(V)/dV$ for $\nu = 1/2$ for several finite temperatures. To explain the experimental observations they suggest to calculate the tunneling current $I(V)$ by (5.21) where the electronic spectral function $A(\varepsilon)$ is modeled by two Gaussian peaks as

$$\begin{aligned} A(\varepsilon) \quad &= \nu \cdot [2\pi\delta^2]^{-1/2} \exp\{-(\varepsilon + \Delta)^2/2\delta^2\} \\ &\quad + (1-\nu) \cdot [2\pi\delta^2]^{-1/2} \exp\{-(\varepsilon - \Delta)^2/2\delta^2\} \end{aligned} \tag{5.80}$$

where $\delta = (\alpha k_{\text{B}} T \Delta)^{1/2}$ is the width of the peaks and α is an adjustable parameter. This model spectral function is motivated by the activated behavior of the zero-voltage conductance $G(V = 0)$ observed in the experiment. Choosing $\alpha = 5.3$ Turner et al. (1996) find good agreement between the model and the experiment for $G(V)$ at several temperatures T. On the other hand, by the modified SC-RPA theory we have derived a spectral function $A(\varepsilon)$ of precisely the same form: Eqs. (5.67) and (5.80) are identical for $\alpha = 2$, up to a shift of the energy scale. Thus, our modified SC-RPA theory supports the model by Turner et al. 1996 on a microscopic level where, however, the value of α does not agree.

5.5 Magnetization of FQHE electron systems

Usually, in theories of the FQHE for $0 < \nu < 1$ it is assumed (Prange and Girvin 1987) that the motion of the electrons is restricted to the lowest spin-polarized Landau level so that the system is assumed to be completely spin polarized. The most prominent example is the Laughlin wave function for the FQHE states with fractions $\nu = 1/m$ (Laughlin 1983). However, in general complete spin polarization is not justified. For electron systems realized in $GaAs$ according to the inequality (5.6) and the ratio (5.9) the bare Zeeman energy $\Delta\varepsilon_s = g\mu_B B$ is very small compared to the characteristic interaction energy. Thus, the spin polarization of electron systems in the FQHE regime is a highly nonperturbative and nontrivial effect. There will be strong correlations also with respect to the spin degrees of freedom.

In a recent NMR experiment (Barrett et al. 1995) the magnetization of the quantum Hall system has been measured via the Knight shift for filling factors $0.66 < \nu < 1.76$ and temperatures $1.55\,\mathrm{K} < T < 20\,\mathrm{K}$. At very low temperatures it has been found that the system is completely polarized (in a ferromagnetic ground state) only for $\nu = 1$, while for other fillings ν the magnetization is strongly reduced. This demagnetization for $\nu \neq 1$ has been related to the existence of charged spin texture excitations or skyrmions (Lee and Kane 1990, Sondhi and Karlhede 1993, Fertig et al. 1994). Further experiments have been performed to study skyrmions based on transport (Schmeller et al. 1995) and optical (Aifer et al. 1996) measurements.

On the other hand the temperature dependence of the magnetization $M(T)$ has been measured for $\nu = 1$ which does not agree with simple theories (Barrett et al. 1995). Because of the very small Zeeman energy, in a system of noninteracting electrons the magnetic polarization occurs at too low temperatures. Exchange interaction effects lead to a considerable enhancement of the effective Zeeman energy. The Hartree–Fock theory, which incorporates exchange effects on a mean-field level, strongly overestimates the effective Zeeman energy leading to a magnetic polarization of the system at much too high temperatures.

Kasner and MacDonald (1996) calculated the magnetization $M(T)$ within a many-particle quantum-field-theoretic approach, which goes beyond Hartree-Fock theory because spin-wave excitations are included via particle-hole ladder diagrams. They argue that the magnetization is suppressed by fluctuations related to thermally excited spin waves. As a result they obtain a magnetization $M(T)$ which yields a polarization of the system at a considerable lower temperature which, however, is still too high compared to the experiment. Furthermore, Kasner and MacDonald have varied the screening length of an effective screened Coulomb interaction and also determined the filling factors of the spin levels self consistently. However, the theory is not satisfactory, the magnetization curve is too far away from the experimental data and the polarization of the system occurs at still too high temperatures. In a complementary approach Read and Sachdev (1995) considered

a continuum quantum-field theory for the spin-vector field and focused on the collective aspect of the physics. Evaluating the magnetization $M(T)$ for $SU(N)$ and $O(N)$ symmetries in the limit $N \to \infty$ and tuning the spin stiffness ϱ_s as a parameter, they obtained results which lie in the range of the experimental data.

Now, we calculate the magnetization $M(T)$ within our modified SC-RPA theory. From the gauge-transformed fermion Green's function $\tilde{G}_{n\sigma}(\tau)$ we obtain the filling factors $\nu_{n\sigma}$ of the several spin-polarized Landau levels by $\nu_{n\sigma} = -\tilde{G}_{n\sigma}(\tau = -0)$. We define the magnetization by

$$M = \nu_\downarrow - \nu_\uparrow \tag{5.81}$$

where $\nu_\sigma = \sum_n \nu_{n\sigma}$ are the filling factors with spin direction σ and $\nu = \nu_\downarrow + \nu_\uparrow$ is the total filling factor. By solving the self-consistent equations (5.39), (5.52), (5.46), and (5.44) of the modified SC-RPA theory for several temperatures, we obtain the magnetization $M(T)$ as a function of temperature T where the total filling factor ν is kept constant.

A considerable simplification of the modified SC-RPA theory occurs if the motion of the electrons is restricted to the lowest Landau level $n = 0$. We have done this in Sect. 5.4. The gauge-transformed fermion Green's function $\tilde{G}_{0\sigma}(\tau)$ is just a free Green's function with shifted energies, given by (5.56) or (5.58). Consequently, the filling factors $\nu_{0\sigma}$ of the levels with spin polarization σ are given by a Fermi distribution function as

$$\nu_{0\sigma} = 1/[\exp\{\beta(\bar{\varepsilon}_{0\sigma} - \mu)\} + 1] \,. \tag{5.82}$$

In this formula the energies $\bar{\varepsilon}_{0\sigma}$ of the shifted levels are nontrivial and defined by (5.57) together with (5.48) and (5.53) where $n = n' = 0$. By (5.45) we may add $\Delta\varepsilon^{\mathrm{F}}_{0\sigma}$ and $\Delta\varepsilon^{\mathrm{D}}_{0\sigma}$ together so that we obtain

$$\bar{\varepsilon}_{0\sigma} = \varepsilon_{0\sigma} - \frac{2\pi\ell^2}{\lambda\beta} \int \frac{\mathrm{d}^2k}{(2\pi)^2} \left\{ \frac{1}{2} u(k) + \left(\nu_{0\sigma} - \frac{1}{2}\right) \frac{u(k)}{1 + u(k)} \right\} \tag{5.83}$$

where $u(k)$ is the dimensionless interaction potential defined in (5.62) and λ is given by (5.63). Clearly, the shifted energies $\bar{\varepsilon}_{0\sigma}$ depend on the filling factors $\nu_{0\sigma}$. Thus, Eqs. (5.82) and (5.83) together with (5.62) and (5.63) form a set of self-consistent equations which can be solved easily by iteration to determine $\nu_{0\sigma}$ and $\bar{\varepsilon}_{0\sigma}$. Then, the magnetization is obtained from $M = \nu_{0\downarrow} - \nu_{0\uparrow}$ while $\nu = \nu_{0\downarrow} + \nu_{0\uparrow}$ is the total filling factor. In (5.82) we adjust the chemical potential μ so that ν is a given constant. Performing the calculations for several temperatures, we obtain $M(T)$ for constant ν.

In Hartree–Fock approximation the shifted energies are given by $\varepsilon^{\mathrm{HF}}_{0\sigma} = \varepsilon_{0\sigma} + \Delta\varepsilon^{\mathrm{F}}_{0\sigma}$. In (5.57) this means that the last contribution is omitted. Equivalently, in the last term of (5.83) the denominator $1 + u(k)$ is replaced by unity so that we obtain

$$\varepsilon^{\mathrm{HF}}_{0\sigma} = \varepsilon_{0\sigma} - \nu_{0\sigma} \frac{2\pi\ell^2}{\lambda\beta} \int \frac{\mathrm{d}^2k}{(2\pi)^2} u(k) \,. \tag{5.84}$$

For Coulomb interaction the k integral can be evaluated explicitly so that $\varepsilon_{0\sigma}^{\mathrm{HF}} = \varepsilon_{0\sigma} - \nu_{0\sigma}(\pi/2)^{1/2}e^2/\varepsilon\ell$. We obtain the filling factors $\nu_{0\sigma}$ and hence $M(T)$ in Hartree–Fock approximation by solving (5.82) and (5.84) as self-consistent equations.

For an explicit calculation of the magnetization $M(T)$ the bare Zeeman energy $\Delta\varepsilon_{\mathrm{s}} = \varepsilon_{0\uparrow} - \varepsilon_{0\downarrow}$ and the total filling factor ν are needed as input parameters. Barrett et al. (1995) have measured the magnetization $M(T)$ versus temperature T in a $GaAs$ sample for $\nu = 0.98$ and $B = 7.05\,\mathrm{T}$. For this system the magnetic length is $\ell = (\hbar c/eB)^{1/2} = 97\,\text{Å}$ which implies the characteristic interaction energy $e^2/\varepsilon\ell = 11.5\,\mathrm{meV}$. The bare Zeeman energy is $\Delta\varepsilon_{\mathrm{s}} = g\mu_{\mathrm{B}}B = 0.18\,\mathrm{meV}$. Thus, we perform our calculations for $\nu = 1$ and

$$\Delta\varepsilon_{\mathrm{s}} = \varepsilon_{0\uparrow} - \varepsilon_{0\downarrow} = 0.016\, e^2/\varepsilon\ell\ . \tag{5.85}$$

In Fig. 5.10 the result of our modified SC-RPA theory, obtained from (5.82) and (5.83), is shown as full line. The data of the NMR experiment (Barrett et al. 1995) are shown as crosses. One clearly sees that our theoretical curve is quite close to the experimental data without any adjustable parameters.

For comparison we have plotted the magnetization of the Hartree–Fock theory obtained from (5.82) and (5.84) as dotted line. Clearly, the Hartree–Fock result is far away from the experimental data. It predicts a polarization of the system at much too high temperatures, about 7.5 times higher than

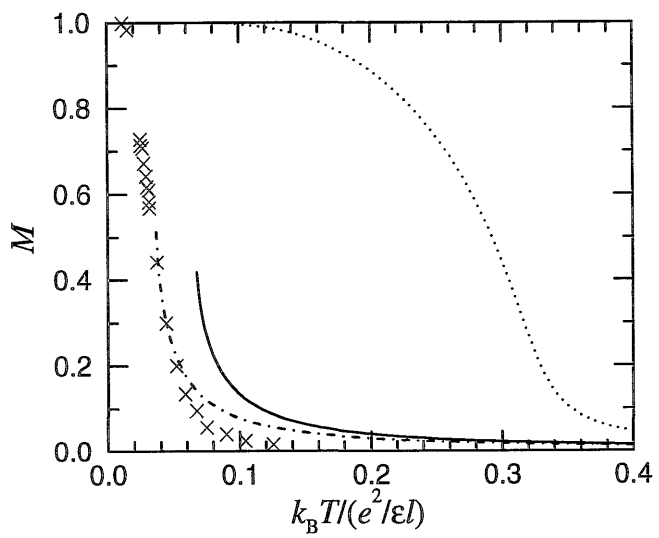

Fig. 5.10. The magnetization $M(T)$ versus temperature T for filling factor $\nu = 1$ obtained from the modified SC-RPA theory (full line) and from the Hartree–Fock theory (dotted line). The dash-dotted line is obtained by including also finite thickness corrections with $d = 3.11\,\ell$. The experimental data of Barrett et al. (1995) are shown as crosses.

found in the experiment. On the other hand, the noninteracting theory predicts the polarization of the system at a temperature related to the bare Zeeman energy, $k_B T \approx \Delta\varepsilon_s$, which is by a factor of 4.5 too low. Thus, simple theories based on a conventional perturbation-series expansion do not explain the experimental data. However, our modified SC-RPA theory which goes beyond perturbation theory works quite well.

Until now we have assumed always that the electron system is perfectly two-dimensional. However, in the real system (Barrett et al. 1995) the electrons are confined in a *GaAs* quantum well of thickness $d = 300\,\text{Å} = 3.11\,\ell$, which in units of the magnetic length ℓ is quite considerable. Thus, we expect corrections due to the finite thickness d of the electron layer. In the quantum well, the perpendicular motion of the electrons is described by the lowest subband wave function $\Psi(z)$, which implies that the charge is distributed in z direction over a layer of thickness d by $\varrho(z) \sim |\Psi(z)|^2$. Consequently, the electrons moving effectively two-dimensional in the lowest subband of the quantum well will interact via an effective potential $V_d(k)$ which depends on the thickness d. For simplicity we assume a quantum well with infinite barriers at $z = \pm d/2$, so that $\psi(z) = \theta(d^2/4 - z^2)(2/d)^{1/2}\cos(\pi z/d)$. Then we obtain the effective potential

$$V_d(\mathbb{k}) = \Big[\frac{2}{kd} + \frac{kd}{(kd)^2 + (2\pi)^2} - 2\Big(\frac{1}{kd} - \frac{kd}{(kd)^2 + (2\pi)^2}\Big)^2 (1 - \mathrm{e}^{-kd})\Big]\, V(\mathbb{k}) \tag{5.86}$$

where $V(\mathbb{k}) = 2\pi e^2/\varepsilon k$ is the two-dimensional Fourier transform of the Coulomb interaction potential. The finite thickness corrections imply a reduction of the interaction strength, $V_d(\mathbb{k}) \leq V(\mathbb{k})$. Thus, we expect a shift of the magnetization curve $M(T)$ to lower temperatures. In Fig. 5.10 this means that our theory comes even closer to the experimental data: the dash-dotted line shows the result of the modified SC-RPA theory including a finite thickness correction via (5.86) with $d = 3.11\,\ell$.

The curves in Fig. 5.10 are calculated with the assumption that the motion of the electrons is restricted to the lowest Landau level. In the experiment of Barrett et al. (1995) the charge carrier density corresponds to a plasma parameter $r_s = 1.5$ so that the Landau-level spacing $\hbar\omega_c$ and the characteristic interaction energy $e^2/\varepsilon\ell = \hbar\omega_c \cdot r_s(\nu/2)^{1/2}$ are nearly equal. Thus it is not obvious, why the higher Landau levels may be neglected. We have performed the numerical calculations also including the higher Landau levels by solving the four self-consistent equations (5.39), (5.52), (5.46), and (5.44) of the modified SC-RPA theory. As a result we obtain magnetization curves $M(T)$ for layer thicknesses $d = 0$ and $d = 3.11\,\ell$ which are quite close to the full line and the dash-dotted line in Fig. 5.10, respectively. Thus, the higher Landau levels imply only small perturbations, the curves are slightly shifted to lower temperatures. Also, the spectral functions $A_{0\sigma}(\varepsilon)$ of the lowest Landau level are affected only weakly by the higher levels. It turns out that for $r_s = 1.5$ the interaction is still too weak for a significant occupation of the higher Landau

levels. We find $\nu_{n\sigma} < 0.03$ for $n \geq 1$ for low temperatures $k_{\mathrm{B}}T \leq 0.1\, e^2/\varepsilon\ell$. Nearly empty levels cannot have a significant effect. Thus, the neglection of the higher Landau levels is indeed justified here.

Earlier we have stated that the modified SC-RPA theory will break down for low temperatures. This breakdown is expected to happen for $k_{\mathrm{B}}T \lesssim \varepsilon_{\mathrm{mr}} \approx 0.1\, e^2/\varepsilon\ell$ where the thermal energy is smaller than the characteristic energy of the collective excitations, because the modified SC-RPA theory does not yield the correct spectrum for the collective excitations. In Fig. 5.10 this breakdown is indeed clearly seen: our theory is valid only for temperatures $k_{\mathrm{B}}T \gtrsim 0.065\, e^2/\varepsilon\ell$ (full line) or $k_{\mathrm{B}}T \gtrsim 0.045\, e^2/\varepsilon\ell$ (dash-dotted line) where the magnetization is sufficiently small, i.e. $M \lesssim 0.4$. The observed breakdown temperatures are slightly lower than the expected one. For $\nu = 1$ below the breakdown temperature the magnetization suddenly jumps to $M \approx 1$ because the parameter λ defined in (5.63) jumps to zero so that the modified SC-RPA theory jumps to the Hartree–Fock theory. For $\nu \neq 1$ the breakdown is softened because in this case $\lambda \geq \nu(1-\nu)$ will never be zero so that the breakdown temperature is not sharply defined. Nevertheless, for all ν the modified SC-RPA theory will fail at low temperatures somewhere below $k_{\mathrm{B}}T_{\mathrm{mr}} = \varepsilon_{\mathrm{mr}} \approx 0.1\, e^2/\varepsilon\ell$.

Because of the very good agreement of the dash-dotted curve in Fig. 5.10 with the experimental data the modified SC-RPA theory appears to be very accurate in the temperature range where it is valid. We do not have a well founded and convincing explanation for why the modified SC-RPA theory works so well. However, we have tested our method with simple models, for which the exact solutions are known. In all cases the modified SC-RPA theory is very close to the exact solution above a certain usually quite small temperature. Below this temperature the modified SC-RPA theory breaks down. As an example we have considered (Haussmann 1997) the model of interacting fermions on one site with two spin degrees of freedom (which is equivalent to the Hubbard model in the atomic limit). This model is exactly solvable and has a quite similar structure as the FQHE system with the motion of the electrons restricted to the lowest Landau level. For average fermion number $N = 1$ we have calculated the magnetization $M(T)$ as function of temperature T where the bare Zeeman energy is assumed to be much smaller than the interaction energy. The result looks quite similar like Fig. 5.10. Here, the result of the modified SC-RPA theory is very close to the exact magnetization, in the same way as in Fig. 5.10 the dash-dotted line is close to the experimental data (Haussmann 1997).

For the filling factors $\nu_{0\sigma}$ and the magnetization $M = \nu_{0\downarrow} - \nu_{0\uparrow}$ the modified SC-RPA theory appears to have a similar structure as the Hartree–Fock theory: in both cases the filling factors $\nu_{0\sigma}$ are given by a Fermi distribution function (5.82) where the energies of the levels given by (5.83) or (5.84), respectively, depend on $\nu_{0\sigma}$ again so that the equations are self consistent. The essential difference of the modified SC-RPA theory is the effective screened

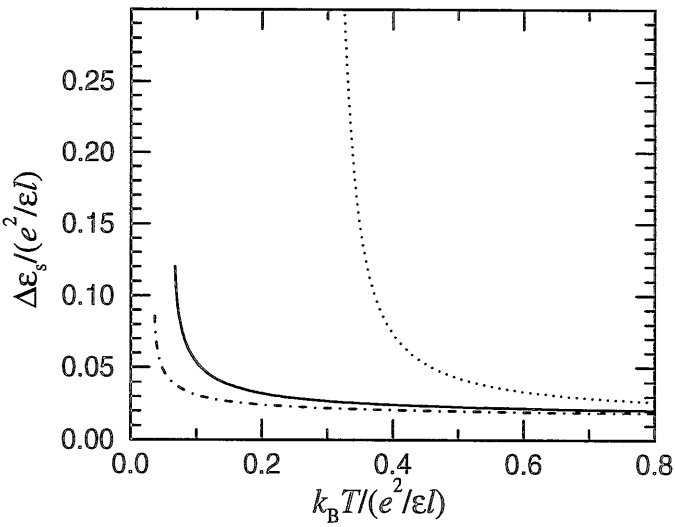

Fig. 5.11. The effective Zeeman energy $\Delta\varepsilon_s$ versus temperature for the modified SC-RPA theory (full line) and the Hartree–Fock theory (dotted line). The dash-dotted line corresponds to the modified SC-RPA theory including finite-thickness corrections with $d = 3.11\,\ell$.

interaction potential $u_{\rm eff}(k) = u(k)/[1+u(k)]$ in the last term of (5.83). For a better understanding of the reason why the modified SC-RPA theory works so well we consider the effective Zeeman energy

$$\Delta\bar{\varepsilon}_s = \bar{\varepsilon}_{0\uparrow} - \bar{\varepsilon}_{0\downarrow} = \Delta\varepsilon_s + M\frac{2\pi\ell^2}{\lambda\beta}\int\frac{{\rm d}^2k}{(2\pi)^2}\,\frac{u({\rm k})}{1+u({\rm k})}\,. \tag{5.87}$$

In Fig. 5.11 we have plotted $\Delta\bar{\varepsilon}_s$ versus temperature as full line and as dash-dotted line corresponding to the respective lines in Fig. 5.10. For comparison the effective Zeeman energy of the Hartree–Fock theory defined by

$$\Delta\varepsilon_s^{\rm HF} = \varepsilon_{0\uparrow}^{\rm HF} - \varepsilon_{0\downarrow}^{\rm HF} = \Delta\varepsilon_s + M\frac{2\pi\ell^2}{\lambda\beta}\int\frac{{\rm d}^2k}{(2\pi)^2}\,u({\rm k}) \tag{5.88}$$

is plotted as dotted line. While for higher temperatures all curves are close to each other, for the Hartree–Fock theory (dotted line) we observe a dramatic increase of the effective Zeeman energy if the temperature is lowered below $k_BT \approx 0.4\,e^2/\varepsilon\ell$. This nearly sudden increase of $\Delta\varepsilon_s^{\rm HF}$ is related to a spontaneous magnetization at the critical temperature $k_BT_c^{\rm HF} = 0.313\,e^2/\varepsilon\ell$ which is softened by the small but finite bare Zeeman energy $\Delta\varepsilon_s = 0.016\,e^2/\varepsilon\ell$. On the other hand, for the modified SC-RPA theory the effective Zeeman energy (full line for $d = 0$ and dash-dotted line for $d = 3.11\,\ell$) increases only slowly with decreasing temperature until $k_BT \approx 0.1\,e^2/\varepsilon\ell$. Here the denominator in (5.87) becomes large and causes screening for $k_BT \lesssim 0.4\,e^2/\varepsilon\ell$ so that the

increase of the effective Zeeman energy and the polarization of the system is delayed to lower temperatures. In the limit $\Delta\varepsilon_s \to 0$ we find the critical temperatures for spontaneous magnetization $k_B T_c = 0.041\, e^2/\varepsilon\ell$ for $d = 0$ and $k_B T_c = 0.016\, e^2/\varepsilon\ell$ for $d = 3.11\,\ell$. These values lie in the range of temperatures where the experimental $M(T)$ changes from 0 to 1. The integrand in (5.87) can be viewed as a RPA like effective screened potential so that the modified SC-RPA theory appears to be a Hartree–Fock theory with an effective screened potential.

6. Further applications

The self-consistent quantum-field theory modified by a gauge transformation appears to be a quite general and powerful approach for quantum liquids to describe phenomena beyond the conventional perturbation theory. In this work we have applied the approach to several interacting fermion systems. First, we have shown how the exact solutions of the Luttinger model and of the independent-boson model can be obtained by our quantum-field-theoretical approach in an elegant way. Secondly, we have applied our method to the two-dimensional electron system in a strong magnetic field in the FQHE regime as a perturbation theory for systems with degenerate levels. Here we describe some further applications of the modified self-consistent quantum-field theory. First of all, our method can be used as a bosonization technique for interacting fermion systems in $d = 1$ and $d > 1$ dimensions alternatively to existing approaches. The method allows a combination of bosonization with perturbation theory to investigate Fermi-liquid versus non-Fermi-liquid behavior. We have discussed this possible application briefly at the end of Sect. 4.3.

6.1 Coulomb plasma

We consider a three-dimensional system of electrons moving in a homogeneous positively charged neutralizing background. The electrons are interacting with each other by the Coulomb potential $V(\boldsymbol{r}) = e^2/|\boldsymbol{r}|$. The average distance between the electrons a is defined by writing the electron density in the form $\varrho = 1/[(4\pi/3)a^3]$. This system, usually called the Coulomb plasma, is described by three characteristic energies: the thermal energy $\varepsilon_{\mathrm{T}} = k_{\mathrm{B}}T$, the characteristic interaction energy $\varepsilon_{\mathrm{C}} = e^2/a$, and the characteristic energy of the quantum fluctuations $\varepsilon_{\mathrm{F}} = \hbar^2/ma^2$ (which is related to the Fermi energy). Fixing the energy scale there remain two dimensionless parameters which describe the physics of the system: the temperature parameter $\Gamma = \varepsilon_{\mathrm{C}}/\varepsilon_{\mathrm{T}}$, which is the strength of the interaction related to the thermal fluctuations, and the plasma parameter $r_{\mathrm{s}} = \varepsilon_{\mathrm{C}}/\varepsilon_{\mathrm{F}} = a/a_0$, which is the strength of the interaction related to the quantum fluctuations. (Here, $a_0 = \hbar^2/me^2$ is the Bohr radius.) In Fig. 6.1 the phase diagram of the Coulomb plasma is shown qualitatively. There is a transition between a liquid and a solid state, which

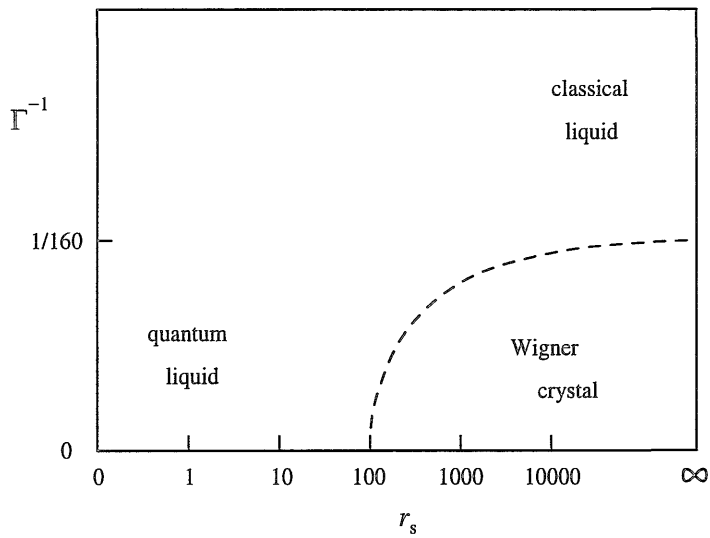

Fig. 6.1. The phase diagram of the Coulomb plasma in $d = 3$ dimensions. The dashed line indicates the first-order transition between the liquid state and a Wigner crystal.

is indicated by the dashed line. While for large temperatures the Coulomb plasma is a liquid, for low temperatures it is a Wigner crystal supposed the quantum fluctuations are not too strong. Furthermore, the system shows a crossover between a quantum liquid (Fermi liquid) and a classical liquid depending on the value of the plasma parameter r_s. For $r_s \lesssim 100$ the quantum fluctuations are so strong that the system remains a liquid even for zero temperature. In the limit $r_s \to \infty$ the Coulomb plasma is a classical liquid which is known to crystallize for $\Gamma \gtrsim 160$.

For small r_s quantum fluctuations are dominating so that the system is a weakly interacting Fermi gas. It turns out that for $r_s \lesssim 1$ the fermion Green's function $G(\mathbb{k}, \omega_n)$, the electronic spectral function $A(\mathbb{k}, \varepsilon)$, and the fermion distribution function $n(\mathbb{k})$ can be calculated by the conventional SC-RPA theory. The usual results of a weakly interacting Fermi liquid are obtained. However, for larger values of r_s nonperturbative effects will be relevant which are not included in the SC-RPA theory. For $r_s \gtrsim 1$ the pair correlation function $g(r)$ is negative for small distances r, which is unphysical and indicates the failure of the conventional SC-RPA theory. While there have been several theories to describe the electron gas for larger values of the plasma parameter up to $r_s \approx 6$ (see e.g. Mahan 1990), until now there does not exist a satisfactory theory for the electronic excitation spectrum $A(\mathbb{k}, \varepsilon)$ in the liquid state for large r_s.

We have applied our modified SC-RPA theory to the Coulomb plasma with the intention to consider large r_s. In Sect. 4.2 we have derived the related

self-consistent equations for the d-dimensional interacting quantum many-particle system. These equations are given by the Dyson equation (4.40) for the gauge-transformed fermion Green's function $\tilde{G}(\boldsymbol{k}, \omega_n)$ together with (4.53)-(4.59). For the three-dimensional Coulomb plasma we just set $d = 3$, $g_s = -2$, and insert $V(\boldsymbol{k}) = 4\pi e^2/\boldsymbol{k}^2$ for the Coulomb interaction. The success of our theory depends on the choice of the gauge-field propagator $D(\boldsymbol{r}, \tau)$ if it is possible to achieve a cancellation of the nontrivial frequency-dependent terms in the self energy $\tilde{\Sigma}(\boldsymbol{r}, \tau)$ defined by (4.55)-(4.58). It turns out that a complete cancellation is not possible because of the gradient terms in (4.57). While the first term of (4.57) may cancel (4.56), the two other terms of (4.57) remain and need not be small. We have found that the best choice is a space-independent gauge-field propagator $D(\tau)$. For this choice the gradient terms are just zero so that the self energy given by (4.55)-(4.58) reduces to

$$\tilde{\Sigma}(\boldsymbol{r}, \tau) = [-U_{\text{eff}}(\boldsymbol{r}, \tau) + (\hbar\partial_\tau)^2 D(\tau)]\, G(\boldsymbol{r}, \tau) \; . \tag{6.1}$$

According to (4.53) the nontrivial frequency dependent part of the effective interaction is defined by

$$\Delta U_{\text{eff}}(\boldsymbol{k}, \Omega_n) = -[V(\boldsymbol{k})]^2 \chi_{\varrho\varrho}(\boldsymbol{k}, \Omega_n) \; . \tag{6.2}$$

In the self energy (6.1) a complete cancellation of $\Delta U_{\text{eff}}(\boldsymbol{r}, \tau)$ can be achieved only for the fixed space variable $\boldsymbol{r} = \boldsymbol{0}$. For this reason we determine $D(\tau)$ by the condition

$$-\Delta U_{\text{eff}}(\boldsymbol{r} = \boldsymbol{0}, \tau) + (\hbar\partial_\tau)^2 D(\tau) = -V \cdot \hbar\, \delta(\tau) \tag{6.3}$$

where V is an arbitrary constant. This equation has the same form as (5.49), so that we may proceed in the same way as in Sect. 5.3 to determine V, $D(\tau)$, and $\Phi(\tau) = D(0) - D(\tau)$. Solving (6.3) for $(\hbar\partial_\tau)^2 D(\tau)$ and inserting the resulting terms into (6.1) we eventually obtain the self energy

$$\begin{aligned} \tilde{\Sigma}(\boldsymbol{r}, \tau) = & \left\{ V(\boldsymbol{r}) n(\boldsymbol{r}) + \Delta U_{\text{eff}}(\boldsymbol{0}, \Omega_n = 0)[n(\boldsymbol{r}) - \tfrac{1}{2}\delta(\boldsymbol{r})] \right\} \cdot \hbar\, \delta(\tau) \\ & - [\Delta U_{\text{eff}}(\boldsymbol{r}, \tau) - \Delta U_{\text{eff}}(\boldsymbol{0}, \tau)] \cdot \tilde{G}(\boldsymbol{r}, \tau) \end{aligned} \tag{6.4}$$

where $n(\boldsymbol{r}) = -\tilde{G}(\boldsymbol{r}, \tau = -0)$ is the Fourier transform of the fermion distribution function $n(\boldsymbol{k}) = -\tilde{G}(\boldsymbol{k}, \tau = -0)$. While the terms in the first line of (6.4) only imply a modification of the dispersion relation $\varepsilon_{\boldsymbol{k}} \to \bar{\varepsilon}_{\boldsymbol{k}}$, the second line represents the nontrivial frequency dependent contribution. Clearly, the second line of (6.4) nearly cancels if the gauge-transformed fermion Green's function $\tilde{G}(\boldsymbol{r}, \tau)$ is nonzero only for small $\boldsymbol{r}$, i.e. for $\boldsymbol{r} \approx \boldsymbol{0}$.

We have solved the self-consistent equations with the self energy (6.4) by a numerical calculation. We find that for sufficiently high temperatures (i.e. sufficiently large Γ^{-1}), where the system is a classical liquid, $\tilde{G}(\boldsymbol{r}, \tau)$ has a sharp peak at $\boldsymbol{r} = \boldsymbol{0}$ and $\tau = +0$ and is nearly zero elsewhere. Thus, in this case the major part of the second line of the self energy (6.4) indeed cancels.

Consequently, we obtain reasonable results for the electron Green's function $G(\boldsymbol{r},\tau) = \mathrm{e}^{\Phi(\tau)}\tilde{G}(\boldsymbol{r},\tau)$ and furthermore for the electronic spectral function $A(\boldsymbol{k},\varepsilon)$. The plasma parameter r_s does not have an essential influence on the cancellation in (6.4) so that r_s may be any value between zero and infinity. We conclude that the modified SC-RPA theory is a useful approach to calculate the electronic excitation spectrum $A(\boldsymbol{k},\varepsilon)$ of a Coulomb plasma for small and for large r_s, supposed the temperature is sufficiently high so that the system is a classical liquid.

The quantum-field theory for many-particle systems at finite temperatures (the Matsubara formalism) is designed as a perturbation theory for high temperatures where $\beta = 1/k_\mathrm{B}T$ is the expansion parameter. Thus, we expect that also the conventional SC-RPA theory may be used to calculate $G(\boldsymbol{r},\tau)$ and $A(\boldsymbol{k},\varepsilon)$ for high temperatures and all values of r_s between zero and infinity. This is indeed true. However, it turns out that the modified SC-RPA theory considered above works much better because of the cancellation in the self energy (6.4). We have solved the self-consistent equations numerically for several temperatures where r_s is kept constant, e.g. $r_\mathrm{s} = 30$. While for high temperatures the cancellation in (6.4) is nearly perfect, for decreasing temperature we obtain an increase of the nontrivial frequency-dependent term in the self energy $\tilde{\Sigma}(\boldsymbol{k},\omega_n)$ so that the degree of cancellation decreases. Below a certain temperature the nontrivial term of $\tilde{\Sigma}(\boldsymbol{k},\omega_n)$ is so large that there is no cancellation any more. Thus, the modified SC-RPA theory fails for low temperatures. However, it turns out that we can reach lower temperatures by the modified SC-RPA theory than by the conventional SC-RPA theory.

6.2 Interacting boson systems

Systems of interacting bosons as e.g. liquid ^{4}He may become superfluid for temperatures below a certain critical temperature T_c. Due to Bose–Einstein condensation in the superfluid state a macroscopic quantum coherence between the bosons is formed which implies a long-range order in the system. The order parameter is defined by the average of the boson field operator as $\langle\Psi(\boldsymbol{r},\tau)\rangle$. While for $T > T_\mathrm{c}$ in the normal fluid state the order parameter is zero, for $T < T_\mathrm{c}$ in the superfluid state it is

$$\langle\Psi(\boldsymbol{r},\tau)\rangle = \eta \cdot \mathrm{e}^{\mathrm{i}\varphi} \tag{6.5}$$

where the amplitude $\eta = \eta(T)$ is a function of temperature. The occurrence of the phase φ in (6.5) reflects a symmetry breaking by the superfluid transition. Since the value of φ may be arbitrary, the superfluid state actually is degenerate: at $T = 0$ for each value of φ there exists a superfluid ground state with the same ground-state energy. Thus, for a theoretical description of superfluid interacting boson systems a quantum-field theory, which represents

a perturbation theory for systems with degenerate levels, may be the appropriate approach. Our modified self-consistent quantum-field theory described in Chap. 4 may be a possible candidate for this purpose.

Conventionally, the quantum-field theory for superfluid boson systems is constructed in the following way (Abrikosov, Gorkov, and Dzyaloshinskii 1963, Fetter and Walecka 1971). From the boson field operators the average values are separated by

$$\Psi(\boldsymbol{r},\tau) = \eta\,\mathrm{e}^{\mathrm{i}\varphi} + \Delta\Psi(\boldsymbol{r},\tau)\ , \qquad \Psi^{+}(\boldsymbol{r},\tau) = \eta\,\mathrm{e}^{-\mathrm{i}\varphi} + \Delta\Psi^{+}(\boldsymbol{r},\tau) \tag{6.6}$$

so that $\langle\Delta\Psi(\boldsymbol{r},\tau)\rangle = 0$ and $\langle\Delta\Psi^{+}(\boldsymbol{r},\tau)\rangle = 0$. Then by inserting (6.6) the Hamiltonian H or equivalently the action functional S of the functional integral are expressed in terms of the new boson field operators $\Delta\Psi(\boldsymbol{r},\tau)$ and $\Delta\Psi^{+}(\boldsymbol{r},\tau)$. The free boson Green's function and the interaction terms for the new boson fields are obtained by inspection of S and identified by the respective elements of the Feynman diagrams. Eventually, the quantum-field theory for the superfluid boson system is obtained as a perturbation theory for the new bosons, i.e. the bosonic quasiparticles. The success of this theory depends on the assumption that a nonzero order parameter (6.5) exists indeed, which is true for a Bose liquid as e.g. ^{4}He in $d > 2$ dimensions in the thermodynamic limit (infinite system size). However, in some cases strong fluctuations of the phase φ destroy the order parameter. The right-hand side of (6.5) is just averaged to zero so that $\langle\Psi(\boldsymbol{r},\tau)\rangle = 0$. This happens e.g. in Bose liquids if the volume is finite or if the dimension is $d \leq 2$. While these systems may show superfluid-like behaviors at low temperatures, the conventional quantum-field theory for superfluid boson systems fails. In the following we show by considering a simple exactly solvable model of interacting bosons that our modified self-consistent quantum-field theory may be successful to describe superfluid interacting boson systems where the order parameter is $\langle\Psi(\boldsymbol{r},\tau)\rangle = 0$.

We consider a system of interacting bosons on one site which is described by the Hamiltonian

$$H = \varepsilon_0 b^{+}b + \tfrac{1}{2}U b^{+}b^{+}b\,b \tag{6.7}$$

where b and b^{+} are the Bose operators. This model is exactly solvable: $E_n = \varepsilon_0 n + \frac{1}{2}Un(n-1)$ are the eigenenergies and $|n\rangle$ are the eigenstates where $n = 0, 1, 2, \ldots$ is the number of the bosons. Since there is only one bosonic degree of freedom, the order parameter is always $\langle b\rangle = 0$ while on the other hand $\langle b^{+}b\rangle = N$ is the average boson number. For very large N the one site is macroscopically occupied with bosons so that the system must show some similarities to a Bose–Einstein condensation and superfluidity. Now, we apply the modified SC-RPA theory to the interacting boson system (6.7) in the same way as we have done in Chap. 5 for the FQHE system. We derive the four self-consistent equations to determine the gauge-transformed boson Green's function $\tilde{G}(\Omega_n)$. Since there is only one bosonic degree of freedom, there are no space variables. Thus, the nontrivial frequency dependent part of the

effective interaction can be canceled completely by the gauge-field propagator $D(\tau)$ by implying a condition analogous to (6.3) or (5.49). Hence, as a result for $\tilde{G}(\Omega_n)$ we obtain a free boson Green's function with a shifted energy.

We want to calculate the entropy S of the interacting boson system as a function of temperature T for fixed average boson number N. To do this we calculate the grand-canonical thermodynamic potential $\Omega(T,\mu)$ by (4.52) and (4.50) together with the functional $\tilde{\Xi}[\tilde{G}, U_{\text{eff}}]$ in modified SC-RPA which is given by the first-order diagrams shown in Fig. 4.13. Then, the entropy is obtained from the derivative $S = -\partial\Omega/\partial T$. We eliminate the chemical potential μ in favor of N so that eventually $S = S(T,N)$ depends explicitly on T and N. Thus, we obtain

$$S = k_{\text{B}}\big\{(N+1)\ln(N+1) - N\ln N \\ - \tfrac{1}{2}[\ln(1+u) - u/(1+u)]\big\} \tag{6.8}$$

where $u = N(N+1)U/k_{\text{B}}T$. This result of our modified SC-RPA theory is remarkably simple. While the first line is the entropy of a noninteracting boson system, the second line contains the interaction effects. For comparison we calculate the entropy exactly by evaluating the grand-canonical partition function $Z = \sum_n \exp\{-\beta(E_n - \mu n)\}$ to obtain $\Omega(T,\mu) = -k_{\text{B}}T\ln Z$ and $S = -\partial\Omega/\partial T$. In Fig. 6.2 the entropy S versus temperature T is shown for $N = 100$. The full line represents the result (6.8) of our modified SC-RPA theory while the dashed line represents the exact entropy. We clearly see that our theory agrees quite well with the exact result for temperatures $k_{\text{B}}T \gtrsim 0.3\,U$. For very low temperatures $k_{\text{B}}T \lesssim 0.3\,U$ our modified SC-RPA theory fails. Here the ground state freezes out so that the entropy becomes zero according to the third law of thermodynamics. This effect at very low temperatures is not described by our theory. For high temperatures $k_{\text{B}}T \gtrsim N(N+1)U$ the interaction effects are small compared to the thermal fluctuations so that the interaction contribution of the entropy (6.8) is small. Thus, in the high-temperature limit S will approach the entropy of the noninteracting boson system which is constant for fixed N and given by the first line of (6.8). In Fig. 6.2 we clearly see that S approaches this constant asymptotic value for $k_{\text{B}}T \gtrsim N(N+1)U \approx 10^4 U$ where $N = 100$.

There is an intermediate region of temperature $0.3\,U \lesssim k_{\text{B}}T \lesssim N(N+1)U$ which is essentially large if the average boson number N is large. In this region the entropy S is a logarithmic function of temperature T which is clearly seen in Fig. 6.2 by the straight lines with finite slope. This logarithm is obtained from (6.8) in the limit $N \to \infty$. We find

$$S = k_{\text{B}}\left[\tfrac{3}{2} + \tfrac{1}{2}\ln(k_{\text{B}}T/U) + \mathcal{O}(N^{-2})\right]. \tag{6.9}$$

The logarithm is also found in the exact entropy. For this purpose in the grand-canonical partition function Z we replace the sum over the boson number n by an integral and approximate the exponential function by a Gaussian peak around $n = N$. As a result we obtain

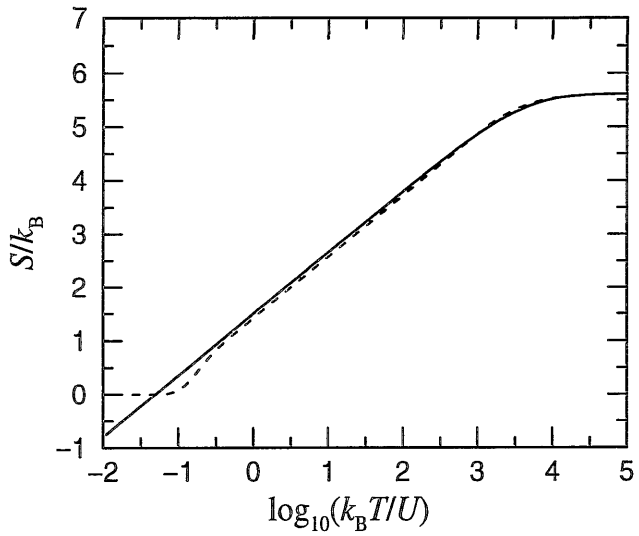

Fig. 6.2. The entropy $S = S(T, N)$ versus temperature T for fixed average boson number $N = 100$. The full line represents (6.8) of our modified SC-RPA theory, while the dashed line represents the exact entropy.

$$S_{\text{exact}} = k_B \left[\tfrac{1}{2}\ln(2\pi) - \tfrac{1}{2} + \tfrac{1}{2}\ln(k_BT/U)\right] \tag{6.10}$$

for temperatures in the intermediate region. The difference of the two entropies $S - S_{\text{exact}} = k_B[1 - \frac{1}{2}\ln(2\pi)] = 0.081\, k_B$ is quite small. For this reason the full line and the dashed line in Fig. 6.2 are very close to each other for intermediate temperatures. It turns out that conventional quantum-field-theoretical approaches work well for high temperatures $k_BT \gtrsim N(N+1)U$ but fail for intermediate and low temperatures $k_BT \lesssim N(N+1)U$. For example, the Hartree–Fock theory yields the constant entropy of the noninteracting boson system which in the exact theory is the high-temperature limit. Also, the conventional SC-RPA theory fails. However, our modified SC-RPA theory works well for high and intermediate temperatures and fails only for very low temperatures for which the ground state freezes out.

To investigate fluctuation effects we consider the boson fields $b(\tau)$ and $b^*(\tau)$ in the coherent-state representation where these fields are just complex numbers. For high temperatures $k_BT \gtrsim N(N+1)U$ the interaction effects are small so that $b(\tau)$ fluctuates like a free boson field over a certain two-dimensional region in the complex plain where the most probable value is $b_0 = 0$. For intermediate and low temperatures $k_BT \lesssim N(N+1)U$ the interaction effects restrict the fluctuations of $b(\tau)$ into a ring-like area in the complex plain around zero, so that now the most probable values are $b_0 = \sqrt{N}e^{i\varphi}$ where the phase φ may be arbitrary. If we interpret the most probable value b_0 as a mean-field order parameter, then we find a mean-field superfluid transition at a critical temperature $k_BT_{c,\text{mf}} \approx N(N+1)U$. How-

ever, since in the present system there is only one bosonic degree of freedom, the phase fluctuations are so strong so that $\langle b(\tau)\rangle = 0$ for all temperatures. The superfluid transition is destroyed by the phase fluctuations.

The most important observation is that our modified SC-RPA theory works quite well for intermediate temperatures $0.3\,U \lesssim k_{\mathrm{B}}T \lesssim N(N+1)U \approx k_{\mathrm{B}}T_{\mathrm{c,mf}}$ below the critical temperature of the mean-field superfluid transition. While (6.7) is the simplest interacting boson system, we may apply our modified SC-RPA theory to more general and more realistic interacting boson systems with many bosonic degrees of freedom. There may be systems as e.g. the three-dimensional Bose liquid for which the phase fluctuations are weaker and do not destroy the superfluid transition. We expect that our modified SC-RPA theory works successfully also for these systems below T_{c} in the superfluid state. However, in contrast to the conventional quantum-field theories (Abrikosov, Gorkov, and Dzyaloshinskii 1963, Fetter and Walecka 1971) our approach does not need a nonzero order parameter, it works for $\langle \Psi(\mathbf{r},\tau)\rangle = 0$.

References

M. Abramowitz and I. A. Stegun, *Handbook of mathematical functions* (Dover, New York 1972).

A. A. Abrikosov, L. P. Gorkov, and I. E. Dzyaloshinskii, *Methods of quantum field theory in statistical physics* (Dover, New York 1963).

I. L. Aleiner, H. U. Baranger, and L. I. Glazman, Phys. Rev. Lett. **74**, 3435 (1995).

R. C. Ashoori, J. A. Lebens, N. P. Bigelow, and R. H. Silsbee, Phys. Rev. Lett. **64**, 681 (1990); Phys. Rev. B **48**, 4616 (1993).

E. H. Aifer, B. B. Goldberg, and D. A. Broido, Phys. Rev. Lett. **76**,680 (1996).

D. J. Amit, *Field theory, the renormalization group, and critical phenomena* (McGraw-Hill, New York 1978).

J. Bardeen, L. N. Cooper, and J. R. Schrieffer, Phys. Rev. **108**, 1175 (1957).

S. E. Barrett, G. Dabbagh, L. N. Pfeiffer, K. W. West, and R. Tycko, Phys. Rev. Lett. **74**, 5112 (1995).

G. Baym, Phys. Rev. **127**, 1391 (1962).

G. Baym and L. P. Kadanoff, Phys. Rev. **124**, 287 (1961).

M. Bijlsma and H. T. C. Stoof, Phys. Rev. A **54**, 5085 (1996).

J. D. Bjorken and S. D. Drell, *Relativistic quantum fields* (McGraw-Hill, New York 1965).

K. M. Brown, N. Turner, J. T. Nicholls, E. H. Linfield, M. Pepper, D. A. Ritchie, and G. A. C. Jones, Phys. Rev. **B50**, 15465 (1994).

C. Castellani, C. Di Castro, and W. Metzner, Phys. Rev. Lett. **72**, 316 (1994).

A. H. Castro Neto and E. Fradkin, Phys. Rev. Lett. **72**, 1393 (1994); Phys. Rev. B **49**, 10877 (1994); Phys. Rev. B **51**, 4084 (1995).

L. N. Cooper, Phys. Rev. **104**, 1189 (1956).

A. S. Davydov, *Quantum mechanics* (Pergamon, Oxford 1965).

C. De Dominicis and P. C. Martin, J. Math. Phys. **5**, 14 and 31 (1964).

P. J. H. Denteneer, Guozhong An, and J. M. J. van Leeuwen, Europhys. Lett. **16**, 5 (1991).

G. Dev and J. K. Jain, Phys. Rev. B **45**, 1223 (1992).

M. Drechsler, diploma thesis, Universität Göttingen 1991 (unpublished).

M. Drechsler and W. Zwerger, Ann. Phys. **1**, 15 (1992).

I. E. Dzyaloshinskii and A. I. Larkin, Sov. Phys. JETP **38**, 202 (1974).

A. L. Efros and F. G. Pikus, Phys. Rev. B **48**, 14694 (1993).

J. P. Eisenstein, L. N. Pfeiffer, K. W. West, Phys. Rev. Lett. **69**, 3804 (1992); Surf. Sci. **305**, 393 (1994).

J. P. Eisenstein, L. N. Pfeiffer, K. W. West, Phys. Rev. Lett. **74**, 1419 (1995).

G. Fano, F. Ortolani, and E. Colombo, Phys. Rev. B **34**, 2670 (1986).

H. A. Fertig, L. Brey, R. Côté, and A. H. MacDonald, Phys. Rev. B **50**, 11018 (1994).

A. L. Fetter and J. D. Walecka, *Quantum theory of many-particle systems* (McGraw-Hill, New York 1971).

R. P. Feynman, *Statistical mechanics* (Benjamin, Reading, MA 1972).
H. C. Fogedby, J. Phys. C **9**, 3757 (1976).
R. Frésard, B. Glaser, and P. Wölfle, J. Phys. Condens. Matter **4**, 8565 (1992).
V. M. Galitskii, Sov. Phys. JETP **7**, 104 (1958).
S. M. Girvin and A. H. MacDonald, Phys. Rev. Lett. **58**, 1252 (1987).
S. M. Girvin, A. H. MacDonald, and P. M. Platzman, Phys. Rev. Lett. **54**, 581 (1985); Phys. Rev. B **33**, 2481 (1986).
L. P. Gorkov and T. K. Melik-Barkhudarov, Sov. Phys. JETP **13**, 1018 (1961).
M. Greiter, Phys. Lett. B **336**, 48 (1994).
P. Grüter, D. Ceperley, and F. Laloë, Phys. Rev. Lett. **79**, 3549 (1997).
F. D. M. Haldane, J. Phys. C. **14**, 2585 (1981).
F. D. M. Haldane, Phys. Rev. Lett. **51**, 605 (1983).
F. D. M. Haldane, Helv. Phys. Acta **65**, 152 (1992).
F. D. M. Haldane and E. H. Rezayi, Phys. Rev. B **31**, 2529 (1985a).
F. D. M. Haldane and E. H. Rezayi, Phys. Rev. Lett. **54**, 237 (1985b).
B. I. Halperin, Phys. Rev. Lett. **52**, 1583 (1984).
B. I. Halperin, P. A. Lee, and N. Read, Phys. Rev. B **47**, 7312 (1993).
Y. Hatsugai, P.-A. Bares, and X. G. Wen, Phys. Rev. Lett. **71**, 424 (1993).
R. Haussmann, Z. Phys. B **91**, 291 (1993).
R. Haussmann, Phys. Rev. B **49**, 12975 (1994a).
R. Haussmann, Acta Physica Slovaca **44**, 417 (1994b).
R. Haussmann, Phys. Rev. B **51**, 10755 (1995).
R. Haussmann, Phys. Rev. B **53**, 7357 (1996).
R. Haussmann, Phys. Rev. B **56**, 9684 (1997).
R. Haussmann, H. Mori, and A. H. MacDonald, Phys. Rev. Lett. **76**, 979 (1996).
S. He, P. M. Platzman, and B. I. Halperin, Phys. Rev. Lett. **71**, 777 (1993).
A. Houghton and J. B. Marston, Phys. Rev. B **48**, 7790 (1993).
A. Houghton, H.-J. Kwon, and J. B. Marston, Phys. Rev. B **50**, 1351 (1994a).
A. Houghton, H.-J. Kwon, J. B. Marston, and R. Shankar, J. Phys. C **6**, 4909 (1994b).
C. Itzykson and J.-B. Zuber, *Quantum field theory* (McGraw-Hill, New York 1980).
J. K. Jain, Phys. Rev. Lett. **63**, 199 (1989).
J. K. Jain, Phys. Rev. B **41**, 7653 (1990).
J. K. Jain, Adv. Phys. **41**, 105 (1992).
P. Johansson and J. M. Kinaret, Phys. Rev. Lett. **71**, 1435 (1993); Phys. Rev. B **50**, 4671 (1994).
L. P. Kadanoff and G. Baym, *Quantum statistical mechanics* (Benjamin, New York 1962).
M. Kasner and A. H. MacDonald, Phys. Rev. Lett. **76**, 3204 (1996).
L. V. Keldysh, Sov. Phys. JETP **20**, 1018 (1965).
K. von Klitzing, G. Dorda, and M. Pepper, Phys. Rev. Lett. **45**, 494 (1980).
P. Kopietz, *Bosonization of interacting fermions in arbitrary dimensions* (Springer, Berlin 1997).
P. Kopietz and G. E. Castilla, Phys. Rev. Lett. **76**, 4777 (1996).
P. Kopietz, J. Hermisson, and K. Schönhammer, Phys. Rev. B **52**, 10877 (1995).
P. Kopietz and K. Schönhammer, Z. Phys. B **100**, 259 (1996).
L. D. Landau and E. M. Lifshitz, *Course of theoretical physics, vol. 3: quantum mechanics* (Pergamon, London 1958).
L. D. Landau and E. M. Lifshitz, *Course of theoretical physics, vol. 9: statistical physics, part 2, theory of the condensed state* (Pergamon, Oxford 1980).
R. B. Laughlin, Phys. Rev. Lett. **50**, 1395 (1983).
R. B. Laughlin, Surf. Sci. **142**, 163 (1984).
D. K. K. Lee and Y. Chen, J. Phys. A **21**, 4155 (1988).

D.-H. Lee and C. L. Kane, Phys. Rev. Lett. **64**, 1313 (1990).
A. J. Leggett, in: *Modern trends in the theory of condensed matter*, edited by A. Pekalski and J. Przystawa (Springer, Berlin 1980), p. 13.
A. Lopez and E. Fradkin, Phys. Rev. B **44**, 5246 (1991).
A. Luther, Phys. Rev. B **19**, 320 (1979).
A. Luther and I. Peschel, Phys. Rev. B **9**, 2911 (1974).
J. M. Luttinger and J. C. Ward, Phys. Rev. **118**, 1417 (1960).
J. M. Luttinger, Phys. Rev. **119**, 1153 (1960).
J. M. Luttinger, Phys. Rev. **121**, 942 (1961).
J. M. Luttinger, J. Math. Phys. **4**, 1154 (1963).
G. D. Mahan, *Many-particle physics* (Plenum, New York 1990).
T. Matsubara, Prog. Theor. Phys. **14**, 351 (1955).
D. C. Mattis and E. H. Lieb, J. Math. Phys. **6**, 304 (1965).
W. Metzner and C. Di Castro, Phys. Rev. B **47**, 16107 (1993).
T. Moriya, *Spin fluctuations in itinerant electron magnetism* (Springer, Berlin 1985), chap. 4.
K. Moulopoulos and N. W. Ashcroft, Phys. Rev. Lett. **66**, 2915 (1991).
Y. Nambu, Phys. Rev. **117**, 648 (1960).
J. W. Negele and H. Orland, *Quantum many-particle systems* (Addison-Wesley, Redwood City, CA 1988).
P. Nozières and S. Schmitt-Rink, J. Low Temp. Phys. **59**, 195 (1985).
R. E. Prange and S. M. Girvin (editors), *The quantum Hall effect* (Springer, New York 1987).
J. Rammer and H. Smith, Rev. Mod. Phys. **58**, 323 (1986).
M. Randeria, J.-M. Duan, and L.-Y. Shieh, Phys. Rev. Lett. **62**, 981 (1989); Phys. Rev. B **41**, 327 (1990).
N. Read and S. Sachdev, Phys. Rev. Lett. **75**, 3509 (1995).
G. Röpke, Ann. Phys. **3**, 145 (1994).
C. A. R. Sá de Melo, M. Randeria, and J. R. Engelbrecht, Phys. Rev. Lett. **71**, 3202 (1993).
R. T. Scalettar, E. Y. Loh, J. E. Gubernatis, A. Moreo, S. R. White, D. J. Scalapino, R. L. Sugar, E. Dagotto, Phys. Rev. Lett. **62**, 1407 (1989).
A. Schmeller, J. P. Eisenstein, L. N. Pfeiffer, and K. W. West, Phys. Rev. Lett. **75**, 4290 (1995).
J. R. Schrieffer, *Theory of superconductivity* (Benjamin, New York 1964).
J. W. Serene and D. Rainer, Phys. Rep. **101**, 221 (1983).
J. O. Sofo, C. A. Balseiro, and H. E. Castillo, Phys. Rev. B **45**, 9860 (1992).
J. Sólyom, Adv. Phys. **28**, 201 (1979).
S. L. Sondhi, A. Karlhede, and S. A. Kivelson, Phys. Rev. B **47**, 16419 (1993).
S. Stintzing, Ph. D. thesis, Universität München 1996 (unpublished).
J. Stoer, *Einführung in die numerische Mathematik 1* (Springer, Berlin 1983).
H. T. C. Stoof, Phys. Rev. A **45**, 8398 (1992).
H. L. Störmer, A. Chang, D. C. Tsui, J. C. M. Hwang, A. C. Gossard, and W. Wiegmann, Phys. Rev. Lett. **50**, 1953 (1983).
D. J. Thouless, Ann. Phys. (N. Y.) **10**, 553 (1960).
A. Tokumitu, K, Miyake, and K. Yamada, J. Phys. Soc. Jpn. **60**, 380 (1991); Prog. Theor. Phys. Suppl. **106**, 63 (1991).
S. Tomonaga, Prog. Theor. Phys. **5**, 544 (1950).
S. A. Trugman and S. Kivelson, Phys. Rev. B **31**, 5280 (1985).
D. C. Tsui, H. L. Störmer, and A. C. Gossard, Phys. Rev. Lett. **48**, 1559 (1982).
N. Turner, J. T. Nicholls, E. H. Linfield, K. M. Brown, G. A. C. Jones, and D. A. Ritchie, Phys. Rev. B **54**, 10614 (1996).

R. L. Willett, R. R. Ruel, M. A. Paalanen, K. W. West, and L. N. Pfeiffer, Phys. Rev. B **47**, 7344 (1993).
J. Yang, Phys. Rev. B **49**, 5443 and 16765 (1994).
S. C. Zhang, Int. J. Mod. Phys. B **6**, 25 (1992).
S. C. Zhang, T. H. Hansson, and S. Kivelson, Phys. Rev. Lett. **62**, 82 (1989).

Index

action functional, 33, 82, 112
– gauge transformed, 83
AlGaAs, 118

BCS theory, 27, 51
– order parameter, 45
Bethe–Salpeter equation, 3, 20, 36, 47
– renormalized, 43
binding energy, 29, 53, 64
Bohr magneton, 118
Bose commutation relations, 107
Bose gas
– weakly interacting, 27, 29, 53
Bose liquid, 14, 165, 168
Bose–Einstein condensation, 27, 59, 164
bubble diagram, 19

cancellation
– of effective interaction, 100, 144, 163, 166
– of Hartree diagram, 96, 104, 137
– of interaction, 102, 138
characteristic energies, 119, 120
Chern–Simons theory, 127
closed-loop theorem, 78, 89, 104, 108
composite bosons, 31, 64
composite fermions, 124
connected diagrams, 12
conserving approximation, 1, 17, 42, 46, 56
continuity equation, 17
Cooper pairs, 27
Coulomb plasma, 161
crossover region, 30, 60
current-voltage characteristic, 132, 150
cyclotron frequency, 119

density-density correlation function, 99, 128, 147
dimensional regularization, 44, 47
dissociation, 28
double-peak structure, 129, 132, 142, 146, 149
Dyson equation, 11, 34, 46, 94, 137

effective boson mass, 59, 65
effective screened interaction, 18, 95, 137, 157, 163
energy gap, 123, 129
– collective excitations, 127
entropy
– for interacting bosons, 167
external field, 9, 16

Fermi gas
– weakly interacting, 27
Fermi liquid, 14, 78, 81, 111
fermion occupation number, 67
fermionic quasiparticles, 30
– energy dispersion, 51
– lifetime, 69
– spectrum, 68
Feynman rules
– gauge-transformed particles, 84
– independent-boson model, 113
– interacting particles, 12, 82
– Luttinger model, 102
– superfluid fermion system, 33
– two-dimensional electron system, 135
field operators, 8, 81
– fermion, 2, 117
– gauge transformation, 83, 101
filling factor
– of spin-polarized Landau levels, 141
– total, 119, 141
finite thickness corrections, 156
Fock diagram, 18, 44
FQHE, 73, 117, 122
functional integral, 10, 33, 81, 85

GaAs, 118
gauge transformation, 75, 83, 113
– action functional, 83

- field operators, 83, 101, 134
- Green's function, 86, 94, 103, 115, 134
- partition function, 83
gauge-field propagator, 85, 134, 138, 140, 163, 166
Ginzburg–Landau equation
- time-dependent, 61
Goldstone mode, 23, 24
Gorkov equations, 50
Green's function
- anomalous, 51
- exact or dressed, 9, 15, 74, 94
- fermion, 133
- free, 9, 10, 12, 35, 82, 106, 112, 134
- gauge transformation, 86, 94, 103, 115, 134
- higher-order, 17
- Matsubara, 128
- normal, 51
- one-particle, 8
- two-particle, 17, 20
ground state
- degenerate, 73, 122
- ferromagnetic, 153
- incompressible, 123, 128
- strongly correlated, 73
- superfluid, 164

Hamiltonian
- independent-boson model, 111
- interacting bosons, 165
- interacting electrons, 2, 117
- interacting fermions, 32
- interacting particles, 81
- Luttinger model, 76
Hartree diagram, 18, 44, 96, 104, 137
Hartree–Fock approximation, 18, 49, 50, 121, 154
heterostructure, 118
hierarchy theory, 123

incompressibility, 123, 130
independent-boson model, 75, 111, 140, 143, 145
- Feynman rules, 113
- Hamiltonian, 111
interaction, 8
- Coulomb, 18, 117
- effective screened, 18, 95, 137, 157
- short-range, 19, 32
- two-particle, 12
interaction vertex
- for fermions, 34
- for pairs, 57
IQHE, 117, 121
irreducible diagrams, 9, 111, 137
- one-particle, 14, 94, 103
- skeleton, 16, 94, 104

Jacobi matrix, 22

Keldysh formalism, 7
Knight shift, 153

ladder approximation, 30
- self-consistent, 19, 42
ladder diagrams, 19
Landé factor, 118
Landau levels, 73, 119
- lowest spin-polarized, 122, 146
Laughlin wave function, 122
- generalized, 124
Legendre transformation, 7, 10, 15, 21
linked cluster theorem, 12
Luttinger liquid, 24, 77, 81, 111
Luttinger model, 75, 76, 101
- Feynman rules, 102
- Hamiltonian, 76
- thermodynamic potential, 108
- Ward identities, 24

magnetic length, 123
magnetization, 153–155
- spontaneous, 158
magnetophonon, 143
magnetoroton, 74, 126, 130, 143, 147
- energy, 127, 149
Matsubara formalism, 7, 32, 73, 82, 164
mobility
- electronic, 118
modified SC-RPA, 99, 100, 137, 162, 165
MOSFET, 118

neutralizing background, 1, 18, 96, 118, 137, 161
NMR experiment, 153

pair formation, 23
pair propagator, 21, 38, 150
- particle-hole, 40
- particle-particle, 40
- regularized, 44
- renormalized, 47
partition function
- grand-canonical, 8, 81

Pauli exclusion principle, 31, 58
phase transition
– second-order, 23
– superfluid, 55
plasma parameter, 161
polarization function, 19, 96, 100, 106, 137
pseudogap, 142, 148

quantum Hall effect
– fractional, 73, 117, 122
– integer, 117, 121
quantum well, 118, 141

random-phase approximation, 104
– modified self-consistent, 99
– self-consistent, 19
resummation
– by gauge transformation, 87
– of polarization subdiagrams, 94, 104
– of self-energy subdiagrams, 15, 74
ring diagrams, 18

S matrix, 8
s-wave scattering length
– bosonic, 58
– fermionic, 41, 50
SC-RPA, 19, 162
– modified, 99, 100, 137, 162, 165
scaling invariance, 48
Schrödinger equation
– exact diagonalization, 144
– many-particle, 122
– one-particle, 118
screening, 18
self energy, 11, 35, 45, 47, 106
– gauge transformed, 94, 96, 99, 137, 163
– Hartree–Fock, 51
– SC-RPA, 18
single-mode approximation, 126, 130, 147
skyrmions, 153
spectral function, 69, 140
– collective excitations, 128, 147
– lowest Landau level, 146, 149
– of spin-polarized Landau levels, 142
– pair propagator, 151
– single-particle excitations, 128
structure factor
– dynamic, 126
– static, 126
subdiagrams
– self-energy, 15
superconductivity, 23, 27
superfluidity, 27, 37, 165

T matrix, 20, 40
theorems for resummation, 87
thermodynamic potential
– "enthalpy", 10
– "free energy", 10
– grand-canonical, 12, 72, 98, 108, 166
Thouless criterion, 24, 50, 62
time ordered product, 8
tunneling conductance
– differential, 152
tunneling current, 131, 150
tunneling experiments, 131
two-particle collisions, 20

vertex function, 21, 35, 46
– bare, 33, 36
– generating functional, 17
– irreducible, 21, 36
– unsymmetrized, 42

Ward identity, 23, 24, 49
Wigner crystal, 143, 162

Zeeman energy, 119, 153
– bare, 155
– effective, 158
Zeeman splitting, 118